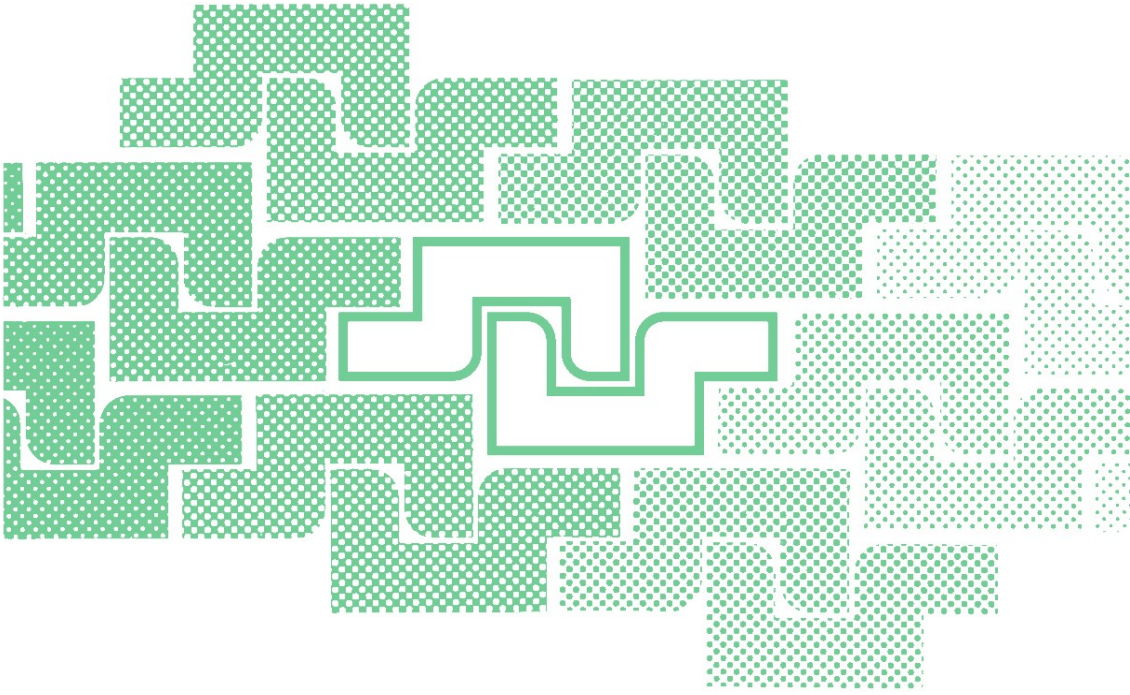

Earthquake Monitoring and Seismic Hazard Mitigation in Balkan Countries

Edited by

Eystein S. Husebye

NATO Science Series

IV. Earth and Environmental Sciences – Vol. 81

CD-ROM INCLUDED

Earthquake Monitoring and Seismic Hazard Mitigation in Balkan Countries

NATO Science Series

A Series presenting the results of scientific meetings supported under the NATO Science Programme.

This Series is published by IOS Press, Amsterdam, and Springer (formerly Kluwer Academic Publishers) in conjunction with the NATO Public Diplomacy Division.

Sub-Series

I. Life and Behavioural Sciences	IOS Press
II. Mathematics, Physics and Chemistry	Springer (formerly Kluwer Academic Publishers)
III. Computer and Systems Science	IOS Press
IV. Earth and Environmental Sciences	Springer (formerly Kluwer Academic Publishers)

The NATO Science Series continues the series of books published formerly as the NATO ASI Series.

The NATO Science Programme offers support for collaboration in civil science between scientists of countries of the Euro-Atlantic Partnership Council. The types of scientific meeting generally supported are "Advanced Study Institutes" and "Advanced Research Workshops", and the NATO Science Series collects together the results of these meetings. The meetings are co-organized by scientists from NATO countries and scientists from NATO's Partner countries – countries of the CIS and Central and Eastern Europe.

Advanced Study Institutes (ASI) are high-level tutorial courses offering in-depth study of latest advances in a field.

Advanced Research Workshops are expert meetings aimed at critical assessment of a field, and identification of directions for future action.

As a consequence of the restructuring of the NATO Science Programme in 1999, the NATO Science Series was re-organized to the Four Sub-series noted above. Please consult the following web sites for information on previous volumes published in the Series.

http://www.nato.int/science
http://www.springeronline.com
http://www.iospress.nl

Series IV: Earth and Environmental/Sciences-Vol.79

Earthquake Monitoring and Seismic Hazard Mitigation in Balkan Countries

edited by

Eystein S. Husebye

Bergen Center for Computational Science,
UNIFOB A/S, University of Bergen,
Bergen, Norway

Published in cooperation with NATO Public Diplomacy Division

Proceedings of the NATO Advanced Research Workshop on
Earthquake Monitoring and Seismic Hazard Mitigation in Balkan Countries
Borovetz, Bulgaria
11–18 September 2005

A C.I.P. Catalogue record for this book is available from the Library of Congress.

ISBN 978-1-4020-6814-0 (PB)
ISBN 978-1-4020-6813-3 (HB)
ISBN 978-1-4020-6815-7 (e-book)

Published by Springer,
P.O. Box 17, 3300 AA Dordrecht, The Netherlands.

www.springer.com

Printed on acid-free paper

CONTENTS

Part V: Seismic Hazard Analysis and Assessment

FOREWORD

Seismology is generally rated the Queen of Earth Sciences due to its ability to provide in ever increasing detail structural information bearing on the Earth interior. The reason for this is twofold: (i) the advanced theoretical foundation of seismology and (ii) extensive scientific cooperation in recording and disseminating data on local, regional and global scales. In contrast, some 40 years ago seismology was a backward science of little interest outside the academics and hence poor funding. This abruptly changed with the political interest in seismology as the principal tool for monitoring compliance with a potential Comprehensive Nuclear Test Ban Treaty (CTBT) banning any kind of nuclear testing in any environment. The political interest become synonymous with major national seismological research programs foremost in USA and an early achievement was the worldwide deployment of 100 modern, identical seismograph stations (the WWSSN network) and with its own data collection and dissemination center. The latter feature is important, so it is no point in network operations unless the earthquake recordings are easily available for the research community. A few years later, the first large aperture array LASA, located in Montana, become operational. Unique features were digital recording for all its 525 sensors, electronic data transmission via leased telephone lines and real-time seismic signal analysis. The early emphasize on modern network and array deployments were not only aimed at better mappings of the Earth interior but also for providing observational basis for further theoretical developments and wave propagation modeling. Outstanding achievements in these regards were advanced source theories, seismic tomography and wave scattering in a heterogeneous Earth. These topics were the subjects of two NATO Advanced Study Institute arranged (i) in Sandefjord, Norway between April 22 and May 3, 1974 (Beauchamp, 1975) and (ii) Oslo, Norway between September 8 to 18, 1980 (Husebye and Mykkeltveit, 1981).

In the 1980s the once backward science of seismology had matured into a modern and advanced science and besides being fully capable to monitor compliance with a CTBT treaty. The latter was not too surprising because most often seismologists act as advisors to the politicians on these matters. In other words, technicalities were no longer a problem, nor an excuse for not agreeing to a test ban treaty which was finally approved by the UN General Assembly in New York in September 1995. Again, also these topics were subject of a NATO Advanced Study Institute arranged in Alvor, Portugal between January 23 and February 1, 1975 (Husebye and Dainty, 1996).

The rapid evolution of seismology to a modern science was to a large extent due to generous government funding in various countries and, not unexpectedly, channeled mainly through government agencies and laboratories. In general, major segments of the seismological community were side-lined during these exciting developments and moreover often deprived of accesses to digital data bases and associated software infrastructures. In other words, being at a disadvantage for undertaking advanced research projects. Fortunately, some distinguished and

foresighted seismologists realized that further research progresses could not be maintained unless more high quality data from ever expanding broadband seismological networks and at that becoming available to the whole seismological community. However, an important prerequisite for successful undertakings here was (and is) extensive and unselfish cooperations between many academic institutions in different countries. If not, funding bodies were unlikely to support these bold new seismological research initiatives for expanding broadband networks and associated data center operations. The required 'distributed responsibilities' for less costly network operations were new to many prominent seismologists so the early 'network' years of for example IRIS and ORFEUS were marked by some internal squabbles. However, the need for constructive cooperations were too obvious so after a few years the mentioned squabbles and quarrels ended. As of today, organizations and network operators like IRIS, GEOSCOPE, ORFEUS, GEOFON, EMSC, MEDNET etc are in harmony and besides closely cooperate in exchange of data, software and often initiate common research projects.

Today, technical nor meager funding do pose insurmountable problems for seismic network operations even on regional scales albeit a number of regions, including Balkans, is lacking a kind of multinational undertaking. This is in a way surprising in view of the regions long history of disastrous earthquakes and its fostering of a number of outstanding seismologists. On the other hand, all the Balkan countries are operating national networks although these are not always up-todate regarding digital seismometry and besides real-time record analysis are not always conducted. However, we see no compelling reasons why not the Balkan countries jointly should be able to monitor local earthquake activities in near real time and subsequently use their data for restoring past prominence in seismological research – this is what this workshop is all about.

The workshop was carried out at a time when the political climate in the world and in particular in Europe had dramatically improved over the last decade. The new regulations in trade and science give more freedom for extensive cooperation and improved societal prospects. Traditionally, seismologists have been closely cooperating in Europe as many countries in Eastern Europe have become members of both EU and NATO. We believe that will see even better coordination and cooperation in seismology both between individual scientists and their respective institutions. Hopefully, our NATO ARW and this book may be rated a token contribution towards this end and also mention that 6 W. Balkan countries are jointly undertaking a NATO sponsored study of historical seismicity in their territories.

The content of the Book is organised in a manner similar to that of the NATO ARW itself. The start or overture is the tectonic framework and geodynamics of the South Balkan region (Burchfiel et al.), then recent GPS measurements of such deformations (Kotzev et al.) while active tectonics and associated large earthquakes in the Aegean and Marmara seas (Taymaz et al.). Several seismicity studies are presented in Part II; Albania by Duni and Kuka, Croatia by Markušić and the Pannonian Basin (Hungary and adjacent areas) by Tóth et al. Greece is dealt with in the hazard analysis of Tsapanos in Part V. Seismic network operations on global, regional and national scales are dealt with in Part III (Kebeasy, Ingate, Mazza et al.,

Hanka and Saul, and Matveeva et al.). Presentations emphasise data collection and dissemination as these services support the research needs of the seismological community. More details on network operations in terms of real time data analysis, signal detection and event location are given in Part IV by Fedorenko et al. (2 articles), Pinsky and Childs et al. Finally, Part V deals with seismic hazard analysis; principle procedures by Kijko, hazard assessment of Greece by Tsapanos while Kebeasy et al. model ground motion amplification due to rugged topography in an area subject to strong shakings during the Lurøy, N. Norway earthquakes in 1819.

A great deal of effort goes into organizing and running an Advanced Research Workshop (ARW). Firstly, I want to express my sincere thanks to my co-director dr. Christova and local organization committee members dr. Nikolova and dr. Raykova often working long hours to make this Workshop possible. Particular thanks go to academician L. Christoskov for his opening address on behalf of the Bulgarian geosience community and likewise dedicated staffers at the Geophysical Institute, Academy of Science in Sofia. To be frank, the Workshop would not have been feasible without the efforts of the Local Organizing Committee for their talent in handling the multitude of tasks like receiving arriving participants, transports, hotel accommodations in both Sofia and Borovetz thus ensuring a memorable and scientifically stimulating workshop in Borovetz, Bulgaria September 11–17, 2005. Let me add, the exceptional editorial skills of Tatiana Matveeva ensured that this book was ever made.

Eystein S. Husebye

References

Beauchamp, K. G. (ed.), 1975. *Exploitation of Seismograph Networks*. NATO ASI Series, Noordhoff Int. Publ. Co., Leiden, The Netherlands, p 645.

Husebye, E. S., Mykkeltveit, S. (ed.), 1981. Identification of Seismic Sources – Earthquakes or Underground Explosions. NATO ASI Series, D. Reidel Publ. Co., Dordrecht, The Netherlands, p 876.

Husebye, E. S., Dainty, A. M. (ed.), 1996. Monitoring a Comprehensive Test Ban Treaty. NATO ASI Series, Kluwer Academic Publ., Dordrecht, The Netherlands, p 836.

Principal Sponsor

NATO Public Diplomacy Division
Collaborative Programmes Section – The Nato Science for Peace and Security Programme, Brussels, Belgium

Co-Sponsors

International Association of Seismology and Physics of the Earth Interior, Boulder, CO, USA
Preparatory Commission of Comprehensive Test Ban Treaty Organization, Vienna, Austria
Cambridge University Press, Cambridge, United Kingdom
Springer Science and Business Media, Berlin, Germany
Kinemetrics Inc., Pasadena, CA 91107, USA

Scientific Directors

Eystein S. Husebye
Bergen, Norway

Cenka Christova
Sofia, Bulgaria

Organizing Committees

Robert E. Engdahl
Boulder, USA

Svetlana Nikolova
Sofia, Bulgaria

Theodoros Tsapanos
Thessaloniki, Greece

Reneta Raykova
Sofia, Bulgaria

Local Organizing Committee

Stoyan Stoyanov, Liliya Dimitrova: Sofia, Bulgaria

LIST OF PARTICIPANTS

SCIENTIFIC DIRECTORS

Prof. Eystein S. Husebye
Bergen Center for Computational Science, UNIFOB/UoBergen, Thormoehlens gt. 55, 2008 Bergen, Norway

Dr. Cenka Christova
Geophysical Institute – BAS Acad. G., Bonchev str., bl 3, Sofia 1113, Bolgaria

LECTURERS

Dr. Remy Bossu
European-Mediterranean Seismological Centre (EMSC), c/o CEA, Bât. Sables BP12, 91680, Bruyères le Châtel, France, bossu@emsc-csem.org

Prof. Clark Burchfiel
Room 54-1010 MIT, Mass., Avenue 77, Cambridge MA 02139, USA, bcburch@mit.edu

Assoc. Prof. Costas
Geophysical Laboratory, University of B. Papazachos Thessaloniki, PO Box 352-1, 54124 Thessaloniki, Greece, costas@lemnos.geo.auth.gr

Eng. Dean Childs
Geophysics Dept. of Bogazici University, 34680 Cengelkoy, Istanbul, Turkey, dean@boun.edu.tr

Dr. Cenka Christova
Geophysical Institute - BAS Acad. G., Bonchev str., bl 3, Sofia 1113, Bolgaria, cenka@geophys.bas.bg

Prof. Dr. Llambro Duni
Engineering Seismology Dept., Rr. "Don Bosko" N60, Tirana, Albania duni@sizmo.edu.al

Prof. Torild van Eck
Observatories and Research Facilities for European Seismology (ORFEUS), P.O.Box 201, 3730 AE De Bilt, The Netherlands, vaneck@knmi.nl

Prof. Yury V. Fedorenko
Polar Geophysical Institute, Kola Sci. Center, Fersman str. 14, Apatity, 184209, Russia, fedorenko@pgi.kolasc.net.ru

Prof. Eystein S. Husebye
BCCS, UNIFOB/UoBergen, Thormoehlens gt. 55,2008 Bergen, Norway, esh@bccs.uib.no

Dr. Shane Ingate
The Incorporated Research Institutions for Seismology, (IRIS), PASSCAL Instrument Center, New Mexico Tech., 100 East Road, Socorro, NM 87801, USA, Shane@passcal.nmt. edu.

Prof. Rashad M. Kebeasy
National Research Institute of Astronomy and Geophysics, Helwan, Cairo, Egypt, rashad_kebeasy@yahoo.co.uk

Dr. Andrzej Kijko
National Manager Council for Geoscience, Private Bag X112, Pretoria, 0001, 280 Pretoria Road, Silverton, Pretoria, South Africa, kijko@geoscience.org.za

Prof. Valentin Kotzev
Central Lab. of Geodesy – DAS, Acad. G. Bonchev str., bl 1, 1113 Sofia, Bulgaria, kotzev@bas.bg

Prof. Dr. Snjezana Markušić
Dept. of Geophysics, University of Zagreb, Horvatovac bb, 10000 Zagreb, Croatia, markusic@irb.hr

Dr. Salvatore Mazza
Istituto Nazionale di Geofisica e Vulcanologia, Via di Vigna Murata 605, 00143 Roma, Italy, mazza@ingv.it

Prof. Gerassimos Papadopoulos
Institut of Geodynamics, National Observatory of Athens, P.O. Box 20048, 118 10 Athens, Greece, g.papad@egelados.gein.noa.gr

Dr. Vladimir Pinsky
Geophysical Institute of Israel, Abaalshemtov 6, POB 182, Lod 71100, Israel, vlad@seis.mni.gov.il

Dr. Joachim Saul
GeoForschungsZentrum Potsdam, Telegrafenberg E220 (PB 2.4), 14473 Potsdam, Germany, saul@gfz-potsdam.de

Prof. Tuncay Taymaz
Istanbul Technical University, Dept. Geophys.-Seismol. Section, Maslak, 34390, Istanbul, Turkey, taymaz@itu.edu.tr

Dr. Laszlo Tóth
Seismological Observatory Meredek u. 18, 1112 Budapest, Hungary, laszlo@seismology.hu

Prof. Theodoros Tsapanos
Dept. of Geophysics, Aristotle University, PO Box 352-1, 54124 Thessaloniki, Greece, tsapanos@geo.auth.gr

PARTICIPANTS

Elena Beketova
Polar Geophysical Institute, Kola Sci. Center, Fersman str. 14, Apatity, 184209, Russia, beketova@pgi.kolasc.net.ru

Prof. Ivan Brlek
Seismological Dept., Federal Meteorological Institute, Bardakcije 12, 71000 Sarajevo, Bosnia and Herzegovina, ivanbrlek@yahoo.com

Acad. Ludmil Christoskov
Geophysical Institute – BAS, Acad. G. Bonchev str., bl. 3, Sofia 1113, Bulgaria, chrst@geophys.bas.bg

Velko Christov
Geophysical Institute - BAS Acad. G., Bonchev str., bl 3, Sofia 1113, Bolgaria, velko@geophys.bas.bg

Dr. Giovanni Costa
Dept. of Earth Sciences, University of Trieste, via E. Weiss 1, 34127 Trieste, Italy, costa@units.it

Liliya Dimitrova
Geophysical Institute – BAS Acad. G. Bonchev str., bl. 3, Sofia 1113, Bulgaria, lidim@geophys.bas.bg

Dr. Francesca Fitzko
Dir. Potezione Civile del FVG, Via Natisone 43, Plamanova, (UDINE), Italy, francesca.fitzko@regione.fvg.it

Dr. Muzaffer Gul B.U.
Kandilli Observatory and Earthquake Research Institute, Dep. of Earthquake Engineering, 81220 Cengelkoy, Istanbul, Turkey, muzaffer.gul@boun.edu.tr

Tamara Jesenko
Environmental Agency of the Republic of Slovenia, Dunajska 47/VI, SI-1000 LJUBLJANA, Slovenia, Tamara.Jesenko@gov.si

Georgios Koravos
Aristotle University of Thessaloniki Dept. of Geophysics, School of Geology, GR-541 24, Thessaloniki Greece, gkor@geo.auth.gr

BSc Kresimir Kuk
Croatian Seismological Survey, Department of Geophysics, Faculty of Science, Horvatovac bb, 10000 Zagreb, Croatia, kresok@irb.hr

Dr. Mohamed EL Idrissi
Kinemetrics Inc., Z.I Le Tresi 3, 1028 Preverenges, Switzerland, midrissi@bluewin.ch

Dr. Svetlana Nikolova
Geophysical Institute – BAS, Acad. G. Bonchev str., bl. 3, Sofia 1113, Bulgaria, sbnik@geophys.bas.bg

Dr. Lazo Pekevski
Seismological Observatory, University "Sv. Kiril i Metodij", P.O.Box 422, 1000 Skopje, Republic of Macedonia, lpekevski@seismobsko.pmf.ukim.edu.mk

Iliana Popova
Geophysical Institute - BAS Acad. G., Bonchev str., bl 3, Sofia 1113, Bolgaria, ilianapopova79@yahoo.com

Slavica Radovanovic
Seismological Survey of Serbia, Tasmajdanski Park BB, P.O.B. 16, 11001 Beograd, Serbia, s.radovanovic@seismo.sr.gov.yu

Dr. Mircea Radulian
Nat. Institute for Earth Physics, Calugareni str, 12, P.O. Box MG-2, 077125, Bucharest- Magurele, Ilfov, Romania, mircea@infp.ro

Dr. Reneta Raykova
Geophysical Institute – BAS, Acad. G. Bonchev str., bl. 3, Sofia 1113, Bulgaria, rraikova@geophys.bas.bg

Assoc. Prof. Manolis Scordilis
Central Seismological Station, Laboratory of Geophysics, Aristotle University, PO Box 352- 1, 54124 Thessaloniki, Greece, manolis@geo.auth.gr

Assoc Prof. Dimcho Solakov
Geophysical Institute – BAS, Acad. G. Bonchev str., bl. 3, Sofia 1113, Bulgaria, dimos@geophys.bas.bg

Stoyan Stoyanov
Geophysical Institute – BAS, Acad. G. Bonchev str., bl. 3, Sofia 1113, Bulgaria, stoyan@geophys.bas.bg

Part I
Tectonic Framework and Geodynamics of the South Balkan Region

Patterns of Cenozoic Extensional Tectonism in the South Balkan Extensional System

B. Clark Burchfiel*, Robert W. King[1], Radoslav Nakov[2], Tzanko Tzankov[3], Nikola Dumurdzanov, Todor Serafimovski[4], Angel Todosov[5], and Bilbil Nurce[6]

Abstract The present day tectonic pattern of the Balkan Peninsula has evolved from three major periods of mainly extensional tectonism: (i) Paleogene extension that is difficult to characterize because its relation to the closing of the Vardar Ocean remains uncertain; (ii) Early to Late Miocene extension related to rollback at the Hellenic subduction zone; and (iii) Late Miocene to Recent extension related to continued trench rollback, but modified by the development of the North Anatolian fault zone and the rapid movement of the Aegean crust to the SSW.

Paleogene extension occurred during and shortly after the time final closure of the Vardar Ocean. The timing of Vardar closing remains uncertain, but is between the early and late Eocene and may be diachronous. Extension occurs from eastern Macedonia through western Bulgaria and northern Greece to northwestern Turkey and lies within a region of thickened crust that may be at least partly undergoing shortening contemporaneous with the earliest stages of extension. However, the exact timing relations between extension and shortening remains unclear, and some evidence suggest they are locally contemporaneous. The tectonic setting appears to be one of transition from subduction related convergence and shortening to subduction rollback convergence with extension. The interpretations of the dynamics for the Paleogene extension are currently controversial.

[1] Massachusetts Institute of Technology, Cambridge, MA, USA

[2] Institute of Geology, Bulgarian Academy of Sciences, Sofia, Bulgaria

[3] Southwest University, Blagoevgrad, Bulgaria

[4] Faculty of Mining and Geology Stip, University of "St. Cyril and Methodius" Skopje, Stip, Macedonia.

[5] Strumica, Macedonia

[6] Department of Geodesy, Construct Engineering Faculty, Tirana, Albania

*To whom correspondence should be addressed. e-mail: bcburch@mit.edu

E.S. Husebye (ed.), *Earthquake Monitoring and Seismic Hazard Mitigation in Balkan Countries.*

By Early or Middle Miocene time, extension within the Balkans was characterized by WSW-ESE extension in western Bulgaria and eastern Macedonia. The NNW striking normal faults were part of an evolving extensional system that was part of the regional Aegean realm and can be related to trench rollback and rotation of large crustal fragments. Short periods of Early or Middle Miocene local compression occur in western Bulgaria and eastern Macedonia that may be related to the time when small, but thick crustal fragments entered the northern Hellenic subduction zone in Albania. Three belts of folds are present in the Thrace basin and are probably related to local transpression along right-lateral strike-slip faults that may be precursors to formation of the North Antatolian fault zone. The age of this folding is poorly constrained and is bracketed only between earliest Miocene and latest Miocene.

Beginning in Late Miocene time the pattern of extension within the Balkans progressively evolved related to complex events in the rollback of the Hellenic subducted slab both to the south and to the west and with the initiation of right-lateral strike slip along the southern branch of the North Anatolian fault zone. E–W extension migrated progressively from western Bulgaria into central Macedonia and Albania, followed to the east by N–S extension that migrated from east to west across central and western Bulgaria into eastern Macedonia. This pattern of faulting dominates the present tectonic pattern in the Balkan Peninsula. The rapid Pliocene development of the northern branch of the North Anatolian fault zone partially decoupled the rapid SSW movement of an Aegean plate from slow N–S extension that increased in magnitude from central Bulgaria and Macedonia into northern Greece.

The present active pattern of tectonism is characterized by a narrow zone of shortening east of the northwest part of the Hellenic trench, that rapidly changes to E–W extension in central Albania and western Macedonia. GPS data and only rare geological data suggest the transitional zone may be marked by distributed right-lateral strike-slip. Slow N–S extension dominates eastern Macedonia and Bulgaria with associated local strike-slip faulting. Although weakly developed, the seismicity generally supports this pattern of tectonism. Slip-rates on faults probably increases southward into northern Greece, a testable hypothesis, based on GPS data that show increasing southward velocity relative to Eurasia. GPS data shows the abrupt change to rapid strike-slip along the North Anatolian fault. The slow N–S extension in the southern Balkan Peninsula may be related to the southward pull of the Aegean plate, with possible slow counterclockwise rotation of the western part of the North Anatolian fault zone.

Keywords cenozoic extension, South Balkan

1 Introduction

The Cenozoic South Balkan Extensional System (SBES) lies within southern Bulgaria, Macedonia, eastern Albania, northern Greece and northwestern-most Turkey (Figure 1). Extension within this region began in Paleogene time during the final closure of the Vardar Ocean and subsequent post-collisional deformation. Subsequently the region was directly part of the more regional Aegean extensional realm before the formation of the North Anatolian fault zone in late Miocene/ Pliocene time (Sengor et al., 2004). Since the development of the North Anatolian fault zone the SBES has been partly isolated from the Aegean extensional realm to the south. The Cenozoic history and evolution of the SBES is largely recorded in the abundant sedimentary basins developed in the region (Figure 2).

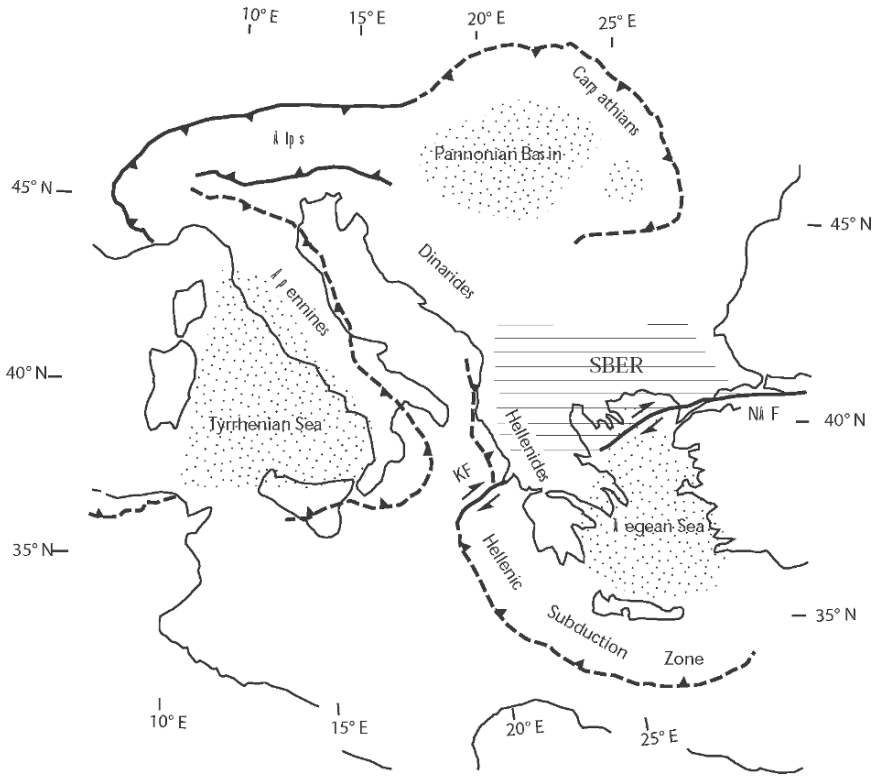

Figure 1 Tectonic map of the Eastern Mediterranean region showing some selected tectonic features. Location of the Southern Balkan Extensional Regime (SBER) is shown by horizontal lines. Dashed lines with barbs are retreating subduction boundary and solid barbed lines are advancing subduction boundaries from late Cenozoic to recent time. Dotted areas are back arc regions of late Cenozoic extension and subsidence. KF = Kefalonia fault zone, NAF = North Anatolian fault, SBER = South Balkan Extensional Regime

Figure 2 Cenozoic sedimentary basins within the South Balkan extensional regime shown with dots and open patterns. These basins contain the record of extensional faulting

In this paper we present only the geometric time space relation of tectonic activity for the Cenozoic without developing the dynamic systems that cause such deformation. The dynamic systems are complex and change spatially and temporally and will be discussed in another publication. Most of the interpretations of the temporal and spatial distribution of deformation presented here are taken from our previous work (Tzankov et al., l996; Burchfiel et al., 2000, 2003, 2006; Nakov et al., 2001a, b; Dumurdzanov et al., 2004, 2005; Kotzev et al., 2001, 2006) plus an extensive literature from this area.

2 Paleogene Time: Closing of the Vardar Ocean and Early Extension

In latest Cretaceous and earliest Cenozoic time the region of the SBES lay on the European plate separated from continental areas to the west and south by the Vardar Ocean (Figure 3; Sengor and Yilmaz, 1981; Brown and Robertson, 2004). The Vardar Ocean closed in early Cenozoic time and its remnants are preserved within central Macedonia, northern Greece and northwestern Turkey, but are largely covered by the northern Aegean Sea (Figure 3). Closure of this ocean by northeastward

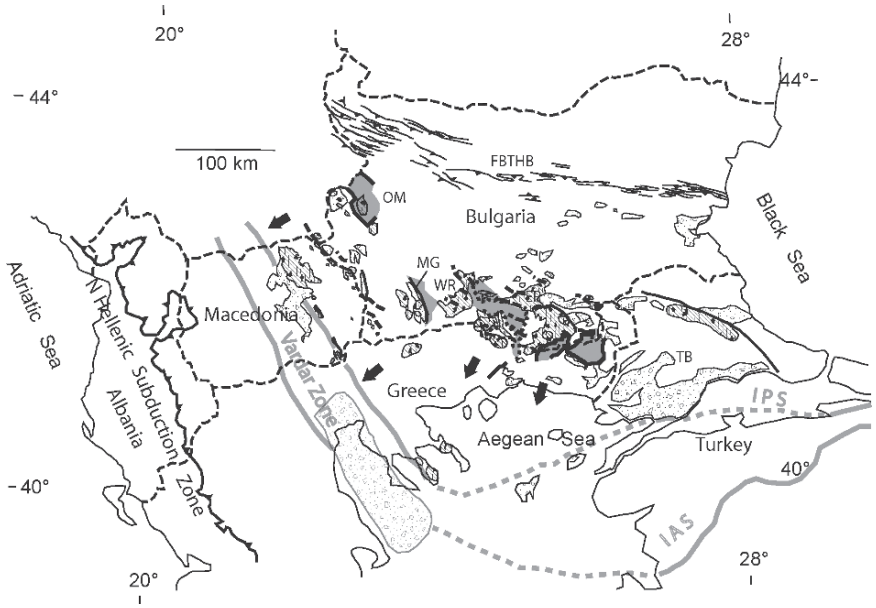

Figure 3 Tectonic elements of Paleogene age within the southern Balkan and northern Aegean region. Dots with open patterned areas are sedimentary basins of Paleogene age (lighter area is the Thermikos basin largely covered by younger sedimentary rocks of water). Lines down to right with black diamonds are areas are dominated by Paleogene volcanic (sometimes dominated by sedimentary rocks) and plutonic rocks. Gray areas are footwalls metamorphic and mylonitic rocks below low-angle detachment faults shown by heavy lines (dotted where inferred). Other heavy solid lines are faults. In northern Bulgaria lines are trends of folds and thrust faults (with tick marks) that form the ForeBalkan fold and thrust belt. Dashed heavy lines are Paleogene dikes. The Vardar zone is bounded shaded broad lines in Macedonia and NW Greece and its eastern branches, the northern Intra-Pontide suture (IPS) and Izmir–Ankara zone (IAS) are shown. Large arrows show general extension directions relative to Europe. The northern Hellenic subduction zone is the location of subduction following closure of the Vardar Ocean. ER = Eastern Rhodope Mountains, FBTHB = ForeBalkan fold and thrust belt, MG = Mesta half-graben, OM = Osogovo Mountains, TB = Thrace Basin, WR = Western Rhodope Mountains

subduction is dated in Macedonia between the latest Cretaceous (possibly Paleocene) and Priabonian time (Dumurdzanov et al., 2005). Recent work by Brown and Robertson (2004) in northern Greece indicate deformation within the Vardar zone was active into the early Tertiary, but overlapping strata are not well enough dated to yield a well-defined date closure. Farther east in western Turkey, geological relations indicate the continuation of the Vardar Ocean consisted of two branches, the Intra-Pontide zone in the north and the Izmir–Ankara zone in the south; the Intra-Pontide Ocean closed by northward subduction between Paleocene and Lutetian time and the Izmir–Ankara zone closed by Oligocene time (Sengor and Yilmaz, l981)

During and after the final stages of closure of the Vardar Ocean extensional tectonism was manifested by deformation of at least two different styles of faulting exposed at the surface. They may however be different expressions of similar processes exposed from different crustal levels. In the eastern Rhodope Mountains of Bulgaria and northern Greece are low-angle faults that expose metamorphic footwalls often associated with mylonitic shear zone overlain by either lower grade or unmetamorphosed rocks and locally synsedimentary rocks in their hanging walls (Figure 3; e.g. Krohe and Mposkos, 2002; Bonev et al., 2006; Ivanov, 1989). Displacements are complex showing relative hanging wall movements to the northeast, southeast and southwest. The extensional areas have geology similar to the well-known and well-described metamorphic core complexes from the western United States and elsewhere (Lister and Davis, l989). Similar core complex-type relations were recently reported by Kounov et al. (2004) in northwest Bulgaria for a southwest-vergent detachment fault of Paleogene (Middle Eocene) age in the Osogovo Mountains (Figure 3). Their data show rapid isothermal decompression during exhumation of high-grade footwall rocks by the detachment faults.

In the western Rhodope Mountains, Burchfiel et al. (2003) presented evidence for a WSW-dipping extensional detachment fault along the eastern side of the Mesta half-graben (Figure 3). East-dipping hanging wall syntectonic sediments derived from plutonic and metamorphic rocks in the footwall are Upper (Middle?) Eocene in age. Magmatic rocks that date between 33 and 28 Ma are syntectonically intruded into the graben sediments and their basement were extruded during sedimentation (Burchfiel et al., 2003). Similar east-dipping sedimentary and volcanic rocks form numerous half-grabens present both in southwestern Bulgaria and eastern Macedonia (see for example Zagorchev l998; Dumurdzanov et al., 2004, 2005). These east-tilted half-grabens have structural and stratigraphic characteristics that indicate they were formed by WSW extension, and may be related to deeper seated west-dipping detachment faults, but such faults have not recognized except in recent a study in northwest Bulgaria (Kounov et al., 2004). The distribution and geometry of these extensional faults is suggestive of a more shallow level of exposure of tectonism than in the core complexes to the east and north, but they may be fundamentally part of the same process.

The Paleogene extension lies within zone of magmatic activity that extends from Serbia in the northwest through the southern Balkan extensional region into and beyond northwestern Turkey to the east (Harkovska, l983, 1984). Such magmatism probably is at least partly responsible for formation of the hot thick crust that facilitated the formation of metamorphic core complex development. Dikes associated with the magmatic belt traverse the crust through the extensional system and have a general E–W to NW trend and Harkovska (l983, 1984) has interpreted them to be a result of N–S to NW/SE extensional tectonism.

During at least the earliest part of this Paleogene extension, the fore Balkan thrust belt was active in northern Bulgaria during Lutetian time. This suggests that at least the earliest part of the Paleogene extension occurred within an overall compressional environment during final closure and post-closure contraction along the Vardar suture zone.

3 Post-Paleogene Shortening

In western Bulgaria and eastern Macedonia there was a short-lived and well-dated period of shortening during latest Oligocene/early Miocene time (Figure 4; Zagorchev, l992, l998; Dumurdzanov et al., 2005). This shortening event we have interpreted to be related to short-lived collision of the Kruja continental fragment at the north Hellenic trench in Albania (Dumurdzanov et al., 2005) causing a temporary change in the stress regime east of the trench before normal subduction roll back was reestablished.

There was also a period of shortening that occurs within the Thrace basin in northwest Turkey, but its age is not well documented (Figure 4). It occurred sometime between deposition of the Danisment Formation of Late Oligocene-early Early Miocene age and the unconformably overlying Ergene Group dated as Late Miocene (?)-Pliocene. Perincek (1991) studied this deformation and considered its three belts of irregular folds to be late Middle Miocene, however there remain and an uncertainty in its age. It appears however, that this deformation while possibly

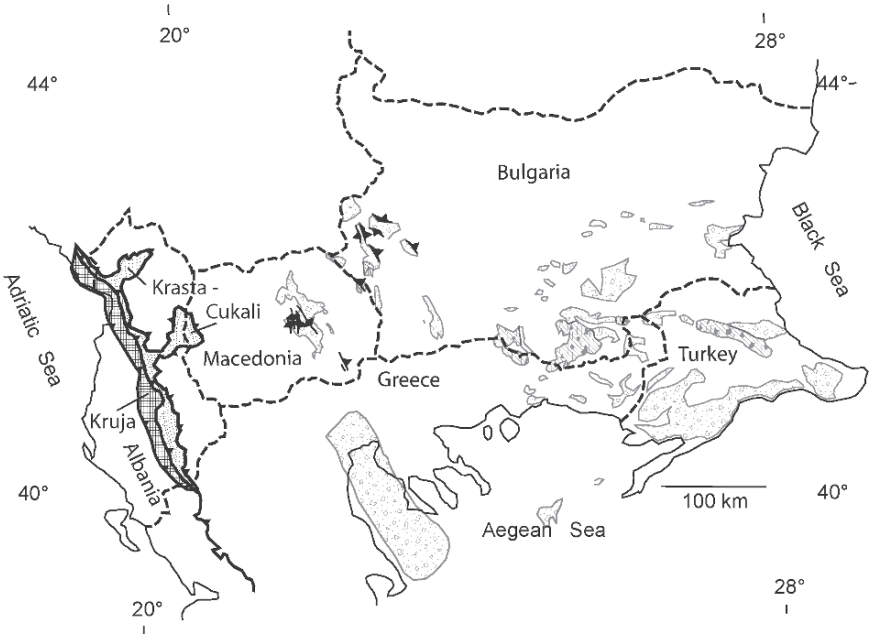

Figure 4 Early Miocene-Latest Oligocene time when a short period of localized compression took place in western Bulgaria and eastern Macedonia. Thrust faults are shown with ticked black lines and folds are shown as black lines with diamonds. The Kruja continental fragment (checked pattern) was accreted into the northern Hellenic subduction zone complex (dotted pattern) at this time. Shaded areas with dotted and open patterns are sedimentary rocks of late Oligocene extending into earliest Miocene time. Shaded areas with lines down to right and solid diamonds are volcanogenic sedimentary and sedimentary rocks

the same age as that in western Bulgaria, it may be younger. Perincek interpreted the folds to be related to step-overs on right-lateral strike-slip faults that strike WNW through the northern part of the Thrace basin. The projection of these faults into Bulgaria would continue them along the Maritza fault zone that flanks the Rhodope Mountains on the north. In the area north of Haskovo, Bulgaria, late Eocene-Oligocene (perhaps as young as earliest Miocene) strata are folded (Nakov et al., 2001b). These folds could be the northern continuation of the folds from the Thrace basin. There is however a broad area between Haskovo and the folded rocks in western Bulgaria where there are no rocks of right age to show if this deformation is present between the two areas. How these two areas might be related both in terms of age and geometry remains unknown. However, if the deformation in western Bulgaria and eastern Macedonia is related to activity at the northern Hellenic trench, it seems unlikely that the deformation in the Thrace basin would be directly related. More likely it is related to strike-slip faulting preceding or in the early part of the evolution of the North Anatolian fault zone.

4 Miocene to Recent Extension

Extension within the southern Balkan region that started the extensional regime of the present-day Aegean realm may be diachronous. In the eastern part of the Balkans this extension may have started in early Late Miocene time whereas in the western part of the Balkans it may have progressed from Paleogene time, but with the short interruption by a brief period of local shortening.

In the western part of the south Balkan region extension of early Middle Miocene time (Badenian) is present with deposition in several extensional basins bounded by NW-striking faults (Figure 5; Dumurdzanov et al., 2004, 2005; Nakov et al., 2001b). Normal faults with this strike migrate westward in time and represent deformation that can be directly related with extension within the larger Aegean realm. The temporal and spatial evolution of extensional faulting and associated basin development shows a progression that can be related to trench roll back at the Hellenic trench that changes in orientation temporally and results in overlapping patterns of faulting (Figures 5–7). The timing of major extension within the Aegean area to the south still remains controversial. The ages interpreted to be related to the beginning of extension in the area of the Aegean Sea ranges from early Tertiary to late Miocene (e.g. see Catlos and Cemen, 2005).

In the western part of the Balkan region the geometry of the extensional faulting suggests the dynamics of extension may have been similar before and after the shortening event. The Paleogene extension occurred above west-dipping detachment faults, however the two main areas where these faults are recognized cannot be obviously directly connected with known faults. The distribution of the small extensional basins in western Bulgaria and eastern Macedonia have the apparent distribution and geometry that suggests they lie above a master west-dipping

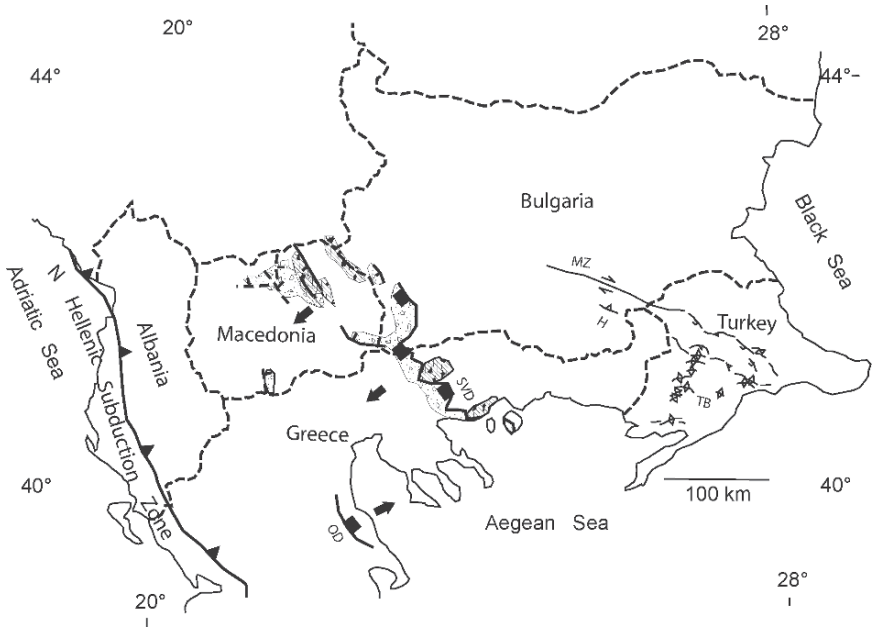

Figure 5 Faults of Middle Miocene time are shown as heavy black lines; with short lines showing direction of dip and squares showing dips of low-angle detachment faults. Thinner black lines in NW Turkey and eastern Bulgaria are faults of probable right-lateral strike-slip with associated folds at constraining bends (black lines with diamonds) and normal faults (small squares) at releasing bends. The age of these structures is poorly constrained and could be early to late Miocene in age. Terrigenous sedimentary rocks in extensional basins are shown in dotted and open patterns and volcanic or plutonic rocks are shown with lines down to right with black diamonds. The position of the north Hellenic subduction zone is shown by black ticked line. H = H = Haskovo, MF= Maritza fault, OD = Olympus detachment, SVD = Strymon Valley detachment, TB = Thrace Basin

detachment fault, but this cannot be proved at present. These basins have sediments that locally were deposited from Paleogene to early Miocene time. By early Middle Miocene time (~15 Ma, Badanian) extension on the west-dipping Strymon Valley detachment fault began in northern Greece and SW Bulgaria (Figure 5; Dinter and Royden, 1993; Zagorchev, 1992). The Strymon Valley detachment parallels the Mesta detachment and has a geometry, kinematics and timing that could be interpreted to be the temporal westward stepping of the Mesta detachment, a pattern of migration of faulting well known in regionally extensional terrains such as the Basin and Range province in the western United States (Lister and Davis, l989). During its evolution the Paleogene Mesta detachment may have begun to be rotated to a more horizontal orientation, similar to detachment faults in the United States, with rotation of the Pirin Mountains in its hanging wall, and younger extension migrated to the west along the western flank of the Pirin Mountains forming the Strymon Valley and Sandanski basins.

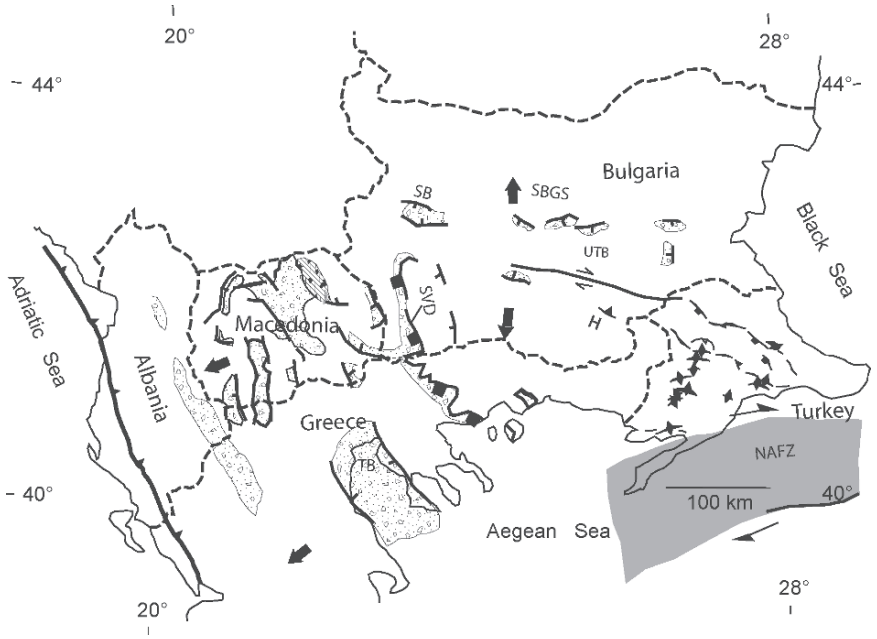

Figure 6 In early Late Miocene time NNW-striking normal faults (thick lines with short perpendicular lines) migrated temporally into western Macedonia and possibly eastern Albania and the major known detachment fault (Styrmon Valley detachment [SVD] – thick line with squares) remained active in SW Bulgaria and northern Greece. E–W striking normal faults were active in central Bulgaria. Sedimentary basins in the hanging walls of these faults are shown by dots and open pattern. Areas of lines down to right and black diamonds are volcanic rocks. Faults (black lines) and folds (black lines with diamonds) shown in NW Turkey and SE Bulgaria are the same as shown for Middle Miocene time in Figure 5 because of uncertainty of their age. North Anatolian fault zone is shown as broad zone of distributed shear which may have begun to form at this time (see Sengor et al., 2004) and southern branch of the fault zone may have been marked by a fault (black line). Black arrows indicate direction of relative extension. H = Haskovo, SB = Sofia basin, SBGS = Sub-Balkan graben system, TB = Thermikos basin. UTB = Upper Thrace basin

The Strymon Valley detachment continued activity into until perhaps Pliocene time (Figure 5; ~3.5 Ma) and new north- trending extensional basins became active progressively farther west reaching western Macedonia and eastern Albania by latest Miocene/early Pliocene time (Figure 6). This progressive formation of more westerly north-trending basins could have occurred in the hanging wall of a master west-dipping detachment (Strymon Valley detachment), but such a geometry cannot be presently demonstrated.

Major east-dipping normal faults are also well known. The oldest, Middle Miocene, is at Mount Olympus in Greece, and east-dipping faults occur also along the west side of the Thermikos basin some of which are presently active (Schermer et al., 1990, 1993). How these east-dipping faults would interact with a master west-dipping detachment fault has not been investigated and is presently unknown.

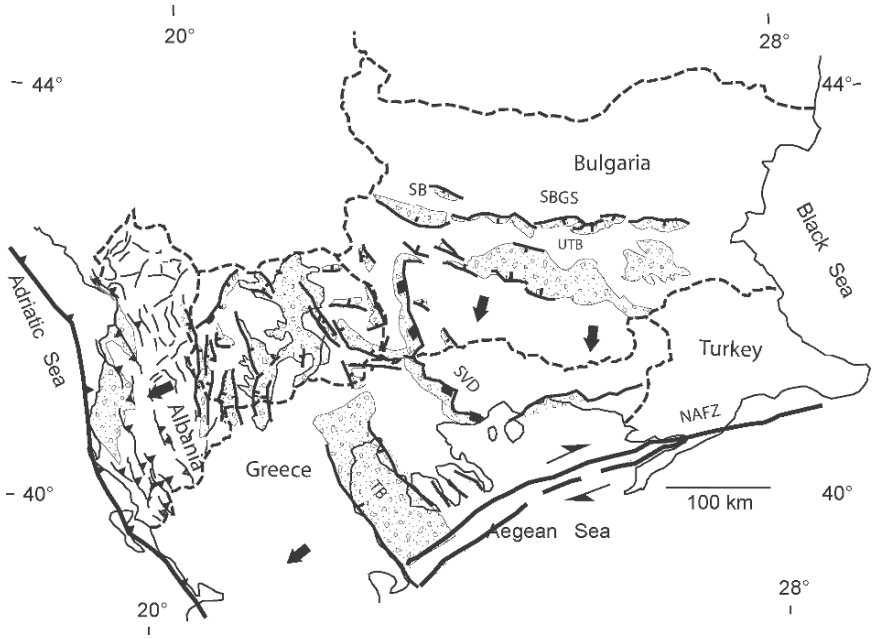

Figure 7 In Latest Miocene to early Pliocene time the North Anatolian fault zone became well developed in the northern Aegean Sea (broad black lines) and N–S extension was active in the Upper Thrace basin (UTB) central and southern B- striking normal faults became less prominent (Strymon Valley detachment – red line with squares) in SW Bulgaria. NNW-striking faults (black lines) became more prominent and into migrated western Macedonia and into eastern Albania. Sedimentary deposits associated with normal faults are shown with dots and open pattern. Shortening occurs in western Albania (black ticked lines) associated with the northern Hellenic Subduction zone (broad black ticked line). SB = Sophia basin, SBGS = sub Balkan graben system

The westward progression of N-trending extensional basins continued into Albania where these basins are presently active in western Macedonia and eastern Albania.

By early Pliocene time the N-trending basins in eastern Macedonia began to be disrupted by E–W-trending basins (Figure 7). These younger basins appear be the result of N–S extension and westward migration of the E–W-trending basins developed first in the eastern part of the Southern Balkan extensional region (Figures 6 and 7; see below). It would suggest that even though movement on the Strymon Valley detachment continued into the middle Pliocene, its activity as a master detachment may have ceased and the eastern limit of N-trending normal faults had migrated first into central Macedonia and then to its present position in western Macedonia. The temporal and spatial pattern of extensional faulting is becoming well established, however the existence of contemporaneous crustal detachments are presently mostly speculation. The westward migration of both the E–W extension and the N–S extension in tandem appears to be real, but the two systems of faults are related to two different dynamic regions; the north and south Hellenic trenches respectively.

The eastern part of the South Balkan extensional region in Bulgaria is characterized by N–S extension that began by Late Miocene time (Figure 6). Middle Miocene strata that could be related to extensional faulting are rare in this region (Nakov et al., 2001), but by Late Miocene time (Late Sarmatian-Early Meotian; 11–8 Ma) strata related to E–W-trending normal faults are present along the north and south sides of the Upper Thracian basin and along the Sofia basin to the west (Figure 5; Tzankov et al., l996; Burchfiel et al., 2000; Nakov et al., 2001b). N–S extensional faults and related strata become more abundant in latest Miocene to early Pliocene time (Figures 6 and 7 to 3.5 Ma) and E–W trending faults and related sediments began to extend westward into eastern Macedonia, at the same time that the N–S striking normal faults migrated westward in western Macedonia and eastern Albania. This pattern of faulting and fault migration continued into the Pleistocene when all of central and southern Bulgaria and eastern t Macedonia was characterized by N–S extension (Figures 6–8). In northern and parts of SE Macedonia and

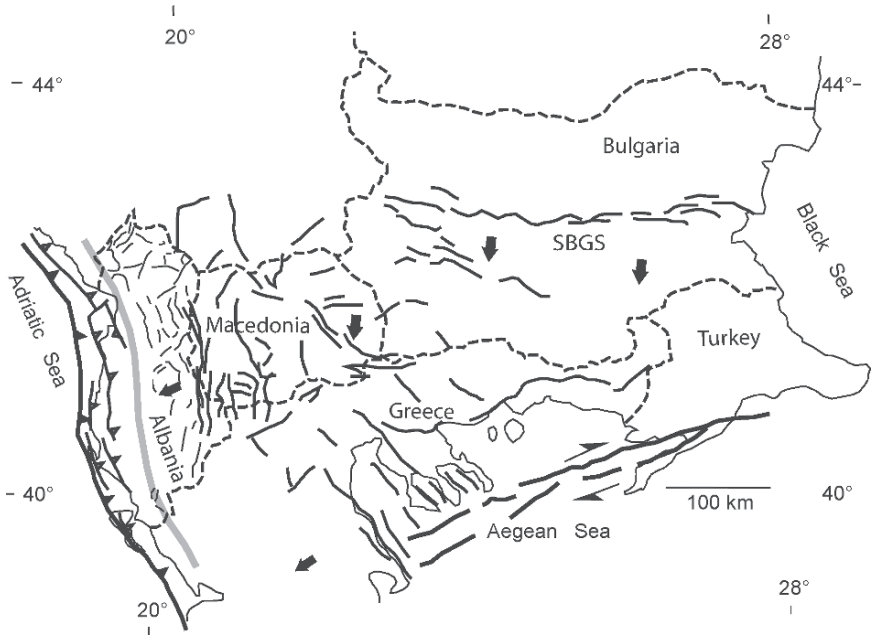

Figure 8 In Pleistocene time N–S extension along E–W striking faults (thick black lines) dominates central Bulgaria and eastern Macedonia and NNW- to N–S- striking normal faults dominates western Macedonia (black lines) and central and eastern Albania (thin black lines). A narrow belt of shortening lies along coastal Albania (black ticked lines) associated with the North Hellenic subduction zone (black ticked line). Shaded line in central Albania separates area of E–W extension from E–W shortening. Some right-lateral strike slip map be present in central Albania but cannot be documented at this time. The North Anatolian fault zone is well developed across the northern Aegean Sea. Black arrows show direction of relative extension. SBGS = Sub Balkan graben system

in NW Greece the two fault provinces overlap. The migration of normal N–S set of faults to the west is temporally related to the propagation of the North Anatolian fault system into the northern Aegean Sea with the southern branch of the fault system forming in late Miocene time and the northern branch being latest forming in Miocene/Pliocene time. When the fault system extended into the northern Aegean it appears to have decoupled the SSW movement of the Aegean region from N–S extension in the eastern part of the Southern Balkan extensional regime.

By late Pleistocene time the present distribution of normal faults had developed and expressed by the distribution of active faults: N–S extension across central and southern Bulgaria, eastern Macedonia and northern Greece, E–W extension in western Macedonia and central and eastern Albania, and shortening in western Albania related to convergence at the northern Hellenic Trench along the Albanian coast (Figures 7 and 8). The two extensional regions are nearly at right angles to each other. This may be because the two dynamic systems causing the extension are somewhat independent.

The distribution of active faulting in the South Balkan extensional region shown in Figure 9 is based on our field observation in Bulgaria and Macedonia (Nakov et al., 2001a, b, Burchfiel et al., 2000; Dumurdzanov et al., 2002, 2005) and from maps of active faults provided by Albanian geologists. Short-term data sets from seismicity and GPS studies support the interpretation presented in Figure 9 (Burchfiel et al., 2006; Kotzev et al., 2006). In particular, GPS data shows an increase in velocities relative to Eurasia southward that indicates that slip-rates on active faults probably increases southward into northern Greece, a testable hypothesis. GPS data shows an abrupt change to rapid right lateral strike-slip movement along the North Anatolian fault. The slow N–S extension in the southern Balkan Peninsula may be related to the southward pull of the Aegean plate, with possible slow counterclockwise rotation of the western part of the North Anatolian fault zone (see Burchfiel et al., 2006; Kotzev et al., 2006).

5 Conclusions

Cenozoic extension within the south Balkan extensional region began in Paleogene time and may have been partly contemporaneous with the final closure and post-closure convergence along the Vardar suture zone and its continuation along two suture zones in northwest Turkey. This early extension was expressed by low-angle detachment faults in the eastern Rhodopian Mountains and in NW Bulgaria and NW-trending half-grabens in western Bulgaria and eastern Macedonia. These two structural types may be the deep and shallow expression of the same extensional processes. Two areas contain minor compressional structures; one in western Bulgaria and eastern Macedonia and a second in the Thrace basin in NW Turkey that may extend into central Bulgaria. Structures in the first area are early Miocene in age and may be related to a short-lived accretion of a crustal fragment into the North

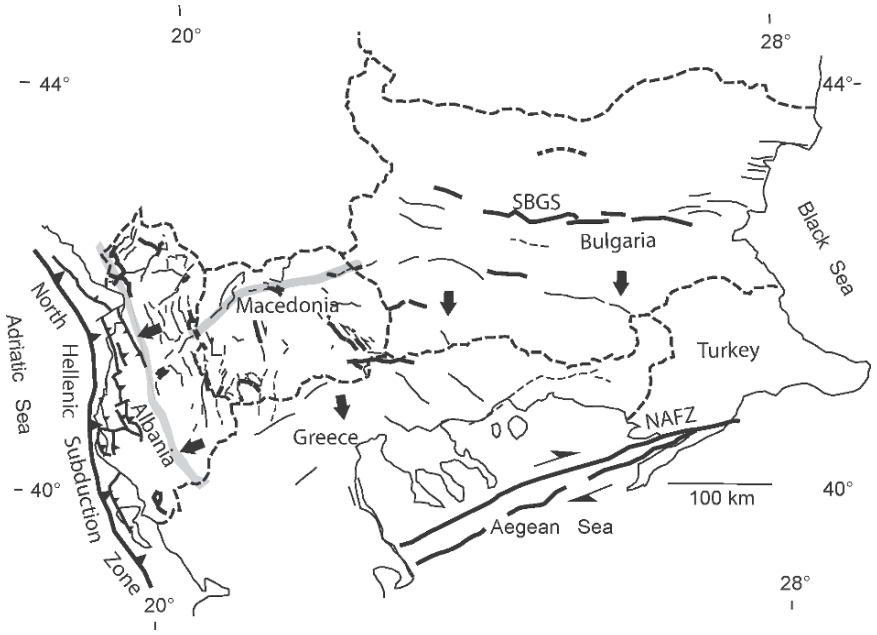

Figure 9 Active faults in the southern Balkan extensional regime. Thick black lines are faults with well-developed features of active faults. Faults with mainly morphological evidence for active faulting shown with thin lines. Small arrows show sense of strike-slip on active faults. Narrow zone of shortening (thrust faults with ticked lines) is present along the Albanian coast associated with the North Hellenic subduction zone (broad black ticked line). Boundary between extension and shortening in Albania is shown by shaded gray line and the northern boundary of southward movement of central and southern Macedonia is marked by an E–W trending gray line. Arrows show the directions of relative extension and shows farther westward migration of N–S extension into to central Bulgaria. NAFZ = North Anatolian fault zone, SBGS = Sub Balkan graben system

Hellenic trench, whereas in the second area the structures were related to oblique transpression and are poorly dated, but are probably younger. By late Early or Middle Miocene extension in the western part of the south Balkan region was characterized by N–S or NNW-SSE normal faults and associated sedimentary basins. Faults of this orientation migrated temporally westward across the region into the active normal faults of western Macedonia and eastern Albania. In the eastern part of the south Balkan region, E–W to WNW-ESE-trending fault became active during Late Miocene time and they migrated temporally westward into western Bulgaria and eastern Macedonia where they were superposed on the older N–S faults. The westward migration of the fault systems were temporally and dynamically related to the propagation of the North Anatolian fault system into the region of the Aegean Sea. In eastern Macedonia and NW Greece the two fault systems overlap and both appear to be presently active. The pattern of active faulting determined by field observations is supported by short-term data from seismicity and GPS studies.

Acknowledgements This study is part of an international cooperative project to understand the Cenozoic and active tectonics of the Southern Balkan Peninsula. It includes the Department of Geodesy, Construct Engineering Faculty, Tirana, Albania, the Central Laboratory of Geodesy, Bulgarian Academy of Sciences, Bulgaria, State Department for Geodetic Survey, Macedonia; Faculty of Mining and Geology, Stip, Macedonia; and the Department of Earth and Planetary Sciences, M.I.T., USA. This study was supported by NSF Grants EAR-9903021 and EAR-9628225.

References

Bonev, N., Burg, J.-P., Ivanov, Z., 2006, Structural evolution of an extensional gneiss dome – the Kesibir-Kardomos dome, East Rhodope, Bulgaria: *International Journal of Earth Sciences* 95*,* 318–340.

Brown, S. A. M., Robertson, A. H. F., 2004, Evidence for Neotethys rooted within the Vardar suture zone from the Voras massif, northernmost Greece: *Tectonophysics* 381, 143–173.

Burchfiel, B. C., Nakov, R., Tzankov, T., Royden, L. H., 2000, Cenozoic extension in Bulgaria and northern Greece: The northern part of the Aegean extensional regime, *in* Bozkurt, E., Winchester, J. A., and Piper, J. D. A. (eds.), Tectonics and magmatism in Turkey and surrounding area: *Geological Society [London] Special Publication* 173, 325–352.

Burchfiel, B. C., Nakov, R., Tzankov, T., 2003, Evidence from the Mesta half graben, SW Bulgaria, for the late Eocene beginning of Aegean extension in the Central Balkan Peninsula: *Tectonophysics* 375,61–76, doi: 10.1016/j.tecto.2003.09.001.

Burchfiel, B. C., Todosov, A., King, R. .W., Kotzev, V., Dumurdanov, N., Sereafimovski, T., Nurce, B., 2006, GPS results for Macedonia and its importance for the tectonics of the southern Balkan Extensional regime: *Tectonophysics* 413, 239–248.

Catlos, E. J., Cemen, I., 2005, Monazite ages and the evolution of the Menderes Massif, western Turkey: *International Journal of Earth Sciences* 94, 204–217.

Dinter, D. A., Royden, L. H., 1993, Late Cenozoic extension in northeastern Greece: Strymon Valley detachment system and Rhodope metamorphic core complex: *Geology* 21, 45–48, doi: 10.1130/0091.

Dumurdzanov, N., Serafimovski, T., Burchfiel, B. C., 2004, Evolution of the Neogene-Pleistocene basins of Macedonia: Geological Society of America Digital Map and Chart Series 1 (accompanying notes), 20 pp.

Dumurdzanov, N., Serafimovski, T., Burchfiel, B. C., 2005, Cenozoic tectonics of Macedonia and its relation to the South Balkan extensional regime: *Geosphere* 1, 1, 1–22.

Harkovska, A., 1983, Spatial and temporal elations between volcanic activity and sedimentation in the stratified Paleogene from the central parts of the Mesta Graben southwest Bulgaria: *Geologica Balcanica* 13, 2, 3–30.

Harkovska, A., 1984, Tertiary magmotectonic zones in southwest Bulgaria, *in* Vozar, J. (ed.), Magmatism of the molasse-forming epoch and its relation to endogenous mineralizaton: Bratislava, *Geologicky ustav Dioyza Stura* 9–34.

Ivanov, Z., l988, Apercu general sur l'evolution geologique et structurale du massif des Rhodopes dans la cadre des Balkindes: *Bulletin De la Société Géologique De France*, 8, IV, 2, 227–240.

Kotzev, V., Nakov, R., Burchfiel, B. C., King. R., Reilinger, R., 2001, GPS study of active tectonics in Bulgaria: results from l996 to l998: *Journal Geodynamics* 31, 2, 189–200.

Kotzev, V., Nakov., R., Georgiev, Tz., Burchfiel B. C., King, R. W., 2006, Crustal motion and strain accumulation in western Bulgaria, *Tectonophysics* 413, 127–145.

Kounov, A., Seward. D., Bernouli, D., Burg, J.-P., Ivanov, Z., 2004 Thermotectonic evolution of an extensional dome: the Cenozoic Osogovo-Lisets core complex (Kriashte zone, western Bulgaria): *International Journal of Earth Science*, 93, 1008–1024.

Krohe, A., Mposkos, E., 2002, Multiple generations of extensional detachments in the Rhodope Mountains (northern Greece): Evidence of episodic exhumation of high-pressure rocks: in Blondell, D. J., Neubauer, F., von Quadt, A. (eds.), The timing and location of major ore deposits in and evolving orogen: *Geological Society London Special Publication* 204, 151–178.

Lister, G., Davis, G. A., l989, The origin of metamorphic core complexes and detachment faults formed during Tertiary continental extension in the northern Colorado River region, USA: *Journal of Structural Geology*, 11, 1/2, 65–94.

Nakov, R. Kotzev, V., Burchfiel. B. C., King, R. W., 2001a, GPS data on the active tectonics of the Bulgarian Rhodopes: *Geologica Balkanica*, 31, 1–2, 123–125.

Nakov, R., Burchfiel, B. C., Tzankov, T., Royden, L. H., 2001b, Late Miocene to recent sedimentary basins of Bulgaria: Geological Society of America Map Chart Series MCH 088, scale 1/200.000, 28 pp.

Perincek, D., l991, Possible strand of the North Anatolian Fault in the Thrace Basin, Turkey – an interpretation: *Bulletin, American Association of Petroleum Geologists*, 75, 241–257.

Schermer, E. R., 1990, Mechanisms of blueschist creation and preservation in an A-type subduction zone, Mount Olympus region, Greece: *Geology* 18, 1130–1133.

Schermer, E. R., l993, Geometry and kinematics of continental basement deformation during the Alpine orogeny, Mount Olympus region, Greece: *Journal of Structural Geology*, 15, 571–591.

Sengor, A. M. C., Yilmaz, Y., 1981, Tethyan evolution of Turkey: A plate tectonic approach: *Tectonophysics*, 75, 181–241.

Sengor , A. M. C., Tuysuz, O., Imren, C., Sakinc, M., Ekyidogan, H., Gorur, N., Le Pichon, X., Rangin, C., 2004, The North Anatolian Fault: A New Look: *Annual Reviews of Earth and Planetary Sciences*: 32, 1–75. C

Tzankov, T., Angelova, D., Nakov., R., Burchfiel, B. C., Royden, L. H., l996, The Sub-Balkan graben system of central Bulgaria: *Basin Research*, 8, 125–142.

Zagorchev, I., 1992, Neotectonic development of the Struma (Kraistid) lineament, southwest Bulgaria and northern Greece: *Geological Magazine*, 129, 197–222.

Zagorchev, I., 1998, Pre-Priabonian Paleogene formations in southwestern Bulgaria and northern Greece: Stratigraphy and tectonic implications: *Geological Magazine*, 135, 101–119, doi: 10.1017/S0016756897008285.

Crustal Motion and Strain Accumulation in the South Balkan Region Inferred from GPS Measurements

Valentin Kotzev*[1], Robert W. King, B. Clark Burchfiel[2], Angel Todosov[3], Bilbil Nurce[4], and Radoslav Nakov[5]

Abstract We present results from GPS observations in Bulgaria, Macedonia, and Albania, which describe a crustal velocity field for the south Balkan region with an accuracy of better than 1 mm/year. Our results show an overall southward motion of the region with respect to Eurasia at a rate of 3–4 mm/year. Much of the area behaves as a single tectonic unit with local zones of slow internal deformation corresponding to the major active tectonic structures. Combined with GPS data for northern Greece, south Balkan data show gradual increase in velocity from north to south to 25 mm/year before reaching the North Anatolian fault. The N–S extension interpreted from the velocity field is consistent with the E–W trend of active faults in southwestern Bulgaria, adjacent southern and eastern Macedonia, and northern Greece. However, some active faults can not be determined from the GPS velocity field because their slip-rates are slower than the uncertainty in the GPS data.

Our GPS data delineate an approximately SE trending extensional boundary at a rate ~1 mm/year that probably marks the northernmost extent of the Aegean extensional region. The boundary encompasses the E–W trending Sub-Balkan graben system of central Bulgaria and its westward continuation into the Sofia graben. At the western portion of the boundary extension at a rate 0.7 mm/year is transferred to the north of the Sofia graben across the westernmost part of the Stara Planina Mountains. Our data show ~1.5 mm/year extension across the central part of the Sub-Balkan graben system which is in a good agreement with the lower bound on the N–S extension rate of 1–2 mm/year, estimated from geological data. There is no consistent velocity pattern that would justify extending the strain belt to the Black Sea coast.

[1] Central Laboratory of Geodesy, Bulgarian Academy of Sciences

[2] Massachusetts Institute of Technology, MA, USA

[3] State Authority for Geodetic Works, Republic of Macedonia

[4] Polytechnic University of Tirana, Albania

[5] Geological Institute, Bulgarian Academy of Sciences

* To whom correspondence should be addressed. e-mail: kotzev@bas.bg

E.S. Husebye (ed.), *Earthquake Monitoring and Seismic Hazard Mitigation in Balkan Countries.*

There are not enough GPS data to map the kinematics in the western part of the south Balkan region. Geological data and focal mechanisms, however, indicate a transitional boundary within southwestern Serbia, eastern Montenegro and western Macedonia, which separates the region of N–S extension to the east from a region of E–W extension in central and eastern Albania, central Montenegro and western Macedonia. That boundary probably marks the western limit of the Aegean extensional domain.

Coupled with GPS data from southeastern Italy, our data indicate that coeval subduction and convergence with a right-lateral strike-slip component along the northern part of the Hellenic trench has not ceased but still proceed at a rate of ~5–10 mm/year.

Keywords crustal strain, GPS, seismicity, eastern Mediterranean, south Balkan region

1 Introduction

The south Balkan region contains a portion of the most active deformational system in the Mediterranean region. This regional system termed Eastern Mediterranean extends westward from the zone of collision between Arabia and Eurasia in northern Turkey and the Caucausus Mountains to the Hellenic subduction zone along which the lithosphere of the Adriatic and Ionian zones is subducting toward the northeast beneath Albania, western Greece, Crete and southern Turkey. The south Balkan region is located in the northwesternmost part of that system where deformation is complex, related to the Hellenic subduction boundary, to the westward motion of Anatolia and to the large-scale topography gradients throughout the region.

The kinematics of the southern part of the south Balkan region and the Aegean have become better known in recent years due to the availability of geodetic measurements with the Global Positioning System (GPS) (Le Pichon et al., 1995; Straub et al., 1997; Clarke et al., 1998; Cocard et al., 1999; McClusky et al., 2000; Kahle et al., 2000; Ayhan et al., 2002; Meade et al., 2002; Flerit et al., 2003; Le Pichon et al., 2003; Nyst and Thatcher, 2004). The overall kinematic pattern provided by GPS generally confirmed the regional tectonic framework developed by McKenzie (1970); Jackson and McKenzie (1988) and Jackson (1992). The GPS results of McClusky et al. (2000) (Figure 1) provided evidence for the existence of an Anatolian plate that moves away from the zone of convergence in eastern Turkey, and an Aegean plate that moves at a different velocity producing extension in the Aegean domain. It was shown that the majority of motion between the Anatolian and Eurasian plates is confined to the relatively narrow zone along the North Anatolian fault. The upper bound of the slip-rate for this fault was estimated at 24 mm/year. The GPS data confirmed that the central and southern Aegean move as a rigid plate toward the southwest at a rate of 30 mm/year and that the northern boundary of the Aegean plate is formed by the North

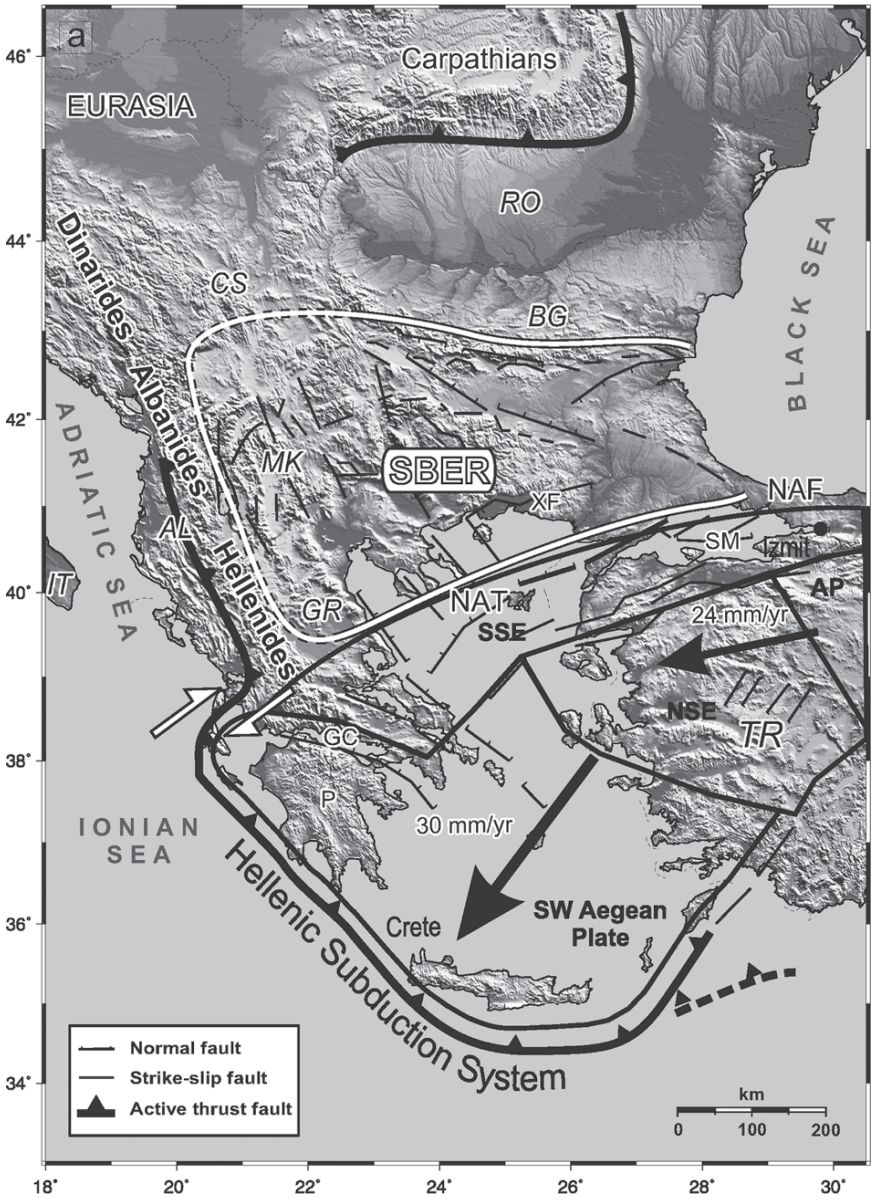

Figure 1 (a) Simplified tectonic map of the eastern Mediterranean and zones of coherent motion adapted from McClusky et al. (2000). Arrows show observed direction of motion relative to Eurasia. Zones of coherent motion: SSE, Strike-slip and extensional zone; NSE, N–S extensional zone. The South Balkan extensional region is shown by thick white line. Abbreviations: AP, Anatolian plate; GC, Gulf of Corinth; NAF, North Anatolian fault; P, Peloponnesus; SM, Sea of Marmara; XF, Xanti fault. Countries: AL, Albania; BG, Bulgaria; CS, Serbia and Montenegro; GR, Greece; IT, Italy; MK, Republic of Macedonia; RO, Romania; TR, Turkey

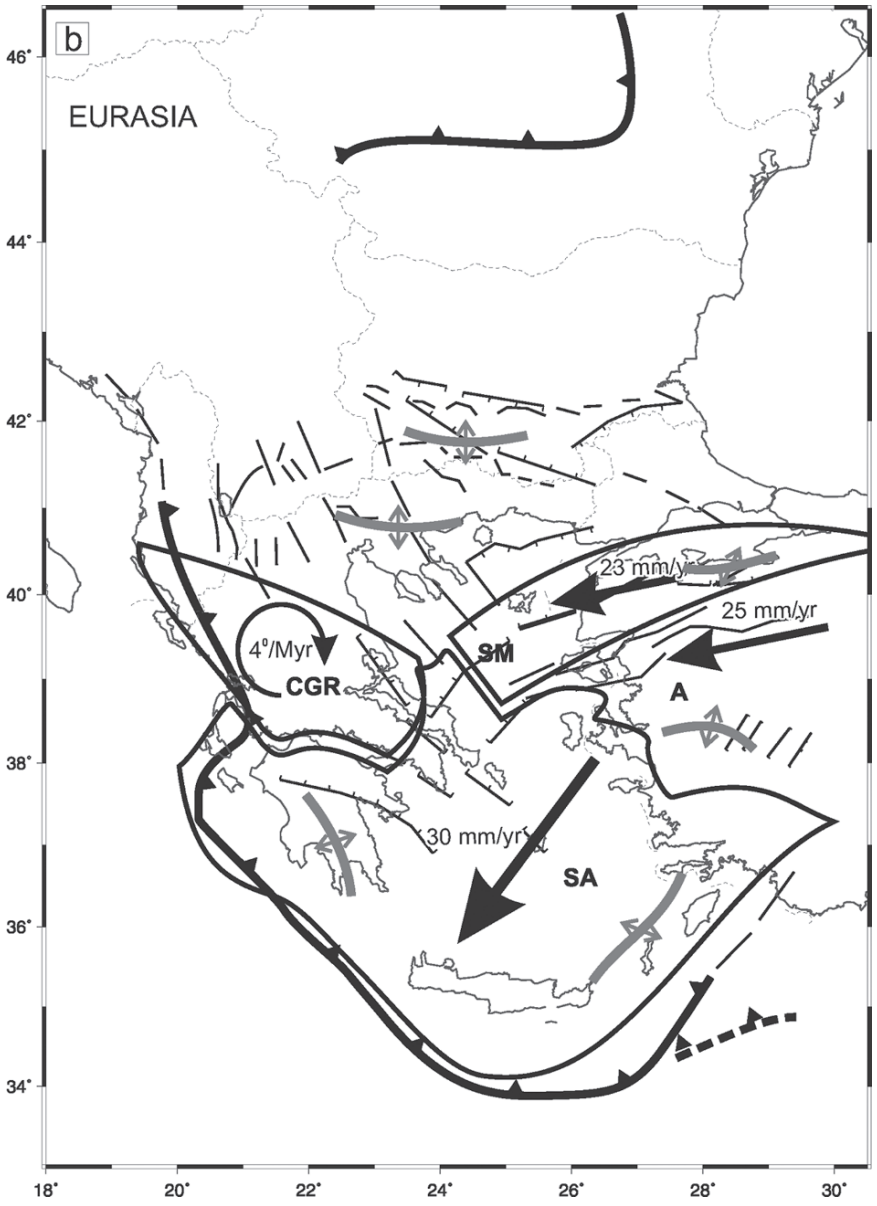

Figure 1 (continued) (b) Kinematic model of the Aegean deformation by Nyst and Thatcher (2004). Microplates: A, Anatolia; CGR, Central Greece; SA, South Aegean; SM, South Marmara. The local zones of extension internal to microplates are shown in grey

Aegean Trough and the Gulf of Corinth and the eastern boundary by a NNW-trending broad zone of left shear and extension.

Besides McClusky et al. (2000), many others developed kinematic descriptions of the Aegean deformation. The pioneering work of McKenzie (1972, 1978) was followed by McKenzie and Jackson (1984), Taymaz et al. (1991), Le Pichon (1995), Armijo et al. (1996), and more recently by Goldsworthy et al. (2002) and Nyst and Thatcher (2004). Using GPS data from six GPS networks in the Eastern Mediterranean, Nyst and Thatcher (2004) found that present-day Aegean deformation is due to the relative motion of 4 microplates: Anatolian moving WSW at 15–25 mm/year relative to Eurasia, South Aegean moving SSW at ~30 mm/year, Central Greece rotating clockwise at ~4˚/Myr around pole in southernmost Albania, and South Marmara moving WSW at 23 mm/year relative to Eurasia. To remove the discrepancies between their model and the observed velocity field Nyst and Thatcher (2004) introduced several isolated deforming zones internal to the microplates: western Peloponnesus (46 nstrain/year E–W extension), SE Aegean (47 nstrain/year E–W extension), SW Anatolia (47 nstrain/year N–S extension), SE of the Sea of Marmara (50 nstrain/year NNE extension). On the basis of very little data, the model gives for northern Greece and southwestern Bulgaria 26 nstrain/year N–S oriented extension.

The south Balkan region is bounded to the west by the northern segment of the Hellenic subduction boundary. Based on tomographic studies, Wortel and Spakman (2000) suggested that subduction has ceased in this area and the trench is no longer active. Seismic data, however, show E–W convergence along the coastal areas from northern Greece and Albania into southwestern Serbia, Montenegro and Croatia, supporting an inference of ongoing subduction. Burchfiel et al. (2004, 2006) suggested that trench roll-back is still occurring along the North Hellenic Trench and induces E–W extension with a component of right lateral-slip in eastern Albania and western Macedonia. The present-day kinematics of the entire Adriatic region is not well constrained, leading to different, often controversial kinematic descriptions. Some authors consider Adria as continuous with Africa or Eurasia (Jimenez-Mundt et al., 2003; Nocquet and Calais, 2003), others as a zone of distributed deformation (Nocquet et al., 2001) or fragmented into 1–2 microplates (Calais et al., 2002; Oldow et al., 2002). Anderson and Jackson (1987) proposed that the region forms a discrete microplate rotating counterclockwise about a pole in northwestern Italy. Using GPS data from southern Italy, Corsica and Sardinia and reinterpreting the velocity results of Altiner et al. (2001), Oldow et al. (2002) suggested that Adria is actively fragmenting into two major subblocks: northeastern and southwestern. Most recently on the basis of GPS data from the Istria peninsula of Slovenia and Croatia and the Po Plain in Italy, Weber et al. (2004) confirmed the microplate model of Anderson and Jackson (1987) and determined a pole of rotation that matches their pole very well. Using data from 30 permanent GPS stations in the region Battaglia et al. (2004) showed that independent microplate models fit better to the GPS velocities than models considering Adria continuous with Africa or Eurasia.

2 South Balkan Extensional Region

Most studies in the Eastern Mediterranean focus on the region south of the North Anatolian fault and its westward continuation. Thus, little is known about the active deformation in the regions to the north. Geological data on young and active faulting indicate that much of the area located to the north of the North Anatoian fault and to the east of the zone of E–W extension adjacent to the North Hellenic Trench has been characterized by extensional tectonism referred to as the South Balkan extensional region (Burchfiel et al., 2000, 2006) (Figure 1). The deformation in this region is not as great as in the Aegean but reconstruction of its extensional regime will provide important constraints on dynamics of the Hellenic system.

The South Balkan extensional region has been separated from the main Aegean regime since ~6–10 Ma by the propagation of the North Anatolian fault zone into the northern Aegean Sea (Armijo et al., 1996; Sengor et al., 2004). After that deformational event, the Aegean region to the south of the North Anatolian fault began to move SSW as a single plate and the extension within the south Balkan region became more N–S oriented and with a lower rate than southward movement of the Aegean plate.

3 GPS Data

The tectonic hypothesis that the Aegean extensional province extends northward into the south Balkan region is critical for understanding the geodynamic processes to the north of the North Anatolian fault zone. The best way to test this hypothesis is by combining GPS geodetic measurements with geologic studies aimed at defining the active structures that accommodate modern deformation field. We began such a study with geological work and GPS surveys in Bulgaria and Macedonia (Burchfiel et al., 2006; Kotzev et al., 2006) where we made the first GPS observations with regional coverage in the south Balkan region that were designed to be integrated with geological studies of active tectonism. In 1996, a Bulgaria-wide network containing 18 stations was established and fully measured during 3 surveys between 1996 and 2001. In 1997, these stations were augmented with a 22 station network for monitoring the strain accumulation in western Bulgaria. That denser network was measured in 1997, 2000, and partly in 2002, 2003 and 2004. The 25 station network in Macedonia was established in 1996 and surveyed twice, in 1996 and in 2000. To obtain evidence for the western boundary of the South Balkan extensional region, in 2002, Bulgarian, Macedonian and Albanian teams surveyed 4 stations in Albania which were measured before in 1996 and 1998.

4 Methods of Analysis

The GPS measurements acquired in the south Balkan region were analyzed using the GAMIT/GLOBK software (King et al., 2003; Herring, 2003) and the approach described in Kotzev et al. (2006). In the first step our GPS data for each day were

merged with observations from 4–10 continuously tracking stations in Europe to obtain loosely constrained estimates for station coordinates and atmospheric, orbital, and Earth-orientation parameters. Those estimates and their covariance matrices were then combined with a similar analysis of the global data performed at the Scripps Orbit and Permanent Array Center (SOPAC) (Bock et al., 1997). The data from all the days of each survey were then combined into a single solution. The parameters estimated in the first step were used as quasi-observations for the second step where all of the GPS surveys were combined to estimate a consistent set of coordinates and velocities allowing stochastic variation of the Earth's rotation.

The dominant errors in GPS measurements are temporally correlated (e.g., Williams et al., 2004), so that any estimation procedure that weights the daily estimates of position equally will generate overly optimistic uncertainties in position and velocity for stations observed for a large number of days (in particular, continuous stations). To compensate for oversampling and to approximate errors with long correlation times we imposed minimum uncertainties of 1 mm on the horizontal position estimates from each survey and added a random walk component of 0.5 mm/√ year.

GPS stations in SE Bulgaria surveyed since August 1999 were significantly affected by the M = 7.4 earthquake on the North Anatolian fault near Izmit, Turkey. To improve the velocity estimates for these stations the offsets were corrected using the predictions computed by R. Burgmann (personal communication, 2003) from the co-seismic model of Reilinger et al. (2000).

The reference frame for the velocity solution was defined at the third step by applying generalized constraints (Dong et al., 1998). To do that, we first estimate a six-parameter transformation (six components of the rate of change of translation and rotation) and then estimate the rotation vectors for one or more groups of stations with respect to the International Terrestrial Reference Frame (ITRF-2000) (Altamimi et al., 2002).

5 Velocity Field for the South Balkan Region

The GPS measurements in Bulgaria, Macedonia and Albania allowed us to determine the velocity field of much of the south Balkan region to an accuracy better than 1 mm/year (Burchfiel et al., 2006; Kotzev et al., 2006). To show the contrast between the rapid motion of Anatolia and southern Aegean toward the Hellenic Trench reaching 30 mm/year and the slow southward oriented motion in the South Balkan extensional region our results were combined with the results of McClusky et al. (2000) into a Eurasian reference frame defined by 16 permanent stations in Europe and western Asia (Burchfiel et al., 2005) (Figure 2).

5.1 Bulgaria

The Eurasian velocities for the Bulgarian stations (Kotzev et al., 2006) are less than 4 mm/year and differences within Bulgaria are only marginally significant (Figure 2). Their coherence within some parts of the network, however, provides a basis for

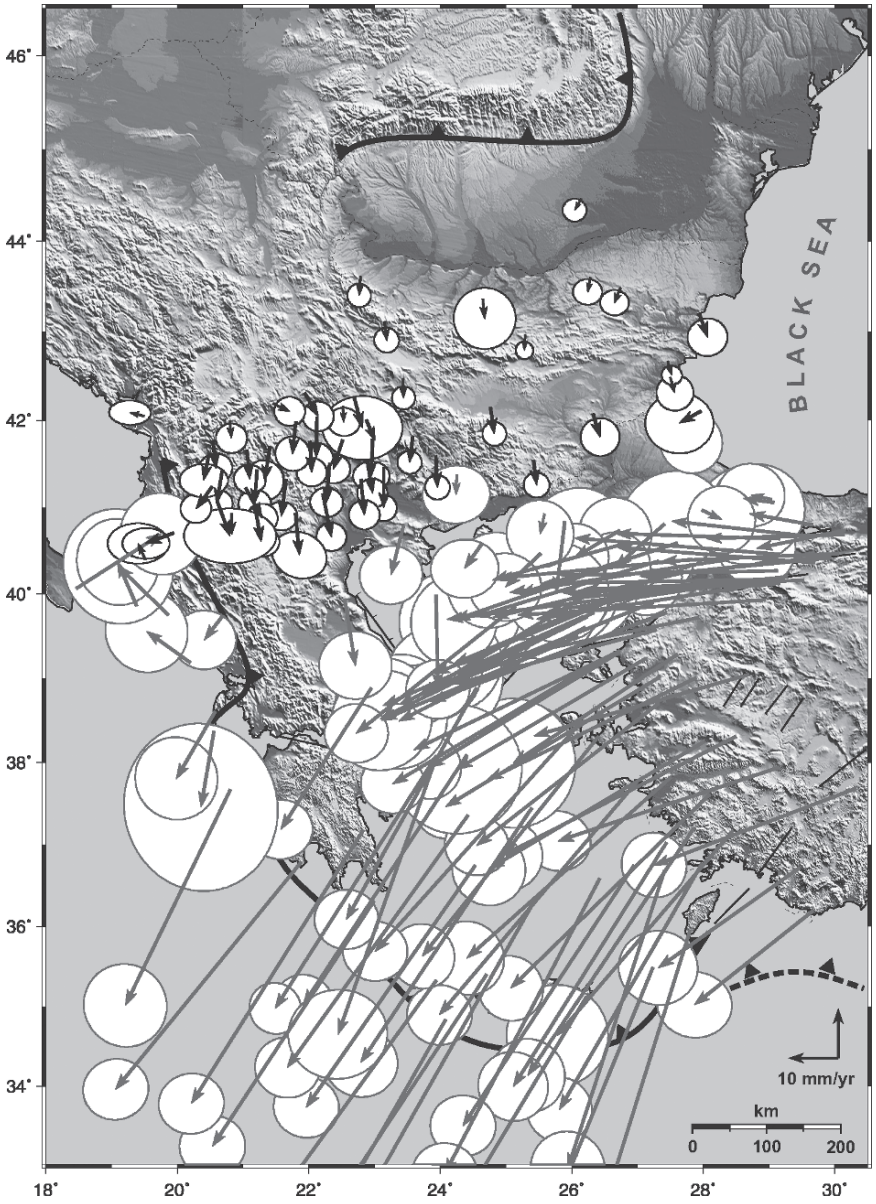

Figure 2 GPS velocities with respect to Eurasia from Kotzev et al. (2006) and Burchfiel et al. (2006). Uncertainties shown at 95% confidence.[1] Velocities in grey are taken from McClusky et al. (2000). Fault symbols used are same as those in Figure 1

defining discrete regions. The six stations to the north of the Stara Planina Mountains move SSW at velocities between 0 and 1.5 mm/year. The Black Sea coast stations do not show a coherent velocity pattern. All stations to the south and west of these regions move south at velocities between 2 and 4 mm/year.

To distinguish strain from motion with respect to Eurasia, the velocity field is presented in a regional frame, termed here as North Bulgarian-fixed reference frame (Figure 3). It is defined by minimizing the velocities of six stations in the stable region of northern Bulgaria plus BUCU, the permanent IGS station in southern Romania (Kotzev et al., 2005).

The relative velocities in the North Bulgarian-fixed reference frame show south-oriented motion at a rate of ~1 mm/year away from the fixed region in northern Bulgaria and southern Romania. That motion develops a clear extensional boundary probably marking the northern limit of the South Balkan extensional region. The boundary encompasses the E–W trending Sub-Balkan graben system of central Bulgaria and its westward continuation into the Sofia graben (Figures 3 and 4). Our data show ~1.5 mm/year extension across the central part of the Sub-Balkan graben system which is in a good agreement with the lower bound on the N–S extension rate of 1–2 mm/year, estimated from geological data (Tzankov et al., 1996). There is no fully consistent velocity pattern that would justify extending the strain belt to the Black Sea coast. To remove the common motion of the stations in southwestern Bulgaria and better display the small relative velocities in this critical region we used a West Bulgarian-fixed reference frame defined by 23 stations in western Bulgaria and eastern Macedonia (Kotzev et al., 2006) (Figure 5).

There are two regions where the consistency in the velocities of three or more stations is strong enough to suggest deformation. The northward motion of VARB, BERK, probably KOZN, and GABR suggests that extension at a rate 0.7 mm/year is transferred to the north of the Sofia graben across the westernmost part of the Stara Planina Mountains (Figures 5 and 6).

In SW Bulgaria and adjacent Macedonia PECH, M119 and M116 move to the south at ~1 mm/year relative to stations to the north and east. This is consistent with N–S extension on the Krupnik fault, the most seismically active area in Bulgaria (Figures 5 and 7). In April 1904 that fault was the locus of one of the strongest earthquakes during the past two centuries in Europe (Vatsov, l905). The magnitude of the earthquake was estimated to be between 7.3 and 7.8 by Gutenberg and Richter (l954) and Christoskov and Grigorova (l968). Using satellite imaginary and geological data Meyer et al. (2002) found that the possible rupture of the Krupnik fault compatible with their observations would account for a magnitude 6.9, significantly smaller than the previous estimates.

[1]The error ellipses are graphical representations of the errors associated with the estimated 2D velocity vectors. Each velocity vector begins at the GPS station. The error ellipse represents the region where there is a particular probability (confidence interval) that the other end of the velocity vector is actually located. If part of the velocity vector is outside of the error ellipse the motion is significant at the particular confidence level. If it is entirely within the error ellipse the motion is insignificant at the particular confidence level.

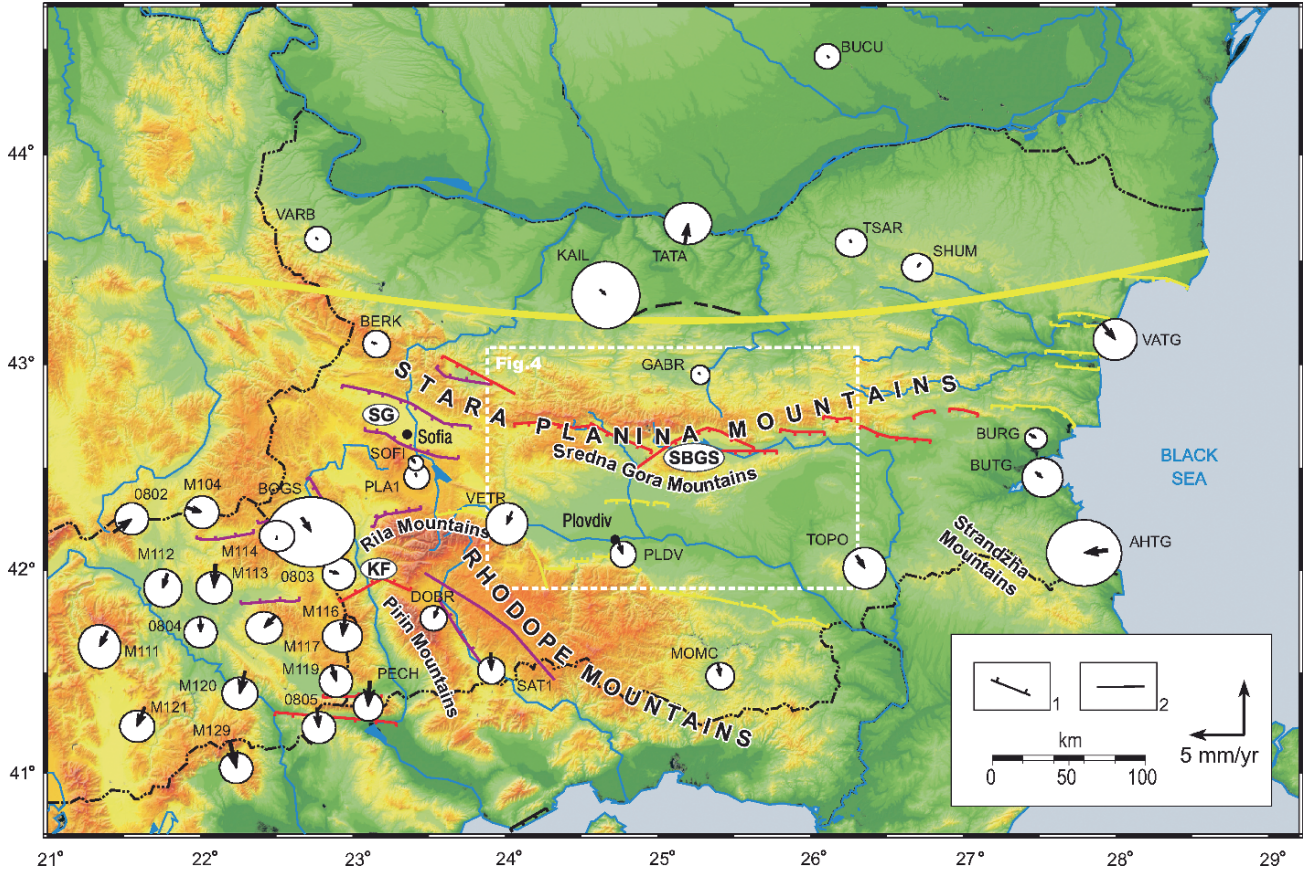

Figure 3 Topographic map with major extensional structures in Bulgaria and station velocities in the North Bulgarian reference frame. Error ellipses represent 95% confidence regions. Faults: 1, normal; 2, fault with unclear type of displacement. Faults in red lines are with the strongest evidence for recent displacements. Faults in violet lines are with well developed morphological evidence and are responsible for present day topography. Faults in yellow have more poorly developed morphological features but still bound modern topographic features. The northern limit of extension is shown by thick yellow line. Abbreviations: KF, Krupnik fault; SBGS, Sub-Balkan graben system; SG, Sofia graben. The white rectangle shows the location of Figure 4

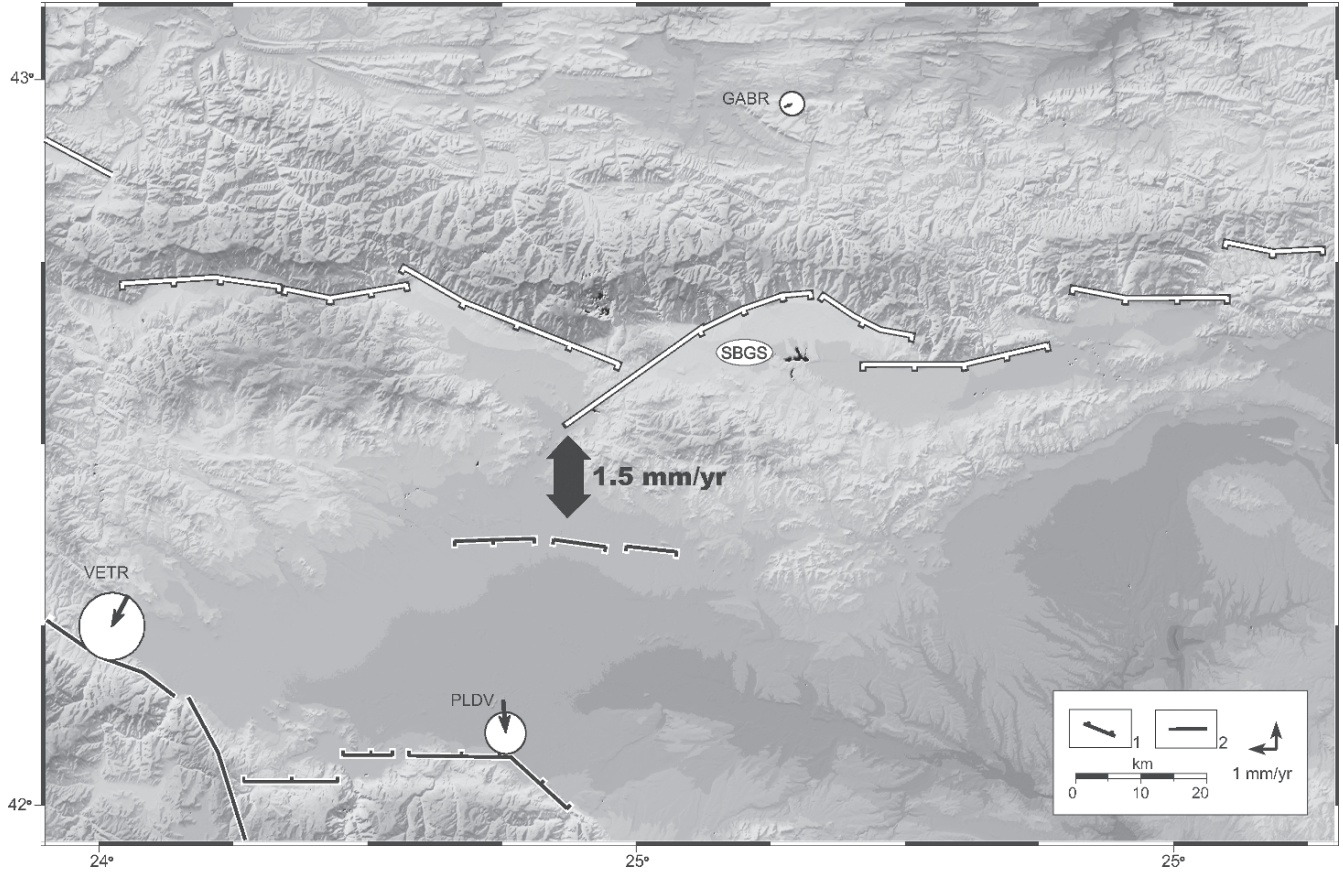

Figure 4 Topographic map of the Sub-Balkan graben system (SBGS) with station velocities in the North Bulgarian reference frame. Error ellipses represent 70% confidence regions. Faults: 1, normal; 2, fault with unclear type of displacement. Faults in white lines (red in Figure 3) are with the strongest evidence for recent displacements. Faults in black (yellow in Figure 3) have more poorly developed morphological features but still bound modern topographic features

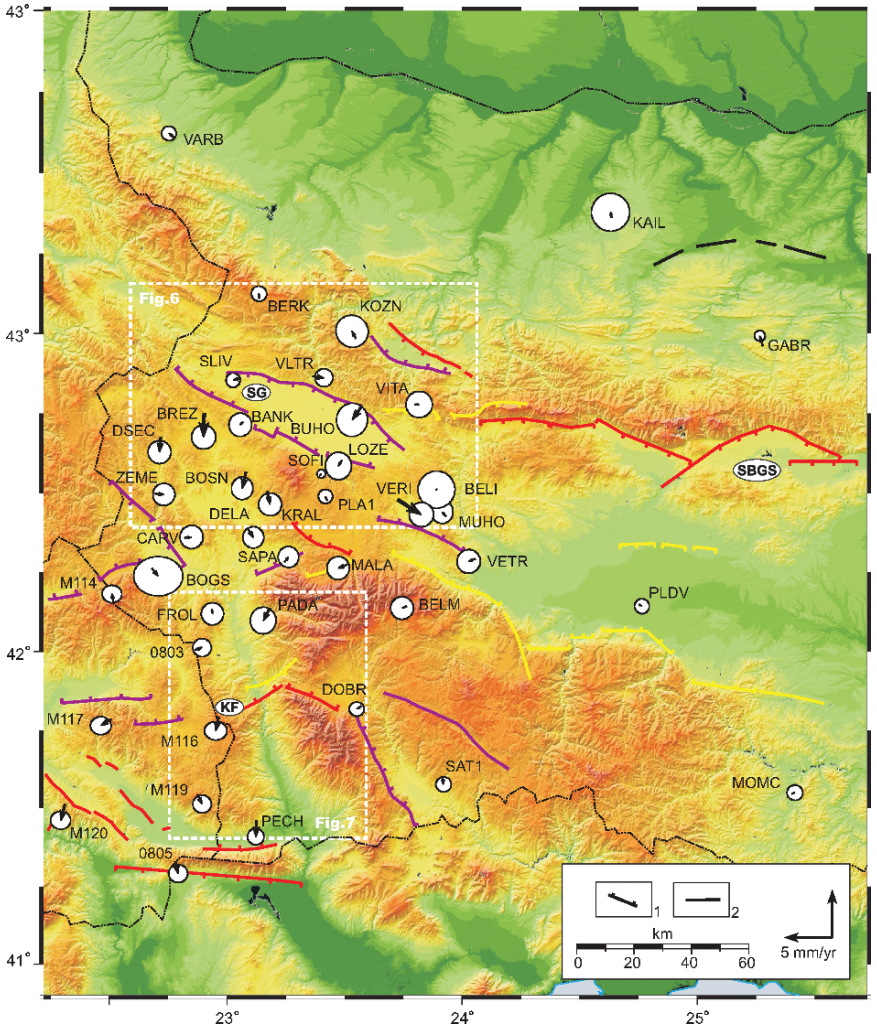

Figure 5 Estimated velocities in the West Bulgarian-fixed reference frame, defined by the 38 stations shown in this figure adapted from Kotzev et al. (2006). The 28 stations used to scale the uncertainties are those south of KOZN, west of GABR, and north of M116 (see text). Uncertainties are shown at 70% confidence for clarity. Faults: 1, normal; 2, fault with unclear type of displacement. Faults in red lines are with the strongest evidence for recent displacements. Faults in violet lines are with well developed morphological evidence and are responsible for present day topography. Faults in yellow have more poorly developed morphological features but still bound modern topographic features. Abbreviations: KF, Krupnik fault; SBGS, Sub-Balkan graben system; SG, Sofia graben. The white rectangles show the locations of Figures 6 and 7

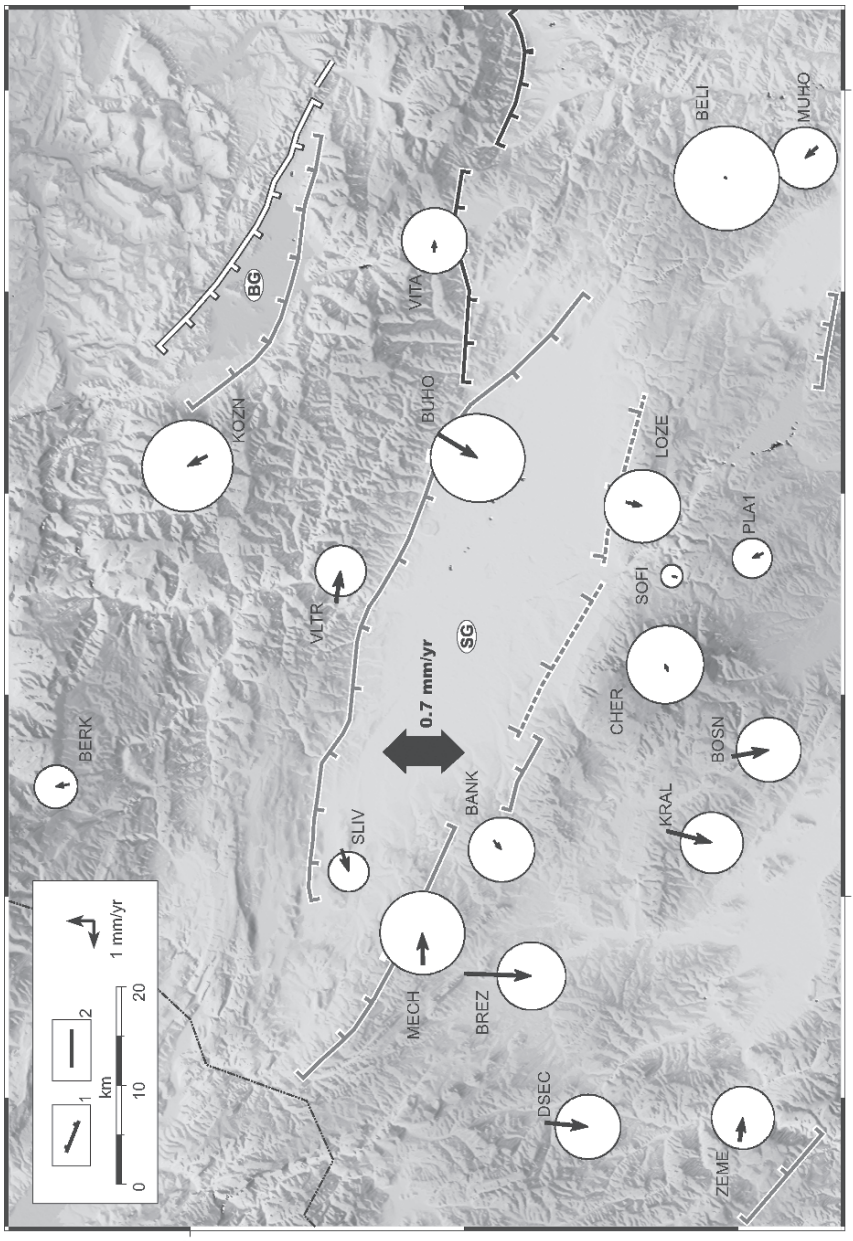

Figure 6 Topographic map of the Sofia graben (SG) with station velocities in the West Bulgarian reference frame. Error ellipses represent 70% confidence regions. Faults: 1, normal; 2, fault with unclear type of displacement. Faults in white lines (red in Figure 5) are with the strongest evidence for recent displacements. Faults in grey lines (violet in Figure 5) are with well developed morphological evidence and are responsible for present day topography. Faults in black (yellow in Figure 5) have more poorly developed morphological features but still bound modern topographic features. Abbreviations: BG, Botevgrad graben

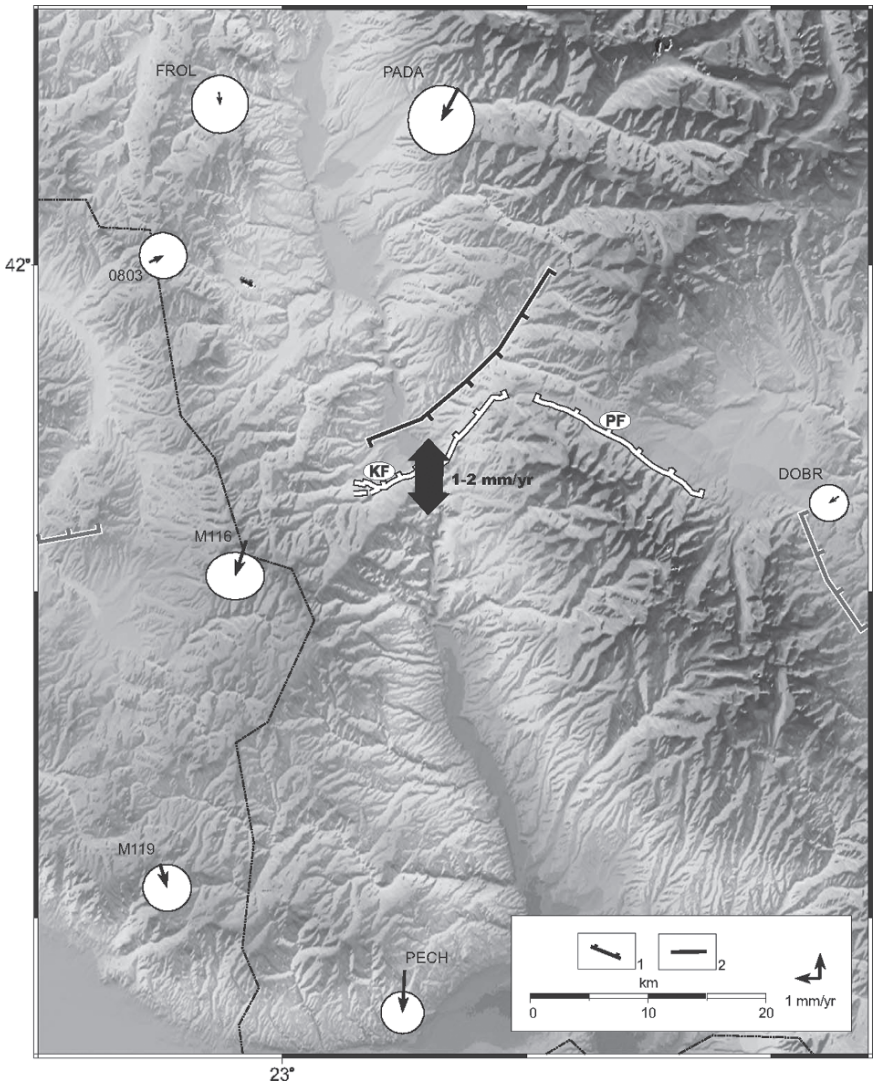

Figure 7 Topographic map of the Krupnik area with station velocities in theWest Bulgarian reference frame. Error ellipses represent 70% confidence regions. Faults: 1, normal; 2, fault with unclear type of displacement. Faults in white lines (red in Figure 5) are with the strongest evidence for recent displacements. Faults in grey lines (violet in Figure 5) are with well developed morphological evidence and are responsible for present day topography. Faults in black (yellow in Figure 5) have more poorly developed morphological features but still bound modern topographic features. Abbreviations: KF, Krupnik fault; PF, Predela fault

5.2 Macedonia

The GPS results from Macedonia (Burchfiel et al., 2006) show an almost uniform southward velocity of 3–4 mm/year relative to Eurasia (Figure 2). That pattern indicates that the entire region is moving to the south as a single crustal unit. The only areas with poorly defined velocity differences are within southwestern and northern Macedonia. To better display the small velocity differences we used a local frame termed here as Central Macedonia-fixed. It is defined by minimizing the velocities of 17 stations in central Macedonia (Burchfiel et al., 2006) (Figure 8).

In southwestern Macedonia GPS velocities indicate E–W extension across the N–S-trending Ohrid and Prespansko grabens (Figures 8 and 9), which is not confirmed by the GPS velocities through the southernmost stations in southwestern Macedonia. It is, however, in agreement with E–W extension interpreted by geological studies on the active faults bounding those grabens.

The second area with velocity differences is within northern Macedonia. It has an E–W trend that passes trough the Skopje graben (Figures 8 and 10), the site of the destructive magnitude 6.5 earthquake in 1963 (Leeds, 1964). Here the GPS data suggest N–S extension with a right lateral component which is not confirmed by geological observations.

Based on geological studies on active faulting Dumurdzanov et al. (2005) divide Macedonia into three regions: eastern dominated by active N–S extension with associated NNW striking left-lateral strike-slip faults, central Macedonia with almost no active faults, and western dominated by NNW-striking normal faults and associated strike-slip faults with right lateral-displacenment. That fault pattern is in general agreements with the distribution and style of seismicity in Macedonia. The uncertainty within the GPS data, however, is too large to discriminate the active tectonics. Neither our GPS measurements or the geology confirm the north–south trending dextral faults passing through central Macedonia suggested by Picha (2002).

5.3 Albania

The Albanides which represent the main geological structures in the territory of Albania (Figure 1) are divided into two major tectonic domains displaying different deformation styles and seismic patterns (Dilek, 2004).

Western Albania is affected by E–W compression resulting from ongoing oblique collision between Apulia and Eurasia. The compression is manifested in N-trending folds, thrust faults and oblique strike-slip fault systems. Active shortening reaches as far north as Montenegro although the deformation field is poorly resolved.

Eastern and central Albania is dominated by E–W extension expressed by a series of large approximately north–south trending grabens bounded by normal and transtensional dextral strike-slip faults that run the length of Albania and southward

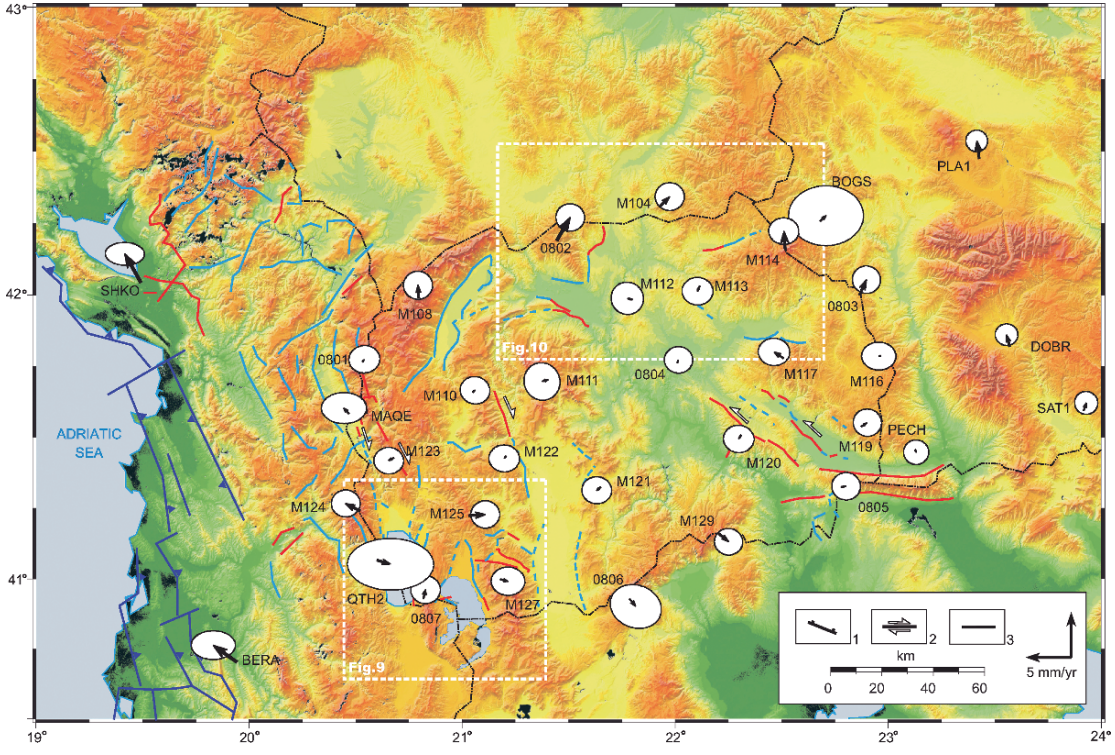

Figure 8 GPS velocities in Macedonia and Albania in the Central Macedonian reference frame adapted from Burchfiel et al. (2005). Error ellipses represent 70% confidence regions. Faults: 1, normal; 2, strike-slip with direction of relative motion; 3, fault with unclear type of displacement. Faults are red where geological evidence shows features of active fault movement. Faults in solid blue lines are associated with well-developed morphological evidence for recent activity. Faults in dashed blue lines are associated with only weak morphological evidence for recent activity. The white rectangles show the locations of Figures 9 and 10

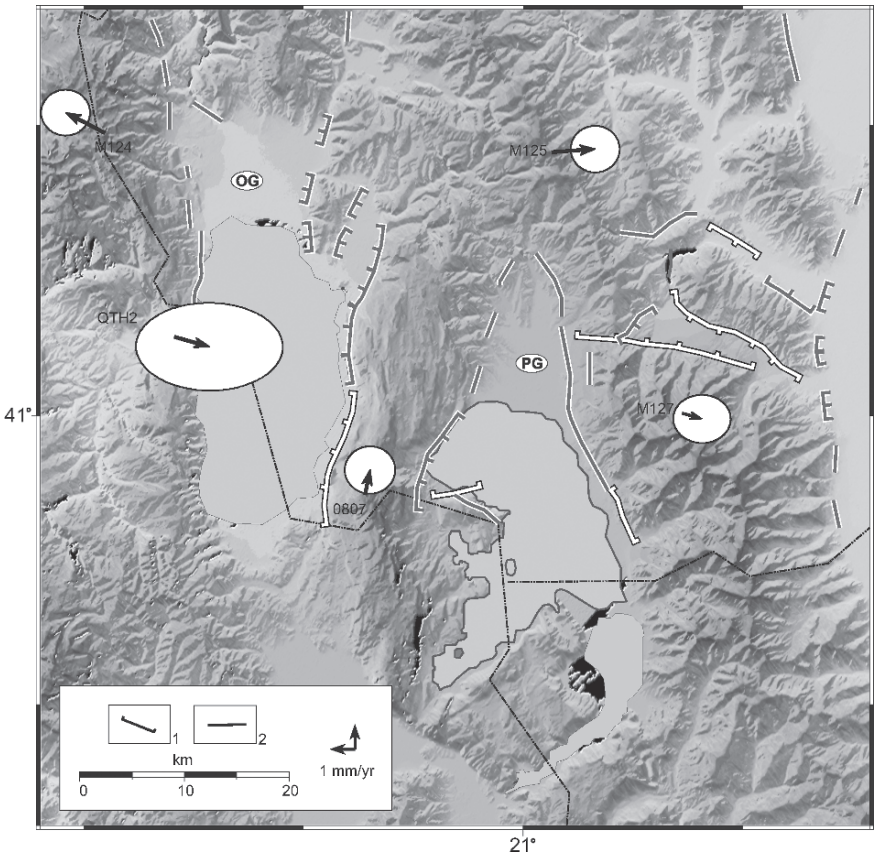

Figure 9 Topographic map of the Ohrid (OG) and Prespansko (PG) grabens with station velocities in the Central Macedonian reference frame. Error ellipses represent 70% confidence regions. Faults: 1, normal; 2, fault with unclear type of displacement. Faults are white (red in Figure 8) where geological evidence shows features of active fault movement. Faults in grey (dashed blue in Figure 8) lines are associated with only weak morphological evidence for recent activity

into Greece. That grabens are approximately parallel to the zone of convergence and probable slow subduction along the coast of Albania, Greece, and adjacent offshore regions.

GPS data from Albania are critical to define the western boundary of the South Balkan extensional region and the nature of the dynamic system bordering it to the west. In Figure 11 the estimated station velocities in Albania (Kotzev et al., 2006) are shown with the mean velocity for the south Balkan region removed to better display the velocity differences. The used reference frame termed here as South Balkan is defined by minimizing the velocities for all stations in the south Balkan region while estimating 3 translation parameters.

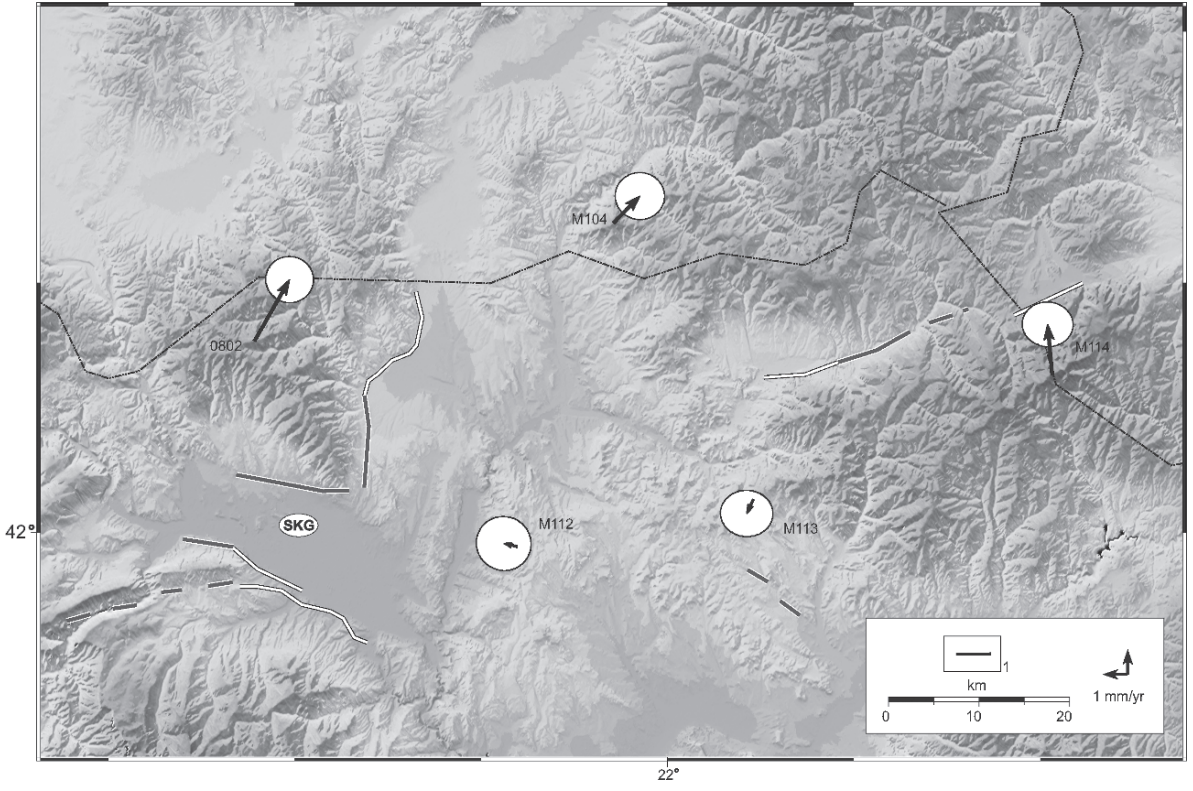

Figure 10 Topographic map of the Skopje graben (SKG) with station velocities in the Central Macedonian reference frame. Error ellipses represent 70% confidence regions. Faults: 1, fault with unclear type of displacement. Faults are white (red in Figure 8) where geological evidence shows features of active fault movement. Faults in grey (dashed blue in Figure 8) lines are associated with only weak morphological evidence for recent activity

Our GPS results generally confirm the established tectonic framework. Combined with data of Oldow et al. (2002) and seismic data they show E–W compression along the Adriatic coast of Albania and E–W extension in eastern and central Albania. Our present data however have insufficient coverage to resolve the western boundary of the South Balkan extensional region. The only indication also confirmed by seismic data is for an extensional zone with a component of right-lateral strike-slip within western Albania. Coupled with the data of Oldow et al. (2002) from Italy, however, our GPS results indicate that probably subduction along the northern part of the Hellenic trench has not ceased as suggested by Wortel and Spakman (2000) but still proceed at rates ~5–10 mm/year. This is supported by seismic data showing east–west convergence along the all coastal area from northern Greece, and Albania into Montenegro and Croatia.

5.4 Romania

Although there is an extensive GPS network in Romania (Becker et al., 1998; Grenerczy et al., 2000) only few data are available. The reason is that most of the first GPS monuments established in 1994–1995 were destroyed. After that poorly determined eccentric points were remeasured instead of the main markers.

Kinematic data from the area to the south of the South Carpatian bend (at ~45°N) in Romania are important to define the northern boundary of the South Balkan extensional regime. Most published velocity and displacement vectors in this region (Becker et al., 1998; Dinter et al., 2001; Hefty, 2004; Grenerczy, 2004) indicate small to insignificant southward oriented motion relative to Eurasia (Figure 2).

Coupled with GPS data from Bulgaria those results suggest N–S extension at a very low rate in southern Romania. Available data, however, are too sparse to determine whether the region joining the southern and eastern Carpathians with its E-striking right lateral faults marks the northern boundary of the South Balkan extensional region as suggested by Burchfiel et al. (2004).

6 Conclusions

Our results show an overall southward motion of the South Balkan region with respect to Eurasia at a rate of 3–4 mm/year. Much of the region behaves as a single tectonic unit. In some places the GPS velocities show local zones of slow internal deformation that correspond to the location of active faults as determined by geological observations.

The GPS data delineate a clear extensional zone that probably marks the northern limit of the South Balkan extensional terrain and the Aegean extensional province. This extensional zone passes through central Bulgaria along an approximately east–west trend separating a northern region with insignificant motion relative to

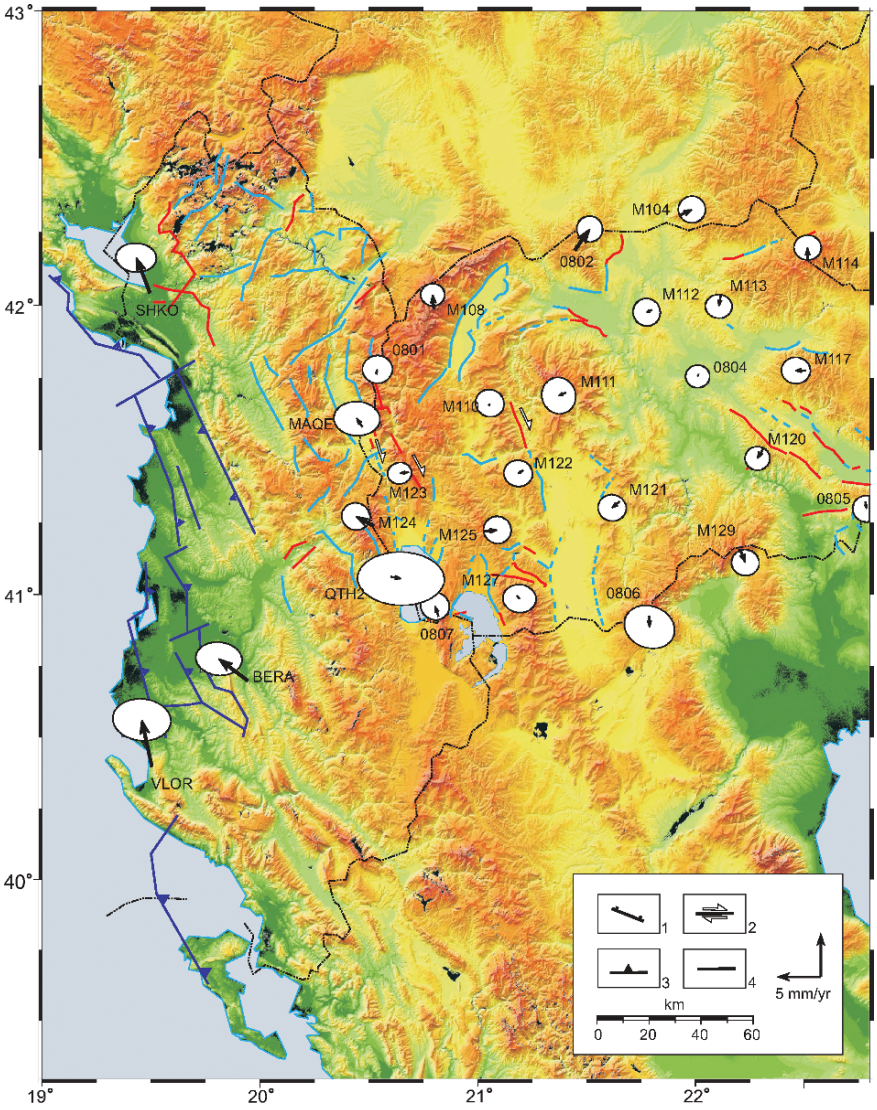

Figure 11 Velocities for GPS stations in Albania and Macedonia in the South Balkan reference frame. Error ellipses represent 95% confidence regions. Faults: 1, normal; 2, strike-slip with direction of relative motion; 3, trust fault; 4, fault with unclear type of displacement. Faults are red where geological evidence shows features of active fault movement. Faults in solid blue lines are associated with well-developed morphological evidence for recent activity. Faults in dashed blue lines are associated with only weak morphological evidence for recent activity

Eurasia from a southwestern region characterized by E–W extensional grabens and increasing southward velocities between 2 and 4 mm/year. The zone of extension passes obliquely trough the east–west trending Stara Planina Mountains of central Bulgaria.

The GPS data allow to define the northern limit of the Aegean extensional province only within central Bulgaria. Elsewhere the location and nature of the boundaries of the Aegean extension are poorly defined. Geological data suggest that the northern limit of extension probably passes through central Serbia and Montenegro where a series of NE to N–S-trending strike-slip faults related to grabens that may be formed as pull-apart structures were shown by Markovic and Djokovic (1995).

South of this E–W trending extensional zone, the area of central and western Bulgaria and eastern Macedonia moves approximately south at a rate of 4 mm/year relative to Eurasia. Throughout most of this area the rates of displacement are uniform within the uncertainties of the measurements, except within the northern and southernmost parts. The GPS data indicate N–S extension at a slow rate of 1–2 mm/year in southernmost Macedonia and Bulgaria.

There is some evidence of NNW-trending transtensional boundary separating southwestern Bulgaria from Macedonia. The relative velocities of the two sides of this boundary are perpendicular to generally ENE to E-trending active normal faults, and in a few places are parallel to strike-slip faults linked to normal faults forming pull-apart structures (e.g. in SE Macedonia).

When combined with GPS data for northern Greece (McClusky et al., 2000; Kahle et al., 2000), Bulgarian and Macedonian data show gradual increase in velocity from north to south to 25 mm/year toward the Aegean Sea (Figure 2). The overall N–S extension produced by the velocity field is consistent with geological and seismic observations in the region. Studies of active faulting in southwestern Bulgaria, adjacent southern Macedonia, and northern Greece show that most of the active and young faults strike generally E–W, WNW, NW and rarely NE. Most of these are normal faults, a few with strike-slip components. To the extent that fault displacements have been dated, the geological data suggest rates of extension from 1–2 mm/year or less in southwestern Bulgaria and adjacent southern Macedonia (Kotzev et al., 2006; Burchfiel et al., 2006) to 3 mm/year in northern Greece (Vamvakaris et al., 2003). Focal mechanisms determined for the region are also consistent with that interpretation showing dominantly N–S extension on east–west trending faults.

The fault pattern in northern Greece contains NNE-striking faults such as the Xanti fault that suggest right lateral strike slip with extension on NW-trending segments. There is no GPS evidence for dextral motion in this area and present GPS networks are too sparse to determine if these faults are the northernmost stands of the North Anatolian fault system, or they were once part of this system but now have mainly N–S extension.

There is not enough GPS data to map the detailed kinematics in the western part of the south Balkan region. Geological data, focal mechanisms and available GPS data in this region indicate a transitional boundary within southwestern Serbia, eastern Montenegro and western Macedonia that probably marks the western limit

of the South Balkan extensional region. That boundary separates the region of N–S extension to the east from a region of E–W extension in central and eastern Albania, central Montenegro, southwestern Macedonia and probably northwestern Greece which may be related to trench roll-back along the still convergent northern Hellenic trench.

Acknowledgements This research was supported by the National Science Foundation Grant EAR-9628225, National Council for Scientific Research Grant NZ-1101/01, National Science Fund Grant NZ-608, and European Union Grant ENV4-CT95-0087. We are grateful for support in data acquisition to personnel from the Central Laboratory of Geodesy, Bulgarian Academy of Sciences; State Department for Geodetic Survey, Skopje; Bundesamt fur Kartographie und Geodasie (BKG), Frankfurt; and the Boulder facility of UNAVCO. We obtained global solution files and most of the IGS tracking data from the Scripps Orbit and Permanent Array Center. The maps in this paper were generated using the public domain Generic Mapping Tools (GMT) software (Wessel and Smith, 1995).

References

Altamimi, Z., Sillard, P., Boucher, C., 2002. ITRF2000: A new release of the International Terrestrial Reference Frame for earth science applications, *J. Geophys. Res*. 107(B10): 2214, doi:10.1029/2001JB000561.

Anderson, H. A., Jackson, J. A., 1987. Active tectonics of the Adriatic region, *Geophys. J. R. Astron. Soc*. 91:937–983.

Armijo, R. B., Meyer, G. C., King, P., Rigo, A., Papanastassiou, D., 1996. Quaternary evolution of the Corinth Rift and its implications for the Late Cenozoic evolution of the Aegean, *Geophys. J. Int*. 126:11–53.

Altiner, Y., 2001. The contribution of GPS data to the detection of the Earth's crust deformations illustrated by GPS campaigns in the Adria region, *Geophys. J. Int*. 145:550–559.

Ayhan, M. E., Demir, C., Lenk, O., Kilicoglu, A., Altiner, Y., Barka, A., Ergintav, S., Özener, H., 2002. Interseismic strain accumulation in the Marmara Sea region, *Bull. Seismol. Soc. Am*. 92:216–229.

Battaglia, M., Murray, M., Serpelloni, E., Burgmann, R., 2004. The Adriatic region: An independent microplate within the Africa-Eurasia collision zone, *Geophys. Res. Lett*. 31, L09605, doi:10.1029/2004GL019723.

Becker, M., Ghitau, D., Marcu, C., Radulescu, F., Reinhard, E., Rosca, V., Rus, T., Seeger, H., 1998. Plate kinematics studies in Romania using GPS, *Rep. in Geodesy of the Warsaw Univ. Techol*. 9(39):89–103.

Bock, Y., Behr, J., Fang, P., Dean, J., Leigh, R., 1997. Scripps orbital and permanent array center (SOPAC) and Southern California permanent GPS geodetic array (PGGA), in: *The Global Positioning System for Geosciences: Summary and Proceedings of a Workshop on Improving the GPS Reference Station Infrastructure for Earth Oceanic, and Atmospheric Science Applications,* National Academy, Washington DC, 55–61.

Burchfiel, B. C., Nakov, R., Tzankov, Tz., Royden, L., 2000. Cenozoic extension in Bulgaria and northern Greece: the northern part of the Aegean extensional regime, in: *Tectonics and Magmatism in Turkey and the Surrounding Area,* E. Bozkurt, J. A. Winchester, and J. D. A. Piper (ed.), *Geol. Soc. Lon. Spec. Publ*. 173:325–352.

Burchfiel, B. C., Dumurdzanov, N., Serafimovski, T., Nakov, R., 2004. The southern Balkan Cenozoic extensional region and its relation to extension in the Aegean realm, *Geol. Soc. Am. Abs. with Prog*. 36(5):52.

Burchfiel, B. C., King, R. W., Todosov, A., Kotzev, V., Dumurdzanov, N., Serafimofski, T., Nurce, B., 2006. GPS results for Macedonia and its importance for the tectonics of southern Balkan extensional system, *Tectonophys*. in press, doi:10.1016/j.tecto.2005.10.046.

Calais, E., Nocquet, J. M., Jouanne, F., Tardy, M., 2002. Current strain regime in the western Alps from continuous global positioning system measurements, 1996–2001, *Geology* 30:651–654.

Christoskov, L., Grigorova, E., 1968. On the relationship between earthquake energy and magnitude for Bulgaria, *Comp. Rend. Acad. Bulg. Sci*. 21(2):127–129.

Clarke, P. J., Davies, R. R., England, P. C., Parsons, B., Billiris, H., Paradissis, D., Veis, G., Cross, P. A., Denys, P. H., Ashkenazi, V., Bingley, R., Kahle, H.G., Muller, M.V., Briole, P., 1998. Crustal strain in central Greece from repeated GPS measurements in the interval 1989–1997, *Geophys. J. Int*. 135:195–214.

Cocard, M., Kahle, H. G., Peter, Y., Geiger, A., Veis, G., Felekis, S., Paradissis, D., Billiris, H., 1999. New constraints on the rapid crustal motion of the Aegean region: recent results inferred from GPS measurements (1993–1998) across the West Hellenic Arc, Greece, *Earth Planet. Sci. Lett*. 172:39–47.

Dilek, Y., 2004. Neotectonics, seismology and the mode of late Cenozoic crustal deformation in the Albanides, Balkan peninsula, *Geol. Soc. Am. Abs. with Prog*. 36(5):52.

Dinter, G., Nutto, M., Schmitt, G., Schmidt, U., Ghitau, D., Marcu, C., 2001. Three dimensional deformation analysis with respect to Plate Kinematics in Romania, *Rep. in Geodesy of the Warsaw Univ. Techol*. 2(57):29–42.

Dong, D., Herring, T. A., King, R. W., 1998. Estimating regional deformation from a combination of space and terrestrial geodetic data, *J. Geodesy* 72:200–214.

Dumurdzanov, N., Serafimovski, T., Burchfiel, B. C., 2005. Cenozoic tectonics of Macedonia and its relation to the South Balkan extensional regime, *Geosphere*, 1:1–22.

Flerit, F., Armijo, R., King, G. C. P., Meyer, B., Barka, A., 2003. Slip partitioning in the Sea of Marmara pull-apart determined from GPS velocity vectors, *Geophys. J. Int*. 154:1–7.

Goldsworthy, M., Jackson, J., Haines, A. J., 2002. The continuity of active fault systems in Greece, *Geophys. J. Int*. 148:596–618.

Grenerczy, G., Kenyeres, A., Fejes, I., 2000. Present crustal movement and strain distribution in Central Europe inferred from GPS measurements, *J. Geophys. Res*. 105(B9):21835–21846.

Grenerczy, G., 2004. The motion of Adria and its effects on the Pannonian basin: Report of CERGOP-2/Environment WP10.3, *Rep. in Geodesy of the Warsaw Univ. Techol*. 4(71):107–114.

Gutenberg, B., Richter, C. F., 1954. *Seismicity of the Earth and Associated Phenomena*, Princeton University Press, Princeton, NJ, p. 310.

Hefty, J., 2004. Work-Package 7 of the CERGOP-2/Environment: Geokinematical modeling and strain analysis. Activity report April 2004–September 2004, *Rep. in Geodesy of the Warsaw Univ. Techol*. 4(71):39–42.

Herring, T. A., 2003. *GLOBK: Global Kalman filter VLBI and GPS analysis program*, Release 10.1, Mass. Inst. of Technol., Cambridge.

Jackson, J., 1992. Partitioning of strike-slip and convergent motion between Eurasia and Arabia in eastern Turkey, *J. Geophys. Res*. 97:12471–12479.

Jackson, J., McKenzie, D., 1988. The relationship between plate motions and seismic tremors, and the rates of active deformation in the Mediterranean and Middle East, *Geophys. J. R. Astr. Soc*. 93:45–73.

Jimenez-Munt, I., Sabadini, R., Gardi, A., Bianco, G., 2003. Active deformation in the Mediterranean from Gibraltar to Anatolia inferred from numerical modeling and geodetic and seismological data, *J. Geophys. Res*. 108(B1), 2006, doi:10.1029/2001JB001544.

Kahle, H.-G., Cocard, M., Peter, Y., Geiger, A., Reilinger, R., Barka, A., Veis, G., 2000. GPS-derived strain rate field within the boundary zones of Eurasian, African and Arabian plates, *J. Geophys. Res*. 105:23353–23370.

King, R. W., Bock, Y., Herring, T. A., McClusky, S. C., 2003. *Documentation for the GAMIT GPS software analysis program*, Release 10.1, Mass. Inst. of Technol., Cambridge.

Kotzev, V., Nakov, R., Georgiev, Tz., Burchfiel, B. C., King, R. W., 2006. Crustal motion and strain accumulation in western Bulgaria, *Tectonophys*, in press, doi:10.1016/j.tecto.2005.10.040.

Leeds, D. J., 1964. *The Skopje, Yugoslavia, Earthquake of July 26, 1963*, University of California, Los Angeles, California.

Le Pichon, X., Chamot-Rooke, N., Lallemant, S., Noomen, R., Veis, G., 1995. Geodetic determination of the kinematics of central Greece with respect to Europe: implications for eastern Mediterranean tectonics, *J. Geophys. Res*. 100:12675–12690.

Le Pichon, X., Chamot-Rooke, N., Rangin, C., Sengör, A. M. C., 2003. The North Anatolian fault in the Sea of Marmara, *J. Geophys. Res*. 108(B4), 2179, doi:10.1029/2002JB001862.

Markovic, M., Djokovic, I., 1995. Neotectonic activity of the Scutari-Pec general area, *Ann. Geol. Penins. Balkans* 59:23–43.

McClusky, S., Balassanian, S., Barka, A., Demir, C., Erginav, S., Georgiev, I., Gurkan, O., Hamburger, M., Hurst, K., Kahle, H., Kastens, K., Kekelidze, G., King, R., Kotzev, V., Lenk, O., Mahmoud, S., Mishin, A., Nadarya, M., Ouzounis, A., Paradissis, D., Peter, Y., Prilepin, M., Reilinger, R., Sanli, I., Seeger, H., Tealeb, A., Toksoz, M. N., Veis, G., 2000. Global Positioning System constraints on plate kinematics and dynamics in the eastern Mediterranean and Caucasus, *J. Geophys. Res*. 105:5695–5719.

McKenzie, D., 1970. Plate tectonics of the Mediterranean region, *Nature* 226:239–243.

McKenzie, D., 1972. Active tectonics of the Mediterranean region, *Geophys. J. R. Astron. Soc*. 30:109–185.

McKenzie, D., 1978. Active tectonics of the Alpine Himalayan Belt: The Aegean Sea and surrounding regions, *Geophys. J. R. Astron. Soc*. 55:217–252.

McKenzie, D., Jackson, J., 1984. The relationship between strain rates, crustal thickening, paleomagnetism, finite strain and fault movements within a deforming zone, *Earth Planet Sci. Lett*. 65:182–202.

Meade, B. J., Hager, B. H., McClusky, S., Reilinger, R. E., Erginav, S., Lenk, O., Barka, A., Ozener, H., 2002. Estimates of seismic potential in the Marmara region from block models of secular deformation constrained by GPS measurements, *Bull. Seismol. Soc. Am*. 92:208–215.

Meyer, B., Armijo, R., Dimitrov, D., 2002. Active faulting in SW Bulgaria: possible surface rupture of the 1904 Struma earthquakes, *Geophys. J. Int*. 148:246–255.

Nocquet, J. M., Calais, E., Altamini, Z., Sillard, P., Boucher, C., 2001. Intraplate deformation in western Europe deduced from an analysis of the International Terrestrial Reference Frame 1997 (ITRF97) velocity field, *J. Geophys. Res*. 106:11239–11257.

Nocquet, J. M., Calais, E., 2003. Crustal velocity field of western Europe from permanent GPS array solutions, 1996 – 2001, *Geophys. J. Int*. 154:72–88.

Nyst, M., Thatcher, W., 2004. New constraints on the active tectonic deformation of the Aegean, *J. Geophys. Res*. 109(B11406), doi:10.1029/2003JB002830.

Oldow, J. S., Ferranti, L., Lewis, D. S., Campbell, J. K., D'Argenio, B., Catalano, R., Pappone, G., Carmignani, L., Conti, P., Aiken, C. L. V., 2002. Active fragmentation of Adria, the north Africa promontory, central Mediterranean orogen, *Geology* 30:779– 782.

Picha, F. J., 2002. Late orogenic strike-slip faulting and escape tectonics in frontal Dinarides-Hellenides, Croatia, Yugoslavia, Albania, and Greece, *Bull. Am. Assoc. Petrol. Geol*. 86:1659–1671.

Reilinger, R., Ergintav, S., Burgmann, R., McClusky, S., Lenk, O., Barka, A., Gurkan, O., Hearn, E., Feigl, K. L., Cakmak, R., Aktug, B., Ozener, H., Toksoz, M.N., 2000. Coseismic and postseismic fault slip for the 17 August 1999, M = 7.5, Izmit, Turkey earthquake, *Science* 289:1519–1524.

Sengor, A. M. C., Tuysuz, O., Imren, C., Sakinc, M., Eyidogan, H., Gorur, N., LePichon, X., Rangin, C., 2004. The North Anatolian Falut: A New Look, *Annu. Rev. Earth Planet. Sci*. 33:1–75.

Straub, C., Kahle, H.-G., Schindler, C., 1997. GPS and geologic estimates of the tectonic activity in the Marmara Sea region, NW Anatolia, *J. Geophys. Res*. 102:27587–27601.

Taymaz, T., Jackson, J., McKenzie, D., 1991. Active tectonics of the north and central Aegean Sea, *Geophys. J. Int*. 106:433–490.

Tzankov, Tz., Angelova, D., Nakov, R., Burchfiel, B. C., Royden, L., 1996. The Sub-Balkan graben system of central Bulgaria, *Basin Res*. 8:125–142.

Vatsov, S., 1905. *Earthquakes in Bulgaria in 1904* (in Bulgarian), Central Meteorological Survey, Sofia.

Vamvakaris D. A., Papazachos, C. B., Savvaidis, P. D., Tziavos, I. N., Karagianni, E. E., Skordilis, E. M., Hatzidimitriou, P. M., 2003. Stress-field and time variation of active crustal deformation in the Mygdonia basin based on the joined interpretation of seismological, neotectonic and geodetic data, *Geophys. Res. Abst*. 5:08794.

Weber, J., Vraec, M., Stopar, B., Pavolvcic-Preseren, P., Dixon, T., 2004, The PIVO-2003 experiment: A GPS study of the Istria peninsula and Adria microplate motion, and active tectonics in Slovenia, in Pinter, N., et al., edis., Ardria microplate, Amsterdam, Kluwer Academic Publisher.

Wessel, P., Smith, W. H. F., 1995. New version of the generic mapping tools released, *Eos Trans. AGU* 76:329.

Williams, S. D. P., Bock, Y., Fang, P., Nikolaidis, R. M., Prawirodirdjo, L., Miller, M., Johnson, D.J., 2004. Error analysis of continuous GPS time series, *J. Geophys. Res*. 109(B03412), doi:10.1029/2003JB002741.

Wortel, M. J. R. Spakman, W., 2000. Subduction and slab detachment in the Mediterranean-Carpathian region, *Science* 290:1910–1917.

Part II
Seismicity Studies in the South Balkan Region

Recent Devastating Earthquakes in Turkey and Active Tectonics of the Aegean and Marmara Seas

Tuncay Taymaz*, Onur Tan, and Seda Yolsal

Abstract The Eastern Mediterranean region, including the adjacent areas of western Turkey and Greece, is indeed one of the most seismically active and rapidly deforming regions within the continents. Thus, the wide range of active deformational processes observed in the Eastern Mediterranean means that this region provides a unique opportunity to improve our understanding of the complex dynamics of continental collision, including strike-slip faulting, subduction and crustal extension, as well as associated volcanism, intense seismic activity and geomorphological events (e.g. tsunamis) and their impacts on societal life and civilization. Recent devastating earthquakes along the North Anatolian Fault Zones (NAFZ) such as the August 17, 1999 Gölcük-İzmit (Mw=7.4) and the November 12, 1999 Düzce (Mw=7.1) earthquakes confirm the complexity of the crustal deformations throughout the region. Furthermore, the source mechanisms and rupture histories of the moderate and large size earthquakes that occured in the last decades contribute to conceive the nucleation and growth of fault system in the region.

In this article, we present novel seismological observations and briefly presented the source characteristics of the recent damaging earthquakes in Turkey and adjacent areas. The latter includes the Marmara and North Aegean Seas, the Lake districts region of SW Turkey, Orta-Çankin of central Turkey and the East Anatolian Fault Zone (EAFZ) in order to display the active tectonic structures associated with seismicity. Investigating and monitoring of the active seismogenic zones will provide a better understanding for predicting the occurences of future earthquakes and hence an improved physical basis for mitigation of their effects on environment and societies in this earthquake-prone region.

Keywords active tectonics, Anatolia, crustal deformations, earthquakes, eastern Mediterranean, source rupture modelling, slip distribution studies, Turkey

İstanbul Technical University (İTÜ), the Faculty of Mines, Department of Geophysics, Seismology Section, Maslak TR-34460, İstanbul, Turkey

*To whom correspondence should be addressed. E-mail: taymaz@itu.edu.tr

E.S. Husebye (ed.), *Earthquake Monitoring and Seismic Hazard Mitigation in Balkan Countries.*

1 Introduction

The complexity of the plate interactions and associated crustal deformation in the eastern Mediterranean region is reflected in the many destructive earthquakes that have occurred throughout recorded history. Turkey, alas, experienced two destructive earthquakes in 1999: the Gölcük-İzmit event on 17 August (Mw = 7.4), and the Düzce event on 12 November (Mw = 7.1); the most devastating earthquakes that this nation has suffered in recent decades (Taymaz, 1999). They took place on segments of the well-known North Anatolian Fault Zone (NAFZ), the most prominent active fault zone in Turkey. It passes close to Istanbul and other major urban centers, and cuts along northern Turkey for more than 1,500 km, accommodating ~25 mm/year of right-lateral motion between Anatolia and the Eurasian plate (e.g. McClusky et al., 2000, 2003; Taymaz et al., 2004a-b). The tectonic evolution of the Eastern Mediterranean region is dominated by deformations tied to ongoing subduction along the Hellenic (Aegean) arc and of continental collision in eastern Turkey (Anatolia) and the Caucasus (e.g. Taymaz, 1990; Taymaz et al., 1991a-b; Sato et al., 2004; Tan and Taymaz, 2006; Podgorski et al., 2007; Georgiev et al., 2007; Kotzev et al. IBID). Northward subduction of the African plate beneath western Turkey and the Aegean region is causing extension of the continental crust in the overlying Aegean province (Taymaz and Price 1992). In contrast, eastern Turkey is instead experiencing crustal shortening and thickening due to northward motion of the Arabian plate relative to Eurasia. The resulting combination of forces: the "pull" from the subduction zone to the west and "push" from the convergent zone to the east, is causing the Turkish micro-plate to move westward, bounded by strike-slip fault zones: the NAFZ to the north and the East Anatolian Fault Zone (EAFZ) to the south. Interplay between dynamic effects of the relative motions of adjoining plates thus controls large-scale crustal deformation and the associated earthquake activity in Turkey (Figure 1, Yolsal et al., 2007a-b). In this presentation we give an overview of active plate tectonics and associated crustal deformation reflected by intense earthquake activity in the Eastern Mediterranean region.

2 Marmara Sea (NW Turkey)

The Sea of Marmara is a marine basin in northwest Turkey that connects the Aegean Sea with the Black Sea, and includes a series of tectonically active basins at the western end of the right-lateral North Anatolian Fault (NAF). Across most of Turkey the NAF is a relatively simple, narrow, right-lateral strike-slip fault zone; however it splits into several fault strands in the vicinity of the Sea of Marmara so that the deformation (surface faulting of the NAF) becomes distributed over a 120 km broad zone (Smith et al., 1995, Taymaz 1999; Le Pichon et al., 2001). The region of the Marmara Sea is a transition zone between the strike slip regime of the NAF and the extension regime of the Aegean Sea, and the Main Marmara Fault (MMF) exhibits all the characteristics of a major through-going active strike-slip fault (Le Pichon et al., 2001; Armijo et al., 2002). We have conducted seismological observations

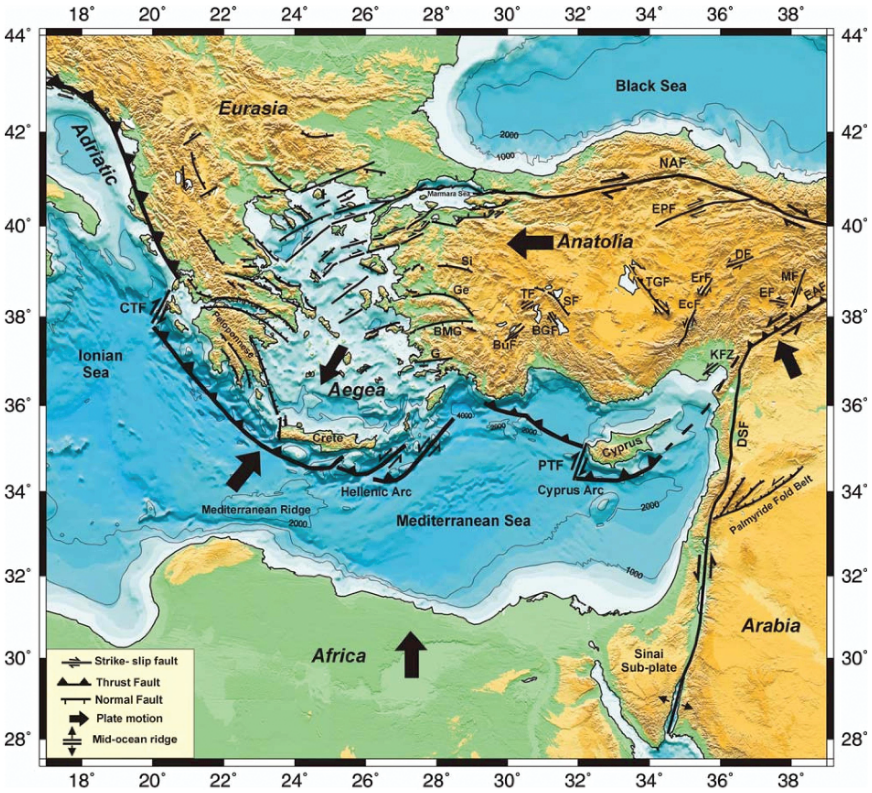

Figure 1 Active tectonic boundaries in the Eastern Mediterranean. Topography and Bathymetry Data are taken from USGS–NOAA / GTOPO30 and GEBCO/97– BODC, respectively. NAF: North Anatolian Fault; EAF: East Anatolian Fault; DSF: Dead Sea Transform Fault; PTF: Paphos Transform Fault; CTF: Cephalonia Transform Fault; BMG: Büyük Menderes Graben; G: Gökova; Ge: Gediz Graben; BuF: Burdur Fault; Si: Simav Graben; BGF: Beyşehir Gölü Fault; TF: Tatarli Fault; SF: Sultandaği Fault; TGF: Tuz Gölü Fault; EcF: Ecemiş Fault; ErF: Erciyes Fault, DF: Deliler Fault, EF: Elbistan Fault, MF: Malatya Fault, KFZ: Karataş-Osmaniye Fault Zone (after Taymaz et al., 2007a; Yolsal and Taymaz, 2007; Yolsal et al., 2007a-b)

within the Sea of Marmara (NW Turkey) in order to investigate the seismicity induced after the Gölcük-İzmit (Kocaeli) earthquake, Mw = 7.4, of August 17, 1999, by using Ocean Bottom Seismometers (OBSs). High-resolution hypocenters and focal mechanisms of micro-earthquakes have been investigated during the Marmara Sea OBS project involving deployment of 10 OBS along each leg within the Çinarcik (eastern Marmara Sea) and Central-Tekirdağ(western Marmara Sea) basins during April–July 2000. This study presents the results of the first marine seismological observations using Ocean Bottom Seismometers (OBSs) in the Marmara Sea to investigate the present status of the detailed micro-seismicity (Sato et al., 2004). We have detected numerous earthquakes within the main basins along the imaged strands of the North Anatolian Fault. Microearthquake seismic activity mainly occurred along

the Main Marmara Fault (MMF) in the Marmara Sea, and is quite high, and focal depth distribution along the fault was shallower than 20 km at the western part, and shallower than 15 km at the eastern part. From high resolution relative relocation studies of the some of earthquake clusters, we suggest that the western Main Marmara Fault is almost vertical and the eastern Main Marmara Fault dips to south about 45°. Composite focal mechanisms show a strike-slip regime at the western Main Marmara Fault and complex (strike-slip and normal type) at the eastern Main Marmara Fault (MMF). The faulting in strike-slip and normal character is present in the eastern part of the Çinarcik basin. On the other hand, the source mechanism of Çinarcik earthquake (Ms = 6.4) of September 18, 1963, also confirms the characteristic of normal faulting with a shallow focal depth (e.g. Taymaz, 1990; Taymaz et al., 1991a) suggesting that there is partitioning of the motion within the Çinarcik basin. Furthermore, intensive scientific efforts are devoted to the Marmara Sea region because of the historical record of damage to large cities such as İstanbul, and the close proximity of the North Anatolian fault which is submerged beneath the Marmara Sea (e.g. Smith et al., 1995; Le Pichon et al., 2001; Armijo et al., 2002; Sato et al., 2004). The most recent probability estimate of a M ≥7 earthquake rupturing beneath the Sea of Marmara is ~35–70% in the next 30 years if a time-dependent model that included coseismic and postseismic effects of the 1999 Mw = 7.4 Gölcük-İzmit earthquake is used (Parson, 2004). The westernmost continuation of NAF into the Sea of Marmara still requires further investigations to better understand the complexity of faulting associated with earthquakes at depth reaching to seismogenic zones.

3 North Aegean Sea and Saros Bay

The most dramatic bathymetric feature of the north Aegean Sea is the North Aegean Trough (NAT), which consists of a series of deep fault-bounded basins. Those in the west have a NE trend, while those in the eastern part of the system trend ENE (see Figure 1). The easternmost basin, the Saros trough, is also the narrowest: in its western part, south of Samothraki, the bathymetry and gravity suggest it is a half-graben bounded by a large normal fault system along its northern margin. Such faulting was probably responsible for the earthquake of 27.3.1975, whose mechanism is consistent with right-lateral and normal slip on a fault dipping south (see e.g. Taymaz, 1990; Taymaz et al., 1991a; Taymaz and Tan, 2003). The fault that crosses the Gallipoli peninsula, and which was responsible for the 1912 earthquake, is a continuation of the ENE trend of the Saros trough. Surface ruptures in 1912 also showed a combination of right-lateral and normal slip, which is reflected in the topography. Thus the faulting associated with the Saros trough is a semi-continuous feature from about 25°E to the western basin of the Sea of Marmara at about 27.5°E, though the asymmetry, and presumably the polarity of the normal faulting, change along strike: with the faults dipping SE in the western part of the trough, NW along the north shore of the Gallipoli peninsula, and SE along Ganosdağ

(Gaziköy) bounding the NW side of the deep offshore basin in the western Sea of Marmara. Such a change in the polarity of tilting and faulting along the strike of a basin occurs also in the North Gulf of Evvia in central Greece, and is a common feature of extensional grabens. Fault plane solutions in the western part of the North Aegean Trough show mainly strike-slip faulting, consistent with right-lateral slip on NE–SW striking faults. The lack of normal faulting solutions is perhaps surprising, and may simply reflect the short time period over which high quality data have been available. The focal mechanisms obtained by Taymaz et al. (1991a) give the impression that the north and central Aegean Sea is dominated by distributed strike-slip faulting: most of it right-lateral with a NE to ENE strike. Normal faulting must, however, be present: strike-slip faulting alone cannot produce the deep basins, and normal faults are obvious in the bathymetry and limited seismic reflection data. Several of the islands appear to be the uplifted footwall crests of such normal faults, and are adjacent to deep basins offshore. There is further evidence from palaeomagnetism that this western region rotates clockwise relative to stable Europe. However, the strike-slip faulting that enters the central Aegean from the east appears to end abruptly in the SW against the NW-trending normal faults of Greece. The geometry of the deformation resembles the behavior of a system of broken slats (see Taymaz et al., 1991a) attached to margins that rotate.

4 Lake Districts of SW Turkey

The Aegean region has been subject to extension since Miocene time, and this extension has left a pronounced expression in the present-day topography. It is further widely accepted that the rapid extension observed in western Turkey is mainly accommodated by large active normal faults that control the geomorphology. The NE–SW trending Burdur, Acıgöl and Baklan, and NW–SE trending Dinar and Sultandağ–Akşehir basins all bounded by large faults form a system of half-graben whose orientation is evident in both the topography and the tilting of Neogene sediments adjacent to them (e.g. Taymaz and Price, 1992; Taymaz, 1993). The Sultandağ lari has a marked morphological expression ~1,000 m in elevation relative to the surrounding plains and is seismically active. December 15, 2000 (Mw = 6.0) Çay–Sultandağ ı earthquake is the first well-recorded seismological event during the instrumental seismology period showing almost pure normal faulting mechanism. The aftershock zone developed following the main shock agrees well with the distributions of damage, and surface ruptures observed in the field.

5 Orta-Çankırı (Central Turkey)

The seismotectonics of the North Anatolian Fault (NAF) in the vicinity of Orta–Çankırı region is examined, and consists of study of a moderate size (Mw = 6.0) earthquake that occurred on June 6, 2000. The instrumental epicenter of this earthquake is about

25 km south of the North Anatolian Fault Zone (NAFZ), and rapid focal mechanism solutions of USGS-NEIC, and Harvard-CMT show a combination of normal and strike-slip faulting, demonstrating that this earthquake is not directly related to the right-lateral movement of the North Anatolian Fault. However, it is the first event with magnitude greater than 5 between Ankara and Çankırı to be recorded instrumentally since 1900, and therefore contains valuable data to improve our understanding of the neotectonic framework of the northwest central Anatolia. Field observations were carried out in the vicinity of Orta town immediately after the earthquake indicating no apparent surface rupture, but reported damage was most intense in the villages southwest of Orta town (Taymaz et al., 2002, 2007a-b). The June 6, 2000, Orta-Çankırı earthquake occurred close to a restraining bend in the E–W striking right-lateral strike-slip fault that moved in the much larger earthquake of August 13, 1951 (Ms = 6.7).

Hence, we tentatively suggest that one possible explanation for the occurrence of the June 6, 2000, Orta-Çankırı earthquake would be localized clockwise rotations due to shear of the lower crust and lithosphere. Furthermore, analysis of a coseismic interferogram, spanning a 10-month interval, revealed a pear-shaped pattern of deformation with ~5 concentric fringes of range increase (subsidence) in the south and ~2 fringes of range decrease in the north. Inversion of these data suggested that the earthquake occurred on the north–south nodal plane: strike 357 ± 15°, dip 55 ± 19°, rake −20 ± 15°, length 9 ± 2.4 km, depth range 3.6 + 1.0/–2.0 km to 7.4 +7.3/–1.71 km, and 1 m of slip. This solution has a seismic moment of **Mo = 14 × 10^{17} Nm**. The InSAR data also suggest that the North–South fault plane was the one that ruptured during the earthquake, and is in good agreement with the solution independently obtained from the inversion of teleseismic P- and SH- body waveforms. The faulting in this anomalous earthquake could be related to the local geometry of the main strike-slip system (the extension fractures that are oriented parallel to the axis of shortening), and may not be a reliable guide to the regional strain field in the northwest central Anatolia.

6 East Anatolian Fault Zone (E Turkey)

The East Anatolian Fault Zone (EAFZ) is a band of active seismicity and tectonism that joins the eastern end of the North Anatolian Fault Zone (NAFZ) to the Mediterranean Sea in the Gulf of İskenderun. It is much less distinct, both morphologically and structurally, than the North Anatolian Fault Zone that ruptured almost along its entire length in a series of large earthquakes between 1939 and 2000. There has been little seismicity associated with the East Anatolian Fault Zone this century, though many large earthquakes are known to have occurred in or near it within the last 500 years (Ambraseys, 1989). Although some clear strands of NE–SW left-lateral strike-slip faulting are clear on satellite images the structure of the zone is more complicated than this: with several pull-apart basins, conjugate fractures, and also considerable thrusting and folding. Structures within the zone are rarely continuous for longer than a few tens of km, and discontinuities between

fault segments may have controlled the extent of rupture in historical earthquakes (e.g. Ambraseys, 1989; Taymaz et al., 1991b). The knowledge of motions in the East Anatolian Fault Zone is also crucial for an understanding of the present-day kinematics of the eastern Mediterranean. East of the junction between the North and East Anatolian Fault Zones (near Karlıova) is a region of mixed strike-slip and thrust faulting that extends from the Turkey–Iran border north of the Caucasus (Podgorski et al., 2007). This region accommodates the shortening between Arabia and Eurasia, which began about 12 Myr ago and which is proceeding today at a rate of about 27 mm/year in a direction 335° based on the NUVEL-1 plate motion model (DeMets et al., 1990). But, recent estimates of GPS measurments during 1988–1997 give the rate of motion at 18 ± 2 mm/year in the direction 335°.

7 Conclusions

We have briefly summarized the characteristics of the recent earthquakes and active tectonics of Turkey and surroundings with an emphasis on the Marmara Sea region. However, the westernmost continuation of NAF into the Sea of Marmara still requires further investigations to better understand the complexity of faulting associated with earthquakes at depth reaching to seismogenic zones (Furlong et al., 2007). Hence, the present active crustal deformation and monitoring provides an improved physical basis for mitigation of the effects of future earthquakes in this vulnerable region.

Acknowledgements We would like to thank the İstanbul Technical University (İTÜ) Research Fund, the Scientific and Technical Research Council of Turkey (TÜBİTAK), and the Turkish Academy of Sciences (TÜBA), in the framework of the Young Scientist Award Program (TT/TÜBAGEBİP/2001-2-17), for their support, and Alexander Von Humboldt (AvH) Foundation, for their support. Constructive comments from drs. Husebye are appreciated.

References

Ambraseys, N. N., 1989. Temporary seismic quiescence: SE Turkey. *Geophysical Journal International* 96, 311–331.

Armijo, R., Meyer, B., Navarro, S., King, G., Barka, A., 2002. Asymmetric slip partitioning in the Sea of Marmara pull-apart: A clue to propagation processes of the North Anatolian fault? *Terra Nova* 14, 80–86.

DeMets, C., Gordon, R. G., Argus, D. F., Stein, S., 1990. Current plate motions. *Geophysical Journal International*, 101, 425–478.

Furlong, K., Beroza, G. C., Brun, J-P., Cowie, P. A., Handy, M. R., Mooney, W. D., Taymaz, T., Teyssier, C., Vauchez, A., Wernicke, B., 2007. Nucleation and Growth of Fault Systems, *In: TECTONIC FAULTS– Agents of Change on a Dynamic Earth*, pp: 78–98, *The Massachusetts Institute of Technology Press*, Cambridge, Massachusetts 02142 USA, 504 pp, ISBN: 978-0-262-08362-1.

Georgiev, I., Dimitrov, D., Belijashki, T., Pashova, L., Shanov, S., Nikolov, G., 2007. Geodetic constraints on kinematics of southwestern Bulgaria from GPS and levelling data. *In:* The

Geodynamics of the Aegean and Anatolia, *The Geological Society of London, Special Publications*, vol: 291, pp. 143–157, ISBN: 978-1-86239-239-7.

Kotzev et al., 2008. Crustal Motion and Strain Accumulation in the South Balkan Region Inferred from GPS Measurements. In E.S. Husebye (ed.). Earthquake Monitoring and Seismic Hazard in Balkan countries. Springer Publishing, Berline, 19–43.

Le Pichon, X., et al., 2001. The active main Marmara Fault, Earth. Planet. *Sci. Lett*. 192, 595–616.

McClusky et al., 2000. Global positioning system constraints on plate kinematics and dynamics in the eastern Mediterranean and Caucasus. *J. Geophys. Res*. 105, 5695–5719.

McClusky, S., Reilinger, R., Mahmoud, S., Ben Sari, D., Tealeb, A., 2003. GPS constraints on Africa (Nubia) and Arabia plate motions, *Geophysical Journal International*, 155 (1),126–138.

Parson, T., 2004. Recalculated probability of M ≥ 7 earthquakes beneath the Sea of Marmara, Turkey. *J. Geophys. Res*. 109, B05304, doi:10.1029/2003JB002667.

Podgorski, J., Hearn, E. H., Mcclusky, S., Reilinger, R., Taymaz, T., Tan, O., Prilepin, M., Guseva, T., Nadariya, M., 2007. Postseismic Deformation Following the 1991 Racha, Georgia Earthquake, Geophysical Research Letters, 34 (4): L04310, doi:10.1029/2006GL028477.

Sato, T., Kasahara, J., Taymaz, T., Ito, M., Kamimura, A., Hayakaw, T., Tan, O., 2004. A study of microearthquake seismicity and focal mechanisms within the Sea of Marmara (NW Turkey) using ocean bottom seismometers (OBSs), Special Issue on Active Faulting and Crustal Deformation in the Eastern Mediterranean Region. *Tectonophysics* 303–314, [Taymaz, Westaway and Reilinger (eds.), 391(1–4), p. 375.

Smith, A. D., Taymaz, T., et al., 1995. High resolution seismic profiling in the Sea of Marmara (NW Turkey): Late Quaternary tectonics and sedimentation. *Bulletin of Geological Society of America* 107, 923–936.

Tan, O., Taymaz, T., 2006. Active Tectonics of the Caucasus: Earthquake Source Mechanisms and Rupture Histories Obtained From Inversion of Teleseismic Body Waveforms. *In: Post-Collisional Tectonics and Magmatism in the Mediterranean Region and Asia, Geological Society of America, Special Paper* 409, pp. 531–578, doi:10.1130/2006.2409 (25).

Taymaz, T., 1990. Earthquake Source Parameters in the Eastern Mediterranean Region. Ph.D. thesis, Darwin College, 244 pp.,University of Cambridge, UK.

Taymaz, T., 1993. The source parameters of Çubukdağ (Western Turkey) earthquake of 11 October 1986. *Geophysical Journal International* 113, 260–267.

Taymaz, T., 1999. Seismotectonics of the Marmara Region: Source Characteristics of 1999 Gölcük-Sapanca-Düzce Earthquakes. Proceedings of ITU-IAHS, International Conference On The Kocaeli Earthquake 17 August 1999, 2–5 December 1999, Istanbul, Turkey, pp. 55–78.

Taymaz, T., Price, S., 1992. The 1971 May 12 Burdur earthquake sequence, SW Turkey: a synthesis of seismological and geological observations. *Geophysical Journal International* 108, 589–603.

Taymaz, T., Tan, O., 2003. Seismotectonics of Saros Bay (NW Turkey) and Surroundings: Source Parameters and Rupture History of July 6, 2003 Mw = 5.7 Saros Earthquake, Recent Progress in Tectonics and Paleoseismology and Field Training Course in Paleoseismology, P. 89, Middle East Technical University: 31 August–12 September 2003, Ankara, Turkey.

Taymaz, T., Jackson, J., McKenzie, D., 1991a. Active Tectonics of the North and Central Aegean Sea. *Geophysical Journal International* 106, 433–490.

Taymaz, T., Eyidoğan, H., Jackson, J., 1991b. Source Parameters of large earthquakes in the East Anatolian Fault Zone (Turkey). *Geophysical Journal International* 106, 537–550.

Taymaz, T., Westaway, R., Reilinger, R., 2004a. Active Faulting and Crustal Deformation in the Eastern Mediterranean Region, *Tectonophysics*, 391, 1–9.

Taymaz, T., Wright, T., Tan, O., Fielding, E., Seyitoğlu, G., 2002. Source Characteristics of Mw = 6.0 June 6, 2000, Orta–Çankiri (Central Turkey) Earthquake: A Synthesis of Seismological, Geological and Geodetic (InSAR) Observations, and Internal Deformation of Anatolian Plate, 1st International Symposium of Istanbul Technical University the Faculty of Mines on Earth Sciences and Engineering, p. 63, Istanbul, Turkey.

Taymaz, T., Tan, O., Yolsal, S., 2004b. Active Tectonics of Turkey and Surroundings: Seismic Risk in the Marmara Sea Region, *In* Fujii, N., Kasahara, J., Higashihara, H., and Ogawa, K.

(Eds.), *The Proceedings of "1st International Workshop on Active Monitoring in the Solid Earth Geophysics (IWAM04)"*, Extended Abstract Book: p. 110–115, Task Group for Active Monitoring, Mizunami City Culture Center, Gifu, Japan.

Taymaz, T., Yılmaz, Y., Dilek, Y., 2007a. The Geodynamics of the Aegean and Anatolia. *The Geological Society of London, Special Publications*, vol: 291, pp. 1–16, ISBN: 978-1-86239-239-7.

Taymaz, T., Wright, T., Yolsal, S., Tan, O., Fielding, E., Seyitoğlu, G., 2007b. Source Characteristics of June 6, 2000 Orta–Çankırı (Central Turkey) Earthquake: a synthesis of seismological, geological and geodetic (InSAR) observations, and internal deformation of Anatolian plate, *In:* The Geodynamics of the Aegean and Anatolia, *The Geological Society of London, Special Publications*, vol: 291, pp. 259–290, ISBN: 978-1-86239-239-7.

Yolsal, S., Taymaz, T., 2007. Source mechanism and rupture histories of the recent Gulf of Gökova and Sığacık Bay earthquakes, European Geosciences Union (EGU) General Assembly 2007, 15–20 April 2007, *Geophysical Research Abstracts*, Vol. 9, Article No: EGU2007-A-01776, Vienna-Austria.

Yolsal, S., Taymaz, T., Yalçıner, A.C., 2007a. Source Characteristics of Earthquakes along the Hellenic and Cyprus Arcs and Simulation of Historical Tsunamis, European Geosciences Union (EGU) General Assembly 2007, 15–20 April 2007, *Geophysical Research Abstracts*, Vol. 9, Article No: EGU2007-A-02306, Vienna-Austria.

Yolsal, S., Taymaz, T., Yalçıner, A.C., 2007b. Understanding Tsunamis, Potential Source Regions and Tsunami Prone Mechanisms in the Eastern Mediterranean, *In:* The Geodynamics of the Aegean and Anatolia, *The Geological Society of London, Special Publications*, vol: 291, pp. 201–230, ISBN: 978-1-86239-239-7.

Estimates of Stress Drop and High Frequency Diminution Parameter from Strong Motion Data Recorded in Albania

L. Lambro Duni* and Neki Kuka

Abstract We analyze ten recent records of the Albanian strong motion network with the aim to estimate the stress drop and high-frequency diminution parameters. Except for the earthquake record of 23/11/2004 in Leskoviku, near the border with Greece (Mw = 5.4), all the others are small intensity records with the value of Mw around Mw = 3.9–4.9. From seven accelerograms we found the value of the stress parameter in the range 15 bars $\leq \Delta\sigma \leq$ 60 bars, with three aftershocks showing the lowest values (15 bars $\leq \Delta\sigma \leq$ 40 bars). After comparison with the actual map of neotectonic zonation of Albania, we conclude that all these events had been generated in a normal faulting environment. The remaining three accelerograms that were recorded in Tirana (Central Albania) and generated in a thrust faulting environment, express higher values of the stress parameter, in the range 200 bars $\leq \Delta\sigma \leq$ 300 bars. The high frequency diminution parameter varies between $0.02 \leq \kappa o \leq 0.04$ for rock sites, ground type A according to Eurocode 8 (EC8) classification, and $\kappa o = 0.07$ for soil sites, ground type B according to Eurocode 8 (EC8). Based on $\Delta\sigma$ estimates and taking into account the variation of this parameter between various tectonic settings of the country, we can establish a stochastic model that could be used for predictions of strong ground motions based on the simple point source model, at least for the areas where the records have been collected.

Keywords strong motion, stress parameter, stochastic model, ground motion simulation

1 Introduction

We are facing increased interest by engineers on seismic acceleration time histories for various kinds of structural analyses in the construction sector. Moreover, the new standards of the building code strongly recommend usages of such information

Institute of Seismology, Academy of Sciences of Albania, Rruga "Don Bosko", No. 60, Tirana, Albania

* To whom correspondence should be addressed. E-mail: duni@sizmo.edu.al

E.S. Husebye (ed.), *Earthquake Monitoring and Seismic Hazard Mitigation in Balkan Countries.*

and analyses. Up to now such undertakings were hampered by the almost totally lack of strong motion records in Albania. Recently, a strong motion network has been put into operation and a small number of records have been collected (Duni et al., 2004). In parallel to the network maintenance and extension we have focused our attention towards the simulation of ground motions. Taking this into account, we have posed the objective to analyze the latest records of the Albanian Strong Motion Network (ASMN) in order to have the necessary data for the construction of a seismological model that could support the simulation of high frequency ground motions based on theoretical models simulations, the most popular of which is the stochastic model of Hanks and McGuire (1981). The most important parameters of this model are the stress parameter ($\Delta\sigma$) and high-frequency diminution parameter (κ_0).

2 Data

The instruments of the ASMN are SMA-1 accelerographs upgraded with the digital QDR kits of Kinemetrics (Duni et al., 2004). After the first installation in June 2002, the network has recorded ten time histories of nine earthquakes, among them five main hocks. These are the earthquakes of March 27, 2003, and June 28, 2004, near Tepelena (Southern Albania); the earthquakes of December 5, 2003, and August 28, 2004, near Tirana (Central Albania) and the earthquake of November 23, 2004, in Leskoviku, near the border to Greece. The remaining events are aftershocks of the June 28, 2004, earthquake. The earthquake of August 28, 2004, is the only event that has been recorded by two instruments situated at the center of the Tirana City on alluvium sediments. All these records have been processed using the SMA software of Kinemetrics. In Figure 1 and Table 1 we present information on these earthquakes and the filters applied during the processing. As it may be seen from Figure 1, except the earthquakes of November 23, 2004 and of August 28, 2004, there is no information of focal mechanisms for the other events.

The seismotectonic features of the areas where the epicenters of these earthquakes are located are presented in the map of Neotectonic Zonation of Albania in Figure 2 (Aliaj et al., 1996). The earthquakes recorded by the TPE station belongs to the external area of the Alpine folding strongly affected by pre-Pliocene compressional movements where reverse faults-thrusts and back-thrusts prevail. The earthquake with the code TIR-03-1 recorded by TIR and the earthquake LSK-04-1 recorded by the LSK station have their epicenters in the internal area of Alpine folding affected by extensional tectonics during the Pliocene to Quaternary. These movements resulted in the establishment of horst-graben structures with mainly normal faults having a strike-slip component. Finally the earthquake TIR-04-1 recorded by TIR2 and TIR3 belongs to the area of periadriatic foredeep strongly affected by post-Pliocene compression movements, also with reverse faults-thrusts and back-thrusts. In general, the dashed line shown in Figure 2 divides the eastern areas characterized

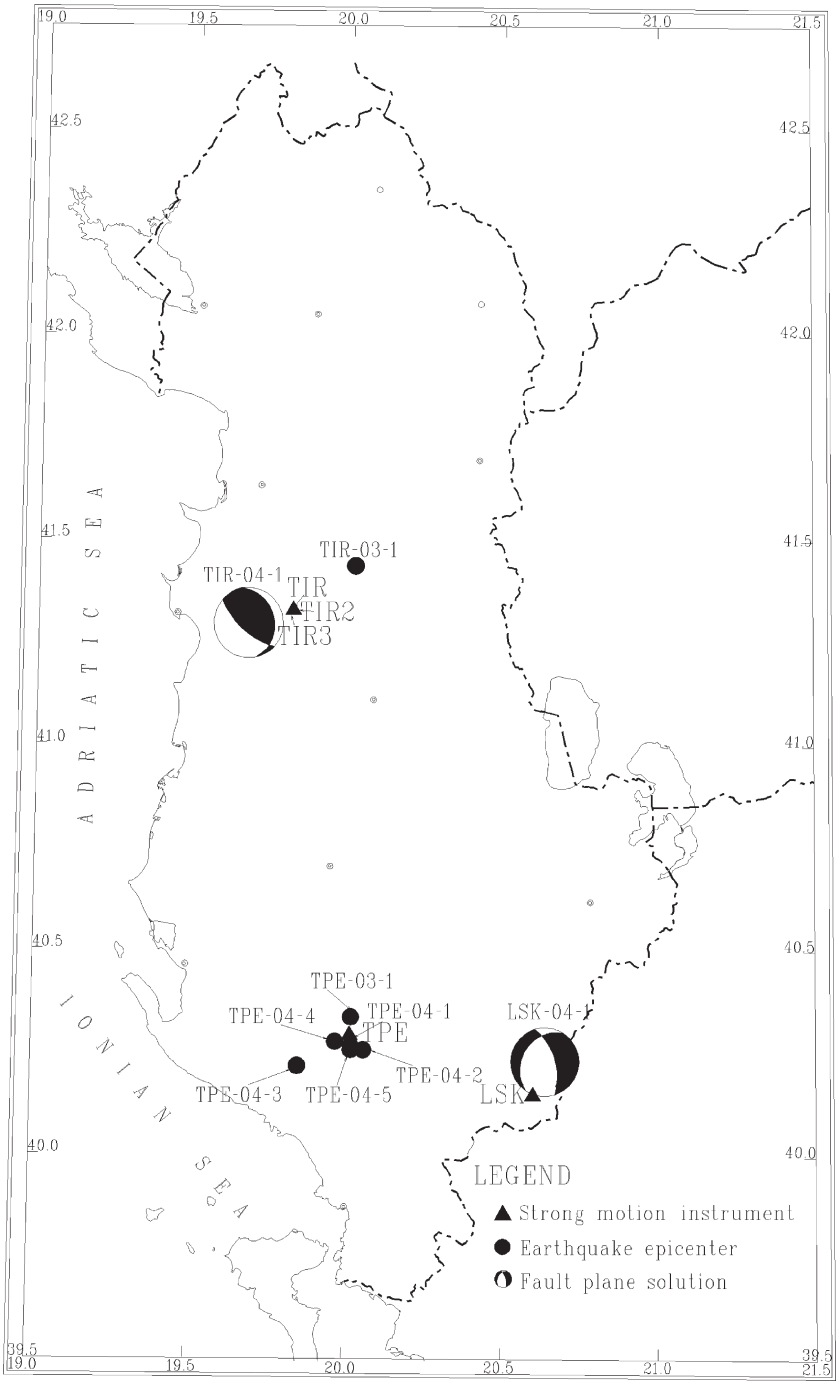

Figure 1 Map of Albania showing earthquake locations, year, month and day of the examined events, as well as the fault plane solution for two of them and accelerographic stations that recorded the events

Table 1 Earthquake and recording information

			Epic. coordinates						Filters (Hz)	
Earthq code	Date (yymmdd)	Time (hhmmss)	Lat	Lon	Geograph. name	Mw	Depth (km)	Ep Dist (km)	Low-c	High-c.
TPE-03-1	030327	043541	40.34	20.02	Bënçë	4.9	20	5.6	1.6–2.0	25–27
TIR-03-1	031205	033149	41.44	20.02	Xibër	4.8	24	16.7	1.6–2.0	25–27
TPE-04-1	040628	174434	40.27	20.02	Tepelenë	4.4	10	2.4	0.4–0.6	25–27
TPE-04-2	040708	174027	40.26	20.06	Tepelenë	4.0	7	5.4	1.9–2.2	25–27
TPE-04-3	040711	131624	40.22	19.85	Lekdush	3.9	5	15.7	2.8–3.6	25–27
TPE-04-4	040712	044240	40.28	19.97	Tepelenë	4.0	1	3.6	0.6–1.0	25–27
TPE-04-5	040712	054050	40.26	20.02	Tepelenë	4.0	1	3.4	2.6–3.0	25–27
TIR-04-1	040828	221648	41.31	19.69	Prezë	4.0	23	11.3	0.8–1.3	25–27
TIR-04-1	040828	221648	41.31	19.69	Prezë	4.0	23	10.9	2.3–2.5	25–27
LSK-04-1	041123	022614	40.23	20.64	Leskovik	5.4	6.9	9.5	0.2–0.3	25–27

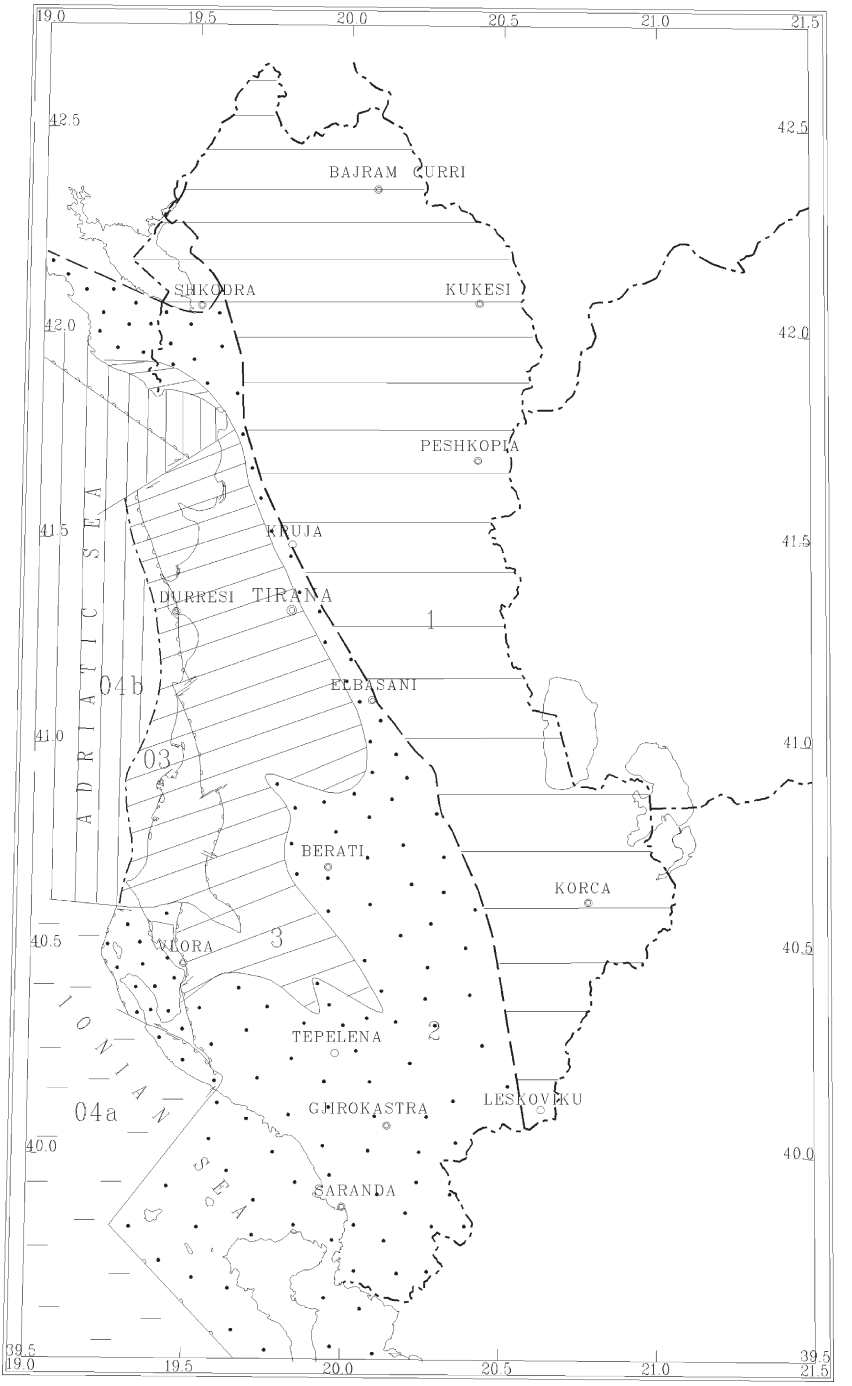

Figure 2 Map of Neotectonic Zonation of Albania (Aliaj et al., 1996) which is subdivided in 4 large neotectonic units. 1. Internal area of Alpine folding affected by extensional tectonics; 2. External area of Alpine folding strongly affected by pre-Pliocene compression movements (02-its offshore sectors); 3. Periadriatic Foredeep strongly affected by post-pliocene compression movements (03-its offshore sectors); 4. Pliocene-Quaternary Foreland in Adriatic and Ionian offshore (04a-Apulian platform; 04b-Albanian basin)

with extensional movements relative those westward with compressional tectonic movements.

We considered only the horizontal components of the above records. Because we are trying to match spectral amplitudes and shapes it is necessary to account for site geology. Following other studies regarding the application of the stochastic method in ground motion predictions and analyses of source parameters (Frankel et al., 1996; Margaris and Boore, 1998), we have assigned each site to one of three classes: B, C and D of the NEHRP (1994) provisions. These are defined in terms of shear-wave velocity averaged over the top 30 m (V30 > 750 m/s for B, between 360 and 760 m/s for C and between 180 and 360 m/s for D). Comparisons made with the classification of ground types given in the EC8 (2003) show that the soil class B of NEHRP (1994) provisions corresponds to type A ground of EC8; soil class C of NEHRP (1994) provisions corresponds to type B ground of EC8, while soil class D of NEHRP provisions corresponds roughly to type C ground of the EC8 classification. In Table 2 we have assigned subjectively the site class B for the TIR, TPE and LSK stations according to the NEHRP (1994) provisions, taken into account that these stations are located on limestone (TPE and LSK) and sandstone (TIR) sediments. For TIR2 and TIR3 site classification we used the value of VS determined by the microzonation study of the Tirana City for the areas where these stations are located. For these two stations we assigned the soil class C according to the NEHRP (1994) provisions.

Regarding Mo evaluations, unfortunately there are no independent estimates of seismic moments for the events listed in Table 1. Exceptions are the LSK-04-1 event for which we have assigned the value of Mo = 1.85 × 1024 according to Harvard and the event TIR-04-1, Mo = 1.16 × 1022 according to SED. Independent evaluations of seismic moments are preferred in many studies of source parameters (Cocco and Roveli, 1989; Roveli et al., 1988; Roveli et al., 1991; Margaris and Hatzidimitriou, 2002). The simultaneous inversion of the ground motion spectrum in terms of both seismic moment Mo and corner frequency fc results in large variations reflecting difficulties in controlling the bias due to their analytical dependence. On the other hand, knowing that the seismic moment is proportional to the low-frequency level Ω of the far-field spectrum, independent estimates of seismic moment are feasible using other types of observation. The reason is that strong motion records are most reliable at high frequencies, but at lower frequencies such analyses are problematic (Roveli et al., 1991).

Table 2 Station information

Station		Geographic coordinates		NEHRP	
code	Station name	Lat	Lon	(1994)	Type
TPE	Tepelena Seismological Station	40.290	20.010	B	QDR
TIR	Tirana Seismological Station	41.350	19.860	B	QDR
TIR2	Building of Academy of Sciences	41.326	19.824	C	QDR
TIR3	Building of UNDP	41.323	19.819	C	QDR
LSK	Leskoviku Seismological Station	40.150	20.600	B	QDR

For the evaluation of seismic moments of our events, we used the relation developed by Muço et al. (2002) who considered the approach of Biswas and Aki (1984) based on coda decay rates:

$$\log M_0 = \log A + 3.25 * \log t + 15.25 \tag{1}$$

where Mo is seismic moment in dyne-cm, A is the peak-to-peak coda-wave amplitude in mm measured on the vertical component of TIR analog seismograms recorded at the gain normalized to 10 dB at time t (s) relative to the origin time. For each earthquake (except the TPE-04-5 event) we measured the input parameters of (1) on the seismograms of TIR. Muço et al. (2002) have also evaluated the relation between Mo and ML in the range $2.2 \leq ML \leq 5.7$:

$$\log M_0 = \frac{1}{0.0493 - 0.0015 M_L} \tag{2}$$

The two equations give roughly the same results for TPE-04-2, TPE-04-3, TPE-04-4 and TIR-04-1 events. Higher values of Mo were found for events TPE-03-1 and TIR-03-1 using (1) instead of relation (2) (2.51 × 1023 versus 9.63 × 1022 for the TPE-03-1 event and 1.51 × 1023 versus 7.68 × 1022 for the TIR-03-1 event). Only for the TPE-04-1 event the evaluation of seismic moment by (1) is smaller than the evaluation made by equation (2) 3.98 × 1022 versus 8.43 × 1022. For the TPE-04-5 event we have only the evaluation taken by (2). This was due to the very small amplitudes of coda waves on the vertical component of TIR for this event. Anyway, for all the other events we have accepted the evaluation of seismic moment made by equation (1). Finally, the well-known relation of Hanks and Kanamori (1979) was used to evaluate the moment magnitude for all our events. These estimates are shown in Table 3. Using our data through equation (1), we have the values Mw = 5.3 for LSK-04-1 and Mw = 4.3 for TIR-04-1, while independent seismic moment results with the value Mw = 5.4 (Harvard) and Mw = 4.0 (SED), respectively. Anyway, we have only two independent seismic moment values for our data, so it is difficult to make comparison with the corresponding estimates of international agencies.

Focal depths and epicentral distances shown in Table 1 were taken from the preliminary Bulletins of the Albanian Seismological Network (ASN). We adopt here the hypocentral distance as the best parameter to be used in our simulations because it is presumed to yield results that correlate more precisely with the observed Fourier spectral values (Cocco and Roveli 1989; Margaris and Hatzidimitriou 2002).

Table 3 Estimates of ML and Mw

Earthquake code	Date (yymmdd)	Time (hhmmss)	Magnitude (ML)	Mo dyne-cm	Mw
TPE-03-1	030327	043541	4.0	2.51 × 1023	4.9
TIR-03-1	031205	033149	4.0	1.51 × 1023	4.8
TPE-04-1	040628	174434	3.9	3.98 × 1022	4.4
TPE-04-2	040708	174027	3.4	1.07 × 1022	4.0
TPE-04-3	040711	131624	2.6	9.12 × 1021	3.9
TPE-04-4	040712	044240	3.1	1.15 × 1022	4.0
TPE-04-5	040712	054050	3.0	9.49 × 1021	4.0
TIR-04-1	040828	221648	4.0	1.16 × 1022	4.0
LSK-04-1	041123	022614	4.8	1.85 × 1024	5.4

3 Method of analysis

The spectrum model considered has the form (Boore 1983; Joyner and Boore, 1988; Boore 1996; Boore, 2002):

$$R(f) = C \cdot S(f) \cdot A(f) \cdot D(f) \cdot I(f) \tag{3}$$

where C is a scaling factor, given by:

$$C = \frac{F_s R_{\theta,\phi} P}{4\pi\rho\beta^3 R\Delta} \tag{4}$$

we take into account the effects of the free surface by the correction Fs, the average radiation pattern Rθ,φ; and the partition of energy between the two horizontal components by P. The density is ρ; the shear-wave velocity in the lithosphere β; and distance RΔ. In equation (3) S(f) is the source spectrum, A(f) is the site amplification factor, D(f) is the diminution factor and I(f) = (2πf)p is a factor that includes instrumental response (p = 1 or 2, for velocity and acceleration respectively) and type of filters used in the processing. For the source spectrum S(f) we adopted an ω-square model for shear waves for the ground acceleration and the standard expression:

$$S(f) = \frac{Mo}{1 + (f / fo)^2} \tag{5}$$

where Mo is the seismic moment and fo is the corner frequency given by the relation:

$$f_0 = 4.9 \times 10^6 \beta (\Delta\delta / M_0)^{1/3} \tag{6}$$

Mo and fo are the two basic parameters that characterize the source radiation. Another parameter determined in this study on a site-by-site basis is κ (kappa), the high cut-off filter, which controls the path-independent high-frequency decay of the spectrum. The diminution function D(f) in (3) is given by:

$$D(f) = e^{-\pi(r/Q(f)\beta+k)f} \tag{7}$$

The path-dependent part of the diminution is controlled by the function Q(f) or the inelastic absorption. In fact, the source spectrum diminishes with distance from the source as a result of geometric spreading (1/R) and inelastic attenuation. Geometric spreading reduces the entire spectrum, whereas inelastic attenuation and scattering combine to alter its shape by absorbing higher signal frequencies faster with distance than lower frequencies (Boore and Atkinson, 1987). Due to the fact that fault-to-station distances in our study are relatively small, Q(f) does not influence the results significantly. We have used the Q function given by Boore (1984) which is detailed in Table 5. This function has been used by other authors dealing with analysis of strong motion data from our area and with good results (Margaris and Boore, 1998; Margaris and Hatzidimitriou, 2002).

An important aspect of our analyses is the proper choice of the amplification factor A(f). The stress parameter we intend to estimate through our analysis depends on the amplification we apply in the simulations (Margaris and Boore, 1998; Margaris and Hatzidimitriou, 2002). Unfortunately, there are no studies describing the frequency-dependent amplification factors in Albania. A small number of geophysical-geotechnical studies have been carried out during the microzonation studies of different towns thereby describing the distribution of VS with depth mainly for soil site conditions but not extended to analyze the frequency-dependent amplification. For this

Table 4 Amplification factors according Boore and Joyner (1997), as given in Margaris and Boore (1998)

Site Class B		Site Class C		Site Class D	
Freq. (Hz)	Amplification	Freq. (Hz)	Amplification	Freq. (Hz)	Amplification
0.01	1.00	0.01	1.00	0.01	1.00
0.10	1.06	0.09	1.21	0.09	1.44
0.24	1.13	0.16	1.32	0.16	1.73
0.45	1.22	0.51	1.59	0.51	2.62
0.79	1.38	0.84	1.77	0.84	3.12
1.38	1.65	1.25	1.96	1.25	3.42
1.93	1.86	2.26	2.25	2.26	3.86
2.85	2.05	3.17	2.42	3.17	4.07
4.03	2.17	6.05	2.70	6.05	5.11
6.34	2.28	16.60	3.25	16.60	5.11
12.54	2.38	61.20	4.15	61.20	5.11
21.23	2.42				
33.39	2.44				
82.00	2.46				

Table 5 Parameters of the Stochastic Model similar to that given in Margaris and Boore (1998)

No.	Source properties
1.	Material properties
	P = 2.75 gm/cm3
	β =3.65 km/s
2.	Single-corner frequency ω-2 spectra and stress parameter Δσ on a site-by site basis as given inTable 8
	Path properties
1.	Q
	Q = 275 (f/0.1) − 2.0, f ≤ 0.2
	Q = 88 (f/1.0) + 0.9, f ≥ 0.6
	Qfor0. [Q for 0.2 < f < 0.6 determined from power-law fit to values of Q at f = 0.2 and f = 0.6 Hz (see Boore 1996). The Q function is that given in Boore (1984)]
2.	1/r geometrical spreading
3.	Duration = 1/fo + 0.05 r
	Site properties
1.	Partition factor = 0.71
2.	Radiation coefficient = 0.63
3.	Free surface factor = 2.0
4.	Site amplification and kappa on a site-by site basis, as given in Tables 4 and 7.

reason, we found it appropriate to use the amplification factors given by Boore and Joyner (1997) for generic rock sites in WNA and divided in three categories according to the site categories specified by the NEHRP (1994) provisions. These amplification factors are shown in Table 4. All the input parameters used in equation (3) are shown in Table 5.

4 Data analyses

In our study we considered only the horizontal components of the records. The basic data for the stochastic-model are the Fourier amplitude spectra, 5%-damped pseudorelative velocity spectra (PSRV) as well as peak acceleration, velocity and displacement from the 20 horizontal-component accelerograms. The Fourier spectra were computed for windows that included the consistent parts of the S-wave arrivals and were not smoothed. The PSRV spectra were computed for the whole waveform. The main purpose was to define the Brune stress parameter ($\Delta\sigma$) and high-frequency diminution parameter, kappa (κ) from our present data set by fitting observed PSRV spectra with a single corner-frequency source model. According to Margaris and Boore (1998), the use of PSRV spectra as the main datum from which these parameters are derived is justified for several reasons: (i) PSRV is more closely related to engineering needs than Fourier amplitude spectrum (FAS), (ii) PSRV is not sensitive to window length as is FAS estimates, and (iii) we want a model that provides a reasonable approximation over a wide frequency range, and

this is best determined by fitting a spectrum rather than a few peak ground-motion parameters (Margaris and Boore, 1998).

Our analysis started with determination of the band-pass filter parameters in order to remove the noise from the records. The corner frequencies of the filter were determined by visually comparing the Fast Fourier Transform (FFT) amplitude spectrum of the signal to that of the preceeding noise. We used mostly the pre-event portions of each uncorrected record for the comparisons because post-event signals show generally larger amplitude spectra. The filters applied on the uncorrected records are given in Table 1, while in the Table 6 we present the peak values of acceleration, velocity and displacement of all components of all recorded events.

4.1 Measurement of High Frequency Diminution Parameter κ and Determination of KO

For the measurement of κ we applied Anderson and Hough's (1984) procedure. For this reason we used for every horizontal component a time window beginning with the shear wave arrival which was extended to include the most significant part of the uncorrected accelerograms. The data sets were windowed by means of a 10 per cent cosine tapering and the resulting spectra were corrected for the instrument response in the frequency domain. In Figure 3 we present the uncorrected horizontal components of all the earthquakes included in our analysis and the windows used for computing the Fourier amplitude spectrum needed in the determination of κ. According to the Anderson and Hough (1984) procedure we applied a least-squares-mean algorithm in the band up to 15–25 Hz (subjectively chosen), depending on the level of high-frequency noise in the spectrum. Each component was considered separately. Figure 4 displays the spectra and the regression fits. The measured values of κ are given in Table 7 and include site amplification and whole-path attenuation. If we used κ for κo in equation (7), we would be counting twice the site amplification and whole-path attenuation, at least as far as the high-frequency diminution of the spectrum is concerned (Margaris and Boore 1998).

For this reason we used the procedure proposed by Margaris and Boore (1998) by correcting the measured κ for the effect of the site amplification and the whole-path attenuation by first computing the spectral amplitudes using the equation (3) with $\kappa_o = \kappa$ and the appropriate site amplification from Table 4. We then used Anderson and Hough's (1984) procedure to find κ' for this simulated spectrum and obtained κ_o from the equation

$$\kappa_0 = k + (k - k') \tag{8}$$

The corrected κ_o are shown in Table 7. This procedure gives κo values that are consistent with the parameters in the simulations and the κ-values obtained from

Table 6 Peak values of acceleration, velocity and displacement

		Acceleration (cm/s/s)			Velocity (cm/s)			Displacement (cm)		
Earthquake code	Station ID	Z	E–W	N–S	Z	E–W	N–S	Z	E–W	N–S
TPE-03-1	TPE	−1.35	16.82	−20.20	0.247	0.305	0.387	0.007	0.009	−0.007
TIR-03-1	TIR	12.91	25.76	22.66	−0.205	−0.647	−0.420	0.006	−0.020	−0.011
TPE-04-1	TPE	41.63	−78.25	−74.07	−0.662	−1.757	−1.230	−0.030	−0.106	0.071
TPE-04-2	TPE	−0.44	−46.46	−30.44	−0.421	−0.716	−0.377	−0.008	−0.013	−0.009
TPE-04-3	TPE	6.77	20.04	22.36	0.129	0.250	0.253	−0.003	−0.006	0.006
TPE-04-4	TPE	27.69	55.05	−59.08	−0.427	−0.646	−0.812	−0.009	−0.029	0.026
TPE-04-5	TPE	12.37	−46.02	47.66	−0.161	−0.375	−0.425	−0.003	−0.006	0.005
TIR-04-1	TIR2	27.88	−46.87	−3.99	−0.358	0.639	−0.081	−0.009	−0.011	−0.003
TIR-04-1	TIR3	4.05	35.47	7.33	−0.101	1.121	−0.248	−0.004	−0.043	−0.010
LSK-04-1	LSK	−4.70	−52.65	88.84	−3.139	−5.627	8.475	−0.771	1.316	1.477

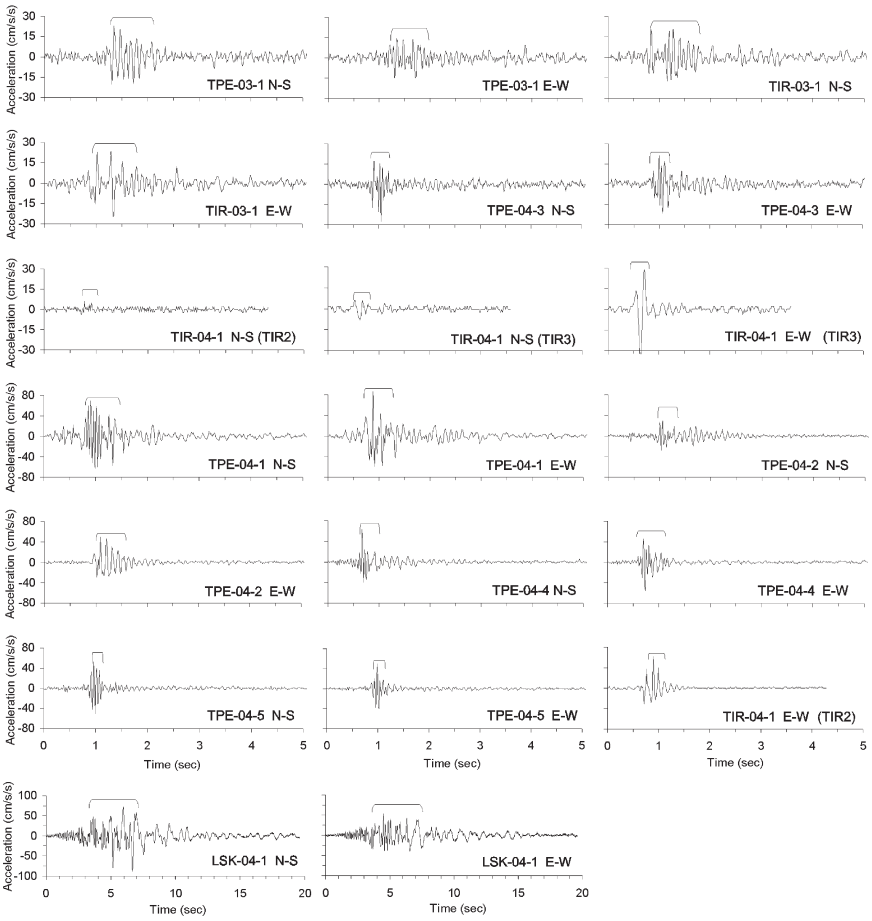

Figure 3 Horizontal uncorrected component records of the data set and the windows used for the computing the Fourier-amplitude spectrum needed in the determination of κ

the recordings at each site (Margaris and Boore, 1998). The difference of the measured values between two components in each record is not large, except for the TIR3 station records. The mean values of κo for the two components of each recording are also shown in Table 7; in general, the modifications to κ are small.

In Figure 5 we have presented the distribution of κo values versus magnitude and hypocentral distance in order to investigate any possible dependence of κo on these two parameters. No particular trend is observed and the κo parameter may be considered constant in the range 0.02–0.04 for all events regardless of their magnitudes and paths. However, the number of large earthquakes is very limited and we are dealing with small hypocentral distances in our data set. The majority of stations have rock sites that correspond to Class A soil according to EC8, while for the

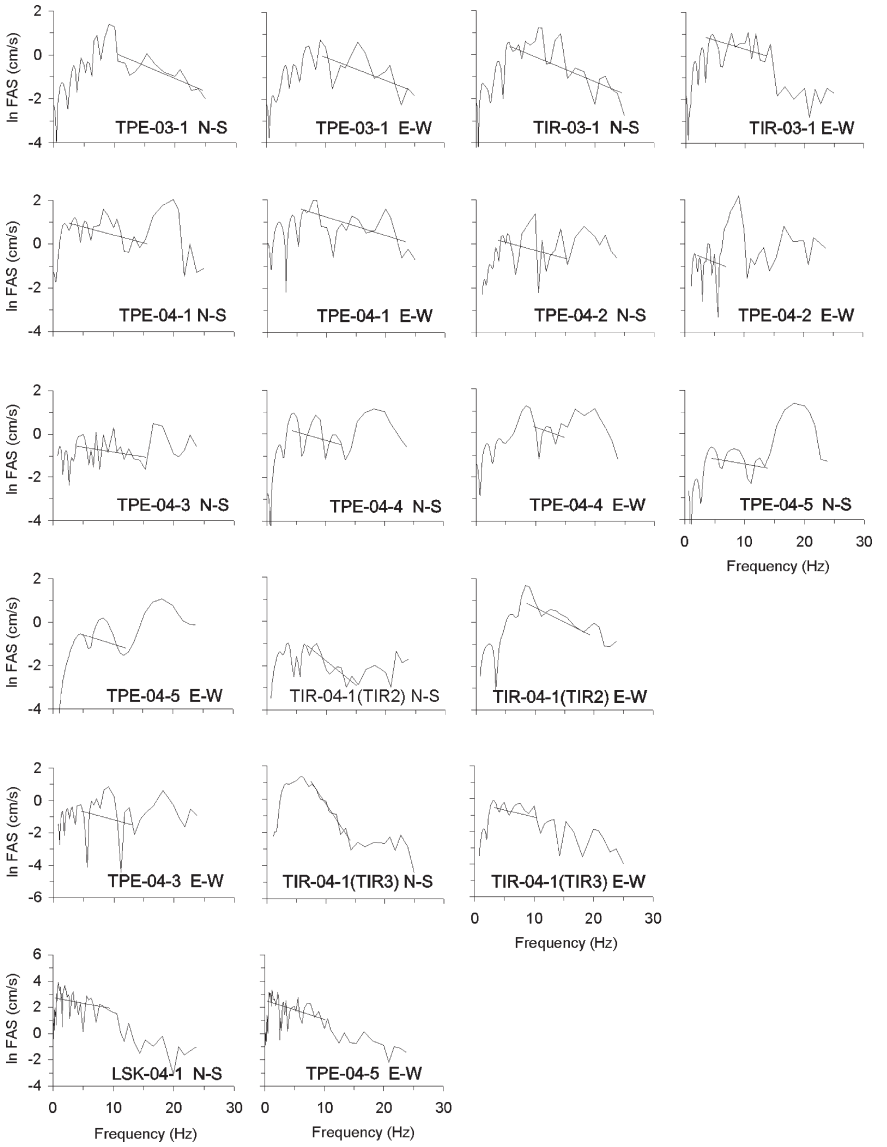

Figure 4 Measurement of κ for each horizontal component. The straight lines show the regression fits to ln spectral amplitudes versus frequency

TIR2 and TIR3 sites we observe larger value for κo. Accordingly, the generalized soil profiles formulated during the microzonation study of Tirana City for these two sites being only located 400 m apart (Koçiu et al., 1988), they belong to site class B according to the EC8 standard.

Table 7 Kappa values

Earthquake code	Date (yymmdd)	Time (hhmmss)	Station	κ (N–S)	κ (E–W)	κ (Average)	κ'	κo
TPE-03-1	030327	043541	TPE	0.0370	0.0341	0.0355	0.0348	0.0362
TIR-03-1	031205	033149	TIR	0.0420	0.0255	0.0338	0.0335	0.0341
TPE-04-1	040628	174434	TPE	0.0255	0.0209	0.0232	0.0228	0.0236
TPE-04-2	040708	174027	TPE	0.0175	0.0297	0.0236	0.0230	0.0242
TPE-04-3	040711	131624	TPE	0.0225	0.0183	0.0204	0.0198	0.0210
TPE-04-4	040712	044240	TPE	0.0290	0.0478	0.0384	0.0379	0.0389
TPE-04-5	040712	054050	TPE	0.0223	0.0219	0.0221	0.0195	0.0247
TIR-04-1	040828	221648	TIR2	0.0665	0.0578	0.0622	0.0561	0.0683
TIR-04-1	040828	221648	TIR3	0.1150	0.0211	0.0681	0.0633	0.0729
LSK-04-1	041123	022614	LSK	0.0291	0.0344	0.0318	0.0313	0.0323

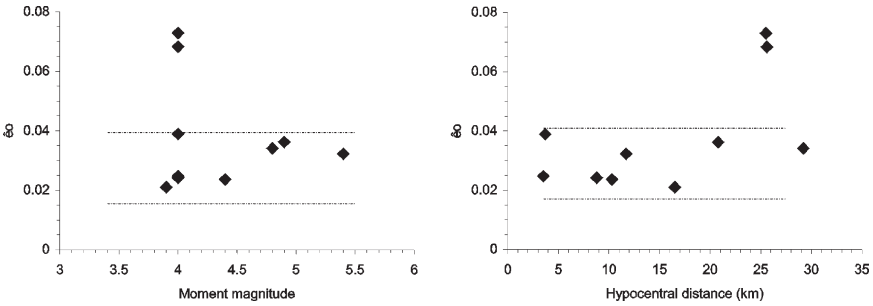

Figure 5 κ versus moment magnitude (left) and hypocentral distance (right). Fluctuations appear to be randomly distributed with no evident dependence on earthquake size and distance for TPE and LSK stations (Class A sites according to EC8). Two points in the upper part belongs to the κ values determined for the TIR2 and TIR3 stations (Class B sites according to EC8)

4.2 Determination of Stress Drop (Δσ)

For the determination of the stress drop parameter for each earthquake in our data set we used the parameters of Table 5 to compute PSRV spectra for a suite of stress parameters. The simulations were done using the random-vibration version of the stochastic model (Boore, 2002). We tried to make a comparison visually to provide a subjective assessment of the adequacy of the single corner-frequency and ω-2 source model. The simulated and the observed response spectra are plotted in Figure 6 for all the recordings considered in this study.

From the plots presented in Figure 6 we can observe that all earthquakes recorded by the TPE station and the earthquake recorded by the LSK station have stress drops between 15–60 bars. The three main shocks recorded on these two stations, those are the earthquakes TPE-03-1; TPE-04-1 and LSK-04-1 have stress drop values between 50–60 bars. These are typical values for earthquakes with normal faulting mechanisms in Greece (Margaris and Boore, 1998). As shown earlier in this study, for

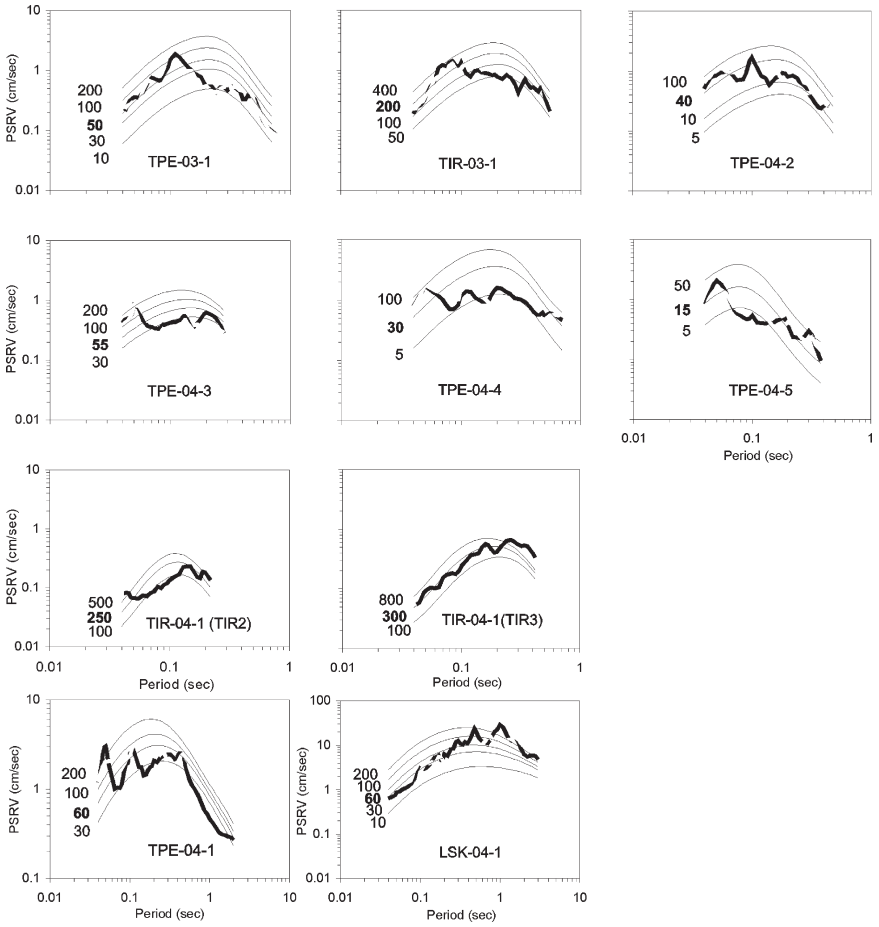

Figure 6 Plot of PSRV spectra from all recordings (10) with simulated curves for different suites of stress parameter. Each plot is labeled with the earthquake code. Thick lines are the response spectra computed from the observed horizontal components, while the thin lines are the simulated spectra. The bolded number in each plot represents the stress drop values for which we have the best fit, both in terms of shape and peak ground motion parameters

these three events, only the earthquake of 041123 near Leskoviku has normal faulting according to the mechanism solution of Harvard. We do not have fault mechanism solutions for the other two events. As far as the other four events is concerned, those with the codes TPE-04-2, TPE-04-3, TPE-04-4 and TPE-04-5 correspond to aftershocks of the TPE-04-1 earthquake, the estimates of stress drop varies from 15–55 bars. Two events have stress parameter values of 40 bars and 55 bars, while the two last events have stress values of 15–30 bars respectively.

For the other two events we found larger stress drop values. The TIR-03-1 event gave a stress drop of 200 bars, while the earthquake TIR-04-1 is characterized by values in the range $\Delta\sigma$ = 250–300 bars. While the $\Delta\sigma$ estimation procedure for the

TIR-03-1 earthquake is the same as for all the other earthquakes analyzed it is different in the case of the TIR-04-1 earthquake. The observed horizontal PSRV spectra on the two stations, TIR2 and TIR3 are distinguished by different intensity levels. The spectra on the E-W component have larger amplitudes over the entire frequency than the range N–S ones and demonstrating a strong directivity effect of this earthquake. It is very difficult to fit simulated spectra with PSRV spectra from the E–W component. We tried to do this and found unreasonable values of the stress-drop parameter. In this case we think it is appropriate to consider only the N-S component for our analyses and thus not being "disturbed" by the directivity phenomenon. The values found from the two records of this event do not differ too much from each other.

According to many published papers (Roveli et al., 1988, 1991; Cocco and Roveli, 1989; Margaris and Boore, 1998; Margaris and Hatzidimitriou, 2002) higher values of Brune stress drop can be found for areas characterized with thrust faulting as compared to normal and strike-slip fault earthquakes. In Greece for example, this difference is evaluated to be roughly 4.5, although determined by a small data set for thrust events (Margaris and Hatzidimitriu, 2002). Similar results are given by for areas of Northern Italy composed by thrust faulting types (Cocco and Roveli, 1989). In our case, analyses of fault mechanism solution is available only for one event, TIR-04-1, which solution is thrust faulting (SED). For the other TIR-03-1 events, $\Delta\sigma$ = 200 bars and we may assume the same thrust mechanism here.

The same features represent also the strong motion record of the event that hit Tirana on 09/01/1988 with MS = 5.7, shown in Figure 7. The E–W component show a very peaked PGA value 0.4 g (Muço et al., 2001). This earthquake had the

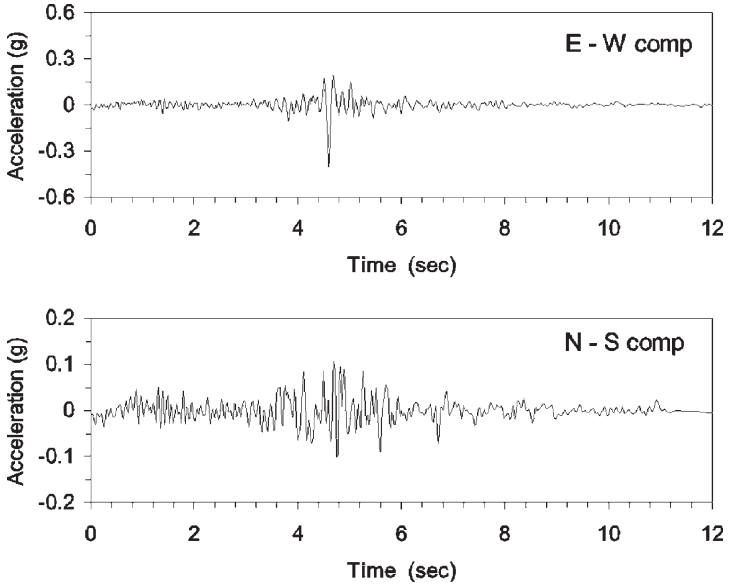

Figure 7 Two horizontal components of the strong motion record of 09/01/1988 event near Tirana

Table 8 Brune stress-drop values and values of peak ground motion parameters

Earthquake				Stress drop	PGA (cm/s/s)		PGV (cm/s)		PGD (cm)	
code	Date (yymmdd)	Time (hhmmss)	Station	(bars)	Rec.	Sim.	Rec.	Sim.	Rec.	Sim.
TPE-03-1	030327	043541	TPE	50	20.2	19.7	0.39	0.49	0.009	0.018
TIR-03-1	031205	033149	TIR	200	25.8	26.4	0.65	0.62	0.020	0.021
TPE-04-1	040628	174434	TPE	60	78.3	55.2	1.76	1.46	0.110	0.086
TPE-04-2	040708	174027	TPE	40	46.5	31.7	0.72	0.58	0.013	0.017
TPE-04-3	040711	131624	TPE	55	22.4	15.9	0.25	0.27	0.006	0.007
TPE-04-4	040712	044240	TPE	30	59.1	51.6	0.81	1.25	0.029	0.043
TPE-04-5	040712	054050	TPE	15	47.7	45.7	0.43	0.48	0.006	0.006
TIR-04-1	040828	221648	TIR2	250	3.99	4.24	0.08	0.07	0.003	0.002
TIR-04-1	040828	221648	TIR3	300	7.33	6.48	0.25	0.17	0.010	0.006
LSK-04-1	041123	022614	LSK	60	88.8	106.0	8.48	5.23	1.480	0.920

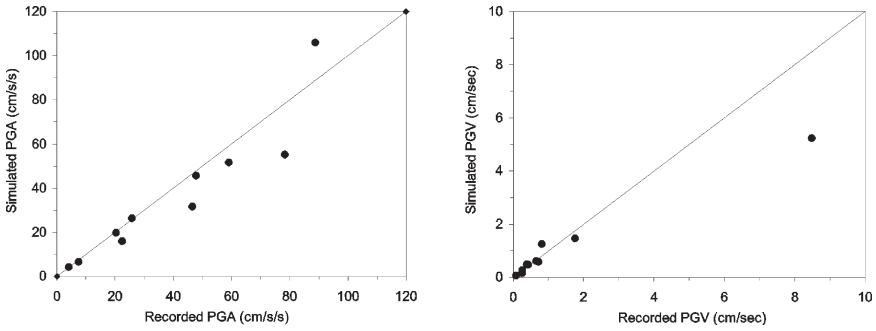

Figure 8 Scatter plots of observed and simulated peak acceleration and velocity

epicenter in the same area as the TIR-04-1 event we are discussing in this study. This is turn may constitute a matter of concern for seismic hazard estimates of Tirana City. Strong directivity effects may be observed in this city from earthquakes generated by the thrust faults environment that surrounds it.

The stress drop values obtained in our analyses as well as recorded and simulated values of PGA, PGV and PGD are presented in Table 8. In Figure 8 presented is the scatter between simulated and recorded values of PGA and PGV for all the events subjected to analysis in this study. These measures of ground motion were computed in the same manner as for the PSRV spectra through the stochastic model, using the derived $\Delta\sigma$ from each earthquake and the other parameters presented in Table 5. On the basis of the comparison presented in Figure 8 we think that the derived stress-drop is consistent with available PGA and PGV values.

4.3 Comparison of Simulated and Observed Fourier Spectra

The last step in our stress-drop analyses is the comparison of the recorded Fourier amplitude spectra and the simulated ones according to the theoretical models described by the equation (3). The simulated and the observed Fourier spectra shown in Figure 9 are in good agreement within a distance of 29.2 km (the maximum hypocentral distance used in our calculations).

Although the majority of the observations shown in Figure 9 fit the simulated spectral models very well, there are a number of recordings with differences. The strongest events recorded by the TPE station, TPE-03-1, TPE-04-1 and TPE-04-2 exhibit an amplification in the frequency range 6–12 Hz for both components. An explanation of the mismatch may be the topography at the recording site of TPE, which is situated on a mountain slope. The same phenomenon is observed also for the LSK-04-1 event, where amplifications are observed on both components of record in the frequency range 0.8–2.5 Hz. As far as the mismatch observed on the N–S components for the recording of 040828 event in Tirana, namely in the TIR2

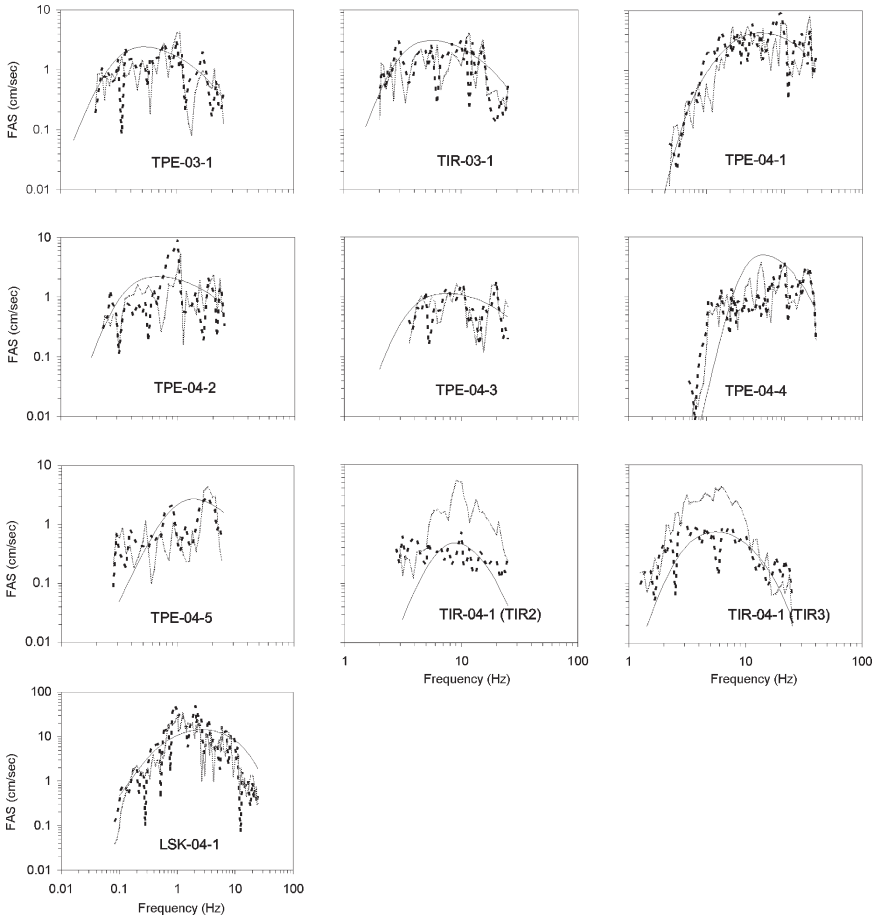

Figure 9 Comparison of the observed spectra of both horizontal components versus theoretical ω-square spectra, computed by using the source parameters estimated for these events

and TIR3 records, this is due to the strong directivity effect, which caused an underestimate of the amplitude of the spectra in N–S components. Anyway, the adoption of simplified models cannot always accurately simulate the real complexity of seismic radiation and the parameters of equation (3), may introduce deviations that, in general are difficult to quantify in detail (Margaris and Hadzidimitriou, 2002).

5 Discussion and Conclusions

We have shown the adequacy of the single corner-frequency ω-2 source model in estimating stress-drop parameters through comparing visually simulated and observed PSRV response spectra. These were derived from a small number of

recordings taken at five stations of ASMN.. We observed two distinct variation intervals of Brune stress-drop in analyzing the records of our data set. The first interval is related to values between 15 bars and 60 bars with main shocks having the largest values $\Delta\sigma$ = 50–60 bars, typical for areas of normal focal mechanism. The second interval is characterized by values in the range $\Delta\sigma$ = 200–300 bars, but the estimates are based on only three records generated by two earthquakes. These latter values are typical for thrust focal mechanism. Returning to the map of the Neotectonic Zonation of Albania presented in Figure 2 (Aliaj et al., 1996). There is some kind of disagreement between our results of stress-drop estimates by analyzing the strong motion records from the TPE station and those stemming from nearby earthquakes and the configuration of areas presenting compressional and extensional movements on that map. According to these estimates of stress-drop, all the earthquakes recorded by the TPE station listed in Table 1 should have normal focal mechanisms. Of course, we do not exclude that normal faults can occur in areas of compressional tectonic movements any eventual shift in the west direction of the contact between compressional and extensional movement zones should be carefully investigated (Margaris and Boore, 1998, and articles referenced therein). The reason is that a narrower area of compressional tectonic movements in south-western Albania has implications on the seismic hazard assessment of the entire country.

Estimates of the high-frequency diminution parameter κ o by our data set have differenced the ground type A according to the EC8 by values in the range $0.02 \leq \kappa o \leq 0.04$, while for ground type B the estimates for the two sites are quite similar with $\kappa o = 0.07$. These values are corrected for site amplification and the whole-path attenuation and clearly the difference between the measured values and the corrected ones are small. These results can constitute a starting point for predictions of ground motions in Albania by taken into account not only the different $\Delta\sigma$ values found for the two main tectonic zones characterized by compressional and extensional movements, but also the κo and amplification factors used in this study. Anyway, it should be noted that the simulation of ground motions through the stochastic model are based on the simple point source model and can be applied for earthquakes with small up to medium magnitude range $M \leq 6.0 \sim 6.5$. For larger magnitudes it would be necessary to use more sophisticated hybrid (deterministic + stochastic) methods and amplification factors that take into account larger time durations and the nonlinear soil behavior under high accelerations.

Acknowledgments We had the assistance of our colleagues E. Dushi and Sh. Shubleka from the Department of Seismological Network who provided the epicentral coordinates and depths for the events listed in this study. We thank Mrs. A. Çollaku for the help with the preparations of some figures presented in this article. We have benefited from discussions with Dr. N. Theodulidis from ITSAK, Thessaloniki, Greece and Dr. A. Pitarka from URS Corporation, Pasadena, USA. This work was supported by the Academy of Sciences of Albania, research project AS-IS No. 01-2003-2004.

References

Aliaj, S. H., Melo, V., Hyseni, A., Skrami, J., Mehillka, L. L., Muço, B., Sulstarova, E., Prifti, K., Pasko, P., Prillo, S., 1996. Neotectonic structure of Albania (in Albanian). Final report. Archive of Seismological Institute of Academy of Sciences, Tirana.

Anderson, J. G., Hough, S. E., 1984. A model for the shape of the Fourier amplitude spectrum of acceleration at high frequencies. *Bull. Seism. Soc. Am* 74: 1969–1994.

Biswas, N. N., Aki, K., 1984. Characteristics of coda waves: central and south-central Alaska. *Bull. Seism. Soc. Am* 74: 493–507.

Boore, D., 1983. Stochastic simulation of high-frequency ground motions based on seismological models of the radiated spectra. *Bull. Seism. Soc. Am* 73: 1865–1894.

Boore, D., 1984. Use of seismoscope records to determine ML and peak velocities. *Bull. Seism. Soc. Am* 74: 315–324.

Boore, D., 1996. SMSIM-Fortran programs for simulating ground motions from earthquakes. Version 1.0. US Geol. Survey, Open-File Report, 96-80-A and 96-80-B: 1–73.

Boore, D., 2002. SMSIM–Fortran programs for simulating ground motions from earthquakes. Version 2.0 – A Revision of the OFR 96-80-A", Open-File Report, United States Department of the Interior USGS: 1–56.

Boore, D., Atkinson, G., 1987. Stochastic prediction of ground motion and spectral response parameters at hard-rock sites in Eastern North America. *Bull. Seism. Soc. Am* 77: 440–467.

Boore, D., Joyner, B., 1997, Site amplifications for generic rock sites. *Bull. Seism. Soc. Am* 87: 327–341. Open-File Report 84–763: 483–499.

Cocco, M., Roveli, A., 1989. Evidence for the variation of stress drop between normal and thrust faulting earthquakes in Italy. *J Geophys Res* 94, No B7: 9399–9416.

Duni, L.L., Aliaj, S.H., Kuka, N., Skrami, J., 2004. The reorganization of the Albanian Strong Motion Network (in Albanian). Project Report No 01/2001. Archive of Seismological Institute of Academy of Sciences, Tirana: 1–18.

Eurocode 8, 2003. Design of structures for earthquake resistance; Part 1: General rules, seismic actions and rules for buildings. Draft No. 6; Version for translation (Stage 49), Doc CEN/TC250/SC8/N335, European Committee for Standardization: 1–30.

Frankel, A., Mueller, C., Barnhard, Th., Perkins, D., Leyendecker, E.V., Dickman, N., Hanson, S., Hopper, M., 1996. National Seismic-Hazard Maps: Documentation June 1996. US Department of the Interior, US Geological Survey, Open-File Report 96–532: 69.

Hanks, T. C., Kanamori, H., 1979. A moment magnitude scale. *J Geophys Res* 84: 2348–2350.

Hanks, T. C., McGuire, R., 1981. The character of high-frequency strong ground motion. *Bull. Seism. Soc. Am* 71: 2071–2095

Harvard Seismology: Centroid-Moment Tensor Project, http://www.seismology.harvard.edu/projects/CMT/

Joyner, W., Boore, D., 1988. Measurements, characterization and prediction of strong ground motion. In: Proc. Earthquake Engineering and Soil Dynamics II GT Div/ASCE, Park City, Utah: 43–102.

Koçiu, S., Aliaj, S. H., Pitarka, A., Peçi, V., Konomi, N., Dakoli, H., Prifti, K., Koçiu, A., Kero, J., Shehu, V., Goga, K., Goro, N., Kume, L., Kapllani, L., Papadhopulli, P., Eftimi, R., Kondo, M., Puka, N., 1988. Microzonation of Tirana City (in Albanian). Technical report. Archive of Seismological Institute of Academy of Sciences, Tirana: 1–201.

Margaris, B,, Boore, D., 1998. Determination of $\Delta\sigma$ and κ_0 from response spectra of large earthquakes in Greece. *Bull. Seism. Soc. Am* 88: 170–182.

Margaris, B., Hatzidimitriou, M., 2002. Source spectral scaling and stress release estimates using strong-motion records in Greece. *Bull. Seism. Soc. Am* 92: 1040–1059.

Muço, B., Vaccari, F., Panza, G. F., 2001. Seismic zonation of Albania using a deterministic approach. AJNTS 10: 5–19.

Muço, B., Kuka, N., Shubleka, S. H., 2002. Development of a moment magnitude relation for Albania. *Bull. Seism. Soc. Am* 92: 1136–1140.

NEHRP, 1994. Recommended provisions for seismic regulations for new buildings, FEMA 222A/223A 1 (Provisions) and 2 (Commentary).

Papazachos, C., Scordilis, E., Peçi, V., 2004. P and S-Deep velocity structure of the Southern Adriatic-Eurasia collision obtained by robust non-linear inversion of travel times. NATO Science for Peace Programme, Final Report, Sub-Project 3, 1–12.

Roveli, A., Bonamassa, O., Cocco, M., Di Bona, M., Mazza, S., 1988. Scaling laws and spectral parameters of the ground motion in active extensional areas in Italy. *Bull. Seism. Soc. Am* 78: 530–560.

Roveli, A., Cocco, M., Console, R., Alessandrini, B., Mazza, S., 1991. Ground motion waveforms and source spectral scaling from close-distance accelerograms in a compressional regime area (Friuli, Northeastern Italy). *Bull. Seism. Soc. Am* 81: 57–80.

SED Moment Tensors- http://www.seismo.ethz.ch/mt/

Seismicity of Croatia

Snježana Markušić*

Abstract Paper presents the analysis of the Croatian earthquake catalogue (CEC) for the period from 373 BC to 2004. The CEC is estimated to be complete for events with $M_L \geq 4.0$ since 1900 and for events with $M_L \geq 3.2$ for the last three decades. The coastal part of Croatia (the Dinarides) is the most seismically active, because of tectonic processes related to the collision of the Adriatic Platform and the Dinarides. The northern part of Croatia (the Pannonian Basin) is characterized by rare occurrences of large earthquakes and thus being typical of intraplate seismicity.

Keywords seismicity, Croatia, earthquake catalogue, Dinarides, Adriatic

1 Introduction

The scope of this contribution is a brief presentation of the Croatian seismicity supplemented with details on the most important and destructive earthquakes ever taking place in this country.

Croatia which is part of the Alpine–Mediterranean seismic region, comprises several geotectonic units. The dominant ones are the Pannonian Basin to the north, Eastern Alps, the Dinarides, the Dinarides–Adriatic Platform transition zone and the Adriatic Platform itself. The seismicity is unevenly distributed albeit most earthquakes occur in the coastal area of the country – the Dinarides. This is commonly explained by the ongoing collision between the Adriatic Platform and the Dinarides (e.g. Aljinović et al., 1984; Anderson and Jackson, 1987; Pribičević et al., 2002; Nocquet and Calais, 2004; Kotzev et al., 2008). The seismogenic faults here are mostly reverse ones, and the tectonic movements have predominantly tangential components. The Pannonian Basin exhibits typical intraplate seismicity characterized

Department of Geophysics, Faculty of Sciences, University of Zagreb, Horvatovac bb, 10000 Zagreb, Croatia

*To whom correspondence should be addressed. E-mail: markusic@irb.hr

E.S. Husebye (ed.), *Earthquake Monitoring and Seismic Hazard Mitigation in Balkan Countries.*

by rare occurrences of large events. In this area the tectonic movements are predominantly vertical on steeply dipping faults (e.g. Aljinović et al., 1984, 1987; Prelogović et al., 1997; Pribičević et al., 2002).

2 The Croatian Network – instrumentation

The first seismological station on Croatian territory was opened in Pula in 1900, equipped at first with a Vicentini, and afterwards also with Conrad and Wiechert seismographs. The station was closed in 1918, after the collapse of the Austro–Hungarian empire. It is not known what happened to the instruments and the seismogram archive. Besides Pula, the following stations were operative in the first half of the 20th century:

- Rijeka (1901–1918, seismograph Vicentini)
- Sinj (1914–1924, seismograph Conrad)
- Šibenik (1926–1940, seismograph Conrad, temporary operation)
- Dubrovnik (1927–1929, seismograph Conrad)
- Zagreb (1906–)

The Zagreb (ZAG) seismological station was founded when the first seismological instrument (the Agamemnone electrical seismoscope) was acquired by the Academy in 1901. At the conference of directors of meteorological institutes, held in Innsbruck in 1905, Dr. Andrija Mohorovičić, head of Meteorological Institute in Zagreb, asked Dr. Konkoly from Budapest to lend him one of the Vicentini seismographs. This instrument was installed in the basement of the Geophysical Institute in Zagreb on April 6, 1906. It was operational for 18 years. Unhappy with the instrument's performance, Mohorovičić purchased the Wiechert seismograph with a mass of 80 kg that recorded horizontal ground motion and installed it in Zagreb in 1908. Soon afterwards, in 1909, a new horizontal instrument was obtained with a mass of 1,000 kg. A vertical Wiechert instrument (1,200 kg) was acquired in 1932. These seismographs operated with almost no disruption until 1983 when they were moved to the Institute's new location in Horvatovac, Zagreb. These seismographs have recently been restored and are now in operating condition.

Electromagnetic seismographs (Sprengnether, SKM-3, Vegik) were obtained in early 1970s, within the framework of the UNESCO project "Survey of the seismicity of the Balkan region". At that time, the strong-motion network was installed too. The new instruments were used to open the new permanent stations Puntijarka (PTJ, 1972), Hvar (HVAR, 1973), Dubrovnik (DBK, 1986) and Rijeka (RIY, 1988). In addition to the permanent stations, a number of temporary ones were installed all over Croatian territory, some of which are still active.

The first 16-bit digital instrument was installed in Zagreb in 1989. The modern Croatian seismic network is based on seven broad-band seismometers with 24-bit digitizers, which were obtained in 1999. Presently, ten BB (broad band) seismometers operate on Croatian territory.

3 The Croatian Earthquake Catalogue (CEC)

After the great Zagreb earthquake of 9 November 1880, the sporadic earthquake research efforts evolved into systematic ones. Immediately after the earthquake, the Yugoslav Academy of Science and Arts in Zagreb established the "Committee for observation of earthquake-related phenomena". The main task of the Committee was to study Croatian earthquakes and methodically collect all relevant data. In the first volume of its Papers, the Academy published the extensive report on the Zagreb earthquake (Torbar, 1882), where the phenomena related to that event were not only described, but also explained. The Academy's Committee later also collected and published all available information on Croatian earthquakes for the period 361–1906. This data set was used as solid basis for scientific study of the natural phenomenon (Kišpatić, 1891, 1892, 1895).

In January 1892, Andrija Mohorovičić became director of the Meteorological Observatory in Zagreb (later Geophysical Institute). In 1893 he initiated a systematic collection of earthquake related data which were regulary published (since 1906) in the Seismic Reports. Following the strong earthquake of 17 December 1901 near Zagreb, Kišpatić and Mohorovičić made every effort to have an operational seismic station in Zagreb. After the first seismoscopes and seismographs were obtained in the beginning of the 20th century, Mohorovičić realized the importance of accurate time-keeping. He therefore initiated regular observation of times of passage stars through the local meridian, thus founding the Croatian time service.

The first catalogue compilation was initiated within the framework of the UNDP/UNESCO project "Survey of the seismicity of the Balkan region" (Shebalin et al., 1974). The resulting catalogue was published in two volumes (Part I – earthquakes in the period 1901–1970; Part II – earthquakes before 1901). Its subset consisting of earthquakes on the Croatian territory formed the nucleus of the CEC. It has been revised and supplemented for the years after 1970 (e.g. Herak et al., 1988a, b, 1991; Herak, 1989; Herak and Cabor, 1989; Markušić et al., 1990, 1993, 1998; Herak et al., 1996; Ivančić et al, 2001/02, 2006). As a rule, new entries were added to the catalogue with a delay of 1–2 years, allowing proper times for collecting additional data and hypocenter relocations.

For historical earthquakes only macroseismic information was used. In the early years of 20th century, instrumental data were rare and available only for strong earthquakes. For that period, when it was impossible to obtain a reliable instrumental, locations of the epicentres were determined also on the basis of macroseismic data.

Whenever it was possible to collect instrumental data of sufficient quality, the hypocentral coordinates were determined using the HYPOSEARCH program (Herak, 1989) and the appropriate velocity models for the investigated area (B.C.I.S., 1972; Herak, 1990; Herak and Herak, 1995). The depth of the Mohorovičić discontinuity as well as the values of the seismic wave velocities within the crust and the uppermost mantle were taken as reported on the basis of

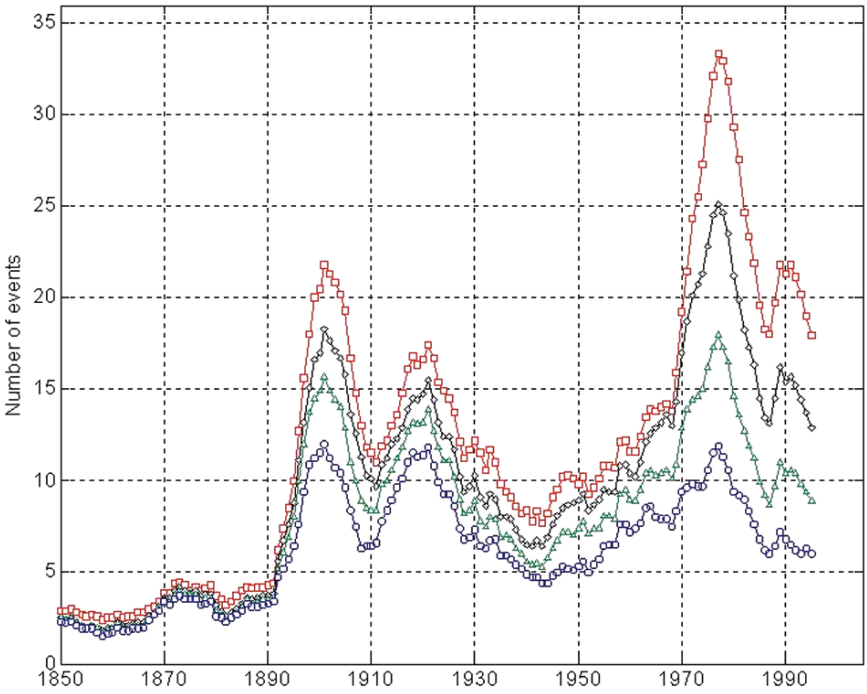

Figure 1 Number of mainshocks with magnitude within the particular magnitude interval as a function of time (red squares: M ≥ 3.6; black diamonds: M ≥ 3.8; green triangles: M ≥ 4.0; blue circles: M ≥ 4.2)

several DSS profiling surveys (e.g. Geofizika Company, 1963–1982; Dragašević, 1973/74; Dragašević and Andrić, 1975) Seismic wave velocities were also derived from studies of Seismological recordings (B.C.I.S., 1972; Skoko et al., 1987; Aljinović et al., 1987, Herak, 1990; Herak and Herak, 1995). The Moho beneath the Pannonian Basin is the shallowest (≈25 km) and its depth increases towards the Dinarides where it exceeds 45 km.

Figure 1 presents the number of mainshocks with magnitude greater or equal to four assumed magnitude thresholds M_c (3.6, 3.8, 4.0, 4.2) as a function of time. Windows of 10 years were shifted along the mainshock subcatalogue, 1 year at the time, and the corresponding value was plotted on the left window edge. As it can be seen, after 1900 the number of mainshocks stabilizes for M ≥ 4.0.

4 Features of Croatian Seismicity

The seismicity of Croatia was analysed on the basis of the CEC comprising of 13,195 earthquakes in the from 373 BC to 2004. The seismically active regions in Croatia are shown on the seismicity map presented in Figure 2. Of special interest

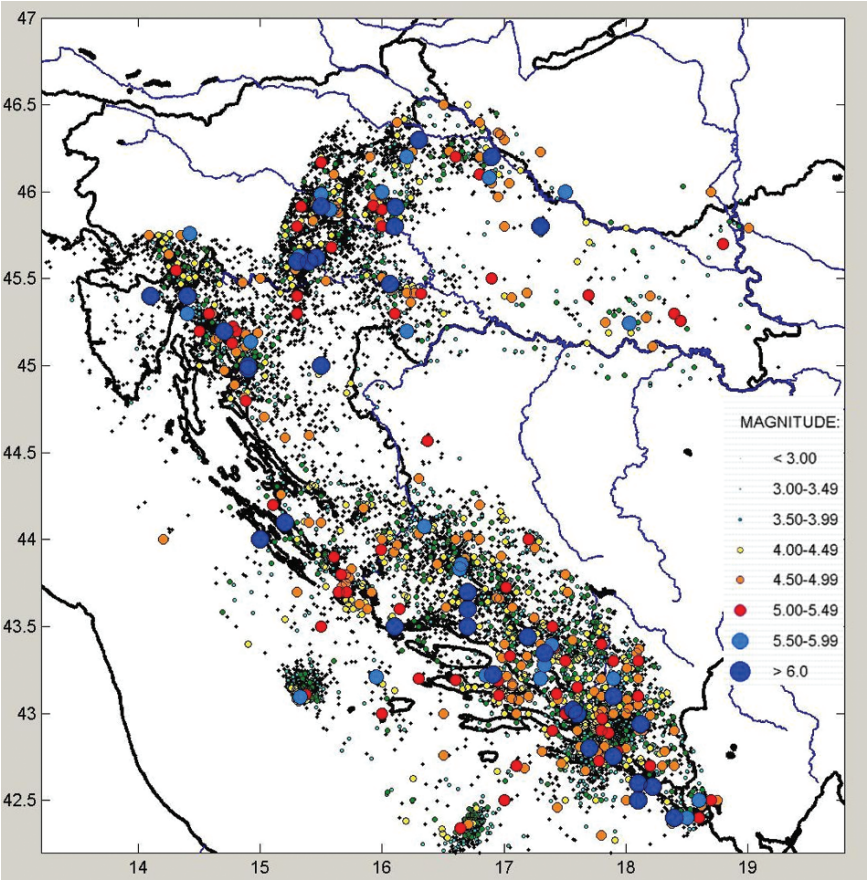

Figure 2 Epicentres of all earthquakes in Croatia in the CEC for the period from 373 BC to 2004

are clear concentrations of epicentres in the southern part of the country (Central External Dinarides). These event clusters are elongated and perpendicular to the direction of the Dinaric Mountains, thus indicating the existence of numerous transverse seismically active faults in this area. Also note worthy is the considerable seismic activity in the Adriatic which is highest at the boundary of the Central and Southern Adriatic along the Gargano ridge and in the vicinity of Jabuka Island.

4.1 Historical Seismicity

Below we will discuss some of the strongest historical earthquakes (I ≥ IX °MCS) in Croatia (Figure 3) that occurred in the period before 1900.

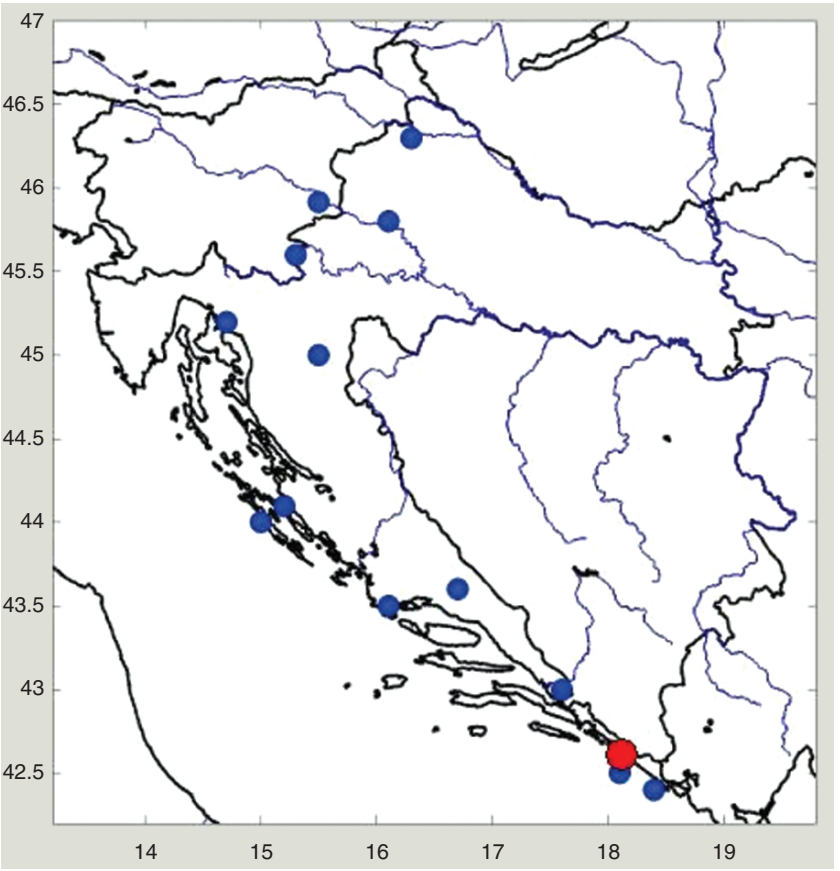

Figure 3 Epicentres of earthquakes with intensities I ≥ IX °MCS in Croatia for the period before 1900 (red circle denotes epicenter of great Dubrovnik earthquake in 1667 with I = X °MCS)

Before 1900, the most seismically active part of Croatia was the wider Dubrovnik area. Among the 8 historical earthquakes of intensity IX or X °MCS in the 15th, 16th and 17th centuries, the strongest and most important was the catastrophic Dubrovnik earthquake of 1667 (I = X °MCS). This earthquake killed more than 5,000 citizens, including the Rector, and destroyed over three fourths of public buildings.

Besides the earthquake just mentioned, in the coastal part of Croatia the following earthquakes occurred with estimated intensity of IX °MCS:

- In the 15th century with epicenter near Metković
- Destructive earthquake in the 15th century with epicenter in Dalmatia (Kišpatić, 1891), but its location and intensity are uncertain
- In the late 19th century with epicenter near Sinj

- In the central part of the Croatian coast (Zadar area) unreliable sources mention large earthquakes in the 13th, 14th, 15th and 18th centuries
- In the northern part of the Croatian coast historical sources mention disastrous earthquakes in the 13th and 16th centuries with epicentres in the vicinity of Vinodol and Senj, and in the 18th century in the Rijeka area

In the seismic area that stretches along the Croatia–Slovenia border, between Karlovac and Novo Mesto, references of strong earthquakes with intensities up to IX °MCS are found in the historical documents from the 6th and 11th centuries (Cvijanović, 1980).

The seismically active area that includes the Zagreb metropolitan area which is the most densely populated area in Croatia. It is part of the contact zone of the Alps, the Dinarides and the westernmost region of the Pannonian Basin, with complex tectonic and structural relationships. Two main epicentral areas may be distinguished there: Brežice-Krško in the Croatia–Slovenia border region (a large number of strong earthquakes occurred there in the 17th century, of which the largest one had the intensity of IX °MCS), and Medvednica Mt. near Zagreb (the largest earthquake there occurred in 1880 – the great Zagreb earthquake – Figure 4).

The archives mention also a strong earthquake in 1459, with the epicentre near Varaždin (I = IX °MCS) in the northern part of Croatia.

Figure 4 Damages of St. Stephen's Cathedral situated in the center of Zagreb after the great Zagreb earthquake in 1880

4.2 Recent Seismicity (Since 1900)

Several brief descriptions of the important earthquake sequences in Croatia since 1900, shown on Figure 5, are given below.

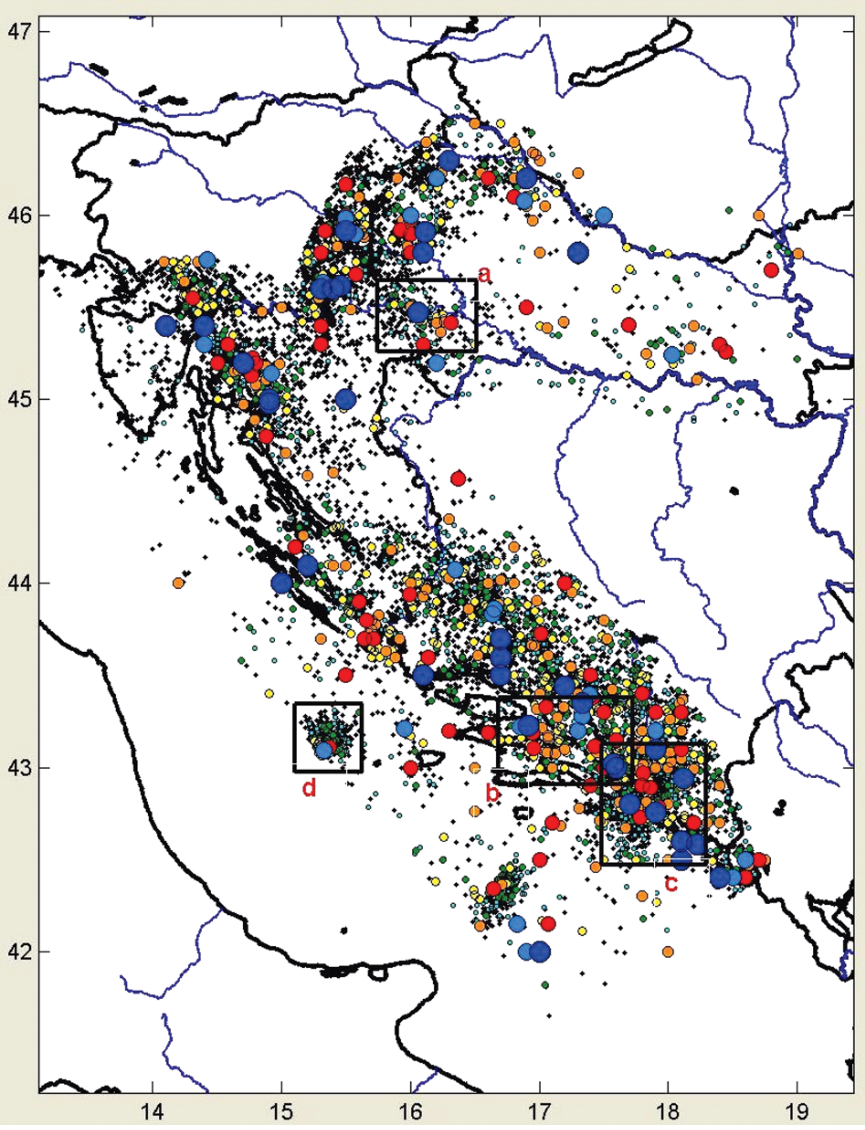

Figure 5 Positions of the following earthquake sequences in Croatia: (a) Kupa Valley (north), 1909–1910; (b) Biokovo Mt., 1962; (c) Ston-Slano (south), 1996; (d) Jabuka Island (off coast), 2003

4.2.1 Kupa Valley Earthquakes (1909–1910)

The main shock of 8 October 1909 is probably the most famous earthquake that has occurred in Croatia and furthermore is firmly entrenched in the history of seismology. By studying its seismograms Andrija Mohorovičić was able to prove the existence of a boundary layer – the Mohorovičić discontinuity – between the Earth's crust and mantle (Mohorovičić, 1910). By this discovery he established himself as one of the greatest and most renowned Croatian scientists of all times. His studies of the Kupa Valley earthquake also resulted in a new and unique procedure for locating an earthquake focus and an analytical expression for the increase of elastic wave velocity with depth (Mohorovičić's law). The locations of 49 events belonging to the Kupa Valley earthquake series are presented in Figure 6. The main shock lies at the perimeter of the group of aftershocks which is elongated and parallel to the direction (NW–SE) of the Vukomeričke Gorice hills. The maximum intensity was observed in the Kupa river valley (I_{max} = VIII °MCS).

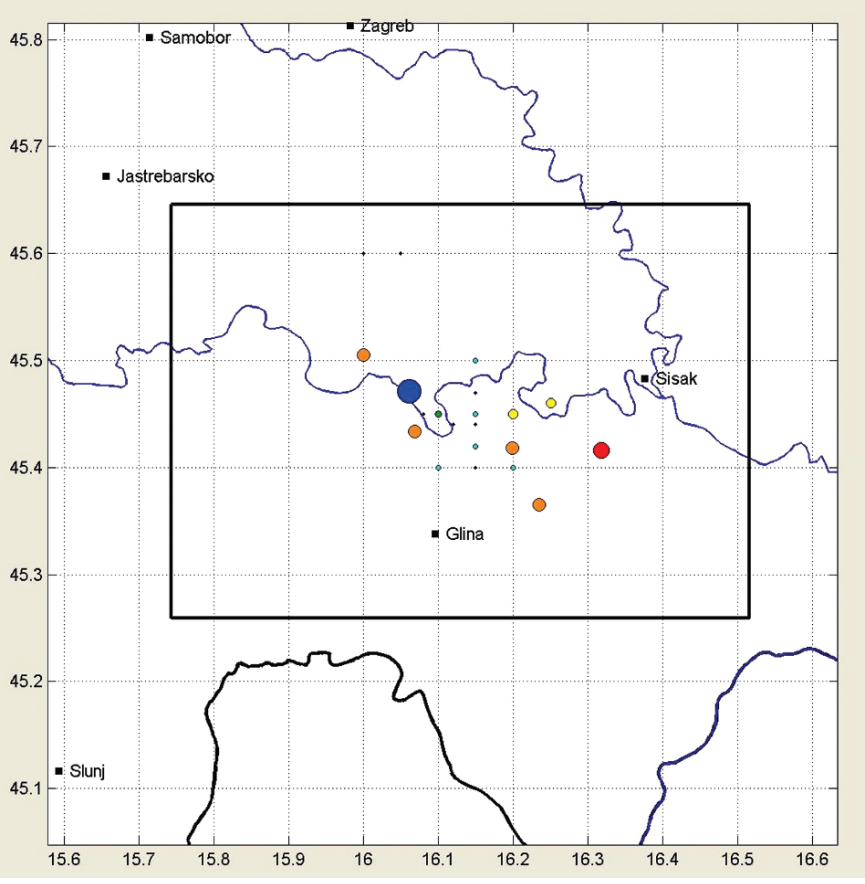

Figure 6 Kupa Valley earthquake sequence (1909–1910)

4.2.2 Biokovo Mt. earthquakes (1962)

This is one of the most important series of earthquakes that has occurred in the coastal part of Croatia in the last century. The two largest events had magnitudes of M = 5.9 and M = 6.1, and were felt with intensities of VII and VIII–IX °MCS, respectively. These earthquakes caused large damages essentially in the Biokovo area, and define the earthquake hazard there. Although there was only one seismograph operating in Croatia at that time, a sufficient amount of microseismic data was collected to reliably locate 46 of the 63 events recognized in the Zagreb recordings. The majority of earthquakes had epicentres in the channel between the islands of Brač and Hvar (Figure 7). The epicentral zone is some 60 km long, extending in the NE–SW direction. There is, however, a group of epicentres (including the largest events) that are aligned in the direction of the coastline and intersects the aforementioned group near the northern coast of the Hvar Island. This suggests that the largest earthquakes occurred in the

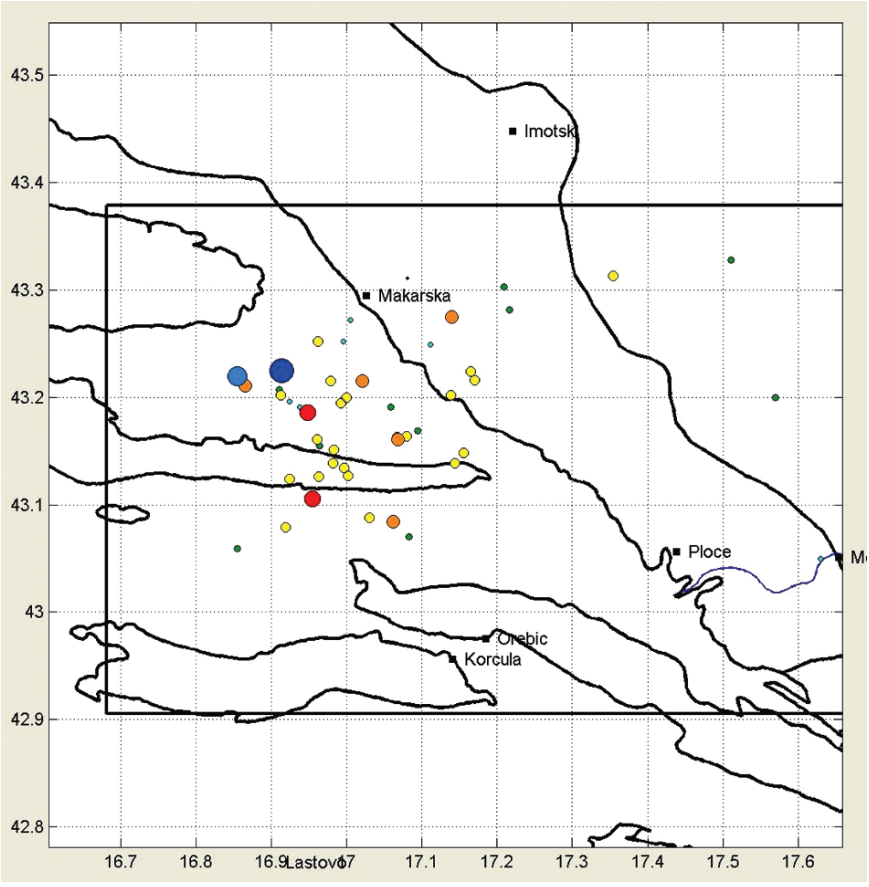

Figure 7 Biokovo Mt. earthquake series in 1962

intersection zone of two fault systems – one striking NE–SW, and the other NW–SE. The two nodal planes obtained as the fault plane solution for the strongest event by McKenzie (1972), strike at azimuths of 197° and 292°.

4.2.3 Ston-Slano Earthquakes (1996)

The Ston-Slano earthquake sequence, with the main shock of M = 6.0, completely destroyed three villages, and caused heavy damage in a number of southern Dalmatian cities. It is the largest sequence of earthquakes in the greater Dubrovnik area since the catastrophic one (I_{max} = X °MCS) of 1667. The peak near-field ground acceleration recorded in Ston was as high as 0.65 g. The a posteriori analysis of seismicity pattern in a larger area of Southern External Dinarides (using CN algorithm-a scheme for intermediate-term medium-range earthquake prediction purposes) revealed significant seismicity pattern anomalies (TIP-Times of Increased Probability) 1 year prior to this earthquake (Markušić et al., 1998). The main shock was followed by thousands of aftershocks, of which 1,350 have been reliably located. Figure 8 at depth down, the aftershock epicentres fall into a well defined elongated ellipse with the major axis directed NE–SW. The seismotectonic model, proposed on the basis of geotectonic data, hypocentral locations and the available fault-plane solutions, implies basic movements of the Adriatic Platform towards NNW and the related resistance of the Dinaric structures. Most of the foci lie within the reverse structures of the Dinarides at depth down to 20 km. The CMT best double couple solution indicates that the main shock was caused by reverse faulting on a NW–SE striking fault system dipping towards NE and thus is in agreement with the system of faults in this area.

4.2.4 Jabuka Island Earthquakes (2003)

This earthquake sequence, one of the strongest ever recorded within the Adriatic microplate, occurred near the Jabuka Island in the very centre of the Adriatic Sea (Figure 9). The mainshock (M = 5.5) was preceded by over 150 foreshocks, and followed by many aftershocks, more than 4,600 of which were recorded on the closest station HVAR (about 90 km to the east). As the epicentres were off-coast and hence the absence of nearby stations, only 597 of these events were confidently located.

Epicentres lie in a well-defined area of about 300 km^2, located to the W and NW of the Jabuka island as shown in Figure 10. The fault-plane solution of the main shock based on the first-motion polarity readings agrees well with the CMT solutions and indicates faulting caused by a S–N directed tectonic compression, on a reverse, dip-slip fault. This is in very good agreement with the seismotectonic framework of the area (e.g. Herak et al., 2005).

This earthquake sequence is also very important in a tectonic context as the Adriatic is considered Adriatic microplate is a single, rigid and nearly aseismic

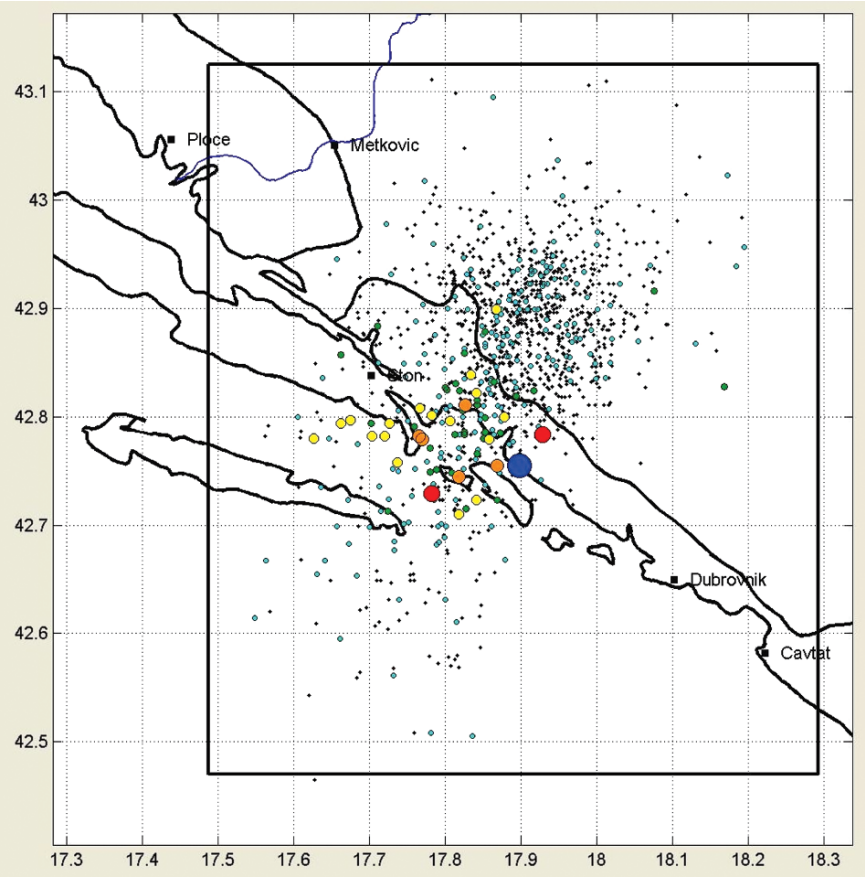

Figure 8 Earthquake sequence in the Ston-Slano region (1996)

block, whose contemporary motion as a whole is described by anticlockwise rotation around a pole in Northern Italy (e.g. Mantovani et al., 1985; Anderson and Jackson, 1987). This rotation is also confirmed on the basis of GPS data (e.g. Nocquet and Calais, 2004; Serpelloni et al., 2005).

Figure 11 presents a spatial distribution of mainshocks, with $M_L \geq 3.2$, for the last 30 years, extracted from the CEC. It implies that the area of the Central Adriatic Sea bounded approximately by the Ancona–Zadar line to the north and the Gargano–Dubrovnik line to the south (AZ and GD), exhibits seismicity which is much more intense than in the rest of the microplate. The ramification of this seismological observation is that Adriatic tectonic plate should not be considered as a single, rigid block. GPS velocities measurements (e.g. Oldow et al., 2002) also indicate that Adriatic no longer behaves as a rigid tectonic plate and is divided into at least two or more sub-plates.

Figure 9 Photo of the non-inhabited Jabuka Island

The CEC lists 7 mainshocks with magnitude 4.5 and above since 1974 in the Central Adriatic Sea (between the lines AZ and GD, counting only events located at least 40 km off-shore). However only 8 such earthquakes reported in the whole area along the Croatian coast and within the External Dinarides between Rijeka and Split, where many strong events have occurred in the past. Three events with $M_L \geq 5.0$ have occurred in the Central Adriatic in the last 20 years ($M_L = 5.0$ in 1986 in the open sea, $M_L = 5.3$ in 1988 near the island of Palagruža, and $M_L = 5.5$ in 2003 near the Jabuka Island). This is more than in any of the seismic zones in Croatia or in the neighbouring territories.

These observations suggest that the seismic potential of the area may be significantly higher than assumed up to now. Every effort should therefore be made to investigate the seismotectonic framework and seismicity of the Central Adriatic Sea by studying recent activity in ever increasing details. Identification of active faults in this area should also lead to improved hazard estimation. This will be of particular importance for the inhabited Croatian islands, where hazard today is almost

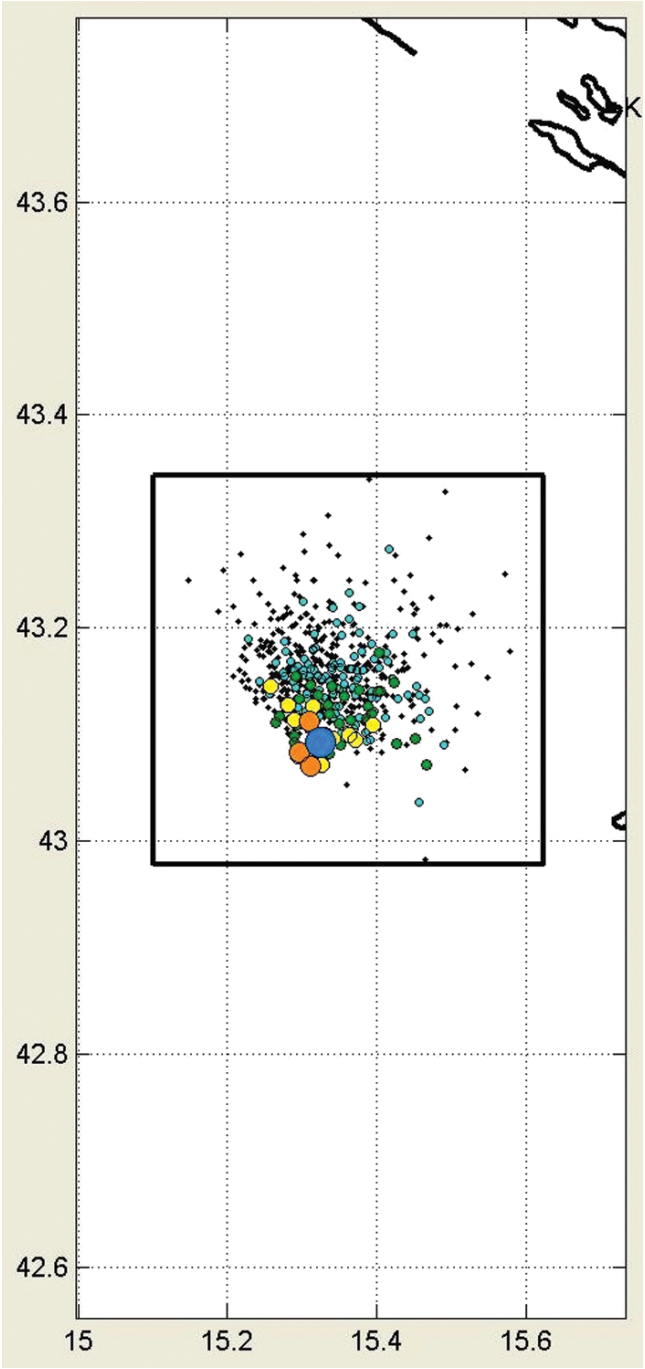

Figure 10 Earthquake series in 2003 close to Jabuka Island in the center of the Adriatic Sea

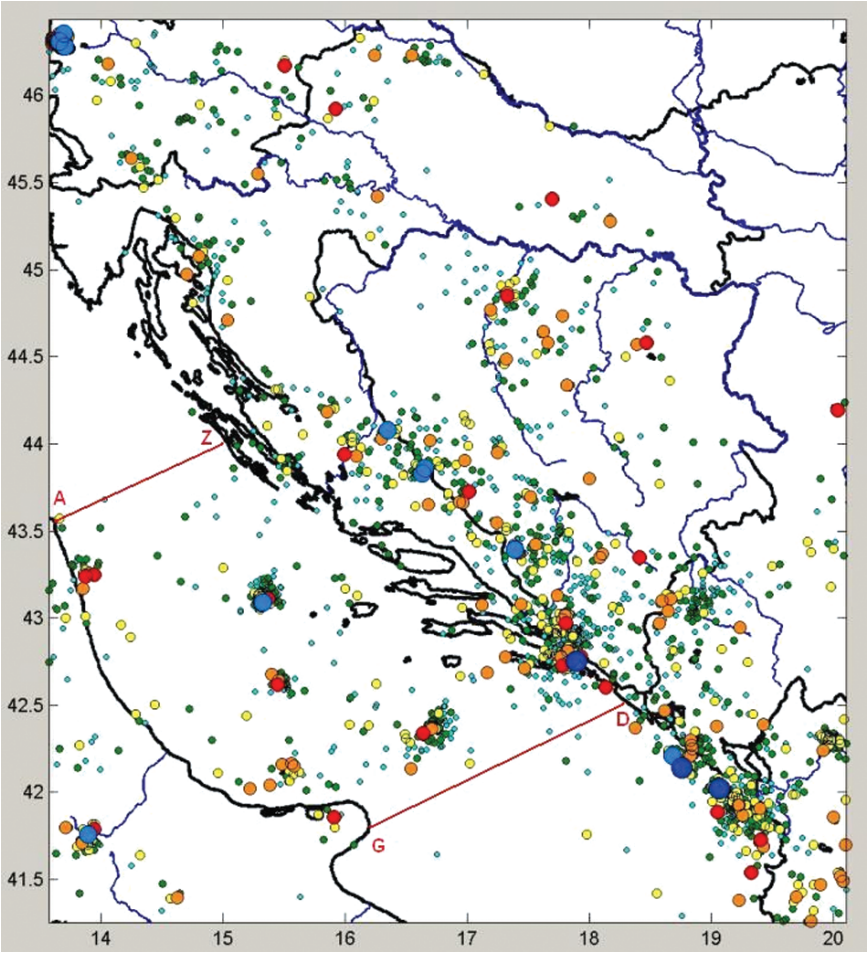

Figure 11 Spatial distribution of mainshocks with $M_L \geq 3.2$ in Croatia and adjacent regions in the period 1970–2004

exclusively defined on the basis of seismicity within the Dinarides and along the collision front between the Adria and the Dinarides (Markušić and Herak, 1999; Slejko et al., 1999; Markušić et al., 2000) For these reasons, the analyses of the Jabuka Island earthquake sequence are most important.

Along with several other sequences which occurred in the last two decades, these earthquakes force us, as already metioned, to change our perception of Adria as a nearly aseismic, compact and rigid block. In fact, it turns out that the recent seismicity of the Central Adriatic Sea is comparable to the seismicity of several well known earthquake-prone areas in the circum-Adriatic region.

5 Focal Depths

According to the analysis of focal depths distribution for reliably located events since 1970, Herak et al, (1996) obtained the following results. Most earthquakes in the Dinarides region occur between 3 and 11 km, and the lower crust is nearly aseismic (95% of the foci lie above 20 km). The earthquakes in the Pannonian Basin tend to be somewhat deeper, with most events occurring at depths between 6 and 18 km.

6 Conclusions

Earthquake catalogues are among the most important products of seismology. They provide a comprehensive database useful for numerous studies, and an outstanding one is investigating the seismicity of an area. Analysing the Croatian Earthquake Catalogue for the period from 373 BC to 2004 the following conclusions could be made. The coastal part of Croatia is the most seismically active. There is also significant seismicity in the Central Adriatic which has been mapped in very detail recently due to Qualitative and Quantitative upgrading of the Croatian Seismic Network during the last decades. All well located earthquakes occurred in the upper part of the Earth's crust with range in depth between surface and 20 km.

References

Aljinović, B., Blašković, I., Cvijanović, D. Prelogović, E. and Skoko, D., 1984. Correlation of geophysical, geological and seismological data in the coastal part of Yugoslavia, *Boll. Ocean. Teor. Appl*. **2**, 77–90.

Aljinović, B., Prelogović, E., Skoko, D., 1987. New data on deep geological structure and seismotectonic active zones in region of Yugoslavia, *Geološki vjesnik* **40**, 255–263 (in Croatian with English abstract).

Anderson, H., Jackson, J., 1987. Active tectonics of the Adriatic region, *Geophys. J. R. Astron. Soc*., **91**, 937–983.

B.C.I.S., 1972. Tables des temps des ondes seismiques (Hodochrones) pour la region des Balkans (Manuel d'utilisation), Strasbourg.

Cvijanović, D., 1980. Seizmičnost područja SR Hrvatske, Ph.D. thesis, University of Zagreb, Zagreb (in Croatian).

Dragašević, T., 1973/74. Present day structure of the Earth's crust and the upper mantle on the territory of Yugoslavia, *Vesnik Zavoda za geol. i geof. istraživanja knj*. **14/15 (C)**, 41–51 (in Serbian with English abstract).

Dragašević, T., Andrić, B., 1975. Dosadašnji rezultati ispitivanja grade Zemljine kore dubokim seizmičkim sondiranjem na području Jugoslavije, *Acta Seismol. Iugosl*. **2–3**, 47–50 (in Serbian).

Geofizika Company, 1963–1982., Investigation of the Earth's crust by DSS in the Dinarides and the Adriatic area, Documentation fund, Zagreb (in Croatian).

Herak, D., Herak, M., Prelogović, E., Cabor, S., 1988a. Some characteristics of the Adriatic Sea earthquake sequence (January–February 1986), *Boll. Geofis. Teor. Appl*. **30 (119–120)**, 385–394.

Herak, D., Herak, M., Cabor, S., 1988b. Some characteristics of the seismicity and the earthquake catalogue of the wider Dinara Mountain for the period 1979–1987, *Acta Seismol. Iugosl*. **14**, 27–59 (in Croatian with English abstract).

Herak, D., Cabor, S., 1989. Earthquake catalogue for S. R. Croatia (Yugoslavia) and neighbouring regions for the years 1986 and 1987, *Geofizika* **6**, 101–121 (in Croatian with English abstract).

Herak, D., Herak, M., Sović, I., Markušić, S., 1991. Seismicity of Croatia in 1989 and the Kamešnica Mt. earthquake, *Geofizika* **8**, 83–99.

Herak, D., Herak, M., 1995. Body-wave velocities in the circum-Adriatic region, *Tectonophysics* **241**, 121–141.

Herak, D., Herak, M, Prelogović, E., Markušić, S., Markulin, Ž., 2005. Jabuka island (Central Adriatic Sea) earthquakes of 2003, *Tectonophysics* **398**, 3–4, 167–180.

Herak, M., 1989. HYPOSEARCH – an earthquake location program*, Computers & Geosciences*, **15 (7)**, 1157–1162.

Herak, M., 1990. Velocities of body waves in the Adriatic region, *Boll. Geofis. Teor. Appl*. **32 (125)**, 11–18.

Herak, M., Herak, D., Markušić, S., 1996. Revision of the earthquake catalogue and seismicity of Croatia, 1908–1992, *Terra Nova* **8**, 86–94.

Ivančić, I., Herak, D., Markušić, S., Sović, I., Herak, M., 2001/02. Seismicity of Croatia in the period 1997–2001, *Geofizika* **18–19**, 17–29.

Ivančić, I., Herak, D., Markušić, S., Sović, I. and Herak, M., 2006. Seismicity of Croatia in the period 2002–2005 *Geofizika* **23,** 87–103.

Kišpatić, M., 1891. Earthquakes in Croatia, Rad *Jugosl. akad. znan. i umjetn*. **CVII**, Zagreb (in Croatian).

Kišpatić, M., 1892. Earthquakes in Croatia, *Rad Jugosl. akad. znan. i umjetn*. **CIX**, Zagreb (in Croatian).

Kišpatić, M., 1895. Earthquakes in Croatia, *Rad Jugosl. akad. znan. i umjetn*. **CXXII**, Zagreb (in Croatian).

Kotzev, V., King, R.W., Burchfiel, B.C., Todosov, A., Nurce, B., Nakov, R., 2008. Crustal motion and strain accumulation in the South Balkan region inferred from GPS measurements, this volume.

Mantovani, E., Babbucci, D. and Farsi, F., 1985. Tertiary evolution of the Mediterranean region: outstanding problems, *Boll. Geofis. Teor. Appl*. **26**, 67–88.

Markušić, S., Sović, I., Herak, D., 1990. Seismicity of Croatia and the surrounding areas in 1988, *Geofizika* **7**, 121–134.

Markušić, S., Herak, D., Sović, I., Herak, M., 1993. Seismicity of Croatia in the period 1990–1992, *Geofizika* **10**, 19–34.

Markušić, S., Herak, D., Ivančić, I., Sović, I., Herak, M., Prelogović, E., 1998. Seismicity of Croatia in the period 1993–1996 and the Ston-Slano earthquakes of 1996, *Geofizika* **15**, 83–102.

Markušić, S. and Herak, M., 1999. Seismic zoning of Croatia, *Natural Hazards* **18**, 269–285.

Markušić, S., Suhadolc, P., Herak, M., Vaccari, F., 2000. A contribution to seismic hazard assessment in Croatia from deterministic modeling, *Pure appl. geophys*. **157**, 185–204.

McKenzie, D., 1972. Active tectonics of the Mediterranean region, *Geophys. J. R. Astron. Soc*. **30**, 109–185.

Mohorovičić, A., 1910. Potres od 8. X. 1909, Godišnje izvješće zagrebačkog meteorološkog opservatorija za godinu 1909, godina IX, dio IV, polovina 1, Naklada Kr. Hrv.-Slav. Dalm. Zem. vlade, Odjela za bogoštovje i nastavu, Zagreb, 1–56 (in Croatian and German).

Nocquet, J.-M., Calais, E., 2004. Geodetic measurements of crustal deformation in the Western Mediterranean and Europe, *Pure appl. geophys*. **161**, 661–681.

Oldow, J. S., Ferranti, L., Lewis, D.S., Campbell, J.K., D'Argenio, B., Catalano, R., Pappone, G., Carmignani, L., Conti, P., Aiken, C.L.V., 2002. Active fragmentation of Adria, the north Africa promontory, central Mediterranean orogen, *Geology* **30**, 779–782.

Prelogović, E., Saftić, B., Kuk, V., Velić, J., Dragaš, M., Lučić, D., 1997. Tectonic activity in the Croatian part of the Pannonian Basin, *Tectonophysics* **297**, 283–293.

Pribičević, B., Medak, D., Prelogović, E., 2002. Determination of the recent structural fabric in the Alps-Dinarides area by combination of geodetic and geologic methods, *Raziskave s področja geodezije in geofizike 2002*, Kuhar, M. Brilly, M. (eds.), Ljubljana: Fakulteta za gradbeništvo in geodezijo, Univerza v Ljubljani, 57–65 (international peer-review).

Serpelloni, E., Anzidei, M., Baldi, P., Casula, G., Galvani, A., 2005. Crustal velocity and strain-rate fields in Italy and surrounding regions: new results from the analysis of permanent and non-permanent GPS networks, *Geophys J. Int*. **161 (3)**, 861–880.

Shebalin, N. V., Karnik, V., Hadžievski, D., 1974. Catalogue of earthquakes I–II, UNDP/UNESCO Survey of the seismicity of the Balkan region, Skopje.

Skoko, D., Prelogović, E. and Aljinović, B., 1987. Geological structure of the Earth's crust above the Moho discontinuity in Yugoslavia, *Geophys. J. R. Astron. Soc*. **89**, 379–382.

Slejko, D., Camassi, R., Cecić, I., Herak, D., Herak, M., Kociu, S., Kouskouna, V., Lapajne, J., Makropoulos, K., Meletti, C., Muco, B., Papaioannou, C., Peruzza, L., Rebez, A., Scandone, P., Sulstarova, E., Voulgaris, N., Živčić, M., Zupančič, P., 1999. Seismic hazard assessment for Adria, *Annali di Geofisica* **42**, 1085–1107.

Torbar, J.,1882. Report on the Zagreb earthquake of November 9, 1880. JAZU, Knjiga I, Zagreb, 1–144 (in Croatian).

Seismicity of the Pannonian Basin

László Tóth*, Péter Mónus[1], Zoltán Bus[2], and Erzsébet Györi[3]

Abstract This article gives a brief summary of the seismic instrumentation used and the monitored results of earthquake activity in Hungary. Despite the Pannonian basin being characterized as a low-to-medium level seismicity region, the risk of destructive earthquake is still a major concern throughout Central Europe. The high population density in the region, and the number of vulnerable industrial facilities eg. nuclear power plants are being among the most sensitive ones regarding public concern.

Keywords Pannonian basin, seismicity, seismic monitoring, seismic hazard

1 Introduction

The Pannonian basin is located between the seismically very active NE Mediterranean sea and the nearly aseismic East European platform. The formation of the Pannonian basin within the Alpine orogenic belt started in the early Miocene and continued with structural inversions up to the late Pliocene-Quaternary period. Presently, there is clear evidence from GPS geodetic observations and seismic monitoring that the Pannonian basin continues to be deformed (Horváth et al., 2004; Grenerczy et al., 2002, 2005; Tóth et al., 2002, 2006; Bada et al., 1998, 1999; Horváth, 1988; Horváth and Cloetingh, 1996).

[1]Seismological Observatory, Hungarian Academy of Sciences (HAS), Budapest, Hungary, GeoRisk Earthquake Research Institute, Budapest, Hungary

[2]Seismological Observatory, Hungarian Academy of Sciences (HAS), Budapest, Hungary

[3]Research Group of Geophysics and Environmental Physics (HAS), Budapest, Hungary

*To whom correspondence should be addressed. E-mail: toth@georisk.hu

E.S. Husebye (ed.), *Earthquake Monitoring and Seismic Hazard Mitigation in Balkan Countries.*

The monitoring of seismicity in the Pannonian basin is not only vital for seismic risk assessment, within a densely populated area, but also to gain a better understanding of the geodynamics of the region through extensive geophysical mapping, and seismotectonic modeling and research. Seismotectonic models published in the early 1990s for the Alps and the northern Dinarides predict with some confidence where earthquake may occur (Anderson and Jackson, 1987; Slejko et al., 1989, 1998; Carulli et al., 1990; Favali et al., 1990; Del Ben et al., 1991; Console et al., 1993; Mariucci et al., 1999).

Due to the development in seismic instrumentation, computer equipments and communication technology in the last decades, high quality seismic stations became affordable even for industrial and civil applications. Sensitive local and regional networks have been installed in the Euro-Mediterranean area (Burchfiel et al., 2008; Kotzev et al., 2008) and the number of seismic monitoring stations has been dramatically increased even in seismically less active areas like Hungary.

2 Historical Seismicity

Seismic activity in and around the Pannonian basin can be characterized as moderate. There are significant variations in different tectonic domains (Figure 1) with the Vrancea region, in the southeast Carpathians, having the strongest and most frequent earthquakes – three with magnitudes larger than 6.5 within the last 30 years (1977: Ms7.2; 1986: Ms7.0; 1990: Ms6.7), and magnitudes of 5 on almost a yearly basis (Zsíros, 2003a, b). In the less active Pannonian basin – an area of about 206,117 km^2 – the occurrence of a magnitude 6 earthquake is about once in 100 years, while a magnitude 5 event occurs in average every 20 years.

Distribution of focal depths suggests three depth domains. Shallow focal depths within the top 20 km of the earth's crust occur almost exclusively through the whole region except the Vrancea zone. In the Pannonian basin, the majority of events occur between 6 and 15 km below ground level. Earthquakes of the Vrancea region are characterized by intermediate depths, the strongest ones occur between 70–110 and 125–160 km depths within an almost vertical column. Deeper and shallower events also have been recorded but only with small magnitudes.

In studies of focal mechanism (Tóth et al., 2002), strike-slip and thrust faulting occurs almost exclusively throughout the Southern Alps and the Dinarides. The maximum horizontal stress directions clearly show N–S and NNE–SSW compression related to the ongoing collision of Adria with Europe (Bada et al., 1999; Kotzev et al., 2008).

The seismicity is moderate in the Eastern Alps and the western Carpathians, where focal mechanism findings show that the majority have strike-slip mechanisms with NNW–SSE and N–S directions. The horizontal stresses are the largest and the most frequent, but NE–SW directions are nonetheless occasionally observed.

Focal mechanism results in the Pannonian basin are more diverse although thrust and strike-slip faulting seem to be dominant. NNE–SSW and NE–SW directions of

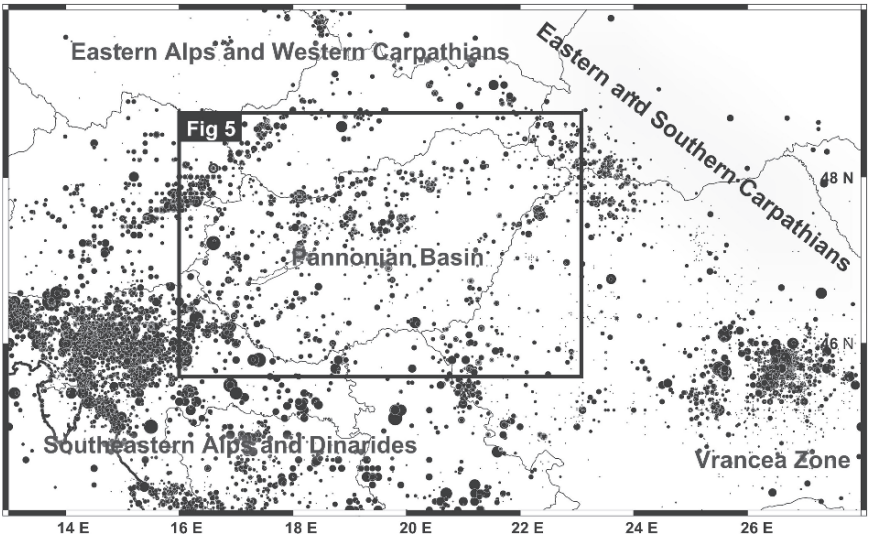

Figure 1 Seismicity of the Pannonian basin and adjacent area (44.0–50.0N; 13.0–28.0E). The regional earthquake database contains more than 22,000 historical and instrumentally recorded events from AD 456 until 2005 (modified from Tóth et al., 2006). Details on the Pannonian basin seismicity are presented in Figure 5

maximum horizontal stresses prevail. However, these features highlight significant differences from those in Western Europe, where the dominant stress directions are perpendicular to those directions. The very few fault-plane solutions from the eastern and southern Carpathians areas indicate thrust faulting along E–W dominant stress axes. Most events in the Vrancea zone are compressional and occur at intermediate depths. Fault-plane solutions of instrumentally recorded large earthquakes show remarkably similar characteristics as they typically strike SW–NE and dip towards NW with the maximum horizontal stress axis characteristically being NW–SE, and in a few cases E–W.

3 Seismic Monitoring

Instrumental seismology is a relatively young science and the first somewhat crude pendulum instruments were installed around the turn of 19th century. The low sensitivity of these mainly ground displacement instruments allowed only for recording of larger magnitude events above $M > 4.5$ for local ones. The first seismograph station in Hungary became operational in 1902 but did not contribute much to the study of local seismicity (Bisztricsány and Csomor, 1981). Hence, macroseismic observations remained the primary source of earthquake occurrences in Hungary to the end of 1980s.

Both instrumentation and seismic record analysis techniques have improved markedly since the mid-1970s. Digital recording has become commonplace and thus permitting use of sophisticated signal processing techniques even in real time. Previously, poor sensitivity of the seismograph stations effectively "prevented" detection of small magnitude earthquakes. Today the problem is the ambient noise level being due to natural and cultural noise sources which sets a lower signal detection level being roughly equivalent to magnitude 2.0 events. Note this level is most difficult to lower further unless local networks are deployed.

In Hungary, a complete overhaul of the traditional analogue seismograph network was commenced in the early 1990s. 16 stations became operational by 2004 with an approx. station density of 1/6,000 km^2. The new national Hungarian network comprises 4 broadband stations (BB-STS2) and the remaining 12 stations are being equipped with 3-component short period seismometers (LE-3D).

Careful site selection and analysis of the ambient seismic noise was carried out before locating the BB stations in the field. Each of the sites has fairly good geology in terms of competent hard rocks. The seismic vaults are constructed according to well proven local standards and besides advantages taken of pre-existing infrastructure (Figure 2). A high speed TCP/IP internet link is used for remote data access at all

Figure 2 The BB field stations are equipped with STS-2 three component broadband seismometers. Seismic data is distributed in near real time by SeedLink servers running on Linux based PCs

Figure 3 The SP field stations each consist of a three component short period seismometer located in a pit, with a digital recorder and time signal receiver housed nearby in a heat insulated steel container building

the BB sites. The stations are equipped with STS-2, three component, broadband seismometers and the seismic data are distributed in near-real-time by SeedLink servers running on inexpensive Linux based PCs.

Each SP field station consists of a three component short period seismometer located in underground pits with a digital recorder and time signal receiver housed nearby in a heat insulated steel container building (Figure 3). The seismometers used are the LE-3D three directional compact size high sensitivity 1 Hz geophones. The digital acquisition system is the Lennartz MARS-88 recorder that uses 20 bit AD converters sampling the data 62.5 times per second. The recorder also performs signal detection by its internal STA/LTA algorithm.

Both event records and continuous data are stored on rewritable magneto-optical disks. This in turn are collected and transferred to the data centre in Budapest on a weekly basis.

The predicted detection capability of the network (Table 1) at average noise conditions (with S/N > 10 at four stations) is equivalent to 1.5–2.0 M_L (Figure 4) so it is unlikely that any felt events would remain undetected in most of Hungary. In other words, 10 years of national network recording have now confirmed its design goal capability.

4 Recent Seismicity

Earthquake activity in the Pannonian basin can be characterized as distributed intraplate seismicity. However specific tectonic structures cannot be identified because incomplete in seismotectonic and geological information does not allow us to determine which fault is associated with a specific earthquake (Figure 5). This is particularly true for events below magnitude 4. For large historical earthquakes, the difficulty mostly stem from inaccurate hypocenter locations.

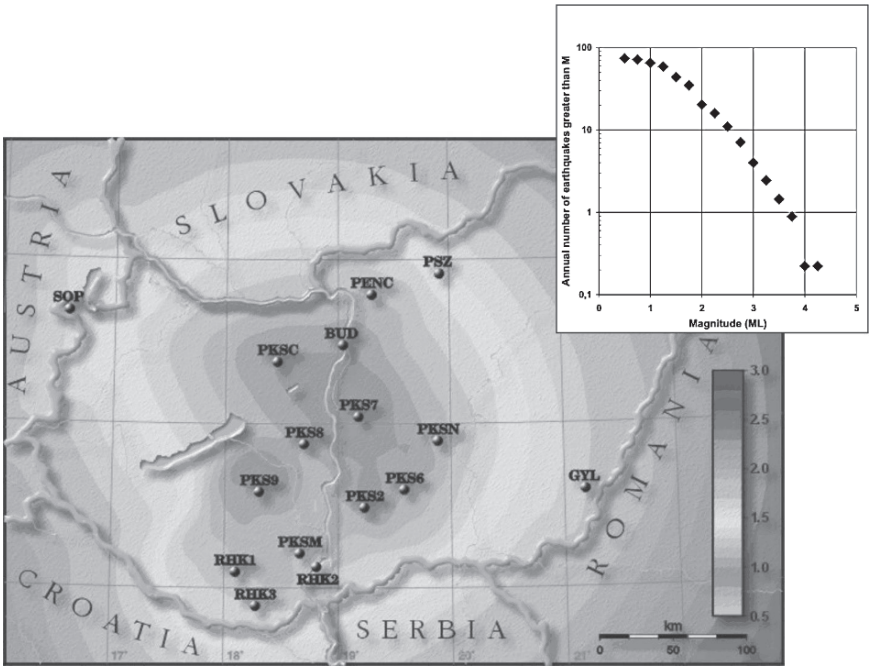

Figure 4 Predicted and observed detection capability of the Hungarian seismograph network. Contour values are local Richter magnitudes (M_L). Criteria for calculation: signal to noise ratio greater than 10 at minimum four stations at average noise conditions. The insert shows the magnitude recurrence curve for Hungary for the recording period 1995–2004

During the 10-year period 1995–2004, the Hungarian seismographic network located some 700 earthquakes within the Pannonian basin and adjacent areas as shown in Figure 5. This total includes two earthquakes of M_L 4; 61 earthquakes of M_L 3; and 249 earthquakes of M_L 2. Out of the mentioned 700 earthquakes 60 were reported felt. Focal depth is also important whether an earthquake would be felt or not and naturally shallow events favor "human detection". These recorded earthquakes are mostly shallow with about 80% in the upper crust that is 6–15 km depth.

Obviously, earthquakes can occur in almost any part of the Pannonian basin, although certain areas have a higher likelihood of occurrence than others. The most earthquake prone areas are the Komárom – Mór – NE of Balaton belt (47.4–47.8N; 18.2E); the Danube bend region (47.8N; 19.0E); the locality of Eger (47.9N; 20.4E) and the area of Jászberény (47.5N; 20.0E). The Vienna basin, in eastern Austria and the northeastern part of Croatia are also relatively active (Markušić, 2008).

The outcome of high sensitivity monitoring over the last 10 years (Tóth et al., 2004) shows that there are in average 4 and 30 earthquakes of magnitude 3 and 2 respectively. The information of magnitude recurrence in the low magnitude range (M_L 2–4) is a very important contributor for the seismotectonic modeling (Bada et al., 2006).

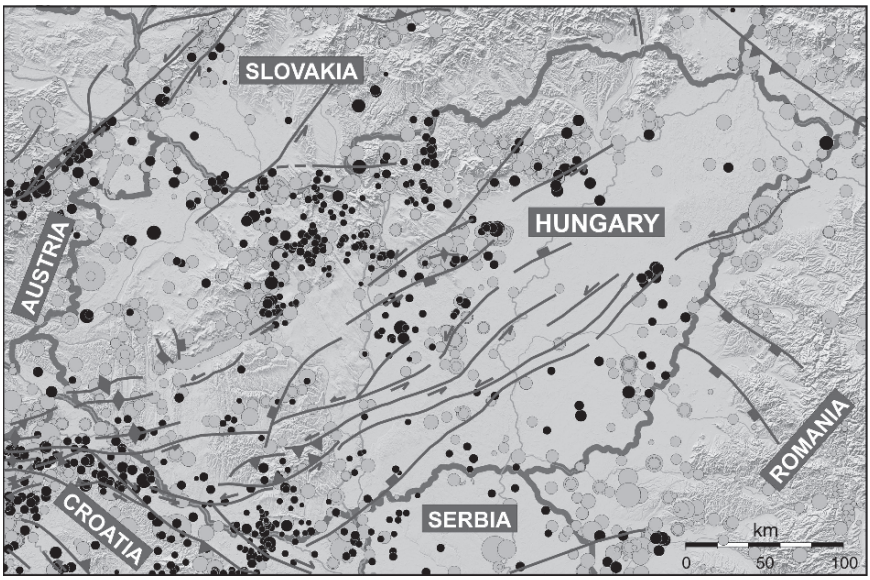

Figure 5 Historical and recent seismicity of the Pannonian basin (Figure 1 insert; 45.5–49.0N; 16.0–23.0E). Grey dots show epicenter distribution of historical (456–1994) earthquakes while black dots represent recent (1995–2004) well located earthquakes. Lines illustrate neotectonic active structures after Horváth et al. (2005)

5 Earthquake Recurrence and Seismic Hazard

In assessing the seismic risk in areas where the extent of faulting in the crustal interior is unknown, the current practice is to represent the temporal occurrence of earthquakes as a Poisson process. For a "complete catalogue" all fore and aftershocks must be removed from the earthquake catalogue, and all earthquakes above a lower bound magnitude (the threshold magnitude M_0) are presumed to be included.

For identifying main shocks, space and time filters are applied - see Table 2. Dieterich (1994) proposed that the aftershock duration T generally increases with the inferred recurrence time of the main shock T_r such that $T \approx T_r/20$. Stein and Newman (2004), following studies in New Madrid zone, Missury USA, put forward the hypothesis of much longer aftershock duration periods for low seismicity intraplate settings. The explanation here is in terms of higher earthquake stress drops and larger normal stresses on intraplate faults. This in turn has a major impact on the assessment of seismic risk in areas of low seismic activity.

The Hungary case; based on empirical weighting, and also on our professional judgment, we used a magnitude-dependent space and time filter to identify main shocks in the catalogue detailed in Table 3.

A simple comprehensiveness test based on "magnitude recurrence fit" shows that our catalogue is complete since 1500 for magnitude $M_0 \geq 6.4$, since 1600 for magnitude

Table 1 The Hungarian seismograph network, the individual stations, their geographical locations, instrumentation and lithologies

Code	Lat (N)	Long (E)	Elev (m)	Site rock	Station type (1)	Sensor type (2)	Record (3)	Org. (4)
BUD	47,4836	19,0239	196	Dolomite	3C BB 3C SP	STS-2 LE-3D	D - C D - E	GGKI GR
PENC RHK4	47,7905	19,2817	250	Alluvium	3C SP	LE-3D	D - E	GGKI-GR
PKS2	46,4920	19,2131	106	Sand	3C SP	LE-3D	D - E	GR
PKS6	46,5998	19,5645	120	Sand	3C SP	LE-3D	D - E	GR
PKS7	47,0473	19,1609	95	Mud	3C SP	LE-3D	D - E	GR
PKS8	46,8787	18,6765	135	Rhyolite tuff	3C SP	LE-3D	D - E	GR
PKS9	46,5870	18,2789	240	Loess	3C SP	LE-3D	D - E	GR
PKSG	47,3918	18,3907	200	Dolomite	3C SP	LE-3D	D - E	GR
PKSM	46,2119	18,6413	170	Granite	3C BB	STS-2	D - C	GGKI
PKSN	46,8972	19,8673	110	Sand	3C SP	LE-3D	D - E	GR
PSZ	47,9184	19,8944	940	Andesite	3C BB	STS-2	D - C	GGKI
RHK1	46,0948	18,0720	297	Limestone	3C SP	SS-1	D - E	GGKI
RHK3	45,8885	18,2521	420	Limestone	3C SP	LE-3D	D - E	GR
RHK5	47,6983	19,0822	213	Limestone	3C SP	LE-3D	D - E	GR
RHK6	47,6741	19,2488	157	Sand	3C SP	LE-3D	D - E	GR
SOP	47,6833	16,5583	260	Gneiss	3C BB	STS-2	D - C	GGKI

(1) 3C – three component seismometer; SP – short period seismometer; BB – broad band seismometer
(2) STS-2 – Streckeisen broad band seismometer; LE-3D – Lennartz three directional 1 Hz geophone; SS-1 – Kinemetrics 1 Hz seismometer
(3) D – digital; C – continuous recording; E – event recording
(4) GGKI – Geodetic and Geophysical Research Institute, HAS; GR – GeoRisk Earthquake Research Institute Ltd

Table 2 Space and time windows used for filtering out the aftershocks and foreshocks in the Hungarian catalogue. In the vicinity of radius **R** of the magnitude **M** main earthquake, all shocks with **M′< M** are regarded as aftershocks or foreshocks conditioned on their origin time differences being less than **T** or **T′** respectively

Magnitude	R (km)	T (day)	T′ (day)
MM ≤ 1.8	5	1	1
1.9 ≤ MM ≤ 2.7	10	2	1
2.8 ≤ MM ≤ 3.3	15	5	1
3.4 ≤ MM ≤ 4.0	20	30	2
4.1 ≤ MM ≤ 4.7	25	130	4
4.8 ≤ MM ≤ 5.4	30	260	10
5.5 ≤ MM ≤ 6.1	35	650	15
6.2 ≤ MM	40	850	30

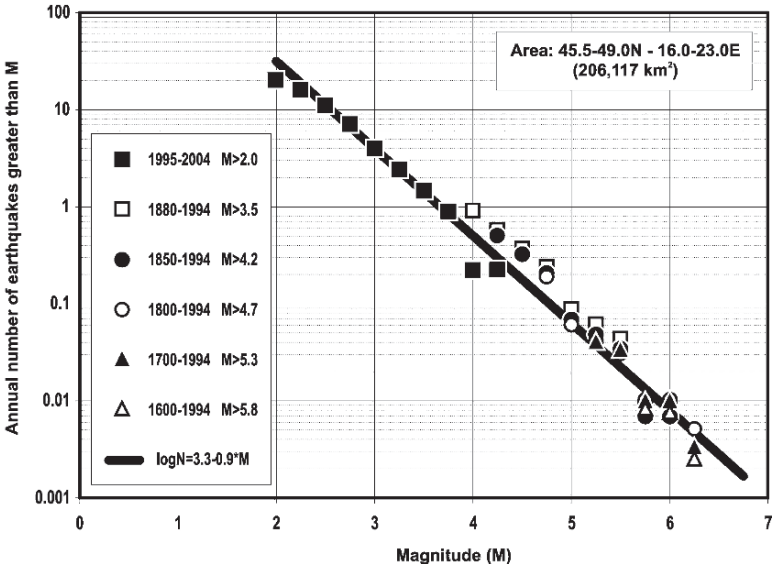

Figure 6 Magnitude recurrence curve for Pannonian basin earthquakes

$M_0 \geq 5.8$, since 1700 for magnitude $M_0 \geq 5.3$, since 1800 for magnitude $M_0 \geq 4.7$, since 1850 for magnitude $M_0 \geq 4.2$, and since 1880 for magnitude $M_0 \geq 3.5$ for the whole Pannonian region related to the human detection threshold mentioned previously.

The probability of earthquake occurrence as a function of magnitude is generally represented by an exponential distribution, as proposed by Gutenberg and Richter (1944): $log\mathbf{N} = \mathbf{a} - \mathbf{bM}$, where **N** is the annual number of earthquakes with magnitude equal or greater than **M**. From the Pannonian basin dataset, we find that **a** = 3.3 and **b** = 0.9 in the $2.0 \leq \mathbf{M} \leq 6.3$ magnitude range (Figure 6).

Using the methodology described in slejko (1998) and particularly in Tóth et al. (2006), seismic hazard maps for the whole Pannonian region were computed. The map shown in Figure 7 depicts the mean PGA with a 90% probability of non-exceedance in 50 years.

Table 3 Completeness test results for the Pannonian region earthquake catalogue

The catalogue is complete	for magnitude
Since 1500	$M_0 \geq 6.4$
Since 1600	$M_0 \geq 5.8$
Since 1700	$M_0 \geq 5.3$
Since 1800	$M_0 \geq 4.7$
Since 1850	$M_0 \geq 4.2$
Since 1880	$M_0 \geq 3.5$

Most of the Pannonian basin has a relatively low seismic risk, with less than 1 m/s^2 expected PGA; however, there are some areas of potential greater risk in the range of 1–2 m/s^2. These are Komárom, northeast of Lake Balaton, east of Budapest, the south-western part of Hungary.

6 Conclusions

To understand how tectonic stress and strain propagates from plate boundaries into continental areas has been a major problem for a long time (Ziegler et al., 1995, 2002. Due to its unusual tectonic environment, the Pannonian basin is an excellent natural laboratory for in-depth investigations here. Stress accumulations and recent deformations in the Pannonian basin are governed by the interaction of plate boundary and intraplate forces being the dominant source of compression. Adding to the complexities is the counterclockwise rotation and N–NE directed indentation of the Adria microplate (also known as "Adria-push"- see also Kotzev et al., 2008). A combination of buoyancy forces associated with elevated topography and lithospheric heterogeneities in the adjacent orogens that result in a complex pattern of ongoing tectonic stresses and deformation activities being projected far into the Pannonian basin.

Observed earthquake activities indicate that current deformation is mainly concentrated in the contact zone between Adria and the Alpine–Dinarides orogen (Figure 1) and some of the movement is transferred into the Pannonian basin resulting in a complex stress/strain pattern. Deformations here may occur whenever the stress exceeds the local shear strength of any given rock mass so neither earthquakes nor other forms of deformation are restricted to block boundaries. Hence a more distributed seismicity pattern as expected is observed (Figure 5), with an added feature of the hot and weak extended Pannonian lithosphere being its characteristic reactivation under relatively low compressional stresses (Lenkey et al. 2002).

Using GPS measurements, Grenerczy et al. (2002) found the largest crustal velocities (1.5–2 mm/year northward) in the Pannonian region in the SW; in the Alpine–Adriatic collision zone. Inside the Pannonian basin itself, the typical velocity was about 1.0–1.5 mm/year directed eastward. Grenerczy at al. (2005) and Kotzev et al. (2008) also concluded that the Alps, Dinarides, and Pannonian basin, take up the shortening caused by the Nubia/Adria convergence. On this basis, we claim ourselves that the Western and Northern Carpathians are no longer active thrust fronts; and now can be considered parts of a stable, and rigid, European Platform.

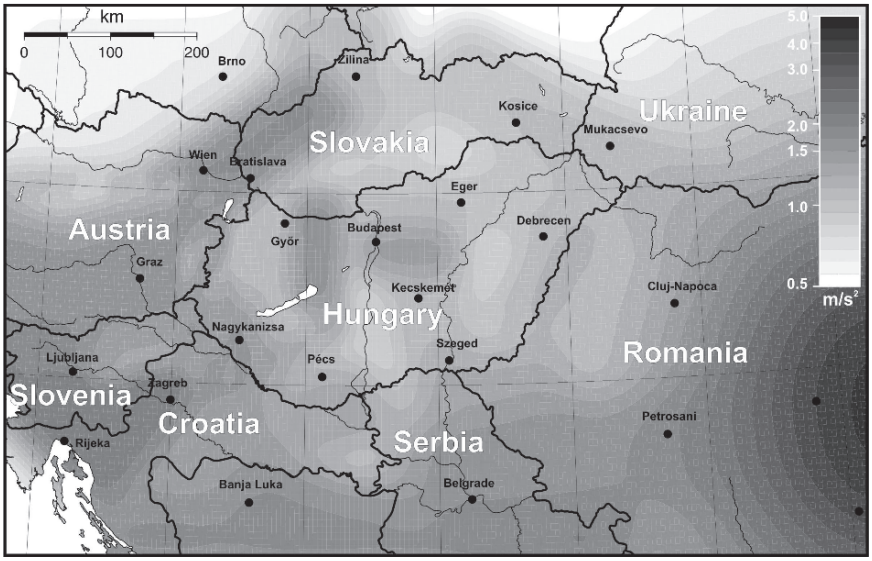

Figure 7 Seismic hazard in the Pannonian basin region. Expected peak ground acceleration in m/s^2 (10% probability of exceedance in 50 years, 475-year return period)

Acknowledgements The research presented in this contribution has been supported by Paks NPP and GeoRisk Ltd. The authors thank Prof. Eystein Husebye for reading the manuscript and for his number of valuable comments.

References

Anderson, H. A., Jackson, J. A., 1987. Active tectonics of the Adriatic region. *Geophys. J. R. Astron. Soc.,* 91: 937–983.

Bada, G., Gerner, P., Cloetingh, S., Horváth, F., 1998. Sources of recent tectonic stress in the Pannonian region: inferences from finite element modelling. *Geophys. J. Int.,* 134: 87–102.

Bada, G., Horváth, F., Gerner, P., Fejes, I., 1999. Review of the present-day geodynamics of the Pannonian basin: progress and problems. *J. Geodynamics,* 27: 501–527.

Bada, G., Grenerczy, Gy., Tóth, L., Horváth, F., Stein, S., Cloetingh, S., Windhoffer, G., Fodor, L., Pinter, N., Fejes, I., 2006. Motion of Adria and ongoing inversion of the Pannonian basin: Seismicity, GPS velocities and Stress Transfer (to appear in a special GSA volume).

Bisztricsány, E. Csomor, D., 1981. 75 years of seismological research in Hungary, Acta Geodaet., Geophys. et Montanist. *Acad. Sci. Hung. Tomus,* 16 (2–4): 423–434.

Burchfiel, B.C., King, R.W., Nakov, R., Tzankov, T., Dumurdzanov, N., Serafi movski, T., Todosov, A., Nurce, B., 2008. Patterns of Cenozoic Extensional Tectonism in the South Balkan Extensional System. In E.S. Husebye (ed.). Earthquake Monitoring and Seismic Mazard in Balkan Countries. Springer publishing, Berline, 3–18.

Carulli, G. B., Nicolich, R., Rebez, A., Slejko, D., 1990. Seismotectonics of the Northwest External Dinarides. *Tectonophysics*, 179: 11–25.

Console, R., Di Giovambattista, R., Favalli, P., Presgave, B. W., Smriglio, G., 1993. Seismicity of the Adriatic microplate. *Tectonophysics*, 218: 343–354.

Del Ben, A., Finetti, I., Rebez, A., and Slejko, D., 1991. Seismicity and seismotectonics at the Alps-Dinarides contact. *Bollettino di Geofisica Teorica ed Applicata*, 33: 155–176.

Dieterich, J. H., 1994. A constitutive law for rate of earthquake production and its application of earthquake clustering. *J. Geophys. Res*. 99(2): 2601–2618.

Favali, P., Mele, G., Mattietti, G., 1990. Contribution to the Study of the Apulian Microplate Geodynamics. *Memorie della Società Geologica Italiana*, 44: 71–80.

Grenerczy, G., Fejes, I., Kenyeres, A., 2002. Present crustal deformation pattern in the Pancardi Region: Constraints from Space Geodesy. In *Neotectonics and surface processes: the Pannonian basin and Alpine/Carpathian system*, S. Cloetingh, F. Horváth, G. Bada, A. Lankreijer (eds.). *EGU St. Mueller Special Publication Series* 3: 65–77.

Grenerczy, G., Sella, G., Stein, S., Kenyeres, A., 2005. Tectonic implications of the GPS velocity field in the northern Adriatic region. *Geophys. Res. Lett*, 32 (16), L16311.

Gutenberg, J., Richter, C. F., 1944. Frequency of earthquakes in California. BSSA; 34: 185–188.

Horváth F., 1988. Neotectonic behaviour of the Alpine-Mediterranean region. In *The Pannonian Basin - A study in basin evolution*, L. H. Royden, F. Horváth (eds.). AAPG Memoir, 45: 49–51.

Horváth, F., Cloetingh S., 1996. Stress-induced late-stage subsidence anomalies in the Pannonian basin. *Tectonophysics,* 266: 287–300.

Horváth, F., Bada, G., Szafián, P., Tari G., Ádám A., Cloetingh S., 2004. Formation and deformation of the Pannonian basin constraints from observational data. In *European Lithosphere Dynamics*, D.G. Gee, R. Stephenson (eds.). *Geol. Soc. London Spec. Publ.*

Kotzev et al., 2008. Crustal Motion and Strain Accumulation in the South Balkan Region Inferred from GPS Measurements. In E.S. Husebye (ed.). Earthquake Monitoring and Seismic Hazard in Balkan countries. Springer Publishing, Berline, 19–43.

Lenkey, L., Dövényi, P., Horváth, F., Cloetingh, S.A.P.L., 2002. Geothermics of the Pannonian basin and its bearing on the neotectonics. In *Neotectonics and surface processes: the Pannonian basin and Alpine/Carpathian system*, S. Cloetingh, F. Horváth, G. Bada, A. Lankreijer (eds.). EGU St. Mueller Special Publication Series, 3: 29–40.

Mariucci, M.T., Amato, A., Montone, P., 1999. Recent tectonic evolution and present stress in the Northern Apennines (Italy). *Tectonics*, 18: 108–118.

Markušić, S., 2008. Seismicity of Croatia. In E.S. Husebye (ed.) Earthquake Monitoring and Seismic Hazard in Balkan countries. Springer Publishing, Berline, 81–98.

Slejko, D., Carulli, G. B., Nicholic, R., Rebez, A., Zanferrari, A., Cavallin, A., Doglioni, C., Carraro, G., Castaldini, D., Iliceto, V., Semenza, E., Zanolla, C., 1989. Seismotectonics of the eastern Southern-Alps: a review. *Bollettino di Geofisica Teorica ed Applicata*, 31: 109–136.

Slejko, D., Peruzza, L, Rebez, A., 1998. Seismic hazard maps of Italy. *Ann. Geophys*., 41: 183–214.

Stein, S., Newman, A., 2004. Characteristic and Uncharacteristic Earthquakes as Possible Artifacts: Applications to the New Madrid and Wabash Seismic Zones. *Seismol. Res. Lett.ers,* 75 (2): 173–187.

Tóth, L., Mónus, P., Zsíros, T. Kiszely, M., 2002. Seismicity in the Pannonian Region – earthquake data. In *Neotectonics and surface processes: the Pannonian basin and Alpine/Carpathian system*, S. Cloetingh, F. Horváth, G. Bada, A. Lankreijer (eds.). *EGU St. Mueller Special Publication Series,* 3: 9–28.

Tóth, L., Mónus, P., Zsíros, T., Kiszely, M., 2004. Micro-seismic monitoring of seismoactive areas in Hungary. Studi Geologici Camerti, Special Issue: Proceedings of the workshop COST Action 625 "Active faults: analysis, processes and monitoring".

Tóth, L., Györi, E., Mónus, P., Zsíros, T., 2006. Seismic Hazard in the Pannonian Region. In: Pinter, N., Grenerczy, Gy., Weber, J., Stein, S., Medak, D. (eds.), The Adria Microplate: GPS Geodesy, Tectonics, and Hazards. Springer Verlag. *NATO ARW Series*, 61: 369–384.

Ziegler, P. A., Cloetingh, S., Van Wees, J.D., 1995. Dynamics of intra-plate compressional deformation: the Alpine foreland and other examples. *Tectonophysics*, 252: 7–59.

Ziegler, P. A., Bertotti, G., Cloetingh, S., 2002. Dynamic processes controlling foreland development - the role of mechanical (de)coupling of orogenic wedges and forelands, in Bertotti, G., Schulmann, K., and Cloetingh, S. (eds.), Continental collision and the tectono-sedimentary evolution of forelands. Katlenburg-Lindau, Germany, European Geosciences Union. *St. Mueller Special Publication Series*, 1: 17–56.

Zsíros, T., 2003a. Earthquake activity and hazard in the Carpathian basin I. *Acta Geod. Geoph. Hung*., 38 (3): 345–362.

Zsíros, T., 2003b. Earthquake activity and hazard in the Carpathian basin II. *Acta Geod. Geoph. Hung.,* 38 (4): 445–465.

Part III
Seismic Network Operations on Global, Regional and National Scales

The CTBTO International Monitoring System and Global Seismicity

Rashad Kebeasy*

Abstract On 10 September 1996, the United Nations General Assembly adopted the Comprehensive Nuclear-Test-Ban Treaty (CTBT), which prohibits all nuclear test explosions in any environment. This treaty was opened for signature on 24 September 1996, in New York and will enter into force after it has been ratified by 44 States, which have been identified in Annex 2 of the Treaty as having nuclear capabilities. As of 2 July 2004, 115 (67%) of the 172 Signatory States of the CTBT (among the 194 UN Member States) have ratified the Treaty. From the 44 States of Annex 2, 41 (93%) have signed the Treaty, with more than two thirds, or 32 (73%), also having completed ratification.

The Comprehensive Nuclear Test-Ban Treaty Organization (CTBTO) with its Preparatory Commission (PrepCom) was established as an international organization by the States Signatories to the Treaty on 19 November 1996. It consists of the policy-making organs of the PrepCom plenary body in conjunction with three working and advisory groups and the Provisional Technical Secretariat (PTS). The PTS started its work in Vienna, Austria in March 1997 and consists, besides administrative and legal divisions, of three technical divisions: the International Monitoring System (IMS), the International Data Center (IDC), and the On-Site Inspection (OSI) division. The IMS – division major responsibilities include the installation, operation and maintenance of the 337 monitoring facilities specified in the Protocol to the Treaty, comprising 321 monitoring stations and 16 radionuclide laboratories.

Keywords CTBTO, Test Ban Treaty, UN General Assembly, IDC Vienna, NDC, Global Monitoring, Seismic, Hydroacoustic, Infrasound, Radionuclide

Background Seismology is generally rated the Queen of Earth Sciences due to its ability to provide in ever increasing detail information bearing on the Earth's interior and to monitore ongoing dynamic processes. The reason for this two-fold; i) the advanced theoretical foundation of seismology and ii) extensive scientific

National Research Institute of Astronomy and Geophysics, Helwan, Egypt

*To whom correspondence should be addressed. E-mail: kebeasy-rashad@yahoo.com

E.S. Husebye (ed.), *Earthquake Monitoring and Seismic Hazard Mitigation in Balkan Countries.*

cooperation in recording and disseminating data in real time on local, regional and global scales. In contrast, some 50 years ago seismology was a backward science of little interests outside the academics and in addition funding was poor both for modern instrumentation and research. This situation abruptly changed with the sudden political interest in seismology as the principal tool for monitoring compliance with a potential Comprehensive Nuclear Test Ban Treaty (CTBT) banning any kind of nuclear testing in any environment. In the early 1950-ties the superpowers plus UK tested their nuclear war heads in the atmosphere and occasionally under water and thus caused pollution of the environment also outside the respective national borders. Other public worries were that the nuclear testing was considered an escalation ladder of the arms race between USA and USSR. This in turn was likely to encourage nuclear weapon proliferations to regional powers. So already in 1955 the test ban issue was on the agenda of the UN Council of Disarmament who met regularly in Geneva – this initiative come from a subgroup of so-called non-aligned countries. Clearly, the public awareness of potential danger to mankind from the atmospheric nuclear tests forced the military to rethink the ways these weapons should be tested in the future. A most spectacular undertaking in this regard was the Rainier underground test in Nevada in 1957. It was remarkable on 3 accounts; i) formal weapon test requirements were fulfilled, ii) no polluting of the free surface environment and iii) this underground nuclear explosion was recorded by seismograph stations hundreds of kilometres away. In other words, testing underground avoided pollution and also offered means for monitoring compliance with future treaties banning all nuclear tests or except those conducted underground. At that time the political climate was cordial and already next year in 1958 did scientific experts from USA, USSR and UK convene in Geneva for elaborating on a seismological monitoring system having global coverage. The expert discussions were not flattering for seismology per se; simply the magnitude estimation varied considerably, the relation between magnitude and weapon yield was not clearly understood, wave propagation in the upper part of the Earth showed strong regional variations and their recording means were primitive. Simply, the seimic monitoring capabilities anno 1958 were highly inadequate for meeting political requirements for verification of a nuclear test ban treaty. Albeit the scientific experts disagreed on many scientific topics they agreed unanimous on the need for launching extensive and fundamental seismological research programs. The above powers all started undertakings and the most and extensive and well known was the VELA Uniform Program of the USA which has continued until presently albeit less vigorous in the last decade. An outstanding achievement in this regard was the deployments and operations of the 2 large aperture arrays LASA (Montana) and NORSAR (Norway). These arrays introduced digital seismometry to the community, demonstrated the feasibility of automatic processing and analysis of seismic records and via ARPANET (forerunner to Internet) bilateral and multinational transfer of huge amount of seismic data. During the 1960- and 1970-ties seismology in a broad sense progressed rapidly from a backward to an advanced modern, mature science. In the 1980-ties scientific experts from many countries experts, still convening twice a year in Geneva, had devised a global monitoring system in

principle capable of monitoring compliance with a comprehensive test ban treaty. For its implementation political agreements were a prerequisite and this come in 1996 – a few years after the cold war ended.

In this article the focus is on the description of the current status of the CTBTO comprehensive monitoring set-up and its daily operation and data products. The scientific foundation upon which the monitoring system rests are far to comprehensive to be dealt with here so only some brief references are made to books literally capturing these research developments over the last 50 years, namely Husebye and Mykkeltveit (1981), Kerr (1985); Husebye and Dainty (1996) anf Lee et al. (2002). The latter book (Vol. 1 & 2) also contains contributions not directly funded by Vela Uniform nor similar national CTBT programs but serve to illustrate the seismological advances over the last decades.

The International Monitoring System of CTBTO, Vienna. The 321 stations (see Figure 1) will monitor the Earth environments for possible nuclear tests: the atmosphere, the oceans and the solid earth. Atmospheric tests will emit infrasonic waves and radionuclide debris as primary products. In addition, there is the possibility of secondary effects namely coupling into seismic and/or hydroacoustic waves. Underwater tests emit hydroacoustic signals, and radionuclides may be vented to the ocean surface from ascending bubbles. These tests will furthermore efficiently convert explosion energy into seismic waves and may also produce infrasonic waves. Underground nuclear explosions have been extensively studied in the past, since they produce characteristic seismic signals observed at the global networks of seismic stations. Besides they may be detected by their emitted 57 infrasound signals and, most likely in marine regions, will be coupled into hydroacoustic waves, called T-phases.

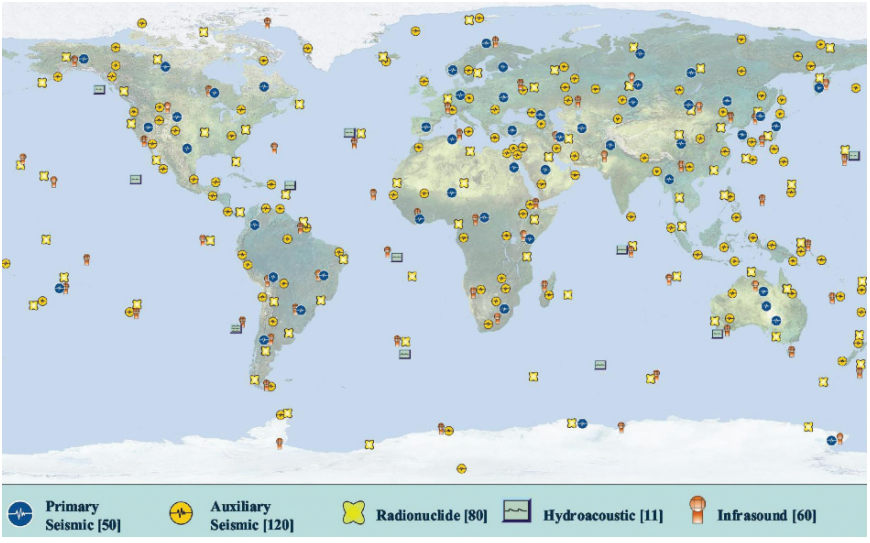

Figure 1 Global distribution of the International Monitoring System stations for the monitoring system of the CTBT comprises of 50 primary and 120 auxiliary seismic stations, 80 radionuclide stations, 11 hydroacoustic/T-phase stations, and 60 infrasound stations

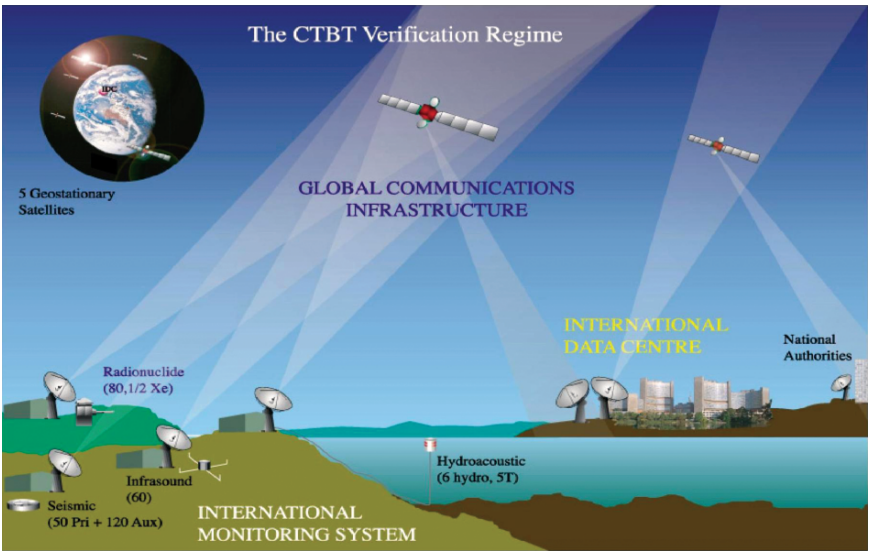

Figure 2 Overview of the different components of the CTBT monitoring system including the GCI communication system and the International Data Center. The later provides data and analysis products to the National Authorities of States Parties

Monitoring efficiencies in these environments will depend on ambient noise levels locally as well by non-random natural sources like chemical explosions, volcanoes, and earthquakes as well as bolides (meteor brusts) and supersonic aircraft in case of infrasound monitoring or whales for hydroacoustic monitoring.

Data handling, management and exchange. A major task for the monitoring system is the forwarding of the data collected by the IMS network to a central processing and archiving site, located at the IDC (division) in Vienna (Figure 2). The 50 primary seismic stations, the 60 infrasound stations and the 11 hydroacoustic stations send continuous waveform data via the Global Communications Infrastructure (GCI) to the IDC. This communication system is based on VSAT technology including the use of 5 space satellites providing for global coverage and currently operates under a 10-year contract. In addition, the 80 radioanuclide stations, the 16 radionuclide laboratories and the 120 auxiliary seismic stations send non-continuous data that is upon request of specific recorded time intervals to the IDC.

As of 30 June 2004, more than 80 certified stations contributed data to the IDC operational processing system. There, the data are automatically archived and processed, interactively analyzed and, on request, forwarded to National Data Centers (NDCs). The IDC carries out its mission in order to support States Parties in support of their verification responsibilities by providing objective analysis and other services which are necessary for an effective global monitoring system. According to the Protocol of the Treaty, the IDC shall: (i) “receive, collect, process, analyze, report on and archive data from IMS facilities, including the results of analysis conducted at

certified laboratories"; (ii) "produce standard reporting products and perform a standard range of services for States Parties, including event screening"; (iii) "apply automatic processing methods and interactive human analysis to raw IMS data on behalf of all States Parties, without prejudice to final judgements with regard to the nature of any event remaining the responsibility of States Parties"; and (iv) "carry out special studies to provide in-depth, Figure 2. Overview of the different components of the CTBT monitoring system including the GCI communication system and the International Data Center. The later provides data and analysis products to the National Authorities of States Parties technical review by expert analysis of data from the IMS, if requested by the Organization or by a States Party".

CTBTO data processing and analysis. The raw data arrive at the IDC within seconds or at most a few minutes after being acquired at the continuously recording monitoring stations (primary seismic, hydroacoustic, infrasound), that is the SHI stations (see Figure 3). In addition, data from auxiliary stations are arriving at the IDC within hours upon requests during later processing stages. For radionuclide stations it usually takes several days to submit their data to the IDC, since raw sample and subsequent data acquisition at the stations are a complicated process taking several 24-h stages. After the data arrive at the IDC they first undergo station processing which outcomes are standard detection lists of extracted waveform features for the SHI data and lists of unusual sample pulse height data in the case of radionuclide data.

For the SHI monitoring data a suite of automatic listed events, i.e. Standard Event List 1, 2, 3 (SEL1, SEL2, SEL3) is formed within about 2, 6 and 12 hours, respectively. The procedures here are tied to associations of detections from the various IMS stations. These processes are called network processing, since detections at the network stations are associated to build relevant events, which typically

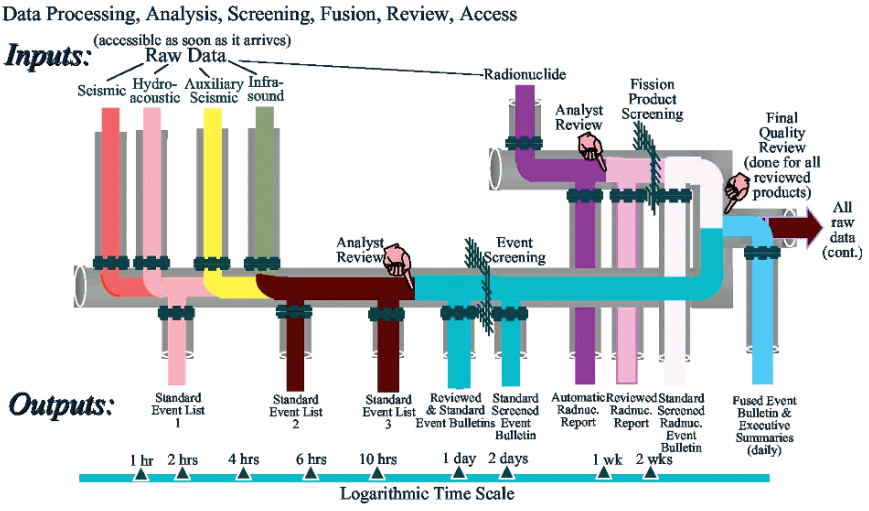

Figure 3 Schematics of the operational pipeline at the IDC illustrating the flow of data and the processing stages carried out for generating the IDC products provided to States Parties

consist of earthquakes and, to a much smaller extent, of mining related explosions. SEL1 is based exclusively on data from the primary seismic and hydroacoustic stations, while infrasound data are included for SEL2. For SEL2 and SEL3 additional data are requested from the auxiliary stations, if they provide an essential contribution to any solution found. On a typical day, as of this writing, the current network of more than 100 SHI stations, among them 60 certified stations, the IDC operational processing (Figure 3) produces nearly 150 events per days for SEL1, with slightly smaller numbers of events for the subsequently produced event lists. These automatic event lists are immediately distributed through a subscription mechanism to requesting States Parties, or can be accessed through an Automatic Data Request Manager (AutoDRM) or via the secure web site of the IDC. The access to the later, however, are restricted for access by authorized users only.

Event bulletins and other data products. Within several days (the Treaty calls for 2 days, but currently a schedule of 10 days or less is in place) the data of the IMS network as well as the final automatic event list SEL3 are reviewed by human analysts to check and refine the solutions generated by the automatic system. Most of this interactive analysis involves improvements of arrival phase parameters such as retiming and adding new arrivals or disassociating unreliable arrivals used by the automatic system. However, during interactive analysis an effort is made to scan the list of detections for any combinations of arrivals that may allow to form a new event. The result of the interactive analysis is the Reviewed Event Bulletin (REB) as the final product concerning the listing of a comprehensive listing of seismo-acoustic event files. The REB typically contains at present about 70 events daily and is based upon recordings and reports from about 100 SHI stations. For the time period from 21 February 2000, when the IDC started producing the REB on a regular basis through June 2004 a total of more than 98,000 seismic events have been located by the IDC. The geographical distribution of the epicenter locations is shown in Figure 4. Besides a clear representation of tectonic plate boundaries it is found that certain areas, such as Central and Northern Europe have disproportional high levels of seismicity, most likely caused by the detection of many chemical explosions stemming from mining and quarrying activities (e.g., see Husebye et al., 2002).

Following the release of the REB two additional products are generated at the IDC: the Standard Event Bulletin (SEB) which is based on the REB and includes additional automatically derived event characterization parameters that can be used by States Parties to conclude on the nature of a particular event. A second product, the Standard Screened Event Bulletin (SSEB), is the result of a so-called "screening process" in which event characterization parameters are used to filter out any events that can be attributed to natural or non-nuclear man-made phenomena.

For the radionuclide data an equivalent schedule is maintained. Automatic station processing of gamma-ray spectra is carried out at the IDC to produce the Automatic Radionuclide Report (ARR). Interactive analysis follows to refine automatic parameter estimates and the outcome is documented in the Reviewed Radionuclide Report (RRR), which also includes event characterization parameters. From 21 February 2000 to 30 June 2004 nearly 600 samples, which were analysed in routine monitoring operations, have been reported with significant levels (levels

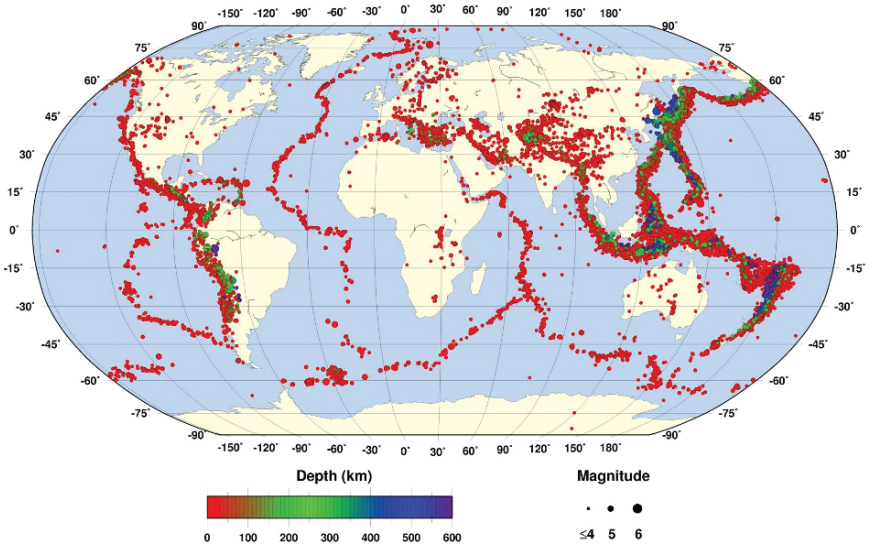

Figure 4 Geographical distributions of all REB events located at International Data Center of the CTBTO/PTS for the year 2003 comprising 2,4701 events of the Earth's seismicity as "seen" by the IMS monitoring system

4 and 5) of anthropogenic radionuclide contents. As for the SHI products, additional automatic post-processing is performed for those samples containing one or more anomalous radionuclides of relevance in a nuclear test context to produce the Standard Screened Radionuclide Event Bulletin (SSREB), which will include details of atmospheric transport modelling.

Summary remarks. Based on its basic obligations under a CTBT, the PTS, and in particular its IDC, provides a number of services to States Parties. As mentioned above are the dissemination of all the data and products obtained and generated at the IDC. Additional services are provided to enable and support States Parties in their verification tasks: support the establishment of National Data Centers and their ability to gain access to data and products: provide technical assistance to National Data Centers; make available processing software used at the IDC in order for States Parties to reassess results obtained at the IDC; and provide training to staff from National Data Centers. Currently, some 80 States Parties actively participate and more than 600 authorized users are registered for the mentioned IDC services.

The current operation of the international monitoring system for the monitoring of the CTBT has highlighted the future technological challenges and scientific opportunities for the seismological sciences. The primary technical challenge is the coherent operation and maintenance of the overall monitoring system at availability levels of nearly 100%. The scientific opportunities are posed by the task of detection, location and characterization of small events near or even below the anticipated detection threshold of body-wave magnitude 4 on a global scale. Fundamental

research in all four technologies is required to enhance our ability to cope with the challenges of CTBT monitoring. On the other hand, the monitoring system with its huge seismological data archives could evolve to a rich source for research institutions involved in different areas of earth and environmental science such as earthquake disaster assessment and Seismic hazard mitigation.

Acknowledgements This unique and original work as reported in this article could not have been realized in such very short time since the foundation of CTBTO in 1997 without the commitment, loyalty and hard work of the staff of the Provisional Technical Secretariat of the CTBTO in Vienna. I also wish to express my gratitude to prof. E.S. Husebye for the invitation to the NATO ARW in Borovets, Bulgaria in September 2005 and his editing efforts for this article.

References

Husebye, E.S., Mykkeltveit, S. (eds), 1981. Identification of Seismic Sources–Earthquake or Underground Explosion. Kluwer Academic Publishers, Noordrecht, The Netherlands. pp 871.

Husebye, E.S., Dainty, A.M. (eds.), 1996. Monitoring a Comprehensive Test Ban Treaty. Kluwer Academic Publishers, Noordrecht, The Netherlands. pp 836.

Husebye, E.S., Fedorenko, Y.V., Karadzhov, Y., 2002. Parameterized seismic source discrimination in aseismic regions. Seismological Research Lett. 73, 356–368.

Kerr, A.U., (ed.), 1985. The VELA Program; A Twenty-Five Year Review of Basic Research. Defense Advanced Research Project Agency (DARPA), US Government, Washington D.C., USA. pp 964.

Lee, W.H.K., Kanamori, H., Jennings, P.C., Kisslinger, C., (eds.), 2002. International Handbook of Earthquake and Engineering Seismology; Part A and B. Academic Press, San Francisco, USA. pp 933 and pp 937–1945.

The IRIS Consortium: Community Based Facilities and Data Management for Seismology

Shane Ingate*

Abstract Our Earth's interior remains one of man's major scientific frontiers. Inaccessible for direct observation beneath a 10–15 km drilling range, Earth's lower crust, mantle and core are seen primarily through illumination by seismic waves. In a major departure from the traditional single investigator approach to research support, the US seismological community has, in 1984, created a consortium of research institutions for the purpose of implementing critically needed national facilities necessary to support seismological research on Earth's interior in the coming decades. IRIS, the Incorporated Research Institutions for Seismology, a non-profit Delaware Corporation, was founded on May 8, 1984. By the first meeting of the Board of Directors on May 13 there were 26 members of the Corporation.

Continuous reliable functioning of the IRIS facilities over more than 20 years and the Consortium's unwavering commitment to free and unrestricted data availability have stimulated profound changes in attitudes among Earth scientists that strongly discourage proprietary data. These attitudes underlay a new era of discoveries about the Earth and explosive growth in Earth science information, including data from EarthScope and broadband seismic networks in many regions of the USA. The consensus in favor of open data facilitates use of research products to serve society in applications that include monitoring of earthquakes, tsunamis, and nuclear tests as well as engineering applications to reduce seismic risk.

Keywords IRIs, Earthscope, Digital seismology, Interior (Earth) illumination, Global seismology

The Incorporated Research Institutions for Seismology, (IRIS), PASSCAL Instrument Center, New Mexico Tech., 100 East Road, Socorro NM 87801, USA

* To whom correspondence should be addressed. E-mail: Shane@passcal.nmt.edu

E.S. Husebye (ed.), *Earthquake Monitoring and Seismic Hazard Mitigation in Balkan Countries.*

1 Formation and Incorporation

The idea for the IRIS Consortium grew from the merging of two independent interests identified by the academic seismology community in the early 1980s. One group was interested in an upgraded global digital seismic network that would expand and modernize the aging and under-funded World Wide Standard Seismographic Network (WWSSN). The other group was interested in developing a new generation of portable seismic instruments for seismological studies of the continental lithosphere. Both of these initiatives were guided by reports from a series of important studies carried out by the National Academy of Sciences and its Committee on Seismology on future instrumentation and data needs in seismology and the Earth sciences. Additional encouragement came from a key report from the Committee on Science, Engineering and Public Policy in 1983 that identified five research areas in which significant dividends can be expected as a result of incremental federal investment in FY1985 including (1) seismic investigations of the continental crust and (2) global digital seismic array.

After a year of intense activity that included numerous workshops and planning meetings, the US seismology community joined together in 1984 to form a new consortium to develop and implement plans for an ambitious new set of facilities to support a wide range of seismological research.

One of the first activities of the corporation was to develop a 10-year proposal that laid out the seismology community's vision. In December 1984, IRIS submitted the proposal entitled "Imaging the Earth's Interior: Detailed Studies of the Earth and of the Seismic Source with New Global and Transportable Arrays" to the National Science Foundation. This proposal requested $107 M for the initial 5 years, and $281 M for the full 10 years of activities, which included the development of a Global Digital Seismic Array, a Mobile Array for continental lithosphere studies, Central Data Management and Distribution Facilities, and a Major Computational Facility.

2 IRIS Today

Twenty one years later, in 2005, IRIS has grown from its 26 original members to a consortium of 102-Member Institutions, comprising virtually every US university with a seismology research program. IRIS also includes a growing number of long-term partners totaling two US Affiliates, more than 43 International Affiliates and 8 Educational Affiliates. Three of the initial four major national facilities outlined in the 1984 proposal have been nurtured by IRIS and the community. The rapid evolution of supercomputer facilities obviated the need for a dedicated seismological computational facility, and IRIS data resources focused on centralized data management. The IRIS core programs currently consist of:

1. IRIS Global Seismographic Network (GSN): a permanent network of over 130 high dynamic ranges, broadband seismological observatories (Figure 1)

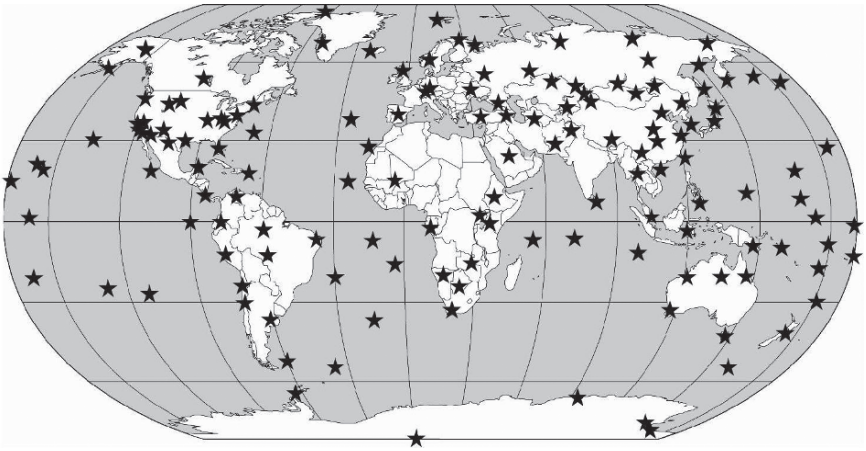

Figure 1 Currently operating stations of the GSN are shown as stars

distributed around the world at 2,000 km spacing that is operated jointly with the US Geological Survey (USGS).

2. IRIS Program for the Array Seismic Studies of the Continental Lithosphere (PASSCAL): A program that supports Earth science experiments through loans of seismic sensors, data acquisition, telemetry and power systems of portable instruments and arrays for use by individual scientists for high-resolution experiments in focused areas, and through services that include planning, shipping, field engineers, data capture, and instrument refurbishment.
3. IRIS Data Management System (DMS): A data system for collecting, archiving and distributing data from the IRIS Data Management Center (DMC), as well as a number of other national and international networks and agencies (Figure 2).
4. IRIS Education and Outreach Program (E&O): A program designed to integrate research and education by making our data and science accessible to non-seismologists through a variety of innovative programs that use seismological data through teacher workshops, student internships, museum exhibits, and classroom seismic stations.

Community activities such as these improve collaboration among member institutions to carry out Earth science research more efficiently and to seek partners among groups outside of seismology, including other Earth science consortia, government agencies, and international organizations.

The GSN and PASSCAL are complementary programs and the primary tools for acquisition of new data. The GSN, along with other cooperating networks, provides a baseline resolution of approximately 1,000–2,000 km on the continents and oceanic islands worldwide. Denser deployments of the PASSCAL instruments allow investigations of focused targets with resolution on the order of hundreds of kilometers down to the sub-meter scale. The DMS and E&O are also complementary programs and the primary means of distributing data for research and education.

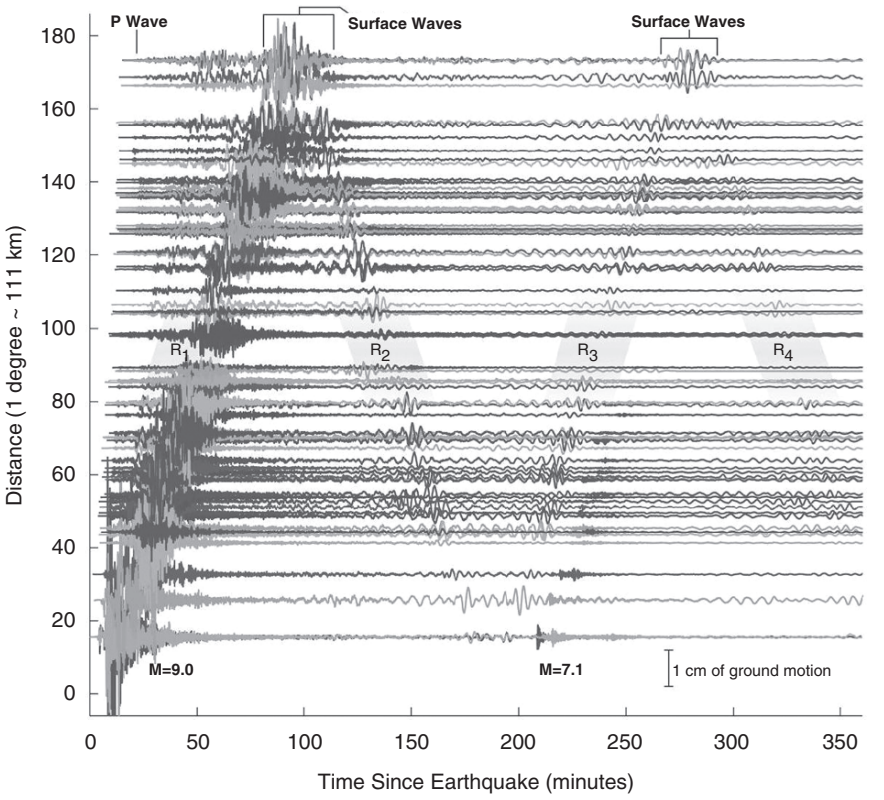

Figure 2 Record section of the December 26, 2004, Sumatran event recorded by the GSN. Data was available in near real-time online through the DMS

By combining and distributing data from different sources, the DMS allows individual investigators to assemble data products tailored to their research objectives.

The DMS also serves as a forum to coordinate international cooperation, establish data and software standards, and promote data exchange.

As these core facilities have grown, so has the demand from the seismological community for the services and products that they provide. IRIS facilities, products and services are now essential for the progress of a large proportion of seismological research funded by the NSF, USGS, DoD, and other US government agencies with programs in the Earth sciences and nuclear monitoring. IRIS facilities and data are also making new styles of scientific investigation possible. A constant goal of IRIS is to improve operation and efficiency of the existing core IRIS facilities.

From the beginning, IRIS facilities and products have also been used for educational purposes. Educators use seismograms or earthquake data obtained from the DMS in the classroom, construct public displays of “live” seismological data from the GSN, and introduce students to field work and research through participation in

PASSCAL deployments. Following the advice of reviewers of the 1996 IRIS proposal, and recognizing the opportunity that IRIS has to facilitate the use of many types of seismological data for educators, in 1998 IRIS established the Education and Outreach (E&O) Program to better address this need for educational materials and services. The E&O Program integrates seismological data with educational programs and public outreach, making IRIS data available and usable, not only for research seismologists, but also for educational institutions and the interested public. The E&O Program also plays an important role in translating scientific results on Earth structure and dynamics into terms meaningful and accessible to the general public.

3 The History of the DMS

The proposal submitted by IRIS to NSF in 1984 sought funding to develop, in parallel with the seismological equipment facilities, "Central Data Management and Distribution Facilities" to provide community access to the data collected, and a "Major Computational Facility" to support analyses of these data. The proposal stressed the development of a central node called the IRIS Data Management Center (DMC). The anticipated requirements were to manage about 500 GB of new data per year and service a few hundred data requests per year. Today, the DMC, which is located at the University of Washington, is adding over 16 TB of waveform data to the archive each year (Figure 3) and servicing over 50,000 requests annually. These numbers have increased significantly since USArray data started flowing.

The fundamental goals of the initial DMS were to coordinate the routine aspects of data gathering and organization and shift these tasks to a central facility accessible to all researchers. The DMS would enable seismologists to focus on their research instead of the more mundane aspects of collecting and assembling the required data sets prior to beginning research.

Over time, the structure of data management within IRIS has changed from the original centralized system that was envisioned to a hybrid system that takes advantage of both centralized and distributed components. While the IRIS DMC is still the largest component of the DMS with a staff of 20, roughly one-third of the financial assets of the DMS are provided to facilities outside the DMC. In the case of the permanent data from the GSN, two Data Collection Centers (DCCs) are co-located with the network operations facilities in San Diego and in Albuquerque. This allows technical staff familiar with the details of the recording systems and their installation to be readily accessible to the technicians dealing with data and metadata issues. The capabilities of these three centers are augmented via smaller and carefully monitored activities at US universities and in some cases, international data centers. Data quality assurance for data generated by the portable deployments of seismometers of the PASSCAL program is funded directly by the PASSCAL but strong and effective interfaces (people and computers) have been forged between the DMS and the PASSCAL programs.

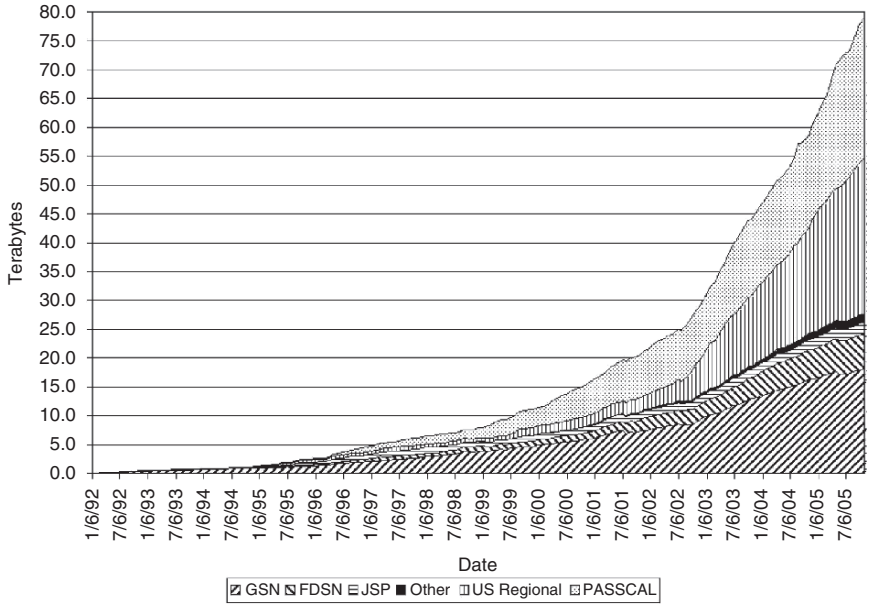

Figure 3 The DMC data archive volume as of July 2005. The contributions to the archive are from bottom to top in this figure: (1) GSN, (2) FDSN, (3) JSP, (4) other sources, (5) US Regional Networks, and (6) PASSCAL active source and passive experiments

The DMS has a short but excellent history of organizing national and international workshops on a variety of topics. These workshops are of tremendous benefit to organizations all over the globe in assisting them in applying modern data management techniques to data from their own networks. The workshop not only demonstrates tools that they can use to manage their data, but portions of the workshop also focus on why management of the metadata is important and necessary for the scientific research community. The benefit to the IRIS community, and the global scientific community, is that these workshops help to make data from a large number of other networks available for scientific research.

4 Data Distribution and Archiving

The primary goal of the DMS is to provide users with a complete and continuous archive of quality-controlled information (waveforms and associated metadata) from all IRIS installations. In developing this complete archive, two pathways have evolved to serve the most common requests:

- **Event Windowed vs Continuous** Many seismological investigations are based on analysis of all available data from specific events (earthquakes or explosions). Once

the origin information (location and time) of an event is known, simple tools can be used to extract the time windows of interest for waves arriving at any seismic station. Since these data segments represent a small fraction of the total archive, they can be stored in on-line disks for rapid access. At the DMC, these on-line resources have been called FARM (Fast Access Recovery Method, for quality controlled data from the archive) and SPYDER (for access to near-real-time data from events, before complete quality control). Since it takes time (minutes to weeks) to create event catalogs and collect data from all stations, these on-line data resources grow with time following an event. This is especially true for the FARM archive, which depends on the completion of quality control procedures.

- **Immediate vs Quality Controlled** In general, most research experiments look for the highest quality, most complete data available, In the case of the DMC, the resource of choice is the permanent archive of continuous data, or the FARM for event-windowed data. There are applications, however, especially in earthquake monitoring and education, where immediate access is more important than completeness or final quality control. To service these types of requests, the IRIS DMC, in collaboration with the USGS, has developed a variety of user tools that collect event related waveforms immediately following notification of an event by the National Earthquake Information Center (NEIC). The core of this system is SPYDER, which uses the NEIC location information to determine the appropriate time segments and gathers waveforms from stations that are available on-line via the Internet.

Waveform data entering the DMC are handled using well-established international data exchange standards for formats and metadata (SEED and miniSEED). Procedures are in place to exchange metadata information with network operators to update needed information related to station configuration. The waveforms are stored for several months in an on-line disk-based RAID system and the metadata are managed in an Oracle Database Management System. Passive-source PASSCAL data are stored in a manner analogous to the way GSN data are archived. Data that are acquired from active-source experiments are received and stored in SEG-Y format and distributed as special volumes of "assembled data sets." The discovery and access tools have recently been significantly enhanced in order to ease the task researchers have in gaining access to these valuable data sets (Figure 4).

In 2001 the DMC upgraded its storage robot to a 6,000-slot capable Powderhorn robot with T9940 tape drives. This system was capable of storing 360 TB of data. As the technology in tape drives evolved the DMC began transcribing data to higher capacity 9940B tape technology in 2004 and the robot's capacity grew to more than 1 petabyte ($1 \times 1{,}015$ bytes). As of October 2005 the DMC data holdings contained roughly 78 TB of data, obtained primarily from five different sources. The GSN data holdings total 17.9 TB, the PASSCAL program holdings total 23.8 TB, regional networks within the USA total 26.4 TB, networks from the FDSN have contributed 6.0 TB and other data sources have contributed roughly 3.5 TB to the DMC archive. The archive is stored in two sort orders, once by time and once by station that allows user requests to be serviced with high efficiency depending

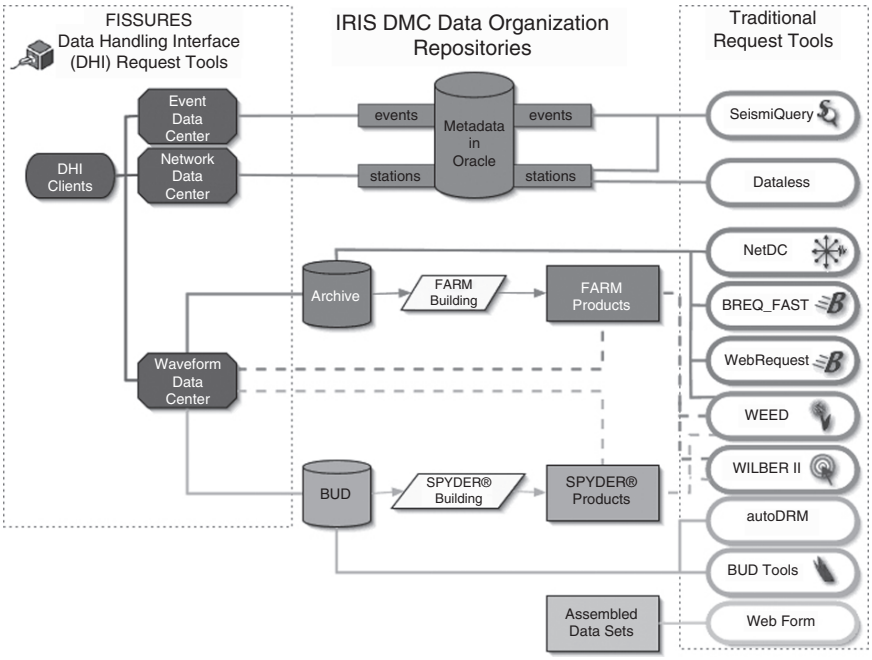

Figure 4 Four data repositories (Archive, BUD, FARM and SPYDER) that exists at the DMC. Continuous data are held in the Archive and the FARM; event-segmented products are in the FARM and SPYDER systems. Data in the Archive and the FARM are quality-controlled whereas BUD and SPYDER data are real-time data with little of no quality control. USArray data will be available through a large variety of data request tools supported at the DMC (as shown on the right) as well as the new FISSUES/DHI tools that support direct data access to clients from the three-types of data center servers (Event, Network, Waveform)

on the nature of the request. Each of the time and station sort orders are stored twice in the Powderhorn and the time-sorted data are also stored on DLT tapes in a secondary library. These DLT copies are transferred routinely to a facility in Colorado for out-of-state safekeeping of all data holdings.

5 IRIS and the International Community

The activities and influence of IRIS, both as a consortium and through its facility programs, have a strong international component. Each of the facility programs conduct activities that continue and expand our ability to interact with international organizations at the scientific level and encourage the longstanding IRIS goals of open data exchange, collaboration, and standardization. GSN, working with international organizations such as the Global Earth Observation System of Systems (GEOSS) and the Federation of Digital Seismograph Networks (FDSN), will

strengthen the coordinated operation of global seismic stations and encourage the expansion into other geophysical observations. The DMS continues to build on the concept of networked data centers and encourage the sharing of data through the FDSN and through direct contacts with national and regional networks throughout the world. PASSCAL continues to support individual PIs in foreign experiments and encourage the development of an organization similar to FDSN to stimulate interactions and exchange in portable seismology.

IRIS was a founding member of the international FDSN and acts as the continuous waveform archive for the Federation. The DMC is used as a primary source of data by researchers throughout the world. In the area of data exchange and instrumentation, formats and procedures established or encouraged by IRIS have been accepted as global standards. By encouraging the acceptance of GSN stations as part of the International Monitoring System, IRIS has made it possible for many nations to fulfill their obligations under the Comprehensive Test Ban Treaty. PASSCAL instruments have been used in a variety of overseas projects, usually involving local and international partners.

IRIS is inherently an international organization due to the geographic distribution of seismic sensors it operates. The DMS has worked with international operators of a variety of networks to develop standardized data formats, data request methods, data distribution techniques and documentation (Figure 5). IRIS involvement in the FDSN has resulted in data exchange with other nations, including Canada, China, France, Germany, Italy, Japan, the Netherlands, Switzerland, and Taiwan. In most instances, these data meet the standards set for data from the GSN. Our international partners consult with IRIS on data management and data distribution methods. Seismological networks around the world are using applications developed by the DMS to archive, distribute and quality control their seismological data. In cooperation with USGS, the DMS has encouraged the exchange of data between other US-supported networks. Many regional networks now contribute data to the DMC and cooperate with the DMS in the development of new techniques for interactions between data centers.

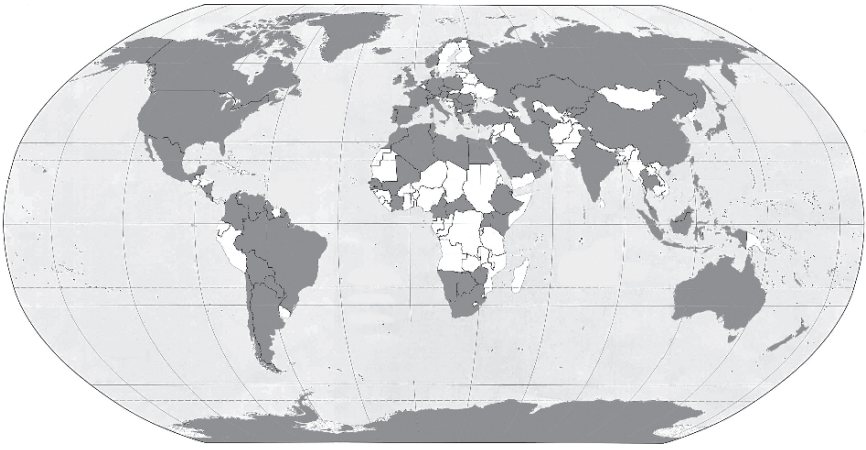

Figure 5 Countries that contribute data to the DMC are shown as shaded

IRIS has developed the concepts of networked data centers (NetDC) and the portable data collection center (PDCC) which have proven to be a powerful way to encourage the global exchange of data while retaining regional authority over data and data quality. In addition to cooperation with US networks, the NetDC procedures are being established at institutions in Japan, China, Netherlands, France, Germany, Italy and Taiwan. It is anticipated that NetDC, along with continuing IRIS developments in real-time data exchange, will be the basis for future IRIS activities to encourage and expand international cooperation. By fully developing and supporting NetDC, IRIS has greatly increased access to and coordination with most of the major international partners. All of these activities are fully coordinated with our international partners through the FDSN.

Recent experience of IRIS staff members and of representatives from our member institutions indicates that the international community recognizes the capability of Earth scientists to contribute simultaneously to capacity-building and natural-hazard mitigation. But success in these areas requires long-term projects that deeply engage the people and institutions of developing countries to an extent that is beyond the scope of a typical seismic experiment. To help IRIS institutions contribute effectively in this area, a central coordination function for international activities is being established within the IRIS Headquarters Office, with the objective of fostering the development of new activities to expand international efforts in seismological education, research, and monitoring. Headquarters staff devoted to this function will assist with activities being carried out by the core facility programs, work at the Consortium level with our member institutions, and engage with the international development organizations to explore opportunities for new funding.

Over the next 5 years we intend this enhanced commitment to international activities to help us bring the strengths, experience, and expertise of IRIS and its member institutions to assist in capacity-building, especially as it relates to improving seismic monitoring and research in the developing world. Following the model being established by the AfricaArray, and previous IRIS experience in Central Asia. This will be done through involvement in workshops and training courses, donation of retired instruments, assistance establishing data centers, and encouragement of educational and research contact with IRIS member institutions. We envision an expansion of the IRIS foreign affiliates program, both in the number and geographic distribution of affiliates and in the commitment of foreign affiliates to principles espoused by IRIS, most importantly free and open access. We anticipate progress in this regard partly because IRIS has a well-established record of making its own data freely available, and a growing record of facilitating use of open data by researchers and other users all over the world.

6 IRIS and EarthScope

The role of the IRIS Consortium in the broader seismological and geophysical research communities in the United States has continued to expand. IRIS has become an organization that successfully facilitates collaboration and cooperation among

seismologists and other Earth scientists. As a consortium of universities, IRIS has been able to develop, present and promote initiatives that have broad support in the academic Earth science community. To that end, IRIS has joined with a broad sector of the Earth science community in the development of EarthScope, a major new NSF-funded initiative that includes a new generation of facilities for seismology and geodesy. EarthScope will combine enhanced geodetic observations in the western United States (Plate Boundary Observatory, PBO), a continental scale seismic array (USArray - see Figure 6) and in situ studies of an active fault zone (San Andreas Fault Observatory at Depth, SAFOD) to provide fundamental new insights into earthquake processes and the structure, evolution and deformation of North America. The IRIS Consortium has joined with UNAVCO, Inc., Stanford University and the US Geological Survey to implement the observational systems that form the foundation of EarthScope.

The USArray component of EarthScope consists of continental- scale, portable seismic and magnetotelluric arrays that will map the structure and composition of the North American continent and the underlying mantle at high resolution. Through its three elements, the Transportable Array, the Flexible Array, and the Backbone Network USArray will be able to capture images that span the continuous range of scales from global, through lithospheric and crustal, and from regional

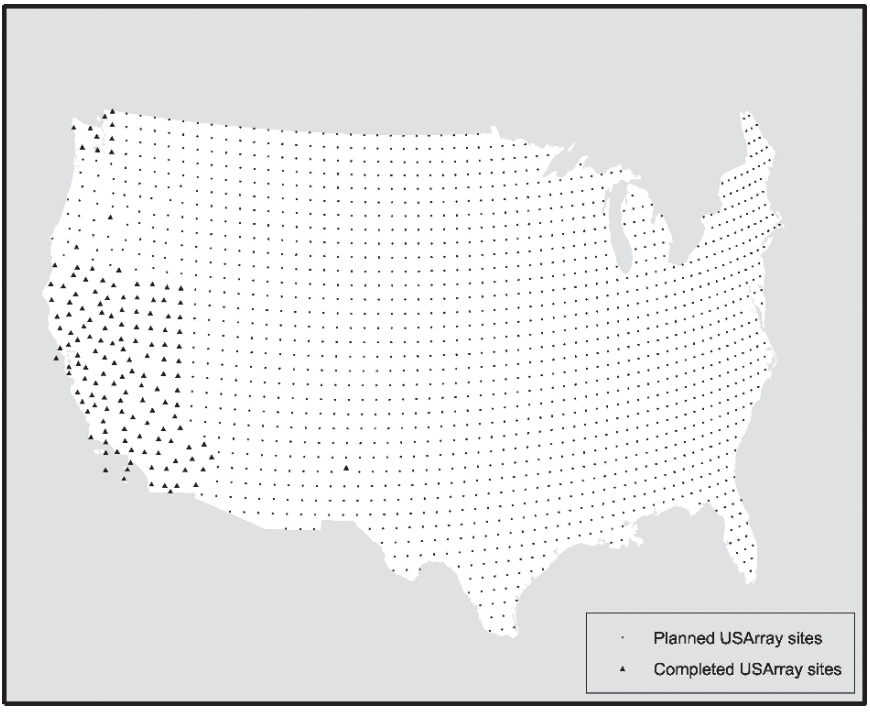

Figure 6 USArray will install permanent and temporary seismic and magnetotelluric stations at nearly all locations shown (Alaska not shown) over the next 10–12 years. Stations indicated by the large triangle symbols have been installed and are operating

to local, complementing and extending the reach of the GSN and PASSCAL facilities. Every IRIS element is contributing to USArray, with GSN coordinating the Backbone Network in collaboration with the USGS, PASSCAL coordinating the Flexible Array and Transportable Array efforts, DMS providing data archival and distribution functions for all of USArray as well as portions of the PBO and SAFOD data sets, and E&O participating in USArray station siting outreach and contributing to EarthScope E&O efforts. An exciting aspect of USArray is that virtually every educational institution in the United States will have the opportunity to take an active role in the investigation.

The community has endorsed the ability of IRIS to carry out this project, particularly regarding the technical capacity and human resources to quickly transfer what the community knows about instrumentation, portable array operations, and data management into practice in fulfilling its obligations to EarthScope. Similarly, the integration of the USArray program within IRIS and the IRIS management and governance structure has meant that the community has come to participate in the operation of USArray through IRIS. It is no surprise that IRIS has been able to call upon its members in order to scale up its core functions to support EarthScope. The size and complexity of USArray should not obscure the fact that it is essentially a facility operation based on protocols and practices that have been well vetted over two decades by IRIS and its membership. IRIS is thus able to move the best ideas of the community into USArray operations. It is important to recognize that while IRIS receives new funding to conduct USArray, the budget for IRIS's distinct core functions has not increased; in fact, over the past 2 years of overall NSF budget austerity, there were reductions in IRIS funding.

The benefits to IRIS of conducting the USArray project have included participation in an exciting major new venture in the Earth sciences and in active engagement of IRIS members in EarthScope research and activities. In some cases, new technical innovations arising from USArray will also be beneficial. For instance, the DMS expects that the technologies developed for EarthScope, such as the product management system, will also be applied to other products at the DMC. Collaborative work with EarthScope will benefit the E&O program in the development of new educational products such as video products for large-scale audiences.

Acknowledgements The author wishes to thank David Simpson for comments. IRIS is supported by the US National Science Foundation (NSF) under Cooperative Support Agreement EAR-0552316. USArray is supported by NSF as part of the EarthScope Project under Cooperative Support Agreement EAR-0323309.

The Mediterranean Broad Band Seismographic Network Anno 2005/06

Salvatore Mazza, M. Olivieri, A. Mandiello, and P. Casale

Abstract The Mediterranean Network (MedNet) presently comprises 22 operating broadband seismic stations installed and maintained in cooperation with 13 geophysical institutions in Italy and in most of the countries adjacent to the Mediterranean Sea. The number of stations may vary as stations are opened or sometimes closed due to different reasons like political, technical, etc., but usually temporarily. All the stations are equipped with Quanterra digitizers and Streckeisen sensors, mostly STS2 with a few STS1. Aim of the network is to contribute to monitoring of one of the most active seismic regions of the World in terms of providing high quality real-time broadband data to the seismological community. Operations started with off-line field data collection and dial-up capabilities were later added at selected sites. At present these have been replaced with more efficient TCP connections that provide for real-time data collection over the whole network. This important technological upgrade allows a prompt contribution to the seismic monitoring of Italy and of most countries bordering the Mediterranean Sea, since data are exchanged in real-time with other seismological observatories. SeedLink protocol has been adopted for data transmission. As for data archiving and distribution, a fast system for retrieving data has been developed. Continuous data streams, collected both from field data tapes and from real-time transfer, are stored at the MedNet Data Center and are directly available at users' request by the standard AutoDRM and NetDC protocols (in GSE and SEED formats respectively). Station metadata and continuous waveforms are archived in a MySQL database on RAID systems and backed up on DLT tapes. Presently, fully automatic network functions include: daily monitoring of state of health; triggered retrieval of event waveforms (with magnitude- and region-specific selection criteria), local and surface wave magnitude determination,

Istituto Nazionale di Geofisica e Vulcanologia, Via di Vigna Murata, 605, 00143 Roma, Italy

E.S. Husebye (ed.), *Earthquake Monitoring and Seismic Hazard Mitigation in Balkan Countries.*

and update of web pages (http://mednet.ingv.it) for events and station information. Rapid semiautomatic moment tensor solutions are calculated by means of a modified Harvard technique, which lowers the Mw threshold down to 4.5 for regional events in those areas with proper station coverage. For smaller earthquakes in Italy a new approach to moment tensor estimation, based on higher signal frequencies, is now being developed. Preliminary tests on earthquake recordings (not only MedNet stations) from the 2002 Molise, South Italy, sequence have proved very successful.

Keywords very broad band seismology, seismic stations, earthquakes, data center organization, real-time data acquisition, request manager, SEED format, seismic noise, moment tensor

1 Introduction

MedNet is a network of very broad band seismic stations installed in countries bordering the Mediterranean area. The project started in 1987, with a final goal of 12–15 stations and a spacing of about 1,000 km between stations. It was motivated both by research interest and by seismic hazard monitoring. Its main objectives were mapping the structure of the Mediterranean region, studying the seismic source properties of intermediate and large events, and applying this knowledge to measures for hazard mitigation and civil protection. In 1988 the MedNet project was incorporated in the framework of the World Laboratory of Lausanne, an organization for the advancement of Science in developing countries, sponsored by the Italian and other European governments. As a result and according to the original plan, station distribution rapidly extended toward the North African countries: Morocco, Algeria, Tunisia and Egypt (Giardini et al., 1992). This significantly increased the number of stations in areas where previously no high quality instrumentation had been deployed (Giardini, 1990).

Over the past 15 years, as both constructive political climate on the one side and technological and scientific development on the other side have progressed significantly, the project also has in a similar manner improved its scientific perspective. Thus slowly it became a “stable” network, albeit with all the inherent difficulties and uncertainties of the region. Although the general objectives have not changed much, the relations between INGV and the other participating institutions are now on a more cooperative base than in the past as the latter increasingly contribute to station management.

For many years data have been collected and archived at the MedNet Data Center (MNDC) in Rome by means of tapes delivered by ordinary mail (Morelli, 1990). In theory tapes ought to have been the safest way to collect data but in practice for many reasons we had poor results. The most tricky problem was that tapes took far too long to arrive at MNDC within 15 days at best and thus matching the time the tape was kept recording (if not years), because they were collected at the station and

sent to Rome only after a certain number had been assembled. As far as data quality and continuity were concerned, this was considered extremely unsatisfactory. For example, seven months' worth of 1994–1995 data from MDT (Midelt, Morocco) were given improper time marks by years. Due to the delay in receiving the tapes, the problem was discovered only a couple of years later when it also was discovered that many tapes following the seven months' period were actually empty.

In the early stages of the Project, particular emphasis was given to site selection. Abandoned mines and old tunnels in remote areas were preferred: BNI (Bardonecchia, Western Alps), VSL (Villasalto, Sardinia), MDT (Midelt, Morocco), GFA (Gafsa, Tunisia), to name only the most prominent sites here.

Good thermal insulation, remoteness and low levels of cultural noise made them attractive sites from a seismological point of view. Their very remoteness, however, had the drawback of making maintenance a difficult task, for both MedNet staff and the local partners as well eg., see examples in Figure 1.

In the following years increased attention was given to the logistic aspects of station installation and operation, in order to ensure a better data production. Nowadays, MedNet sites range from old building cellars (CII, Carovilli, Italy) to a 15th-century

Figure 1 Four examples of MedNet sites: the entrance to the 120-m long tunnel, in the desert region of Gafsa (GFA, Tunisia, top left); L'Aquila Castle, which hosts the station in one of its cisterns (AQU, Central Italy, top right); Vitosha observatory, a few kilometers from Sofia (VTS, Bulgaria, bottom left); the existing excavation (originally used to hide tanks) in the vicinity of Kottamya Astronomical Observatory, about 70 km to the East of Cairo, later improved, to host the instrumentation, to a three floor, 8-m deep hole (KEG, Egypt, bottom right)

castle cistern (AQU, L'Aquila, Central Italy), from an ad hoc-dug vaults (KEG, Kottamya, Egypt; DIVS, Divcibare, Serbia; AIO, Antillo, Sicily; IDI, Crete, Greece) to observatory basements (BGY, Belgrade, Serbia; VTS, Vitosha, Bulgaria).

In 1991, an attempt was made to transmit data in real time from VSL (Villasalto, Sardinia). Despite the success of the operation, real-time transmission was not an option for many years to come (until 1999), because of the high cost of leased lines. For a long time, the use of modem remained the only way of retrieving data from MedNet stations in quasi real time. Modems were installed at many stations, whenever a phone line was available. This proved very useful on many occasions; during the two trade embargoes and the civil war suffered by Yugoslavia, the only data recorded by BGY (Belgrade) were the only ones retrieved via modem. The tape drive at the station was regrettably broken, and it was impossible to replace it due to the embargo.

Over the last three months of 1997, Central Italy was struck by a prolonged earthquake swarm, during which the high level information potential of very broad band recordings was fully exploited. Stations that had been installed for research purposes proved very useful to monitor this sequence. Many investigations were carried out based on quasi real-time data: earthquake parameters commonly extracted were reliable magnitude estimates, directivity effects and moment tensors.

CMT solutions, as well as source properties from long period seismograms (Morelli et al., 2000), were computed for many of the Mw > 4.5 shocks of the sequence (Ekström et al., 1998). Magnitude relations were strongly revised, the duration Magnitude giving 4.7 for an Ml = 5.6. Lastly, three well-placed stations proved sufficient for estimating reliable directivities for many of the largest swarn earthquakes (Pino et al., 1999). Furthermore, the effective monitoring of these events gave the Italian MedNet stations in Italy enhanced visibility and thus overshadowed the importance of other Mediterranean stations for some time.

Around 1999–2000, thanks mostly to the huge reorganization of the Istituto Nazionale di Geofisica ((ING) into the Istituto Nazionale di Geofisica e Vulcanologia (INGV) things have radically improved for MedNet. The new Institution is ensured stable and adequate governmental funding and its research and monitoring responsibilities are established legally. Other recent developments have also much helped MedNet rise from the ashes it was reduced to after its brilliant start. To complete the framework of this new start we must add that:

- In the last few years constructive political and scientific development have taken place in several countries bordering the Mediterranean Sea.
- Technological advancements have made very broad band seismological records easily accessible and thus have serve to close the gap between research and monitoring tasks.
- Many good and fruitful co-operations have started, e.g., those catalyzed by the MEREDIAN Project (all the details about MEREDIAN are available on the ORFEUS website at http://www.orfeus-eu.org/organization/projects/meridian/meridian.html).
- Robust and well-documented software became freely available for network operations.

2 Network Description

2.1 Station Instrumentation

The network presently comprises 22 operating stations, all of them equipped with state of the art seismograph stations. Their deployment is still governed by the principle of increasing broad band station coverage with due regards to the deployment of similar stations by other operators. Figure 2 shows the status at the time of writing.

Seismometers are mostly Streckeisen STS2, with a few STS-1/VBB installed during the early phases of the project. STS1 exhibits a flat response between 0.003 Hz (360 s) and 10.0 Hz (0.1 s), whereas STS2 is flat between 0.01 Hz (100 s) and 100 Hz (0.01 s). Amplitude response details in Figure 3. STS1 have been installed with the protective instrument cover (glass bell, aluminum cover, etc.) as delivered from the factory, with minor variations from site to site like cementing the glass plate to the rock. Later on MedNet shifted instrumentation to Streckeisen STS2 sensors when the factory phased out the STS1 design. Initially the STS2 were installed with small or no shielding against thermal and electromagnetic fluctuations. However, lack of adequate covers proved problematic, so subsequently all STS2 instruments were reinstalled, with a marble base and aluminum and steel boxes filled with glass fiber and foam, according to Wielandt's recipe (Wielandt, 2002).

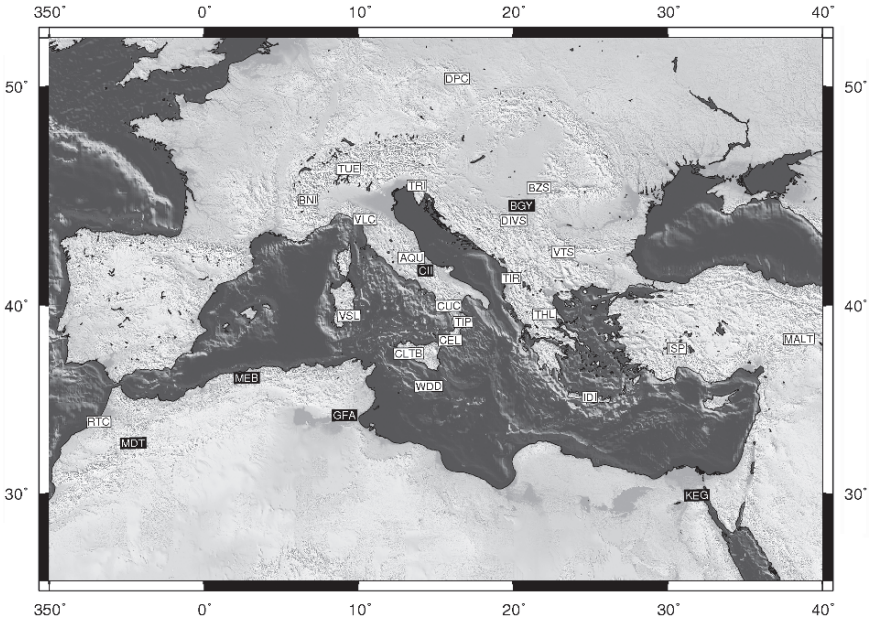

Figure 2 Map of stations: closed stations are shown in red, open stations in green

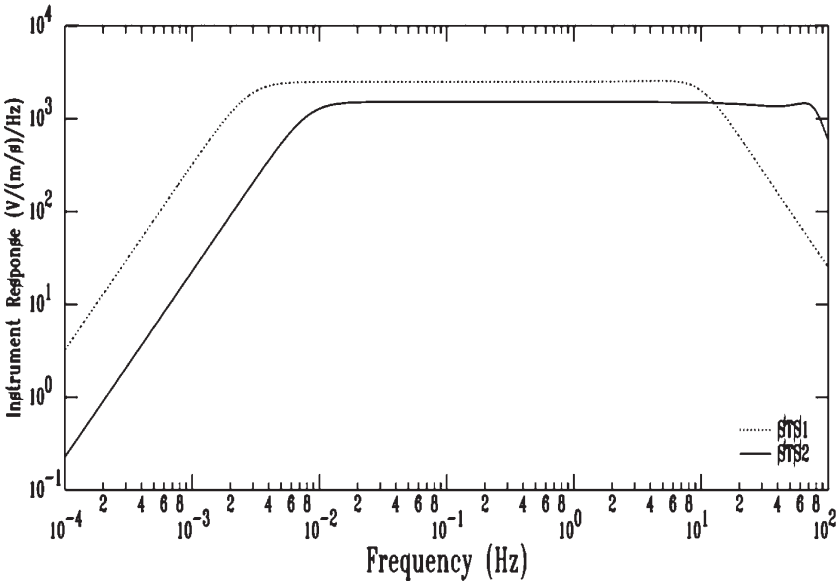

Figure 3 Amplitude response functions for the two types of sensors in use at MedNet stations, Streckeisen STS1-VBB (dotted line) and STS2 (solid)

As for digitizers, in the late 1980s only one type of 24-bit digitizer was available: Quanterra were adopted (then called Quantagrators) and upgraded in the following years. Nowadays 24-bit digitizers are produced by many manufacturers and buyers' choice is no longer a matter of technical specifications, but of convenience and economy. For example, the TIR station (Tirana, Albania) is equipped with a Nanometrics digitizer, in order to take full advantage of the Nanometrics satellite system adopted both by Italy and Albania and thus facilitating data exchange. All the other data-loggers are from Quanterra (Q380-680, Q730, Q4120 and Q330). Table 1 shows, beside coordinates, seismograph-data-logger combination and various sampling rates available.

2.2 Real Time Data Transmission

Data are now transmitted in real time from the stations to Rome using TCP protocol. Several physical links are in use: leased lines, Virtual Private Network, Frame Relay, Internet and satellite link. Figure 4 shows a simplified diagram of the physical connections and the acquisition running at MNDC.

Two separate acquisition systems allow us to get data from "internal" and "external" stations (with respect to INGV Local Area Network). The two servers exchange data with each other, so that inside and outside the firewall the same complete set of data is available.

Table 1 Overview of MedNet station coordinates and instrument configuration (seismograph and data-logger). Rate column shows the maximum sampling rate and the down-sampled data stream rates available from each station. Q×80 is for Q380 (three channels) and Q680 (six channels) data-loggers

Sta	Lat	Lon	Elev (m)	Rate (sps)	*Instruments*
ISP	37.84330	30.50930	1100	80,20,1,0.1	*Q×80-STS1*
MALT	38.31340	38.42730	1120	80, 20,1,0.1	*Q×80-STS2*
AIO	37.97120	15.23300	751.4	80, 20,1,0.1	*Q×80-STS2*
AQU	42.35400	13.40500	710	100, 20,1,0.1	*Q4120-STS2*
BGY	44.80260	20.51580	250	20,1,0.1	*Q52K-STS1*
BNI	45.05200	6.67800	1395	100, 20,1,0.1	*Q4120-STS2*
CEL	38.26030	15.89390	702	100, 20,1,0.1	*Q4120-STS2*
CII	41.72300	14.30500	910	80, 20,1,0.1	*Q×80-STS2*
CLTB	37.57800	13.21600	949	100, 20,1,0.1	*Q730-STS2*
CUC	39.99380	15.81550	637	100, 20,1,0.1	*Q730-STS2*
DIVS	44.09810	19.99170	1000	20,1,0.1	*Q×80-STS1*
GFA	34.33800	9.07300	250	20,1,0.1	*Q52K-STS1*
IDI	35.28800	24.89000	750	80, 20,1,0.1	*Q×80-STS2*
KEG	29.92750	31.82920	460	20,1,0.1	*Q52K-STS1*
MDT	32.81700	−4.61400	1200	20,1,0.1	*Q52K-STS1*
MEB	36.30300	2.73000	500	20,1,0.1	*Q52K-STS1*
RTC	33.98810	−6.85690	50	80,20,1,0.1	*Q×80-STS1*
TIP	39.17940	16.75830	789	100, 20,1,0.1	*Q4120-STS2*
TIR	41.34720	19.86310	247	100, 20,1,0.1	*TRID-STS2*
TRI	45.70900	13.76400	161	100,20,1,0.1	*Q4120-STS1*
TTE	45.66000	13.79000	92	20,1,0.1	*Q52K-STS1*
TUE	46.47223	9.34732	1924	100, 20,1,0.1	*Q4120-STS2*
VAE	37.46900	14.35330	735.1	80,20,1,0.1	*Q×80-STS1*
VLC	44.15940	10.38640	555	100,20,1,0.1	*Q4120-STS2*
VSL	39.49600	9.37800	370	100,20,1,0.1	*Q730-STS1*
VTS	42.61800	23.23500	1490	20,1,0.1	*Q×80-STS1*
WDD	35.86700	14.52300	41	80, 20,1,0.1	*Q×80-STS2*
BZS	*45.61660*	*21.61660*	*260*	*100,20,1,0.1*	*Q330-STS2*

It is worth remarking that data can make long detours before reaching their final destination. For example, data from IDI (Crete) are first collected in Athens, then forwarded to Rome. Similarly, data from ISP (Isparta, Turkey) first go to Istanbul, then to Potsdam and eventually to Rome. All this is automatically accomplished by means of the SeedLink protocol and SeisComP, a software package developed, maintained and freely distributed by GEOFON (GFZ, Potsdam, Germany eg., see Hanka et al., 2000; Hanka and Saul, ibid). On the contrary, most of the stations in Italy send their data via a private network, with a very straightforward connection.

Real time transmission for MedNet commenced in 1999 since such exchange was urgently needed by then. MedNet was lagging behind in this respect. At the same time, the EC project MEREDIAN was launched and one of its main aims was real-time data exchange. Naturally, MedNet in view of its network communication needs was an active participant. Within the MEREDIAN project the SeisComP

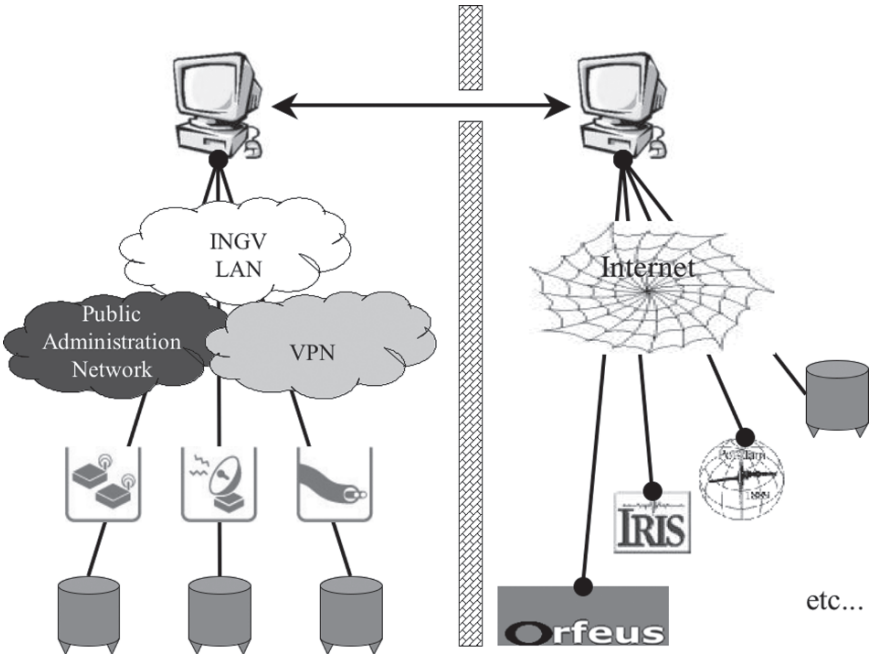

Figure 4 Simplified diagram of the connections from "internal" and "external" MedNet stations, with emphasis on the two SeedLink servers on both sides of the firewall in Rome

software was further developed, with mutual advantage to partners, to software and to data exchange in Europe. It was immediately apparent that the SeedLink protocol suited MedNet needs very well (not without reason, as it was first conceived for GEOFON, a similar network).

Among the many features of this software, the following are particularly relevant to MedNet:

- Open source and free availability
- Easy installation and maintenance
- High modularity
- Server-client structure
- Availability of many plug-ins for a wide range of data-loggers
- Miniseed format
- Simple and widely used archive structure
- Ease of adaptation to specific needs (e.g. de-sampling new streams or introductions of new plug-ins).

Note that, thanks to the server-client structure, a net of connections can be established between data centers and stations. There are no differences between a station SeisComP server and a data center one, other than the differences regarding computer performances and the obvious changes in configuration files. In practice, station servers usually provide data to one data center client, while data center computers

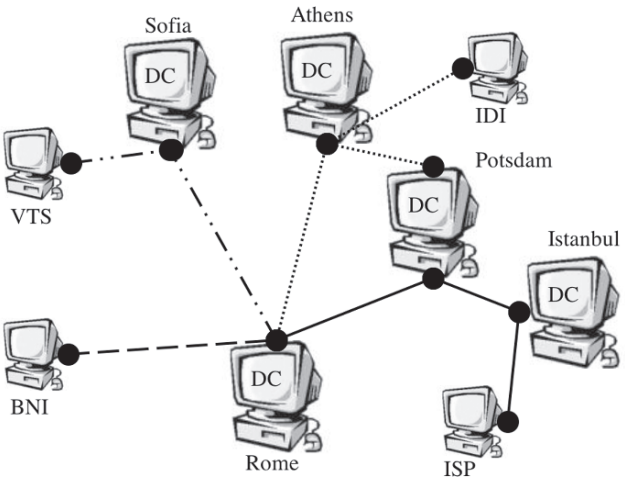

Figure 5 Examples of actual data connections station-data center and data center-data center as practiced within the MedNet network

get data from many stations and provide many stations to other clients. Figure 5 shows a few of the actual data links among MedNet stations and data centers.

2.3 Institutional Network Cooperation

One of the main goals of MedNet is enhancing scientific relationships and cooperation among seismological institutions in countries bordering the Mediterranean Sea. After all, network management would be impossible without the cooperation of local partner Institutions. Occasionally, a station may close down temporarily or even permanently due to political and/or international difficulties. Stations are considered temporarily closed, also over a long period of time, if

- They are not operative and thus non-recording.
- It is not possible for partners to restart it properly.
- No involved Institution has officially declared it permanently closed.

An example is the MEB (Medea, Algeria) station, which has been closed since 1995. In practice, a station has never been closed permanently, except when moved to a better or more convenient site. This happened, for example, with MDT (Midelt, Morocco) that was moved to RTC (Rabat City, Morocco) or BGY (Belgrade, Serbia) moved to DIVS (Divcibare, Serbia). Likewise, TTE (now TRI) in Trieste, Italy was moved to a better site and upgraded to a 3 component STS1 (from vertical only STS1).

Note that TRI is slightly different from a standard MedNet station, as it is fully owned and managed by Università di Trieste (Dipartimento di Scienze della Terra) and Istituto Nazionale di Oceanografia e Geofisica Sperimentale. They contribute their data to the network, getting support for instrumentation whenever needed. Table 2 summarizes locations, operation dates and involved Institutions.

Table 2 List of MedNet station codes, locations and partner institutions

Code	Operation dates	Station location	*Hosting institution*
AIO	1999–present	Antillo, Italy	*INGV, Catania*
AQU	1988–present	L'Aquila, Italy	*INGV, Rome*
BGY	1991–2001	Belgrade, Yugoslavia	*Seismological Institute of Serbia, Belgrade*
BNI	1988–present	Bardonecchia, Italy	*INGV, Rome*
BZS	2005–present	Buzias, Romania	*National Institute for Earth Physics, Bucarest*
CEL	2003–present	Celeste, Italy	*INGV, Rome*
CII	1994–present	Carovilli, Italy	*INGV, Rome*
CLTB	2000–present	Caltabellotta, Italy	*INGV, Rome*
CUC	2003–present	Castrocucco, Italy	*INGV, Rome*
DIVS	2005–present	Divcibare, Serbia	*Seismological Institute of Serbia, Belgrade and Geophysical Institute Slovak Academy of Sciences*
GFA	1989–1999	Gafsa, Tunisia	*Institut National de Météorologie, Tunis*
IDI	1994–present	Crete, Greece	*National Observatory of Athens*
ISP	1996–present	Isparta, Turkey	*Bogazici University Kandilli Observatory and Earthquake Research Institute Congelkoy, Istanbul GEOFON, GFZ, Potsdam*
KEG	1990–1999	Kottamya, Egypt	*National Research Institute of Astronomy and Geophysics, Helwan, Cairo*
MALT	2000–present	Malatya, Turkey	*Bogazici University, Kandilli Observatory and Earthquake Research Institute Congelkoy, Istanbul GEOFON, GFZ, Potsdam*
MDT	1989–1999	Midelt, Morocco	*Centre National pour la Recherche Scientifique e Technique, Rabat*
MEB	1992–1994	Medea, Algeria	*Centre de Recherche en Astronomie, Astrophysique et Geophysique, Bouzareah*
RTC	2002-present	Rabat, Morocco	*Centre National pour la Recherche Scientifique e Technique, Rabat*
TIP	2004-present	Timpagrande, Italy	*INGV, Rome*
TIR	2004-present	Tirana, Albania	*Seismological Center, Academy of Albania, Tirana*
TRI	1996–present	Trieste, Italy	*Università di Trieste & Istituto Nazionale di Oceanografia e Geofisica Sperimentale, Trieste*
TTE	1991–1995	Trieste, Italy	*Università di Trieste & Istituto Nazionale di Oceanografia e Geofisica Sperimentale, Trieste*
TUE	2002–present	Stuetta, Italy	*INGV, Rome*
VAE		Valguarnera Caropepe, Italy	*INGV, Catania*
VLC	2003–present	Villacollemandina, Italy	*INGV, Rome*
VSL	1989–present	Villasalto, Italy	*INGV, Rome*
VTS	1996–present	Vitosha, Bulgaria	*Geophysical Institute, Bulgarian Academy of Science, Sofia*
WDD	*1995–present*	*Wield Dalam, Malta*	*Deptartment of Physics, Malta University, La Valletta*

3 MedNet Data Center

When MedNet first started, data operations were mainly devoted to retrieving data from tapes, converting them to records of 4kilobytes, archiving them on huge optical disks (4 Gbytes, extraordinary at those times!), and indexing which data had been safely archived and where. Distribution just meant forwarding of SEED Volumes (SEED, 2004) in exabyte tapes to ORFEUS Data Center (De Bilt, The Netherlands) and IRIS Data Management Center (Seattle, USA).

All the operations were done on microVax workstations, under VMS. The Data Collection Center (DCC) software (Morelli, 1990) for data retrieving and archiving was provided by Albuquerque Seismological Laboratory (NM, USA) and adapted to MNDC needs. Unfortunately, none of the MedNet staff ever got well acquainted with the source code, even though available. Time after time this led to major difficulties. Changes in hardware, software and SEED definitions (for example the introduction of Steim2 compression algorithm, not managed by the old system) finally blocked the MNDC SEED machine, resulting in an even larger number of unread tapes, which in 1998 exceeded 700.

A new system was clearly needed and after some experimenting the solution was a fairly advanced system. This was the PdccToolkit2.0 by IRIS DMC staff (presently an entirely new version is being distributed (see http://www.iris.edu/manuals/pdcc_intro.htm about the latest release of PDCCToolkit)). In fact, what was available from the Portable Data Collection Center (PDCC) was:

- A user-friendly interface for most of the operations
- A simple, not normalized but practical MySQL database scheme
- A few on-line commands to deal with the main operations of importing and exporting data and information from the database and producing both dataless and full SEED volumes

With the above software and some home made scripting a new, raw, but efficient system was made and put in operation to build up a full archive of the whole MedNet data set from 1990 to present, also recovering the 700 unread tapes.

In 1999 the goal of archiving all MedNet tapes on a RAID system, with a relational database underneath, was achieved and since then various bits and pieces have been added to the system: procedures for miniseed processing, bug fixing, time correction, etc. such as routines from the Quanterra Users Group (QUG) Software Archive (see http://www.ncedc.org/qug/ for QUG documentation and software) or from the SeedStuff package by GEOFON (see http://www.gfz-potsdam.de/geofon/ for SeedStuff software).

3.1 Data Acquisition and Archiving

Data center operations now include real-time data acquisition, quality check, archiving, and distribution toward other data centers or users.

Initially, Quanterra data-loggers at the Italian sites had been plugged in directly on Ethernet, without a SeisComP running PC. Although in principle this was desirable in terms of economy and robustness, it later turned out to be a weak point, because phone lines were much less reliable than expected (at least in Italy). In case of failure, the buffer for data recovering is around 15 minutes or even less. On the contrary, the retransmission inherent to SeedLink protocol is based on a much larger configurable buffer, and data can be stored locally. Therefore, by installing a PC at the station, most of the gaps are already handled by the client-server pair, while a full computer (Linux running) is available to deal with data recover, checks, etc.

Within a short time all stations have been equipped with a SeisComP PC and a procedure has been very recently developed which checks for gaps in the archived data and tries to fill them by getting back to the stations. The procedure is powerful and simple and ensures maximum completeness on data streams.

Data flow from stations to archive consists of the following steps:

- Data packets flow into the MNDC following individual path.
- Data are stored at MNDC in real time.
- Every day data are copied from the acquisition system to the archiving one, so that only a limited amount of days (1 or 2 weeks) are kept on the disk of the real time acquisition server.
- On the archiving computer (which is now a Sun server, with RAID systems) the completeness check is performed and data are recovered as needed.
- Once gaps are rated unrecoverable, data are scanned and gap information is inserted into the database.

3.2 Data Distribution

Data are distributed following three main routes: the fast, but restricted one of real-time distribution, the intermediate one of distributing data grouped by event, and the last one, slow, but very comprehensive, of sending data at users' request via e-mail or ftp, and then extracting them from the archive.

3.2.1 Real Time Distribution

Real time data distribution is based on the SeedLink server. Disregarding the technicalities of how data are actually transmitted, there is one SeedLink server providing all MedNet data, whereas the same server ensures the collection of data from other data centers. Real time data are exchanged on a one-to-one basis between Institutions and are usually regulated by bilateral agreements. Single users are not allowed to access data in real time.

Closely related to real-time distribution, is the prompt updating and dissemination of station information. This is done by means of the so-called dataless SEED volumes,

i.e. files in SEED format in which all the information regarding a station is reported, that is its location, channels, response functions, antialias filters, and whatever is needed to fully describe and use data from a given station. In other words, since data are now flowing separately from the metadata describing them, those metadata must be updated as soon as some modification has taken place in a station configuration (a sensor replacement, a repaired data-logger, etc.). The SEED format, although a little cumbersome, provides the most complete way of distributing station metadata and their updates.

3.2.2 Event Data and MedNet Automatic Web Publisher

Data are published automatically in quasi real time whenever an earthquake with specific characteristics occurs like epicenter location, magnitude, distance from stations, etc. The automatic procedure that extracts, processes and publishes data from the continuous data streams, processes and publishes them was named Muscles and it was first conceived to monitor the activity of the stations in quasi real time.

It was initially a routine check of stations' state of health, carried out by calling the station every night and downloading information, like tape status, last time mark received, and so on. It was soon apparent that visual or simple standard checks were insufficient for quality control of station operations. Thus some additional scientific oriented controlling tasks were added. The following is a typical case: a noise spectrum of the seismic trace is effective in discovering big deviations of the instrument response from the theoretical one, but not a time shift due to some drift of the internal station clock. To discover that, a simple comparison between the theoretical and the observed P arrival times of occurring earthquakes is a far more effective tool.

Data for relevant events in Italy, in the Mediterranean and over the World were then extracted, so that they could be immediately available to users and in turn quality checked by real scientific investigations. By chance the procedure had just been started when the already mentioned 1997 Central Italy seismic sequence occurred, with great advantage for both research and monitoring.

Data quality check and station state of health is now based on other tools, but Muscles is still working as the automatic event builder and data bundles web publisher. In principle, it receives event mails from selected international Agencies like the Italian National Network, NEIC, EMSC, etc. and checks whether the earthquake is of interest according to a priori given specifications. Then all data from the continuous streams (i.e. from the SeedLink server) are collected. Data relative to the event in question are eventually put on the MedNet web site, for downloading by users. In this case, data are in SAC format; although it is not a standard exchange format, it is widely used and it is handy for immediate usage. Beside seismograms, a simple map and a few plots are also presented.

3.2.3 Distribution of Archived Data

All data recorded at MedNet stations are available automatically by sending a request via e-mail to netdc@ingv.it and autodrm@ingv.it, the two different of data

request managers: (i) NetDC (Networked Data Center (Casey and Ahern, 1999)) and (ii) AutoDRM (Auto Data Request Manager (see Kradolfer, 1993, and http://www.seismo.ethz.ch/autodrm/ for AutoDRM documentation and software)). Although they both process e-mail requests to provide station information and data to users, they differ in many respects:

- AutoDRM request syntax is richer and requests can be more detailed.
- AutoDRM default format is GSE2.0, whereas NetDC is SEED.
- NetDC is not just a request manager, but mainly a software for data centers networking.

In other words, installing NetDC also means joining a group of data centers sharing their data so that the whole set of data can be offered to users as if originating from just one place. The user deals with only one data center and does not need to know where data actually reside. Data centers, on the other hand, are all on an equal level; each one acts as a hub only when it receives, processes and forwards a request to the others.

Users are often familiar with only one or the other of the two types of data managers, because of data format, request syntax, etc. It is therefore more convenient for the data center staff to install both request managers than to spend time helping users unfamiliar with one or the other.

There is also a form on the MedNet web pages to help users extract data via NetDC. It is just an interface to prepare the e-mail request and send it to the proper address, netdc@ingv.it. As a matter of fact, NetDC is better maintained and updated at MNDC, if nothing else because SEED is the format adopted from the very beginning. MedNet data are distributed to Institutions like ORFEUS DC and IRIS DC, as well as other data centers: this implies that data are also available from them, through the tools they provide.

4 Products

MedNet main products remain its very broad band, high quality data:

- Continuous data from 1990 to present, through NetDC and AutoDRM
- Event data since 1997, in quasi real time
- Up-to-date station information
- Real-time data from more than 20 stations

A few other products are also available through the MedNet web site, http://mednet.ingv.it. They can be summarized as follows:

- ML and MS magnitude estimates
- Semi-automatic Regional Centroid Moment Tensors for events around the Mediterranean basin, down to Ml ~ 4.2, in case of fortunate station coverage
- Automatic Moment Tensor solutions (still in an experimental phase)
- Daily and monthly noise spectra of every station, as indicators of data quality

Semi-automatic Regional Centroid Moment Tensors (Quick RCMT) are routinely calculated by means of a modified technique with respect to the Harvard standard one on the occurrence of strong earthquakes in the Mediterranean area (Arvidsson and Ekström, 1998). The procedure has never been fully automated out of choice: it can be slow, but being manually checked it is very stable and provide highly reliable results. This piece of scientific software is one outcome of a longstanding cooperation between INGV and the Department of Seismology, Harvard University, USA. S.Pondrelli (pondrelli@bo.ingv.it) is responsible for the operations. Thanks to the signal frequencies taken into account and the technique applied, results are reliable down to Mw = 4.5 (in the most advantageous cases 4.2).

After revision and inclusion of other available stations, the Quick RCMT solutions are included in the RCMT Catalogue (Pondrelli et al., 2002), published on http://www.ingv.it/seismoglo/RCMT/.

As for the automatic moment tensor solutions, they are based on the routines by Fukuyama and Dreger (2000), and are the result of a co-operation between National Research Institute for Earth Science and Disaster Prevention, Japan (NIED) and INGV. F. Di Luccio (diluccio@ingv.it) is responsible for this procedure which, although robust and efficient, is still being tested. The reason is the need for an accurate set of Green functions in order to produce reliable and stable results. Green functions have been determined only for very specific part of Italy (Pondrelli et al., 2003) and the calculated moment tensor solutions are seldom satisfactory.

5 Plans for Future Developments

On the fieldwork side some actions are already underway and others are in planning stages. In this regard, accurate time schedules are difficult as many factors can interfere with operations. The following task implementations have already started:

- The site has already been prepared for a new station to be installed in Thessalia (Greece) near the village of Klokotos: this is in cooperation with the Geodynamics Institute of the National Observatory of Athens (GI-NOA) and the Geophysical Institute of the Academy of Sciences of the Czech Republic (GI-CAS).
- The installation of a Streckeisen STS1/VBB sensor is planned to upgrade DPC (Dobruska/Polom, Czech Republic) station. This will be done in co-operation with GI-CAS, to fully exploit the site excellent quietness.
- Contacts have been re-established with the Institut National de la Météorologie to reopen GFA (Gafsa, Tunisia) station and a field trip to check the station conditions has already taken place. It is planned to equip the station with satellite transmission.

Reopening the other stations in North Africa (KEG, Egypt and MEB, Algeria) and, if possible, improving the station coverage by adding new ones (e.g. in Libya) are never-abandoned plans, which wait suitable times to be realized.

On the data management side, there are two main reasons for a re-organization of the MedNet Data Center: one is a re-organization of the Italian National Network

Data Center, the other is the participation of MedNet, on behalf of INGV, to the European Integrated Data Archive (EIDA), in the framework of the recently approved European Project NERIES. All the details about NERIES are available on the ORFEUS web site at http://www.orfeus-eu.org/neries/neries.html.

Data archiving and distribution, after the integration with the Italian National Network, will follow similar concepts as in the past, but on a different scale, as MedNet data will be only a small percentage of the total archived data.

On the European side, major data centers will provide support for data archiving and distribution to those centers that do not have the resources to do it independently or just want a backup system. Data archiving will be distributed using new software, data structures and protocols. Data centers will take care of exchanging data and making the system complexity transparent to users.

Acknowledgments The authors wish to thank Professor E. Boschi and Dr. A. Amato for their continuous support. They are also deeply indebted to D. Pietrangeli, S. Pinzi, A. Bucci, M. Perfetti and M. Tozzi for the smooth running of MedNet operations.

References

Arvidsson, R., Ekström, G., 1998. Global CMT analysis of moderate earthquakes, using intermediate period surface waves, *Bull. Seism. Soc. Am*., 88, 1003–1013.

Casey, R., Ahern, T., 1999. Technical Manual for Networked Data Centers (NetDC) Protocol, http://www.iris.edu/manuals/netdc/intro.htm.

Ekström, G., Morelli, A., Boschi, E., Dziewonski, A. M., 1998. Moment tensor analysis of the central Italy earthquake sequence of September–October 1997, *Geophys. Res. Let*., 25, 1971–1974.

Fukuyama, E., Dreger, D. S., 2000. Performance test of an automated moment tensor determination system for the future "Tokai" earthquake, *Earth Planets Space*, 52, 383–392.

Hanka W., Heinloo, A., Jaeckel1, K.H., 2000. Networked Seismographs: GEOFON Real-Time Data Distribution, *ORFEUS Newsletter*, 2, 3, December.

Hanka W., Saul, J., 2008. GEOFON and its Role in Earthquake Monitoring and Tsunami Warning. In E. S. Husebye (ed.). Earthquake Monitoring and Seismic Hazard in Balkan Countries. Springer Publishing, Berlin, 151–162.

Giardini D., Boschi, E., Mazza, S., Morelli, A., Ben Sari, D., Najid, D., Benallou, H., Trabelsi, H., Hfaidh, M., Debeasy, R. M., Ibrahim, E. M., 1992. Very-broadband seismology in Northern Africa under the MEDNET Project, *Techtonophysics*, 209, 17–30, Amsterdam, NL.

Giardini D., 1990. MedNet: Network Configuration. In: Boschi, E., Giardini, D., Morelli, A. (eds.), Proceed. 1st Workshop on MEDNET, September 10–14, CCSEM, Erice, Il Cigno – Galileo Galilei Edizioni, Roma, 15–33.

Kradolfer, U., 1993. Automating the Exchange of Earthquake Information, *EOS Trans. Amer. Geophys*. U., 74,. 442,444–445.

Morelli, A., 1990. MedNet: Data Management, In: Boschi, E., Giardini, D., Morelli, A. (eds.), Proceed. 1st Workshop on MEDNET, September 10–14, CCSEM, Erice, Il Cigno –Galileo Galilei Edizioni, Roma, 34–62.

Morelli, A., Ekström, Olivieri, M., 2000. Source properties of the 1997–1998 Central Italy earthquake sequence from inversion of long period and broadband seismograms, *J. Seismol*., 4, 365–375.

Pino, N. A., Mazza, S., Boschi, E., 1999. Rupture Directivity of the 1997 Central Italy Earthquakes, Geophysical Research Letters, *Geophys. Res. Lett*., 26, 2101–2104.

Pondrelli, S., Di Luccio, F., Fukuyama, E., Mazza, S., Olivieri, M., Pino, N. A., 2003. Fast Determination of Moment Tensor for the recent Molise (southern Italy) Seismic Sequence, *Orfeus Electronic Newsletter*, 5.

Pondrelli, S., Morelli, A., Ekström, G., Mazza, S., Boschi, E., Dziewonski, A. M., 2002. European-Mediterranean regional centroid-moment tensors, 1997–2000, *Phys. Earth Planet. Int*., 130, 71–101.

SEED (Standard for the Exchange of Earthquake Data), 2004. V2.4 Reference Manual, http://www.iris.edu/manuals/SEEDManual_V2.4.pdf, August.

Wielandt, E., 2002. Seismometry. In: Lee, W. H. K., Kanamori, H., Jennings, P. C., Kisslinger, C. (eds.). International Handbook of Earthquake and Engineering Seismology. Part A, Academic Press, ISBN 0–12-440652-1, Part A, 283–304.

GEOFON and its Role in Earthquake Monitoring and Tsunami Warning

Winfried Hanka and Joachim Saul[1]

Abstract Although originally not founded nor funded for earthquake monitoring, after the Indian Ocean tsunami disaster in December 2004 this became an important issue for the GEOFON program of GFZ Potsdam. The GEOFON earthquake information system is based on real-time data feeds of the GEOFON Extended Virtual Network (GEVN), a virtual network of about 300 stations worldwide. It comprises most of the GEOFON network stations and many partner network stations distributed globally. The data are acquired by Internet using the SeedLink real-time protocol, a worldwide defacto standard developed at GFZ. The system provides very timely but nevertheless precise automatic earthquake parameter information published on its web page or by email and SMS alerts. Due to its expertise, GEOFON was appointed to design and implement the seismological component of the German contribution to the Indian Ocean Tsunami Early Warning System (GITEWS). Beside the earthquake monitoring and the operation of a major global seismic broadband network GEOFON runs the largest seismological data archive in Europe. In addition, the cooperation and networking of European and other data centers both in terms of real-time data exchange and the setup of distributed data archive structures are promoted and actively supported. Large EU projects like MEREDIAN and NERIES coordinated by ORFEUS are basically relying on GEOFON's innovative concepts and guidance.

Keywords GEOFON, tsunami warning, earthquake monitoring

1 Introduction

The original scope of the GEOFON Program of GFZ (Geoforschungszentrum Potsdam, http://www.gfz-potsdam.de/) is to collect and distribute worldwide high quality seismological data for all kinds of scientific studies (Hanka and Kind, 1994). It consists of three components, the global permanent broadband seismological network, a varying number of mobile network deployments and the GEOFON Data Center

[1]Geoforschungszentrum Potsdam, Germany, hanka@gfz-potsdam.de

E.S. Husebye (ed.), *Earthquake Monitoring and Seismic Hazard Mitigation in Balkan Countries.*

(now called GFZ Seismological Data Center). The latter comprises the earthquake information system; Semicodon a service for real-time data feed distribution and a comprehensive seismological archive. Unlike, e.g. IRIS, as an initiative with a similar scope, GEOFON has to operate on a much lower economic level but attempts to achieve its goals using simple, inexpensive but innovative technical solutions and with intensive cooperation on all levels. This concept has been extremely successful over the past decade and many networks and data centers in Europe and worldwide have adopted it. Therefore GEOFON today; acts more as a support center and networking, integration and capacity building institution for many networks and data centers rather than a just conventional seismic network and data center on its own.

GEOFON plays also a leading role in near real-time data collection and processing of broadband seismological data both on European and global scales. Its SeedLink IP data transmission protocol being part of the GEOFON SeisComP data acquisition and processing software package has become a defacto global standard. It is also adopted as a manufacturer independent real-time data exchange protocol by international organizations and major projects, supported by all major commercial suppliers of seismological equipment. The GFZ Seismological Data Center acquires in near real-time data from more than 300 globally distributed stations that is from GEOFON's own stations and those from partner networks (GEOFON Extended Virtual Network – GEVN). Most of them are located in Europe (derived from the Virtual European Broadband Seismic Network – VEBSN, Van Eck et al., 2004) and SE Asia. Using these real-time data feeds, automatic processes for data quality checks, event detection, localization and source quantification are performed and the resulting rapid but nevertheless highly reliable earthquake information is automatically published on the Internet. Likewise, alerts are distributed by email and SMS messages to a wide spread user community.

For most of its partner networks, the GFZ Data Center not only acquires near real-time data streams for earthquake monitoring purposes, but also archives them. Together with the GEOFON data and the data sets from numerous temporary network deployments the GFZ long-term Seismological Data Archive is formed. From this all data are redistributed to the user community. All data from permanent and temporary networks are in principle immediately and automatically available to anybody, both as real-time feeds (if available) and from the data repository. However, temporary network data have normally a time period of exclusive usage of the project consortium (2–3 years). Some data of GEOFON partner networks is presently also not generally available.

After the Tsunami tragedy in the Indian Ocean, GEOFON was selected to implement the seismological component of the German contribution to the future Indian Ocean Tsunami Early Warning System (GITEWS, Hanka et al., 2006). This appointment is regarded as a recognition of the successful data collection, processing and dissemination strategies implemented over the past decade.

2 The Permanent GEOFON Network

The permanent GEOFON network (FDSN network code GE), presently consisting of 54 stations on all continents, became a multinational initiative. A number of institutions from different countries joined the GFZ efforts to set up a permanent

seismological broadband network in Europe and the Mediterranean as well as to fill gaps in the global broadband network (Figure 1). Cooperations on different levels with similar programs like IRIS, MedNet, Pacific21 and individual national networks and geophysical institutes in many countries have as a result that the GEOFON network has been growing much faster than expected. GEOFON stations

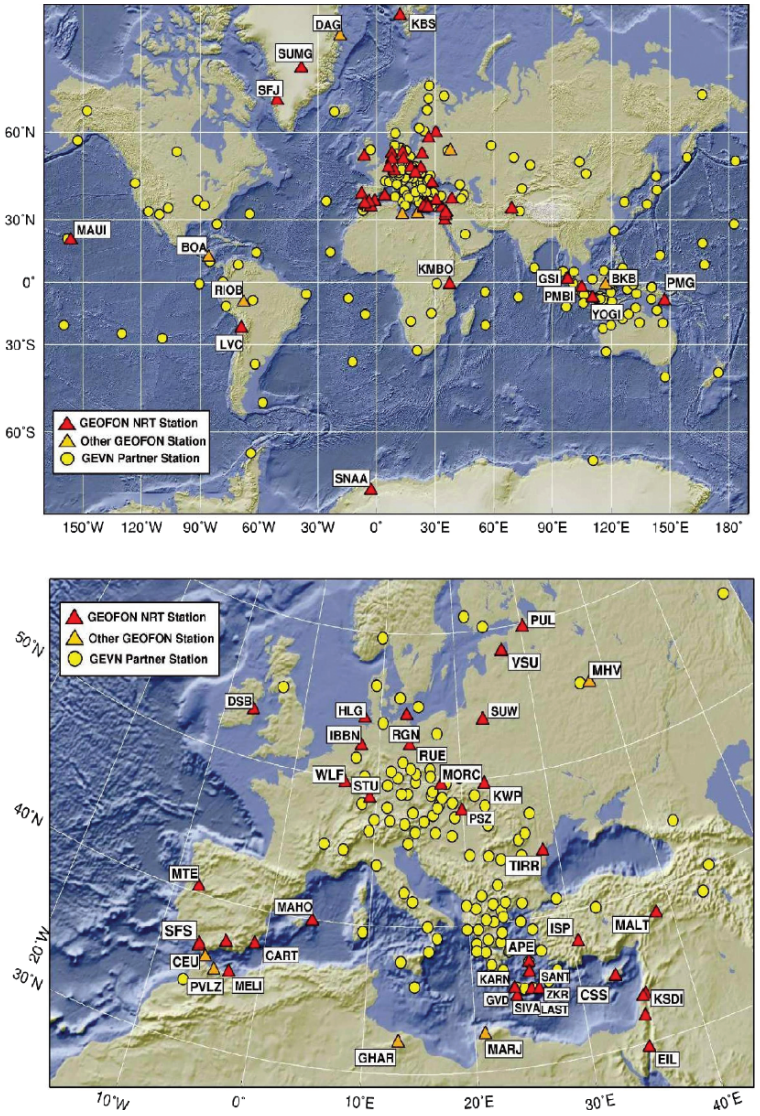

Figure 1 Overview of station distribution of the permanent GEOFON network (triangles, red – online stations, orange offline stations) and the GEOFON partner networks (yellow circles) in EuroMed area and globally jointly acquired at GFZ via Internet and forming the GEOFON Extended Virtual Network GEVN

are normally equipped with Streckeisen STS-2 VBB seismometers with a special shielding (Hanka, 2000) and adequate "true" 24-bit digitizers, which allow the recording of all relevant seismic signals from high frequency local events to the earth tides with sufficient dynamic range. In several "global" sites STS-1 seismometers are used. In older GEOFON stations Quanterra Q380 or Q4120 dataloggers are still used, while in newer or upgraded stations Earth Data PS6-24 digitizers are installed. In the new satellite based Indian Ocean GEOFON sub network Q330 (HR) digitizers are used. These new stations are also equipped with additional strong motion sensors.

The Seismological Communication Processor The core of the GEOFON network is the Seismological Communication Processor (SeisComP) system (Figure 2, http://www.gfz-potsdam.de/seiscomp). It is a concept for a manufacturer independent networked seismographic system, originally developed for the GEOFON network (Hanka et al., 2003) and further extended within the MEREDIAN project (Van Eck et al., 2004) which became meanwhile a defacto standard in Europe and worldwide. Its task is sevenfolded: data acquisition, data recording and real-time communication on the station side, monitoring and controlling, automatic (near) real-time data processing (quality control, event

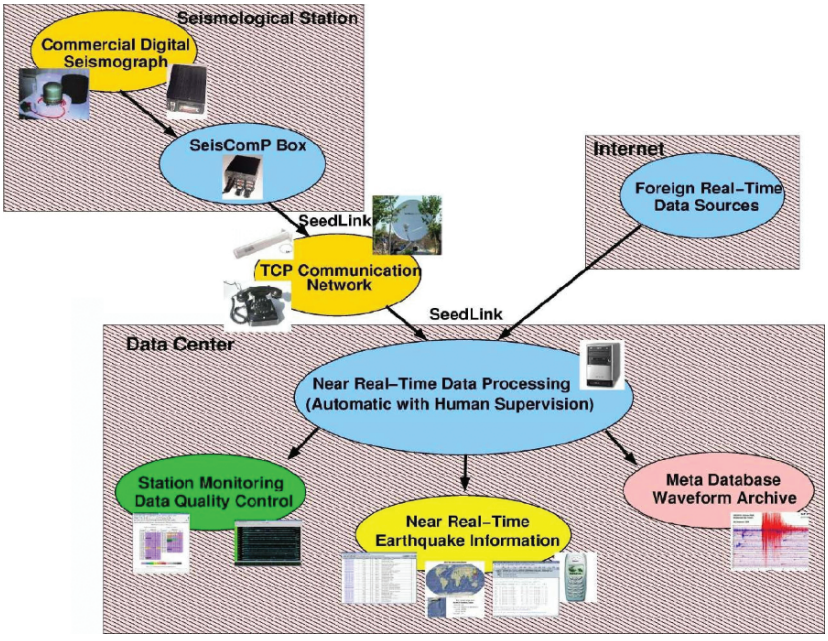

Figure 2 The GEOFON Seismological Communication Processor (SeisComP) concept provides standardized acquisition for all sorts of commercial digitizers and data loggers, data recording and real-time communication on the station side, monitoring and controlling, automatic (near) real-time data processing (quality control, event detection and location), data archival and data distribution on the data center side

detection and location), data archival and data distribution on the data center side. SeedLink, the data acquisition and transmission part of the SeisComP software package makes it easy to deal with heterogeneous commercial hardware. SeedLink supports many different commercial and noncommercial data logger and digitizers, data formats and transfer protocols and provides unified appearance for heterogeneous hardware, formats and protocols within seismological networks. For this, all GEOFON stations are equipped with a so-called SeisComP box, a GFZ developed PC/104 based station and communication processor running the SeisComP software under the Linux operating system. Although a standard office PC would in principle do the job as well, the SeisComP boxes have certain advantages (small size, low (12 VDC battery) power consumption, rugged field design, sophisticated environmental shielding). Most (47) GEOFON stations are directly or indirectly connected to the GEOFON Data Center in Potsdam by SeedLink, mostly by Internet. For this, local Internet service providers or local or regional SeisComP data collection centers at partner institutions with Internet access are used. Different means are used to bridge the "last mile" from the remote seismic vault to the Internet access point. These can be radio, WLAN or satellite links as well as dedicated or dialup telephone or IDSN lines. Using SeedLink, it is possible to transfer the complete data sets from the remote stations in (near) real-time to the GEOFON Data Center.

Many seismological networks in Europe and worldwide have adopted the GEOFON concept of establishing state-of-the-art high quality real-time broadband seismic networks at low costs. In many countries the existing old short period network were transformed into modern broadband networks after a single GEOFON station has been installed as nucleus and the required know-how was transferred. Also the EC project MEREDIAN, carried out under the coordination of ORFEUS, had a substantial impact namely in distributing SeisComP as the European standard system for real-time data exchange among data centers. The major achievement of MEREDIAN, the Virtual European Broadband Seismic Network (VEBSN), consists mainly of a set of SeedLink servers at each contributing data center, offering real-time data access to all or a selected subset of stations available at the centers. SeedLink therefore supplies a realtime data exchange mechanism among data centers and makes it easy to establish crossborder virtual networks. In the USA, the IRIS DMC has adopted SeedLink for distributing its real-time data streams (including those from the FDSN stations and USArray) to the users. In Central America, South and East Africa (including AfricaArray initiative), Japan, Australia, New Zealand and recently South East Asia, many networks are meanwhile using SeisComP and offer real-time data via SeedLink for exchange. Even if in some cases commercial data acquisition software is used, SeedLink provides a unique opportunity to link commercial networks to those from different manufacturers and to the SeisComP and Earthworm community. Altogether, there are presently presumably between 1,500 and 2,000 stations worldwide in principle available via SeedLink.

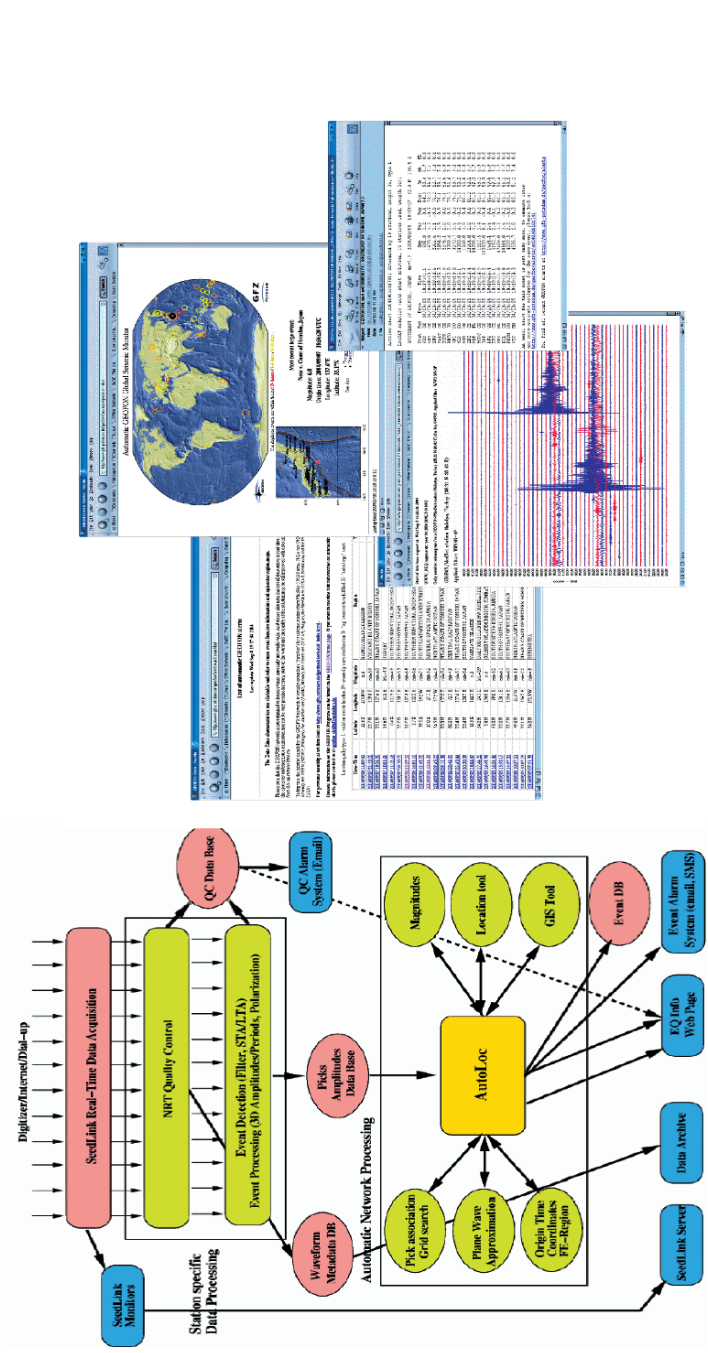

Figure 3 Data and information flow within the GEVN real-time data processing system and resulting Internet products. The system provides presently one of the fastest source of publicly available basic earthquake information on global and regional scale

3 The GEOFON Extended Virtual Network (GEVN) Earthquake Information System

Using these resources, real-time data streams from more than 250 foreign stations are presently acquired at the GFZ Seismological Data Center in parallel to those of the GEOFON itself forming the so-called GEOFON Extended Virtual Network (GEVN). Many stations are from GEOFON partner networks (mainly in Europe), for which also backup archiving at the GFZ Seismological Data Archive is a major issue. But also many additional global stations (namely from IRIS) and from countries in the Indian Ocean area are used for global and regional earthquake monitoring purposes (Figure 1). The near real-time data processing and its results are illustrated in Figure 3. After performing quality control, the incoming single data traces are checked for seismic signals by automatic detectors and a variety of post detection algorithms. The individual event triggers are then associated to event related groups with a grid search method. Additional post-detection parameters like polarization angles, spectral characteristics and duration are determined to better classify questionable arrivals and to distinguish overlapping pick groups from parallel occurring events at different locations within the network. The precise hypocenter for the successfully associated and prelocated pick ensembles is finally determined by standard location programs (e.g. LocSAT). The obtained information is immediately distributed to registered users by email and SMS services and published on the GEOFON Internet page both in the "Seismic Monitor" (http://www.gfz-potsdam.de/geofon/seismon/globmon.html) and the online automatic bulletin (http://www.gfz-potsdam.de/db/eqinfo.php). A separate web page is generated for each event, where the arrival times and magnitudes for all stations are listed. All event pages are accessible from the Automatic Bulletin page. In the "Global Seismic Monitor" the epicenters of all larger earthquakes of the last 2 weeks are marked. The epicenter of the last bigger earthquake is blinking red. "Live" seismograms visualize recent earthquake activity at individual stations to the public (http://www.gfz-potsdam.de/geofon/gfn_liveseis.html). This system provides presently one of the fastest sources of publicly available basic earthquake information on global and regional scale. In Figure 4 the alert delay times are shown as a function of geographical region while in Figure 5 the location performance of the system is illustrated in comparison to NEIC solutions. In both categories the system shows a very good performance for many parts of the world, mainly for EuroMed area and SE Asia. The black dots in Figure 5 indicate events not listed by NEIC. Some of these may be fake events, but many of them are real but weak earthquakes.

4 The GFZ Seismological Data Center

The GFZ Seismological Data Center provides three basic services: the GEVN Earthquake Information Service, the GEVN SeedLink real-time data feed service and the GFZ Seismological Archive. The two later ones are carried out in the

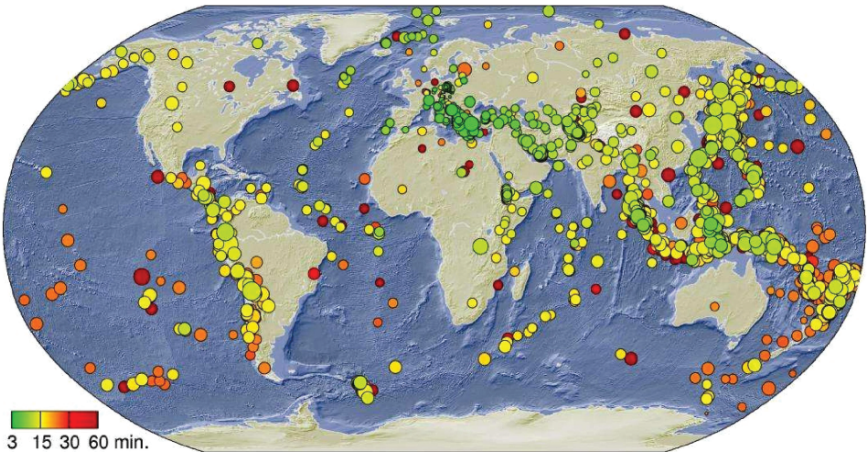

Figure 4 Global alert publication delay times of the GEVN Earthquake Information System in dependence of the geographical region

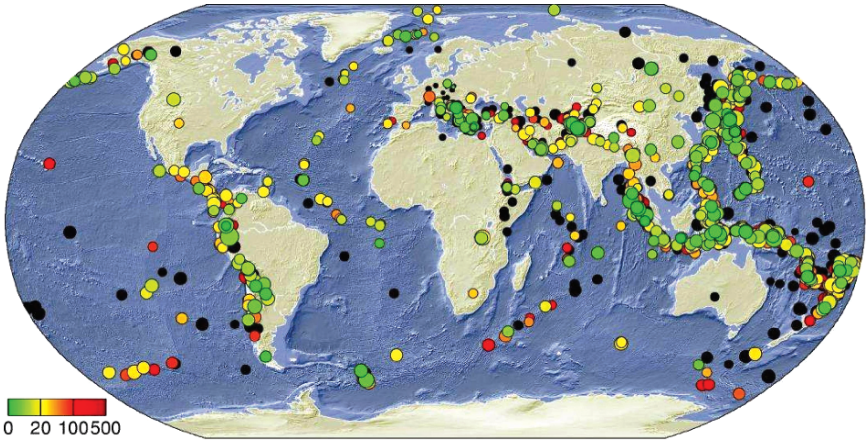

Figure 5 Global location accuracy (in km) for the GEVN Earthquake Information System in dependence of the geographical region and in comparison with NEIC. Black dots indicate nonassociated locations, which might in many cases be "real" events anyway

ORFEUS distributed data center framework being presently setup within the NERIES EC project (http://neries.knmi.nl). In the GEVN SeedLink online data pool (near) real-time data from presently almost 30 worldwide partner networks are acquired parallel to the GEOFON network with in total more than 300 stations. In return, most of these partner networks obtain real-time GEOFON or other GEVN data feeds for their needs. Most of these data feeds are also available for other users. Therefore usually more than 40 institutions worldwide acquire GEOFON and other data in near real-time from the public GEVN SeedLink server (geofon.gfz-potsdam.de:18000).

The GFZ Seismological Data Archive holds all continuous data from the permanent GEOFON network as well as the data from most of the GEVN partner networks, for which it also serves as long-term backup data archive. However, the major part of the archive holdings (presently about 8 TB, the largest data archive in Europe) is data obtained from mobile seismic experiments with the GFZ instrument pool. Data from temporary networks is usually restricted to the project consortium for 2–3 years before it gets released for public use. Although most data sets are derived from broadband stations, also a substantial amount of short period data is archived as well as some strong motion and OBS data. All data is online available on large RAID disk arrays. Backup files of all data are in addition also stored online in a mirrored RAID system and offline in a large tape robot system in the GFZ Central Computer Department. The data retrieval system is automatic, but queued. Request times therefore depend on the number of parallel requests. All data sets are accessible jointly in a unified way by a prototype web request formulation tool (http://www.gfz-potsdam.de/cgi-bin/geofon/request?mode=nform&nettype=perm) or by breq_fast email requests (breq_fast@gfz-potsdam.de). Within the NERIES project, GEOFON is responsible for the implementation of the European Integrated Data Archive (EIDA) as a de-centralized archival system which is more suitable for the situation in Europe than a centralized approach as, e.g. at the IRIS DMC. Its basis is the so-called ArcLink protocol, a SeisComP twin of SeedLink not for real-time feeds but for archive and meta database access. ArcLink was developed in the WebDC project of GFZ and SZGRF (http://geofon.gfz-potsdam.de/new/web_dc.html) is designed as a straight continuation of IRIS' NetDC concept of providing seismic data fully transparent to the user through a single user interface wherever the actual archive is located. In practice, the basic NetDC ideas are just combined with the basic SeedLink ideas to overcome present shortcomings by invoking a direct TCP/IP based protocol instead of email and ftp and a sophisticated web interface for request formulation. Instead of supporting different data acquisition systems through SeedLink plugins, ArcLink request handler plugins support different data archive structures as individual data sources. Presently a distributed data archive for Germany based on ArcLink exists already as a prototype installation and provides combined access to the data sets of the GFZ Seismological Archive and the German Central Seismological Observatory (SZGRF) Archive in Erlangen (http://www.webdc.eu).

5 GEOFON and the Indian Ocean Tsunami Warning System

The tsunami tragedy following the great Sumatra quake of December 26, 2004, included more than 500 German victims among the approximately 230,000 in total. It became obvious to nearly all of us that in today's global village natural disasters can affect everybody. The German human aid program for the Indian Ocean region started immediately after the disaster and included substantial funding (45 M Euro) for the proposed German Indian Ocean Tsunami Early Warning System (GITEWS). The government of Indonesia was the first who accepted the German

offer of providing a substantial part of their planned tsunami early warning system. Meanwhile more cooperative agreements with Sri Lanka and other countries in the region are under negotiation.

GEOFON was appointed to design and implement the land based seismic component of GITEWS, based partly on its expertise in Internet-based near real-time data acquisition, automatic near real-time earthquake alerts and virtual seismic network management. The other components involved are CGPS buoys, ocean bottom units (pressure and presumably seismic broadband sensors), coastal stations (tide gauges, CGPS, strong motion sensors) and CGPS stations.

The challenge for a tsunami warning system for Indonesia is that the tsunamigenic earthquakes happen in the Sunda trench subduction zone very close to the coastline of the Indonesian island chain. Only a few minutes are available not only to detect and locate a potential tsunami generating earthquake, but also to determine as many additional parameters for the extended earthquake source capable to choose the most likely tsunami scenario from several thousands pre-calculated models. Success in tsunami early warning for Indonesia also will benefit the other Indian Ocean rim countries. Therefore international cooperation is the key, both for primary data exchange (e.g. seismic data) but also for the exchange of warning bulletins.

GITEWS station locations are based on an Indonesian proposal that includes densifying its own regional network and using data from 6 CTBTO stations. Locations for the international backbone network (Figure 6) were negotiated with

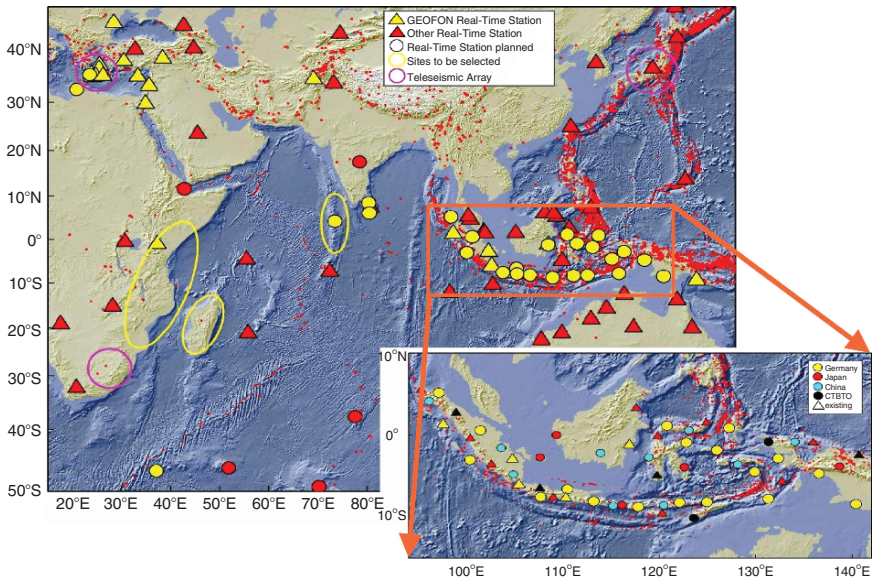

Figure 6 GEOFON network extension in the Indian Ocean area for tsunami warning purposes (yellow symbols). Triangles indicate existing stations, circles planned one. Ellipses indicate areas of interest for more deployments. Pink ellipses show dense national network to be used as teleseismic arrays for rupture tracking for Sunda Trench earthquakes

Germany (25 stations), Japan (NIED, 15) and China (CEA, 10). For an earthquake occurring at any point along the Sunda trench, 2–5 of these stations will receive the first arrivals so quickly that a first internal alert based on rough estimates for location and amplitudes of rupture start can be issued after 1–2 min. More precise values are expected after 3–5 min together with first estimates on rupture direction and fault plane parameters based then on the recordings of more than 20 stations. Each sub-network functions independently, but also feeds data into a single virtual network to be processed jointly.

Comprehensive earthquake monitoring of the Sunda trench and the whole Indian Ocean area requires also data from far regional and teleseismic distances. Open real-time data are presently available from Australia, Malaysia and Singapore, the IRIS GSN and GEOSCOPE. Comprehensive cooperation has been agreed with Australia and South Africa, and direct data exchange with Malaysia and Singapore is arranged. Plans include two new stations and a seismic control center in Sri Lanka, and additional stations may be possible in the Maldives, Madagascar, and East Africa. A fully redundant VSAT system is envisaged with the main hub in Jakarta and a backup in Darwin, and South Africa can also help providing regional gateway functionality. Besides the optimum recording of the full seismic spectrum relevant both for early warning and seismological research, the main station design goal is high reliability and minimum maintenance. The main VBB seismometer is an STS-2 with additional shielding, proved to increase the VLP performance significantly at previous GEOFON stations. A strong motion sensor is also attached to a 6-channel Q330HR. About half of the seismic stations will be co-located with real-time GPS. To protect against humidity, swampy conditions, frequent floods and vermin, the station equipment will be buried in specially designed two-chamber water and air tight fiber vaults with a steel bottom construction providing optimum attachment to a bed of concrete.

Comprehensive software is being developed to provide full functionality, such as operator process and state-of-health visualization and interaction, and sophisticated tools for regional and teleseismic analysis. The system will provide optimum reliability and redundancy including possibilities for advanced distributed real-time data processing, avoiding the necessity to bring all data streams in real-time to one place. Already in 2005 GEOFON stations were installed in Indonesia at four BMG (Meterological and Geophysical Service of Indonesia) sites with existing VSAT links on Nias, Sumatra, Java and Kalimantan, two of them with CGPS. Also two tsunami test buoys with broadband OBS were deployed offshore Sumatra. After installation of a VSAT system in June 2006, completion of the seismic network in Indonesia and Sri Lanka is planned within 2 years. On the eastern side of the Indian Ocean area, a communication concept must be developed first before stations can be sited. As early as June 2005 a copy of the GEOFON automatic near real-time earthquake information system was installed at BMG as a provisional automatic alert system. It was using at first only external stations imported via Internet but the different partners have already installed 28 real-time stations in Indonesia, cutting the alert times for earthquakes in Indonesia to 4–7 min. Research has started for developing methods to obtain quickly reliable automatic magnitudes also for strong earthquakes above M = 7 (Bormann and Wylegalla, 2005).

Acknowledgment The GEOFON project is an initiative funded by GFZ Potsdam and more than 50 institutions worldwide. This is publication no. 5 of the GITEWS project (German Indian Ocean Tsunami Early Warning System), funded by the German Federal Ministry for Education and Research (BMBF), Grant 03TSU01.

References

Bormann, P., Wylegalla, K., 2005. Quick Estimator of the Size of Great Earthquakes. *Eos Transactions, AGU*, 86, 46, 464.

Hanka, W., 2000. Parameters which influence the very longperiod performance of a seismological station: examples from the GEOFON network. *In: (P. Bormann and E. Bergman (ed.)) New Manual of Seismological Observatory Practise.*

Hanka, W., Heinloo, A., Jackel, K. H., 2003. Networked Seismographs: GEOFON RealTime Data Distribution, *In: Proceedings of OHP/ION symposium "LongTerm Observations in the Oceans: Current Status and Perspectives for the Future", January 21–27, 200, Workshop Report, 58–62.*

Hanka, W., Lauterjung, J., & GITEWS Team, 2006. GEOFON and the German Indian Ocean Tsunami Warning System*. IRIS Newsletter, 2, 89.*

Hanka, W., R. Kind, 1994. The GEOFON Program. *Annali di Geofisica, XXXVII, N5, Sept. 1060–1065.*

Van Eck, T., Trabant, C., Dost, B., Hanka, W., Giardini, D., 2004. Setting up a virtual Broadband Seismograph Network Across Europe. *EOS, Transactions, AGU, 85, 13, 125–129.*

The Karelian Regional Seismic Network in NW Russia

Tatiana Matveeva[1], Yury V. Fedorenko[2], and Eystein S. Husebye[3]*

Abstract NW Russia is an aseismic region implying that few and infrequent earthquakes occur. Its seismicity is mainly mapped through analysis of historic macroseismic observations which is incomplete regarding small earthquakes say below ML = 4.5. For the Karelia Region (north of St. Petersburg) most located seismic events are explosions in origin and further more recorded mainly by stations and arrays adjacent to Karelia that is in Kola, Finland and N. Norway. From a Karelian point of view this is not entirely satisfactorily so some initiative has been taken for installing a local seismograph network. Note that deployment and subsequent network operations are a costly undertakings but using the inexpensive and versatile Cossack Ranger II instrumentation a high quality and affordable network operation for Karelia has been achieved. These efforts are the topic of this article.

Keywords Karelia, NW Russia, seismograph network, Cossack Ranger II, earthquake monitoring

1 Introduction

Present days when seismic data acquisition system and network operational cost are becoming affordable, earth scientists pay more attention to the study of tectonic activities of low-seismicity regions. The conditions for seismic monitoring of such regions are dense seismic networks which can guarantee weak event detection down to a ML ~ 1.5. This was the challenge when starting the deployment of the Karelian (NW Russia) seismic network namely the necessity to have an affordable 3-component seismograph, capable of providing adequate seismic records for basic research. An additional requirement is ease of seismograph installation and

[1]*Institute of Geology, KarSC RAS, Petrozavodsk, Russia*

[2]*Polar Geophysical Institute, KSC RAS, Apatity, Russia*

[3]*Bergen Center for Computational Science, UNIFOB/UoBergen, Bergen, Norway*

*To whom correspondence should be addressed. e-mail: esh@bccs.uib.no

E.S. Husebye (ed.), *Earthquake Monitoring and Seismic Hazard Mitigation in Balkan Countries.*

maintenance at remote sites. Considering many seismograph makes, essentially restricted to those based on inexpensive geophone sensor, we found not surprisingly that the Cossack Ranger II seismograph (CR-II) best meet the above requirements. This instrument initially developed by Fedorenko in 1999 has been operated successfully in the most adverse climatic conditions like Kirovsk (Chernouss et al., 1999), W. Norway (Fedorenko et al., 2000) and also in the tropical Costa Rica (Waldo Taylor, pers. communication).

2 CR II – General Description

The Cossack Ranger II 3-component seismic station is an advanced, inexpensive and low-power 3–12 channel seismograph. It consists of four modules being common for most seismic station designs (i) 3-component seismic sensor unit with or without preamplifier, (ii) an A/D-converter unit, (iii) optional GPS clock, and (iv) data logger based on any type of computer (desktop, notebook, Palm Digital Assistant etc.) supporting USB or RS232 port.

CR-II can operate as a 3-component station or 9-element mini-array storing data locally or remotely using TCP/IP protocol via Ethernet, GPRS modem, radio transmitter, wireless 802.11b etc. The CR-II data acquisition software supports continuous, level-triggered and STA/LTA triggered recordings. It can also be easily configured to start and stop data acquisition in given time intervals. While operating in a triggering mode the loads on data links are considerably reduced, and even slow modem connections will be adequate. To synchronize station time to UTC the CR-II timing system uses either the GARMIN GPS 18 clock or Internet Time Protocol service via TCP/IP connection. Recorded data can be stored locally to hard disk or sent to the central Hub in a few minutes after event recording 'terminated'. Optionally, data may be written to a flash memory card which can be exchanged within a few minutes. Adequate power supply protects battery from over-discharging and easy switching to exchange batteries. A standard housing conforming to the IP68 standard is used to protect equipment from dust and liquids.

3 Field installation of the Cossack Ranger II seismograph

Any seismograph installation requires (i) power access, (ii) timing device or clock, (iii) remote data transfer, and (iv) proper siting rock. Since the CR initially was designed for school yard installation we would address the above requirements in this context. First electric power in terms of the 220 V electric network or 9 V batteries. The former is most convenient and our preference is given for the automatic rebooting at power out-gauges say due to lightening. Alternatively, rebooting is performed remotely from the Hub or network center. For remote, stand-alone installations batteries provide adequate power supply but are often somewhat

inconvenient with frequent replacement unless consumption of ADC and data logger is exceptionally low. The CR-II design is flexible permitting stand alone operations with power supply from batteries.

Accurate, absolute timing is a necessity for comparing and jointly analyze recordings from 2 or more stations. Before the advent of the GPS timing device this was often a severe practical problems. Clocks, even expensive ones, had a timing accuracy seldom better then 0.1 s. For field installations, similar accuracy was attainable, using radio clock signals from Potsdam (Germany) and/or Rugby (UK) for calibrations. When we first deployed our CR-stations in W. Norway high schools in 2000/2001 we used the Internet timing system being accurate to +/−0.01 s or better. At that time GPSs were relatively expensive and besides a drawback is its required outdoor monitoring with exposures to rainy weather and theft. Today, the preference is for using highly accurate and inexpensive GPS timing (+/−0.002 s).

For most monitoring systems fast data access at the local center or Hub is mandatory. This has been feasible since the 1970s using say leased commercial telephone lines but high costs have prevented wide spread use of such solutions until recently. Today the relatively easy access to the Internet at almost no costs makes this mean for the data transfer universally praised by seismologists. In case of stand alone station operations most of the events recorded and stored on disks in the field while only an affordable fraction of the data stream is transferred within a reasonable time lag to the Hub. In this context is interesting to 'convert' mobile phones into a data transfer unit (Katkalov and Husebye, 2008). Note, advanced data logger design permit extractions of critical parameters for an epicenter location like P–arrival times and amplitudes and also signal envelopes (1 s sampling) tied to the Hilbert transform of the original waveforms (100–200 Hz sampling).

Proper seismograph siting is critical for the high quality network operations. Preferably site surveys proceed the actual installation measuring the ambient noise field and avoid locations close to fast running machinery. In particular, it is important to avoid any site 'tied to' parts of the housing structure which easily 'transmit' in-house activities. Switching on and off of machinery are occasionally manifested as spikes in the recordings. If the spikes are simple and of a regular form they are easily removed by digital filtering; the CR-II data logger incooperates such a feature.

4 Karelian Seismic Network – CR-II Installation

In Karelia we undertook a special study of siting environments by installing 4 CR stations at very different sites (Figure 1).

The network installation process began in August 2000 when the first station was installed in the Geophysical Yard of the Petrozavodsk University (PTRZE in Figure 1). Seismometer was installed in the basement of a wooden, two-story house on solid rock. Data were transmitted via radio link to the Institute server. This station has provided reliable event recordings for more than 6 years. Then during summer 2006 a new station was installed in a school yard (KOSTE in Figure 1). It

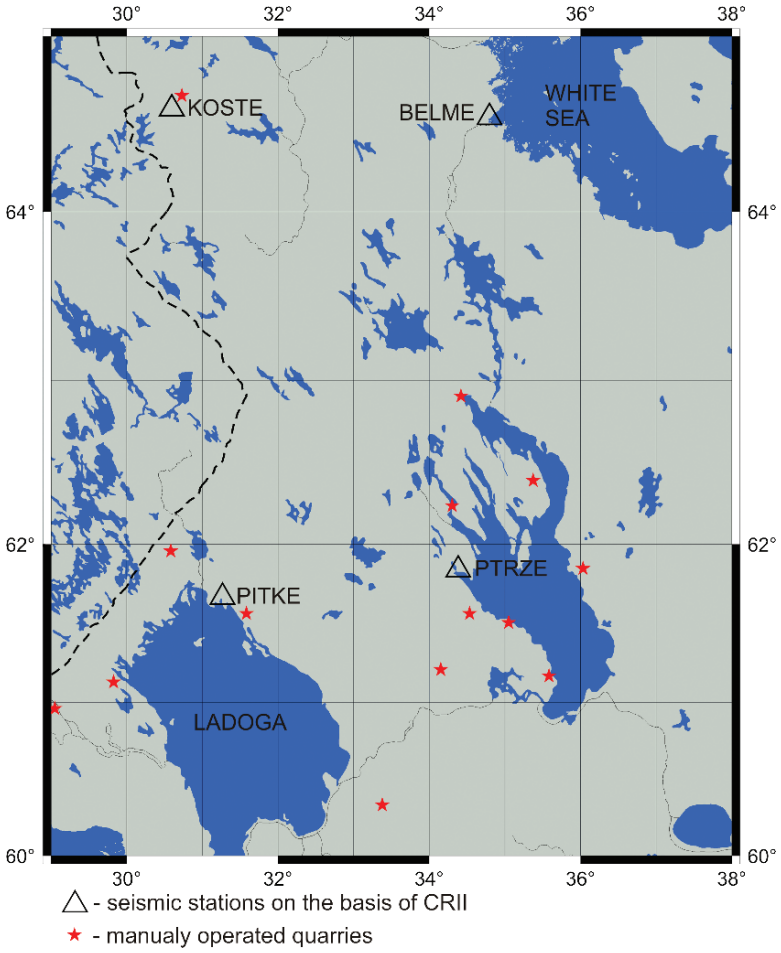

Figure 1 Seismic stations: PTRZE, KOSTE, BELME and PITKE (triangles) with the CR-II instrumentation installed in 2000–2006 in Karelia (NW Russia) and adjacent quarries (red stars). For geoscience investigations in this region, we refer to Sharov (2004)

was impossible to dig a hole close to the data logger and due to a lack of safety for outdoor installation we put sensor on the floor in the school building. As expected, this place was hopeless due to the human activity in the building so only explosions from the nearby mine were recorded during the half year of operation.

The remaining two stations (BELME and PITKE in Figure 1) were installed on the premise of radio masts where service buildings provided stations with proper housing. Therefore one station BELME was installed near the mast in the outskirts of the small town Belomorsk close to the White Sea. The sensor was installed in an abandoned building on exposed rock. The closeness of the town, railway station and White Sea bay made reliable recording impossible of even close occurring events. Only a few teleseismic earthquakes and some explosions were recorded by

this station over 6 months. The other station PITKE was installed near a mast relatively far from any human activity and 3 km away from the Ladoga Lake. Sensor was installed on the solid rock and a wooden shielding was made. This installation turned out to be successful and events of different kind were recorded.

For both of these stations (BELME and PITKE) data transmission and station operation were organized via GPRS modem of mobile phones. An unexpected shortcoming of the GPRS connection was during lunch and dinner time when the cellular network was overloaded causing low speed connection. Contrary to our expectations the electric lines of the radio masts did not produce spikes on the recordings and likewise wind vibrations of the masts had no significant recording influence.

5 Cossack Ranger Recordings in Research

The first Cossack Ranger seismographs were to some extent home made in the sense that besides the individual sensor of cost $60 each, partly 'home made' ADC and an old PC as data logger had a price tag less than $1,000. Some colleagues asked whether such a dirt cheap seismograph was useful for advanced research purposed. This was considered a challenge so the first step in testing recording quality was to site the CR adjacent to a Kinemetrix Ranger seismograph – the ASK station close to the Institute and Bergen city itself. Test was only partly successful as the Kinemetrix recordings obviously were clipped for a local ML ~ 3.5 events. Further tests were a polarization study of Karelian events demonstrating that observed and calculate wavefield polarization properties were similar (Fedorenko et al., 2008a). This would not have been feasible with anomalous phase shift among the sensor components. In another study, we used deformable templates technique for linearly projecting the Lg-wave train from one CR station into another one – the original waveforms replaced by their respective Hilbert transforms. In other context, we subjected the Pg/Pn-coda to an automatic phase picking scheme and then using Bayesian statistics for validating the pickings toward updated focal parameter estimates including depth. The CR is also efficient in monitoring local seismicity since its 2D signal detector is superior to the conventional 1D detector commonly used. A number of relevant references are added to the reference list below and these are; Fedorenko et al., (2008a,b,c), Husebye et al., (2003) and Husebye and Mäntyniemi (2005).

6 Summary

All installed CR-II stations proved to be robust, stable and easy to install (even for a single person) and operate properly. Some of the stations were running for more than a year in Norway and Karelia without any disruption while in some cases water leaked into the instrumentation boxes. This problem was eliminated by using more elaborate box design and also to ensure that the sealing putty in fact stopped water sipping inside the box. We have also operated the CR's in most moistly environments like the jungle

in Costa Rica, the wet west coast of Norway and cold areas like Karelia, Spitsbergen and in the Kirovsk mountains. It has been functioning equally well in all these environments. To summarize, the Cossack Ranger design is well suited for advanced seismological research and network monitoring of local seismicity.

References

Chernouss, P., Zuzin, Yu., Mokrov, E., Fedorenko, Yu.V., Kalabin, G., Husebye, E. S., 1999. Avalanche Hazards in Khibiny Massif, KOLA, and the new Nansen Seismograph Station. *IRIS Newsletter* 1, 12–13.

Fedorenko, Yu. V., Husebye, E. S., Bulaenko, E., 2000. School Yard Seismology. *Orfeus Newsletter* 2, 3, 22.

Fedorenko, Y.V., Matveeva, T, Beketova, E.B., Husebye, E.S., 2008a. Secondary phase validation - phase classification by polarization. M/s submitted Physics Earth Planetary Interiors.

Fedorenko, Y.V., Husebye, E.S., and Matveeva, T., 2008b. A 2-D Seismic Signal Detector for Stand Alone 3-Component Stations. In E.S. Husebye (ed.) Earthquake Monitoring and Seismic Hazard in Balkan Countries. Springer Publishing, Berlin, 171–187.

Fedorenko, Y.V., Husebye, E.S., Matveeva, T., 2008c. Cossack Ranger II – A High Quality, Versatile and Affordable 3-Component Short-Period Station. In E.S. Husebye (ed.) Earthquake Monitoring and Seismic Hazard in Balkan Countries. Springer Publishing, Berlin, 189–196.

Husebye, E.S., Beketova, E.B., Fedorenko, Y.V., 2003. School Yard Seismology. J. Geoscience Education 51, 329–355.

Husebye, E.S., Mäntyniemi, P., 2007. The Kaliningrad, West Russia earthquake on the 21st of September – surprise events in a very low-seismicity area. Physics Earth Planetary Interiors 153, 227–236.

Katkalov, Yu., Husebye, E.S., 2008. Cossack Ranger field operation – efficient data transfer via mobile phones. Manuscript in preparation.

Sharov, N.V., (ed.), 2004. Deep structure and seismicity of the Karelia region and its margins. Karelian Research Center, Institute of Geology, Petrozavodsk, Russia, pp 245–255.

Part IV
Seismic Network Operations, Event Location and 2-D Signal Detection

Cossack Ranger II – A High Quality, Versatile and Affordable 3-Component Short-Period Seismograph

Yu. V. Fedorenko[1], Eystein S. Husebye[2*], and Tatiana Matveeva[3]

Abstract Modern, high quality seismic instrumentation has become very expensive and likewise high costs for fast data transfer from outlying stations to the local analysis center. National network operations are normally a government responsibility including the national tasks of monitoring earthquake activities and advising local authorities on earthquake hazards. Originally, seismographs were developed, deployed and operated by Academia but as stated now such tasks rest with government agencies with very few exceptions. Scientists in geoscience departments would often like to operate their own networks for special research experiments but this is hardly feasible due to the high costs involved. When faced with such problems our 'solution' was to develop a low cost, high quality 3-component short period seismograph with a price tag between $1,000 and $1,800. Operational costs were minimized through an outreach project named SeiSchool aimed at cooperation with local high schools. The latter have permanent access to the Internet so data transfer to the Hub in Institute was free. Some schools even installed their own seismographs locally with only written instructions at hand. Station operations were mostly trouble free and in the most successful schools the Cossack Ranger was in continuous operations for more than a year. In this article we describe in details our Cossack Ranger II seismograph, operational aspects, school cooperation and the use of recordings in research ventures.

Keywords Cossack Ranger II, seismographs, outreach project, networks, school research

[1]*Polar Geophysical Institute, KSC RAS, Apatity, Russia*

[2]*Bergen Center for Computational Science, UNIFOB/UoBergen, Bergen, Norway*

[3]*Institute of Geology, KarSC RAS, Petrozavodsk, Russia*

*To whom correspondence should be addressed. e-mail: esh@bccs.uib.no

E.S. Husebye (ed.), *Earthquake Monitoring and Seismic Hazard Mitigation in Balkan Countries.*

1 Introduction

An essential element in local and regional seismicity studies is a dense seismic network. The cost of instruments and high running expenses are factors that have constrained wide deployments of such seismograph clusters. The challenge we faced some years ago was to construct an affordable seismograph, capable of providing adequate seismic recordings for basic research. Initially, the motivations came from studying avalanches which may be released by seismic loading caused by open pit and underground mining explosions. Our first step here was installation of the Nansen station (Chernouss et al., 1999) on a mountain top near the town Kirovsk (Kola) for monitoring mining explosions being as a potential trigger of adjacent avalanches. Despite a very harsh environment this simple prototype 3-component station is still functioning very well. Successful later installations and further exploitation of the Nansen seismic station design demonstrate that it is feasible to deploy high quality local and regional seismograph networks without excessive investment operational costs. Such operations have taken place in W. Norway, Costa Rica and Karelia (NW Russia) where environmental conditions may be revere.

Our seismograph design, termed the Cossack Ranger (CR) was first deployed near Kirovsk, Kola, in 1999, while the present day version, the CR-II, is much improved technically. This and the large interest in high quality inexpensive seismographs for outreach purposed justify a new presentation of the Cossack Ranger II versus the original one by Fedorenko et al. (2000). In addition, a few examples are given of CR-II recordings in seismological research contexts.

2 Geophones as substituting seismometers

The most expensive part of a modern, high-quality seismograph station has until recently been the seismometer. Up to about 1980 seismometers were essentially expensive mechanical instruments with single short-period sensor costing $20,000–40,000. Note, broadband instruments are far more expensive with costs exceeding $20,000. Anyway, oil industry provides cheap but good geophones so in principle an inexpensive substitute for conventional seismometers is available in the market.

In the 1990s use of geophones as substitute for seismometers became more common in particular for operations where compact size and rugged design were important. Companies world-wide produce many different types of geophones so to choose the type optimal for seismic measurements is not always a simple task. A further complication is that a geophone is coupled to a preamplifier which adds electronic noise to the geophone recordings. Other important design characteristics of seismograph stations are the dynamic range and the sensor response versus the ambient noise field. The former parameter is defined as the ratio between the largest and smallest signal amplitudes which can be handled without distortion by the A/D-converter. Modern and costly broadband stations are equipped with so-called

24-bits A/D-converters which are equivalent to a range of 144 dB or a local event of magnitude 7.0. Such relative costly A/D-converters are not really needed for geophone 'derived' seismometers and in case of the CR-II we found a 22-bits converter entirely adequate. Regarding system or instrumentation signal responses as a function of frequency there is an obvious limitation in geophone seismometers simply because the sensor pendulum mass is modest at 23 gram being equivalent to a lower cut-off frequency around 0.5 Hz. For many earthquakes monitoring purposes this is not much of a shortcoming as the classical short-period seismograph stations operated in the 0.5–50 Hz range. Likewise, geophones in 3-component clusters used for 4D mapping in ocean bottom surveys, permitting S-wave field recordings as well, record signals primarily in the 10–30 Hz range.

Most signal processing schemes presume that the ambient noise is white and Gaussian. Hence an obvious signal processing advantage is to ensure responses 'producing' white ambient noise which in turn may be achieved by designing the geophone seismometer to record ground accelerations of the incoming signals (Figure 1). This contrasts with the classical short-period seismograph measuring ground velocities which besides being slightly skew in the frequency domain. Above we stated that a seismometer should be rugged implying that it is waterproof, insensitive to temperatures typical of both tropic and arctic regions and finally being handy so easy to install (Figure 2).

From the general CR-II description above, we present the technical details in the chapters below. Also we present a few scientific results stemming from analysis of Cossack Ranger recordings in Norway and Karelia, NW Russia.

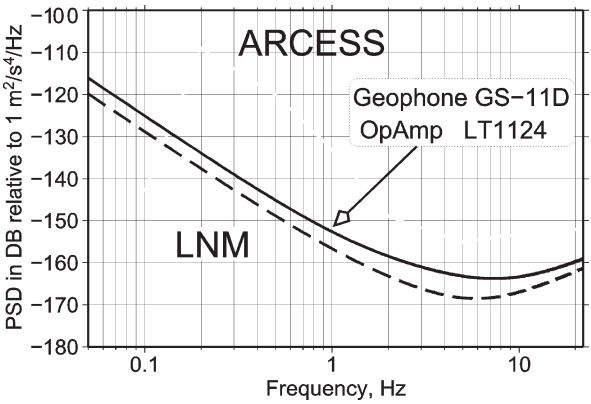

Figure 1 Geophone -based seismic sensor noise versus USGS New Low Noise Model (LNM) and observed ARCESS array (N. Norway) noise and recalculated into acceleration units. Solid curve shows equivalent noise acceleration for geophone based sensor; dashed curve represents dual-geophone sensor (each component uses 2 geophones reducing noise by the factor 1/sqrt2). The sensor noise model includes voltage and current noise sources for both inverting and non-inverting inputs of LT1124 operational amplifier, suspension and thermal (Johnson) noise of geophone and also thermal noise of resistors

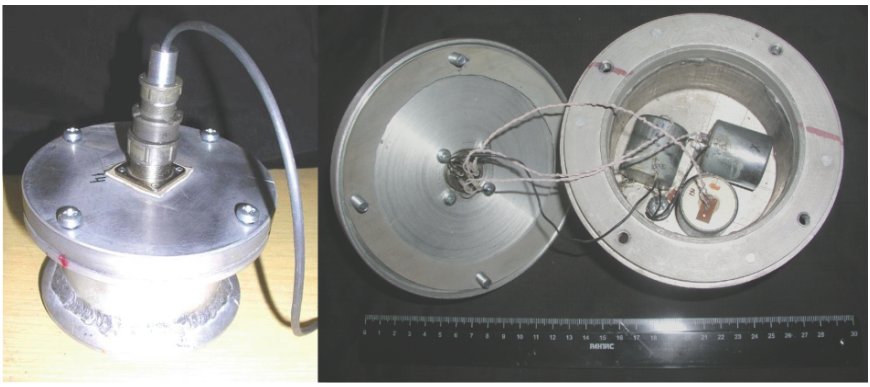

Figure 2 The geophone based shielded sensor and its interior. Sensor cover is made from aluminum alloy and walls are rather thick. The attaching point of cable connector is waterproof so the interior of sensor is absolutely safe. 9-wire cable of connector stands well against splashes. Geophones are glued to the bottom and the grounding point is screwed to the bottom. The cover of the shielding box has a rubber ring for water/moisture protection. Preamplifier can be installed inside of this box (this one is without preamplifier)

3 General Description

The Cossack Ranger II 3-component seismic station is an advanced, inexpensive and low-power 3–12 channel seismograph. It consists of four modules (i) 3-component seismic sensor unit with or without preamplifier, (ii) an A/D-converter unit, (iii) optional GPS clock, and (iv) data logger based on any type of computer (desktop, notebook, Palm Digital Assistant etc.) supporting USB or RS232 port. The schematic structure of the CR-II design and station parts are shown in the Figures 3–5. CR-II can operate as a 3-component station or 9-element mini-array storing data locally or remotely using TCP/IP protocol via Ethernet, GPRS modem, radio transmitter, wireless 802.11b, etc. The CR-II data acquisition software supports continuous, level-triggered and STA/LTA triggered recordings. It can also be easily configured to start and stop data acquisition in given time intervals. While operating in a triggering mode the loads on data links are considerably reduced, and even slow modem connections will be adequate. To synchronize station time to UTC the CR-II timing system uses either the GARMIN GPS 18 clock or Internet Time Protocol service via TCP/IP connection. Recorded data can be stored locally to hard disk or sent to the central Hub in a few minutes after event recording is ‘terminated’. Optionally data may be written to a flash memory card which can be exchanged within a few minutes. Adequate power supply protects battery from over-discharging and easy switching to exchange batteries. A standard housing conforming to the IP68 standard is used to protect equipment from dust and liquids. The main technical units are listed in Table 1.

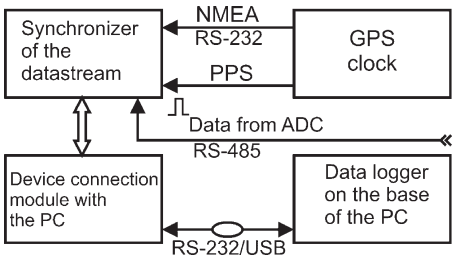

Figure 3 Main modules of the Cossack Ranger II seismic station design: (i) 3-component seismic sensor with or without preamplifier, connected to the; (ii) 22 bits ADC by the wire analog line up to 100 m long; (iii) GPS-clock transmits Pulse Per Second (PPS) and NMEA string, containing date, absolute time and coordinates of the clock and connected to the Time Synchronization device; ADC connected to the Time Synchronization Device by the wire line (up to 100 m) or the radio link (not recommended); Time Synchronization Device connected to the; and (iv) Data Logger, based on any type of PC, and usually operated under Linux

Figure 4 Station parts: Time Synchronization Device (left), GPS-clock and ADC (to the right)

Figure 5 Data logger and the center for the station operation. A laptop is used for the real time data display while the data logger has no graphic interface. Photo taken at the BELME station in Karelia, NW Russia

Table 1 Principal units and operational features of the Cossack Ranger II – 3-component short-period seismograph

1. Sensor type	Geophone GS-11D, Geo Space Inc., LP, Houston, Texas G = 100; R = 4,000; f_0=´4:5´ Hz, f_{max} =´1,000´ Hz
2. Preamplifier	130 dB dynamic range; amplification adjustable by jumper setting in 3 steps by 30 dB each. In order to optimize ADC the preamplifier makes preconditioning of seismic ambient noise to insure that a white noise will be applied to ADC input. Desired response is shaped digitally in datalogger.
3. A/D-converter	Analog Devices AD7716 data acquisition system. Resolution 22 bits, four separate A/D-converter channels. Sigma-delta ADCs include on-chip digital sinc^{3}´ filtering. Data interface to RS232 and RS485 ports is made by PIC18F452 microcontroller.
4. Interface	RS232 and/or RS485 on 115200 baud
5. RS232 Data Word format	3 channels 3-byte each: DB23 … DB2 DB1 DB0 DB21 … DB0 CA0 CA1 Conversion result Channel address
6. Sampling rate	Programmable 20 Hz (23 bits), 50 (22 bits), 100 Hz (22 bits), 200 Hz (21 bits) and 500 Hz (20 bits)

(continued)

Table 1 (continued)

7. Bandwidth	75% of Nyquist frequency for Chebyshev anti-alias filter; 67% for Butterworth filter and 47% for Bessel filter.
8. Antialias filters	Internal AD7716 digital $sinc^3$ with −40 dB/decade external analog RC-filter; Second filter is a causal IIR filter to avoid ripples preceding first arrivals, programmable. It is possible to use Chebyshev (frequency domain optimal), Butterworth (intermediate type) and Bessel (time domain optimal) response types for second filter. Attenuation above Nyquist frequency more than −50 dB.
8. Pre-event record	Programmable 1 … 150 s
9. Post-event record	Programmable 1 … 150 s
9. Data format	Data are stored in GSE2.0 CM6 format in segmented files. This format is commonly used worldwide. Notice that this format is supported in event processing packages such as PITSA.

3.1 Dynamic Range and Data Acquisition System Response

The dynamic range is one of the most important characteristics of a seismic station. It is usually defined as the ratio between the largest and the smallest amplitude which can be handled without distortion by the A/D-converter. We used 4-channel 22-bits AD7716 A/D-converter from Analog Devices Inc. Programmable sampling rates may be chosen in the range from 35 to 1,000 Hz. A common but not strictly correct assumption is that an acquisition system with A/D-converters which have most bits must be most accurate. This is not necessarily the case because dynamic range depends also on signal and ambient noise spectra at the A/D-converter input. The power spectra of internal ADC noise is uniform or, in other words, is white. In order to obtain optimal dynamic range the signal must be preconditioned to make its spectrum as close to white as possible before it will be forwarded to the ADC input. Seismic signals vary widely in spectra contents while the shape of ambient noise spectra vary much less. Hence, we use the design frequency response of DAS's analog part versus the seismic noise spectra which has an approximate roll-off of the 1/f type. In order to achieve better performances we decided on flat acceleration response for our sensor (Fedorenko and Husebye, 1999) while usually seismic measurements are tied to instruments with flat velocity response (Figure 6). The motivation here is twofold; firstly because this is an advantage/requirement for signal conditioning before A/D-conversion and secondly ground acceleration is a common parameter in seismic loading and earthquake hazard studies. Its direct recording makes signal processing in these contexts much easier.

3.2 Signal Amplitude Preconditioning

The Signal-to-Noise Ratio (SNR) obviously can not be improved by amplification. Dynamic range of DAS is defined by the ratio of maximal signal amplitude that the

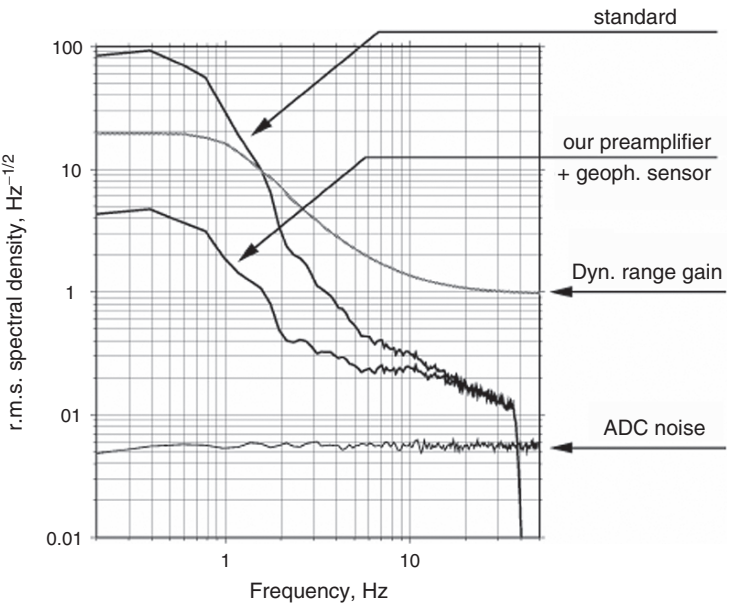

Figure 6 Dynamic range improvement. The 'standard' line indicates typical ambient noise from the ARCESS array recalculated using the 1 Hz sensor response; 'geoph. sensor line' – ambient noise from ARCESS recalculated using our preamplifier and sensor response. 'Dyn. range gain' is the dynamic range gain obtained by replacing the standard flat velocity response by flat acceleration response. The ADC noise at the bottom show the A/D-converter internal electronic noise

ADC can digitize versus the rms of electronic and seismic noise. Both parameters are known while developing the DAS therefore amplification can be calculated as shown by Filatov (2003). Hence, *it is not necessary to introduce any gain and install any extra amplifier besides sensor preamplifier*. In noisy environments where industrial activity is high, it is necessary to keep signal amplitude in the cable connecting sensor and the ADC input as large as possible in order to reduce interference. The latter point demonstrates that the use of amplifiers near the ADC can make SNR worse and also diminish the dynamic range of the DAS. For the Cossack Ranger II seismograph the amplification is pre-calculated using seismic noise level spectra for the area where the station supposed to be installed. Sensor preamplifier has 3 steps of amplification 30 dB each, but there is *no signal conditioning by the ADC*. This simplifies the DAS design and also give better control with proper gain range setting. For example, a local earthquake in W. Norway of moderate ML ~ 3.75 magnitude was properly recorded by a CR-station while a nearby national network seismograph stations 'produced clipped' records. The reason for this was that in the latter case the seismometers were equipped with a 12 dB A/D-converters and gain ranging was set to produce good resolutions for signal frequencies above 5 Hz – for unknown reason.

3.3 Nyquist Theorem and SNR

From the Nyquist theorem it follows that the signal must not contain spectral components above the Nyquist frequency that is half of sampling frequency. If input to the ADC has any such components they will be 'aliased' that is folded back into signals with frequencies below Nyquist. This point is important because violation of this theorem leads to corrupted recordings and reduces the dynamic range. Seismic signals at short distance ranges have broad spectra (up to few hundred Hertz) while sampling rate rarely exceeds 100 Hz hence the risk of aliasing is quite real.

The ΣΔ type ADCs are very popular in seismic instrumentation. Our A/D-converter also uses Analog Devices Inc. AD7716 (Figure 7) which has 4 independent channels of the ΣΔ type. It samples a signal by 1-bit ADC at a very high frequency and reduce digital noise to obtain 22-bits resolution by so-called sinc^3 $(\sin(\pi f)/f)^3$ non-causal digital FIR filter. The first notch frequency of filter is usually equal to the output sampling rate. Because of the high initial sampling rate a simple analog one-pole low-pass *RC* filter is adequate for satisfying the Nyquist Theorem at the initial 1-bit sampling. However the decimation of initial samples is not quite obvious. For example, if the input of the ADC is a signal with flat spectrum in the frequency band 0–100 Hz and output sampling rate F_S is also 100 Hz, the sinc^3 filter together with a simple analog *RC* filter with pole at $f_c = 0.26\ F_S$ yields a dynamic range of only 23–24 dB due to aliasing of frequencies above 50 Hz. This means that the amplitude of

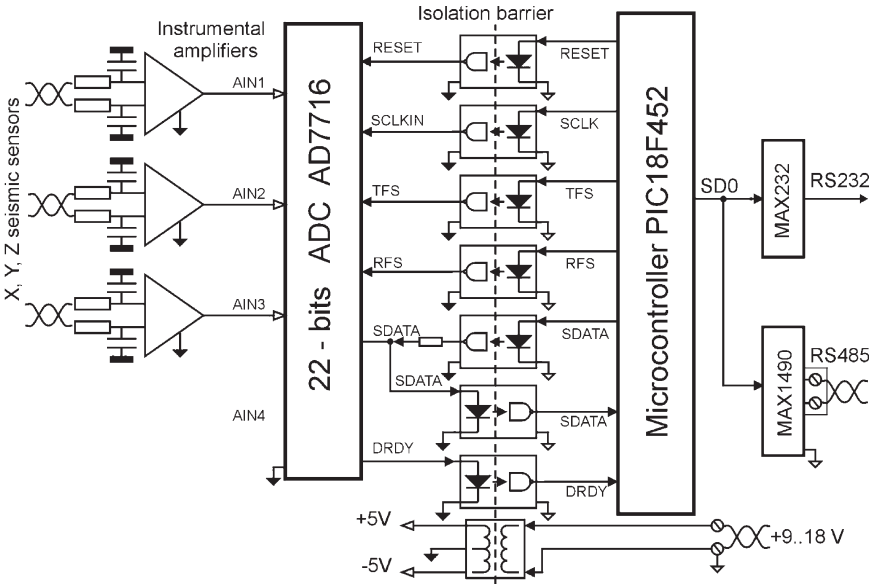

Figure 7 Simplified structure of the A/D-converter

aliased signals is 15 times smaller than amplitude of signals in frequency band of interest and this is unacceptable for the highly detailed signal analysis. With the intention of eliminating aliasing *the CR-II station utilizes oversampling with post-filtering* in its datalogger. The output sampling frequency from ADC is set to 1,000 Hz while the 2-pole passive *RC* filter has a −3 dB attenuation at 75 Hz. Final frequency band is shaped by the digital IIR filter as shown in Table 1. This configuration ensures suppression of the aliased part of the signal spectra with a factor greater than 50 dB.

In many areas, electromagnetic industrial noise may leak into the preamplifier and ruin the CR-II operation. To avoid this, we constructed and used an A/D converter with an isolation barrier (Figures 3 and 7) which guarantee complete separation of the high-sensitive analog part from the noisy digital part and from the site ground. As a result we avoided possible cable grounding loops and suppressed almost all spikes from nearby power lines.

Another feature of the CR-II design is internal biquad equalizer which can convert almost any arbitrary sensor response defined by a pair of complex-conjugated poles into a standard one. Such problem often appears if sensors in seismic networks or profiling surveys are of different types while signal processing schemes require identical responses. The geophone damping by the preamplifier usually is often small to ensure a flat response in the desired frequency range. In these cases the digital IIR equalizer transforms responses in real time gracefully and being invisible to the end user.

3.4 ADC, Event Detection and Time Synchronization

In CR-II we implemented a 2D STA/LTA-detector; 2D in the sense that we utilize both vertical and horizontal components jointly while a conventional 1D STA//LTA (NO2//) detector uses vertical components only. Basic assumption here is that the noise is uncorrelated between components both regarding the original waveforms and also the corresponding envelopes. The STA time serie is a sort of signal envelope. This appears to be the case for all seismic recordings we have analyzed so far. Our 2D detector operates in the three frequency bands 1.5625–3.125 Hz, 3.125–6.25 Hz and 6.25–12.5 Hz. Simple Monte-Carlo statistical simulation yields a false alarm rate about 2 orders lower relative to that of the 1D detector at the same threshold of 2.5. In practice we do not expect the noise components to be entirely uncorrelated, but still we can trade false alarms for a lower threshold value based on operational experience with our 2D detector (Fedorenko et al., 2008, ibid).

Accurate time synchronization is essential in all kinds of seismological observations. All stations of the network should have precise time to provide accurate epicenter location which is derived from the absolute arrivals times of various phases. The CR-II data logger is based on the Unix-like operational systems and may be installed on any cheap PC from Intel 486 DX up to Pentium 4 and compatible processors. It runs under Linux operating system and inherits all advantages

of a Unix-like operational systems. So it can synchronize a data stream with UTC from the Internet time servers using the NTP (Network Time Protocol). The NTP timing accuracy is usually better than ±10 ms depending on quality of the Internet connection at hand. In case the data logger is synchronized from the GPS-clock the accuracy is about ± 0.2 ms.

4 Field installation of the Cossack Ranger II Seismograph

Any seismograph installation requires (i) power acces, (ii) timing device or clock, (iii) remote data transfer, and (iv) proper siting rock. Since the CR initially was designed for school yard installation we would address the above requirements in this context. First, electric power in terms of the 220 V electric network or 9 V batteries. The former is most convenient and our preference is given for the automatic rebooting at power out gauges say due to lightening. Alternatively, rebooting is performed remotely from the Hub or network center. For remote, stand-alone installations batteries provide adequate power supply but are often somewhat inconvenient with frequent replacement unless consumption of ADC and data logger is exceptionally low. The CR-II design is flexible permitting stand alone operations with power supply from batteries.

Accurate, absolute timing is a necessity for comparing and jointly analyze recordings from 2 or more stations. Before the advent of the GPS timing device this was often a severe practical problem. Clocks, even expensive ones, had a timing accuracy seldom better then 0.1 s. For field installations, similar accuracy was attainable, using radio clock signals from Potsdam (Germany) and/or Rugby (UK) for calibrations. When we first deployed our CR-stations in W. Norway high schools in 2000/01 we used the Internet timing system being accurate to ±0.01 s or better. At that time GPSs were relatively expensive and besides a drawback is its required outdoor monitoring with exposures to rainy weather and theft. Present day, the preference is for using highly accurate and inexpensive GPS timing (±0.002 s).

For most monitoring systems today fast data access at the local center or Hub is mandatory. This has been feasible since the 1970s using say leased commercial telephone lines but high costs have prevented wide-spread use of such data transfer solutions until recently. Today the relatively easy access to the Internet at almost no costs make this option for the data transfer universally praised by seismologists. In case of stand alone station operations most of the events recorded and stored on disks in the field while only an affordable fraction of the data stream is transferred within a reasonable time lag to the Hub. In this context is interesting to ‘convert’ mobile phones into a data transfer unit (Katkalov and Husebye, 2008). Note, advanced data logger design permit extractions of critical parameters for an epicenter location like P – arrival times and amplitudes and also signal envelopes (1 s sampling) tied to the Hilbert transform of the original waveforms (100–200 Hz sampling).

Proper seismograph siting is critical for the high quality network operations. Preferably site surveys proceed the actual installation measuring the ambient noise field and avoid locations close to fast running machinery. In particular, avoid any site, 'tied to' parts of the housing structure which easily 'transmit' in-house activities. Switching on- and off- of machinery is occasionally manifested as spikes in the recordings. If the spikes are simple and of a regular form they are easily recurved by a digital filter, the CR-II data logger incooperates such a feature.

4.1 Outreach Efforts: Seischool Norway Seismograph Network & Karelian Seismograph Network

With outreach efforts is meant initiatives in the academics to foster scientific interests among pupils in grade schools and students in high schools. The basic motivation is to encourage students at a later stage to undertake science studies in the universities. The generally worry here is the decreased enrollment in natural science courses which moreover is a global phenomenon. In our case, the prime motivation was to collect our own seismological network data for advanced research undertakings as the recordings from the Norwegian National Seismograph Network were not adequate in this regard. The experience from the design of the Nansen station near Kirovsk indicated that even from our meager research funds we could afford network investment costs (some $5,000) given that operational costs were essentially free of charge. The only solution to the latter requirement was to install the seismograph in school yards and subsequently route the data transfer through the school's Internet connection maintained permanently in 365 days a year. Regarding school teachers; they were quite eager in getting a seismograph installed in their respective school yards but further seismological commitments were modest. Anyway, when the first CR were complete at the Institute in Bergen we went straight for the 'first' school, Aasane Gymnasium, being about 20 km away. We found a hard rock site just 2 meter off the school building wall and the 'instrument foundation' was a tiny $20 \times 20\,\mathrm{cm}^2$ concrete slab. The seismometer was protected by a wooden box, waterproof coverage added and then camouflaged by turf. The cable connecting seismometer and the data logger in the school's data room went through a tiny hole in the wall nearby. With a few trials with record displays on PC screens the Cossack Ranger functioned entirely satisfactorily including data transfer and exchange with the Hub server located in the Institute at the University of Bergen. This first CR school installation gave the SeisSchool project a flying start; just a few days after its installation a local earthquake of ML ~ 3.7 took place nearby and the students analysis of their own seismic records was prominently published in the local newspaper. Our seismological colleagues were less fortunate as their costly national network recordings were severely clipped and hence withstood any serious analysing effort. We were also interested in deploying seismograph stations in N. Norway and also here school teachers were eager to comply to our proposals. A practical problem was remote CR installation as for us travel costs would be formidable. This problem turned out to be

non-existent; instrumentation was shipped to the respective schools including a two-page manual for installation. Some further elaborations were via mails and a few phone calls and within a few hours the new stations were operational. Frequently asked questions from colleagues about our SeisSchool project were about school yard noise levels and the safety of the non-locked seismometer housing. To the first one the reply was that school yards are not particular noisy and for monitoring tasks the closeness to local earthquakes are more critical than 5–10 dB variations in noise levels. In Karelia we undertook a special study of CR siting environments by installing 4 CR stations at very different sites (Figure 8).

The first station was installed in August 2000 in the Geophysical Yard of the Petrozavodsk University (PTRZE in Figure 8) and has provided reliable event

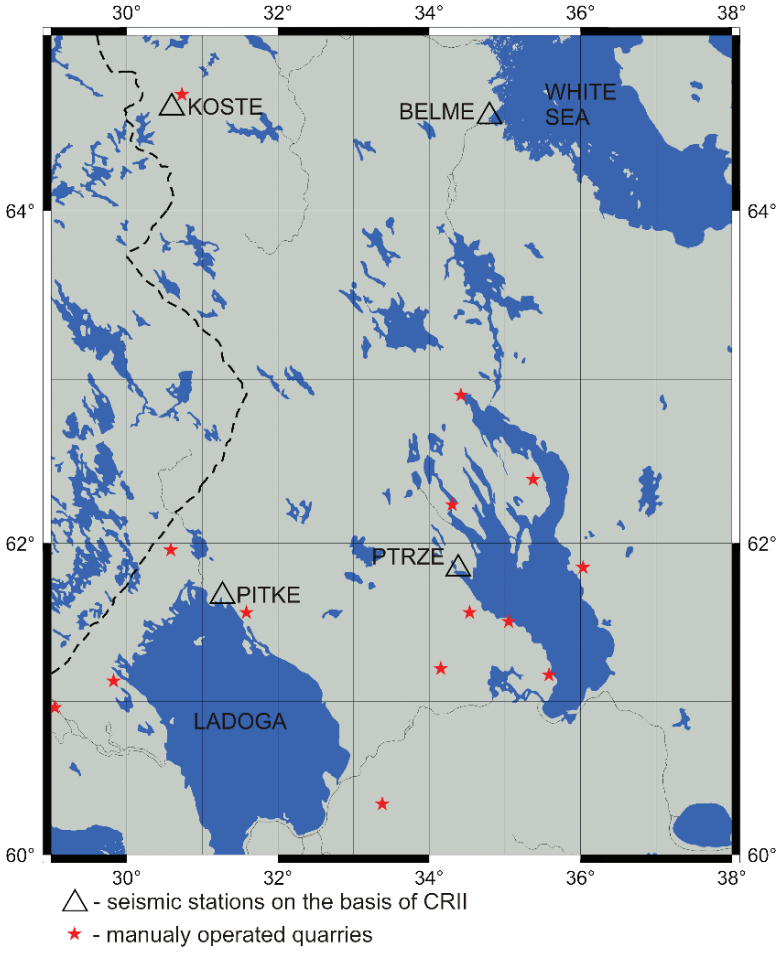

Figure 8 Seismic stations: PTRZE, KOSTE, BELME and PITKE (triangles) with the CR-II instrumentation installed in 2000–2006 in Karelia (NW Russia) and adjacent quarries (red stars)

recordings for more than 6 years. Seismometer was installed in the basement of a wooden, two-story house on solid rock. Data were transmitted via radio link to the Institute server. Then during summer 2006 a station was installed in a school yard (KOSTE in Figure 8). As it was no possibility to dig a hole close to the data logger and due to a lack of safety for an outdoor installation we put sensor on the floor in the school building. As expected, this place was hopeless due to the human activity in the building so only explosions from the nearby mine were recorded during the half year of operation. As we could not find a feasible place for the school yard installation in Karelia we gave attention to a Radio masts where service buildings provided stations with proper housing. Therefore one station (BELME in Figure 8) was installed on the mast in the outskirts of the small town Belomorsk close to the White Sea (Figure 9). The sensor was installed in an abandoned building on exposed rock.
The closeness of the town, railway station and White Sea bay prevented any reliable recording of events occurring on the territory of this region. Only a few teleseismic earthquakes and some explosions were recorded by this station within the 6 months. Another station was installed on the territory of the mast relatively far from any human activity (PITKE, Figure 8), 3 km far from the Ladoga lake. Sensor was installed on the solid rock and a wooden shielding was made. This installation turned out to be successful and events of different kind were recorded. For both of

Figure 9 The Radio mast in the outskirts of the town Belomorsk where one of the CR-II seismic stations was installed. Due to the noise produced by the mast related activity and the proximity of the town infrastructure the operation of this station was a scientific failure

last stations (BELME and PITKE) data transmission and station operation were organized via GPRS modem of mobile phones. An unexpected shortcoming of the GPRS connection was during lunch and dinner time when the cellular network was overloaded causing low speed connection. Contrary to our expectations the electric lines of the radio masts did not produce spikes on the recordings and likewise wind vibrations of the masts had no significant recording influence. Once again, our experience confirmed the obvious thing: it is impossible to install sensors on floors of any building in use.

Regarding safety of installation we have not experienced any problems here like theft which may be more likely in some countries. After the seismometers were covered with turf and similar material it was hardly to find any visible sign of their existence except the small piece of cable on the nearby building wall. Occasionally we had problems in relocating the station even as we knew its position within a few meters (Figure 10).

Some of the stations operated for more was than a year in Norway and Karelia without any problem while in other cases water was leaking into the instrumentation boxes caused disruptions. This problem was eliminated by using more elaborate box design and also to ensure that the sealing putty in fact stopped water sipping inside the box. We have also operated the CR's in most moistly environments like the jungle in Costa Rica, the wet west coast of Norway and cold areas like Karelia, Spitsbergen and in the Kirovsk Mountains and functioning equally well in all these environments. To summarize; the Cossack Ranger design is robust, versatile and inexpensive and thus eminently suited for outreach undertakings for fostering science interest among high school students. From a professional point of view, the CR recordings are well suited for advanced seismological research. These two issues, outreach and research, would be addressed below.

Figure 10 A place of the sensor installation with splendid rock sites. Aluminium shielding with waterproof resistance permits sensor positioning under the soil cover. Obviously it's next to impossible to find the CR-II here unless told how to pinpoint its location

4.2 Outreach Efforts: The Seisschool Project

In general, to ensure successful cooperation between all participants to a 'Project' all of them must gain something being considered beneficial to themselves. In case of our SeisSchool project the advantages to us were proper station sites, installation and operational assistances and permanent free Internet access. Since the CR operation proved to be exceptional stable the school sitting efforts in terms of working hours were moderate. The real problem to us was to find out what the schools that is teachers and students wanted to gain from such cooperation. Geophysics nor seismology do not constitute a major part of the respective school curricula so the challenge was to present 'geophysics' in exciting manners to our school partners. Some of our contributions were a kind of electronic learning in terms of CD-Roms titled the Dynamic Earth and Seismogram Analysis where various aspects of geophysics were presented through snapshots and video clips (Boulaenko and Husebye, 2003). Also, occasionally we were able to form small student teams undertaking small research projects tied to seismicity and local earthquake recordings. The outcome of such efforts in terms of project reports were submitted to the Norwegian Young Scientists competition and got top ranking including visits to Oslo for presentations at their annual meetings. The school interest in geophysics and seismology is on top during earthquake disasters or when earthquakes are widely felt locally while otherwise is on a non-commitment level. This is understandable as stronger, active engagements are equivalent to extra work efforts on subjects peripheral to the daily educational tasks. To us most important was that schools ensured proper station operations and that occasionally a few students with genuine science interest would undertake small geo-investigations. Our school cooperations functioned very well on an informal basis; no contracts or annual reports were desired by the respective schools or by us. On the other hand, the new Head of Institute wanted to formalize cooperation with written contracts, pedagogic formulations, annual reports and so forth but the suggested set-up was uniformly rejected by participating schools. To summarize, we find it stimulating to work and interact with schools and also realized that the science interest in schools are clearly time dependent and foremost that the school working environment is very different from the academics having focus on few subjects at any time (Husebye et al., 2003).

4.3 Cossack Ranger Recordings in Research

The first Cossack Ranger seismographs were to some extent home made in the sense that besides the individual sensor at a cost of $60 each, partly home made ADC and an old PC as data logger had a price tag less than $1,000. Some colleagues asked whether such a dirt cheap seismograph was useful for advanced research purposed. This was considered a challenge so the first step in testing recording quality was to site the CR adjacent to a Kinemetrix Ranger seismograph – the ASK station close to the Institute and Bergen city itself. Test was only partly successful

as the Kinemetrix recordings obviously were clipped for a local ML ~ 3.5 events. Further tests were a polarization study of Karelian events demonstrating that observed and calculate wavefield polarization properties were similar (Fedorenko et al., 2008b). This would not have been feasible with anomalous phase shift among the sensor components. In another study, we used deformable templates technique for linearly projecting the Lg-wave train from one CR station into another one – the original waveforms replaced by their respective Hilbert transforms. In other context, we subjected the Pg/Pn-coda to an automatic phase picking scheme and then using Bayesian statistics for validating the pickings toward updated focal parameter estimates including depth. The CR is also efficient in monitoring local seismicity since its 2D signal detector is superior to the conventional 1D detector commonly used. Recent research activities using Cossack Ranger II recordings are listed in Matveeva et al., 2008 (ibid).

References

Bulaenko, M.E., Husebye, E.S., 2003. Electronic learning modules for high school students in seismology. *Seismological Research Letters*, 74, 570–577.

Chernouss, P., Zuzin, Yu., Mokrov, E., Fedorenko, Yu. V., Kalabin, G., Husebye, E. S., 1999. Avalanche Hazards in Khibiny Massif, KOLA, and the new Nansen Seismograph Station. *IRIS Newsletter*, 1, 12–13.

Fedorenko, Yu. V., Husebye, E. S., 1999. First breaks – automatic phase picking of P- and S-onsets in seismic records. *Geophys. Res. Lett*., 26, 3249–3253.

Fedorenko, Yu. V., Husebye, E. S., Bulaenko, E., 2000. School Yard Seismology. *Orfeus Newsletter*, 2, 3, 22.

Fedorenko, Y.V., Husebye, E.S., Matveeva, T., 2008a. A 2-D Seismic Signal Detector for Stand Alone 3-Component Stations. In E. S. Husebye (ed). In E. S. Husebye (ed.) Earthquake Monitoring and Seismic Hazard in Balkan Countries. Springer Publishing, Berlin, 189–196.

Fedorenko, Y.V., Matveeva, T, Beketova, E.B., Husebye, E.S., 2008b. Secondary phase validation – phase classification by polarization. M/s submitted Physics Earth Planetary Interiors.

Filatov, P. V., Fedorenko, Yu. V., Husebye, E. S., 2003. Seis/School/Norway Project: Equipment, Network Operation, Data Acquisition and Processing System. *Seismol. Res. Lett*., 74, 5, 564–569.

Husebye, E.S., Beketova, E.B., Fedorenko, Y.V., 2003. School yard Seismology. *J. Geoscience Education*, 51, 329–355.

Katkalov, Yu., Husebye, E. S., 2008. Cossack Ranger field operation – efficient data transfer via mobile phones. Manuscript in preparation.

Matveeva, T., Fedorenko, Yu. V., Husebye, E.S., 2008. The Karelian Regional Seismic Network in NW Russia. In E. S. Husebye (ed.). Earthquake Monitoring and Seismic Hazard in Balkan Countries. Springer Publishing, Berlin, 163–168.

A 2-D Seismic Signal Detector for Stand Alone 3-Component Stations

Yu. V. Fedorenko[1], Eystein S. Husebye[*2], and Tatiana Matveeva[3]

Abstract An integral part of modern earthquake monitoring is that of real time signal detection. When digital seismometry was introduced in the early 1970-ties with the deployment and subsequent operations of the LASA and NORSAR large aperture arrays automatic and optimal seismic signal detection become a research issue. Much ingenuity was invested in the signal detector design and some of these efforts were indeed elaborated. However, hardly any of them outperformed the simple 1D STA/LTA-detector – the ratio between Short Term and Long Term Averages of signal RMS-power on exclusively vertical sensors. When digital stand-alone 3-component stations become operational in the 1980-ties the array signal detector was adapted to these stations as well and hence excluding signal presence on the horizontal components. In this article we present a novel 2D signal detector incorporating all seismometer components and also demonstrate that the 2D detector not unexpected outperforms the 1-D detector at local and regional distance ranges.

Keywords 1D STA/LTA detector, 2D signal detector, false alarms, Gaussian noise, signal rectilinarity

1 Introduction

Signal detection research become popular among scientists with the introduction of digital recording in seismology around 1970 not at least because this could relieve the analyst of tedious work tasks. An early design here was the so-called STA/LTA-detector where STA and LTA are short and long term noise and signal power averages. We term it a 1-D detector since only Z-components recordings are used. Despite much ingenuous research, still the STA/LTA-detector is widely popular

[1]Polar Geophysical Institute, KSC RAS, Apatity, Russia

[2]Bergen Center for Computational Science, UNIFOB/UoBergen, Bergen, Norway

[3]Institute of Geology, KarSC RAS, Petrozavodsk, Russia

*To whom correspondence should be addressed. e-mail: esh@bccs.uib.no

E.S. Husebye (ed.), *Earthquake Monitoring and Seismic Hazard Mitigation in Balkan Countries.*

since a simple and robust alternative has not been found so far (e.g., see Goforth and Herrin, 1981; Lee and Stewart, 1981; Harjes and Joswig, 1985). The reason for this may be twofold: (i) noise is not Gaussian so an optimum signal detector in a statistical sense will be hard to find, and (ii) close to the signal acceptance threshold the false alarm rate increases nearly exponentially. In other words, for say 100 detections we have to reject 99 as signal look-alike noise wavelets – a truly hopeless task. Our alternative is to introduce a 2-D STA/LTA-detector; 2-D in the sense that we utilize both vertical and horizontal record components jointly as expressed in the equations below. In many signal detector studies much attention is often given to filter settings for ambient noise suppressions and STA-length in time or samples. The efficient LTA-length often exceeds 1 min in its recursive definition. It should be noted that signal detection often constitutes an integral part of automatic network operation and in this context the problem is to extract seismicity parameters like event magnitude and epicenter location (Mendi and Husebye, 1994; Kværna and Ringdal, 1996). However in this article we first the give principal detector design criteria before presenting our novel 2-D detector extensively tested on the Cossack Ranger stations deployed in several countries (e.g., see Matveeva et al., 2008, ibid; Fedorenko et al., 2008a, ibid).

2 Background

In previous works (e.g. see Fedorenko et al., 1998, 1999) we demonstrated that the wavelet transform may be a more suitable tool than the FFT for signal detection, phase pickings, and signal source recognition. This in turn requires that the ambient noise is white which is equivalent to an approximate flat seismometer acceleration response curve. Since most instruments in use measures ground velocities the noise spectra are in general non-flat as shown in Figure 1 for the ARCESS array (N. Norway) center seismometer. To overcome this drawback in the context of signal detection the preamplifier of the Cossack Ranger seismograph is designed in such a manner as to modify our ground velocity measuring geophones to produce seismometer ground acceleration motions which in case of noise give approximately white spectra in the frequency range 1.5–20 Hz. The spectral hump at lower frequencies in Figure 1, due to relatively strong microseisms, are in practice is of no consequences as this signal part is removed by bandpass filtering in the detector processor prior to forming the STA and LTA estimates.

In our more theoretical detector studies (Fedorenko and Husebye, 1999) we found that the popular STA / LTA detector has an excellent performance in comparison to many other detectors including the non-parametric Kolmogorov-Smirnov (KS) one. It was one exception here namely in case of spiky records often caused by the electric outgauges in buildings where a station may be housed. In such cases the STA/LTA detector become literally blinded while the KS-detector was little affected. Instead safeguarding here in terms of 2 different detector systems we build-in a spike ‘killer’ in the A/D-converter ensuring spike-free records prior to signal detection per se.

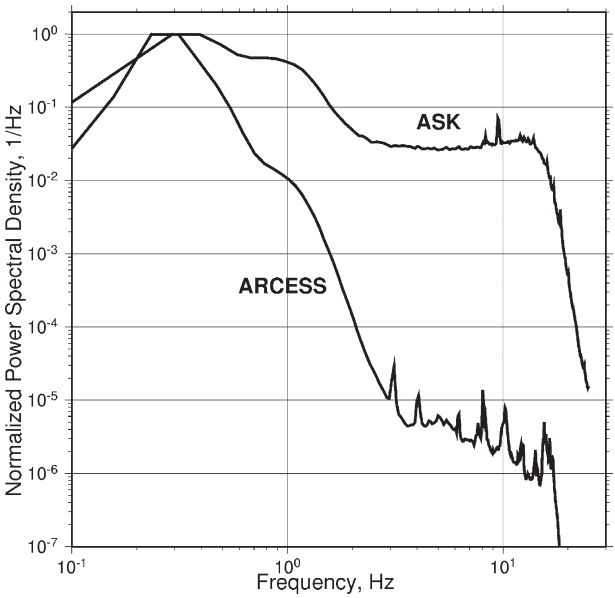

Figure 1 Normalized power spectral density for ARCESS 3C center station (winter time) and our novel station at ASK (summer time) – in both cases Z-components. Since the noise level in winter is high the normalization gives low level of the high frequency noise at ARCESS. Note that above 2 Hz the ARCESS spectra follows approximately the 1/f decay while ASK spectrum is almost flat in this frequency range

Another basic requirement in our 2-D detector design is noise independency between components and the validity of this assumption is demonstrated in Figure 2. As can be seen, there is no significant noise coherency even at low microseism frequencies (f < 0.5 Hz). In a typical signal detector passbands within 2–15 Hz the noise coherency is truly small being less than 0.02 units. Besides component independency also valid for components envelopes the noise appears to be Gaussian as presumed in our theoretical detector study. The above results imply that a 2-D detector will outperform the conventional 1-D STA/LTA detector foremost because more signal information is incorporated in the test statistics.

3 The 2-D signal detector

Our 2-D signal detector operates in the three frequency bands which coincide with the corresponding frequency bands in wavelet transforms, namely 1.5625–3.125 Hz, 3.125–6.25 Hz and 6.25–12.5 Hz. The first step is data preparation prior to the detection process itself using IIR (Infinite Impulse Response) Butterworth filters of order 6 to obtain filtered time histories for the $x_k(t)$(N), $y_k(t)$(E),$z_k(t)$(Z) for our 3 frequency bands k = 1,2,3. The 2-D detector is modeled after the 1-D STA/LTA detector which in the former case is defined as:

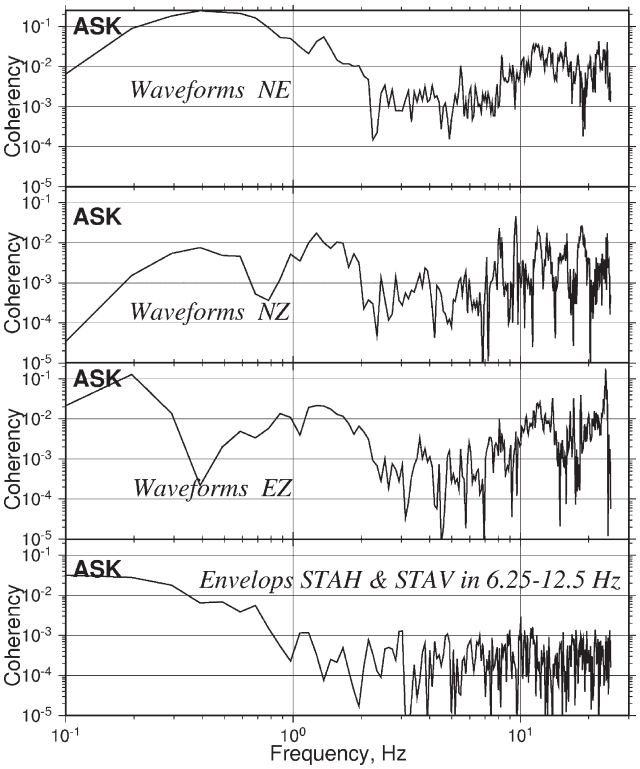

Figure 2 Observed noise coherency between 3-component waveforms and STAH and STAV envelops. This is original noise waveforms recorded by our novel ASK station of length 60 min presumably free of signals. Coherency at levels of 0.01 or less give component independency for the ambient noise field. Also note that similar results were obtained when noise waveforms were replaced by the corresponding envelopes, in this case the coherency is less than 0.001. In tha STA/LTA 2-D detector the test statistics are the noise and signal envelopes

$$STAH_k(t) = IIRF_{STA}(x_k(t)^2 + y_k(t)^2)^{1/2}$$
$$\mathrm{STAV}_k(t) = \mathrm{IIRF}_{STA}(|z_k(t)|) \tag{1}$$

where H = horizontal and V = vertical, $\mathrm{IIRF}_{\mathrm{STA}}$ defines Bessel low pass IIR filter of order 3 with cut-off at 0.5 Hz. The LTAH and LTAV are defined in a similar manner but with a frequency cut-off at 1/300 s. The combination of Butterworth prefiltering and Bessel type of filters for forming the STA and LTA test statistics are motivated by the need of suppressing side-lobe detections that is false alarms caused by noise triggering (Steinert et al., 1975).

Anyway, we may consider $\mathrm{STAH}_k(t)$ and $\mathrm{STAV}_k(t)$ as approximate envelopes of horizontal $a_h(t)$ and vertical acceleration components in the given frequency bands while $\mathrm{LTAH}_k(t)$ and $\mathrm{LTAV}_k(t)$ are estimates of RMS of the ambient noise. Also, this

LTA definition is coincident with the parameter used for record 'denoising' in our wavelet processing scheme for picking automatically P- and S-phase onsets. In order to to keep them from being affected by the seismic signal we freeze these values while the detector is in the detection state. The 2-D detector is taken to be ratio $R_k(t)$ between the STA and LTA that is:

$$R_k(t) = \frac{\left[\mathrm{STAH}_k^2(t) + \mathrm{STAV}_k^2(t)\right]^{1/2}}{\left[\mathrm{LTAH}_k^2(t) + \mathrm{LTAV}_k^2(t)\right]^{1/2}} \tag{2}$$

A signal detection is declared whenever any $R_k(t)$ exceeds a preset threshold currently set at 4.0 for all three bands. This setting is rather conservative since we so far have not observed any clear false alarms. Depending on signal shape and duration the detector may be triggered several times during signal 'passage'. An independent trig requires a time lag of minimum 2 s while detection state is defined as at least 60 sec between the first and last trigger events. We naturally count no of triggs during detection state as this parameter is useful for differentiating between earthquakes and explosions (most 8 triggs) while man made signals like marine air gun activities, human walking near the site etc. often produce more than 20 triggs. The 2-D detector parameterization may be tailor-made for each individual site reflecting local knowledge on ambient noise and signals triggered by human activities.

The horizontal and vertical acceleration envelopes are used to obtain the estimate of the acceleration envelope $a_k^{env}(t)$ and of the apparent incidence angle θ_k

$$\begin{aligned} a_k^{env}(t) &= \left[\mathrm{STAH}_k^2(t) + \mathrm{STAV}_k^2(t)\right]^{1/2} \\ \underline{\theta}_k(t) &= \arcsin\left[\mathrm{STAH}_k(t) / a_k^{env}(t)\right] \end{aligned} \tag{3}$$

Seismic events have $10 < \theta_k(t) < 60$ while spikes and non-seismic events often fall outside this angular interval in degrees.

4 Results – 2-D Detector Performances

Detector performances are not easy to quantify since close to the threshold value it is difficult to validate the event origin – earthquake or false alarms. The problem is severe as circa 40–50% of reported event detections for an array or a station remain unassociated meaning that the potential event has no counterpart in station logs elsewhere. In Figure 3 we have simulated the 2-D signal performances for uncorrelated 3-component Gaussian noise field. Clearly, we expect the 2-D signal detector to be superior to its 1-D counterpart by a factor of $\sqrt{3}$ approximately. In another experiment a CR-II station and a Kinemetrix Ranger station shared the

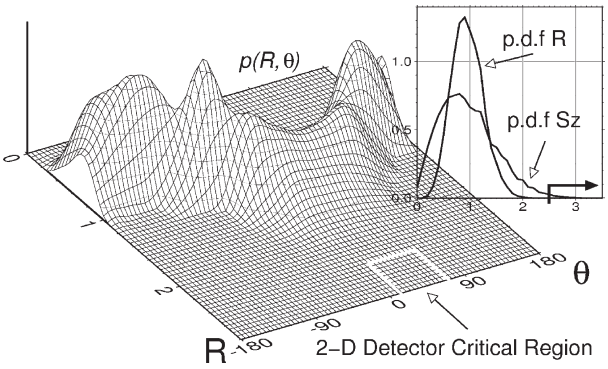

Figure 3 Illustration of 2-D detector performance. Probability density function $p(R, \theta)$ modeled for uncorrelated 3-component Gaussian noise with zero mean and same variance in each component. Critical region for the 2-D detector appear far from 'p.d.f. main body' assuring small false alarm rate. Insert shows one-dimensional p.d.f of R and of conventional STA/LTA ratio Sz = STAZ/LTAZ. It is clear that the R statistics produce less false alarms for uncorrelated noise because its variance is less than variance of the z statistics by a factor of $\sqrt{3}$ approximately

siting at Ask west of Bergen (Norway). The 2-D detector of the CR-II station proved superior to that of the adjacent 1-D detector station.

Signal detector parameters may be utilized for more that just detecting probable seismic event recordings. For example, Mendi and Husebye (1994) demonstrated that the STA parameter would provide a magnitude estimate as well given an assumption about likely epicenter distance. In case of STA measures reflecting pure noise estimates the corresponding magnitude estimates give a lower limit of the stations event detectability.

The detection parameter 'apparent angle of incidence' is observationally limited to the observation interval 10° – 60° for earthquakes and chemical explosions (Figure 3). This implies that horizontal components record parts of the P-wave field even for teleseismic events making 2-D detectors superior to those based on vertical components only. For arrays where vertical sensors are dominant (only four 3-comp. stations in ARCESS) 2-D detectors are of less interest unless the latter ones are used for detecting Lg and Rg-waves. The conservative threshold setting of 4.0 ensure no false alarms due to noise triggering. To lower threshold value, for Gaussian noise a threshold of 2.4 would be acceptable, we would produce many more detections of air gun signals and nearby human activity signals. Such events are of no scientific interest so better removed in this manner than by a less conservative threshold setting.

The novel 2-D signal detector has proved superior to the conventional 1-D STA/LTA for stand-alone 3-component stations. In a monitoring context, we want to extract more information on detected signals per se and this would be feasible using continuous sampled STA parameter for representing the original waveforms. The

STA sampling rate is often 1 Hz while the original waveform may be 50 or 100 Hz so even in under adverse field conditions waveform transfer to the HUB would be affordable say using mobile phones (Katkalov and Husebye, 2008). Two of us, Fedorenko and Husebye, have previously demonstrated that envelope waveforms can be used for highly accurate epicenter locations and source type identification (Husebye et al., 2002; Fedorenko et al., 2008b).

5 Summary Remarks

For efficient monitoring of local earthquake activity a network of stand-alone 3-component stations would be most efficient in comparison to a few small arrays and much more cost efficient. A smart signal detector is an essential element in such an undertaking and the novel 2-D detector presented here is well suited for such tasks. Its performances are better than similar 1-D detectors both in terms of lower signal detection threshold and false alarms rates. In addition, detector outputs in form of envelope traces can be used for desired monitoring results in terms of epicenter locations and source identification.

References

Fedorenko, Yu. V., E. S. Husebye, B. Heincke, B. O. Ruud, 1998. Recognizing Explosion Sites without Seismogram Readings: Neural Network Analysis of Envelope-Transformed Multistation SP Recordings 3–6 Hz. *Geophys. J. Int*., 133, F1–F6.

Fedorenko, Yu. V., E. S. Husebye, B. O. Ruud, 1999. Explosion Site Recognition: Neural Net Discriminator Using Three-Component Stations. *Phys. Earth Planet. Int*., 113, 131–142.

Fedorenko, Yu. V., E. S. Husebye, 1999. First Breaks – Automatic Phase Picking of P- and S onsets in Seismic Records. *Geophys. Res. Lett*., 26, 3249–3253.

Fedorenko, Yu. V., Husebye, E. S., Matveeva, T., 2008a. Cossack ranger II – A High Quality, Versatile and Affordable 3-Component Short-Period Seismograph. In E. S. Husebye (ed.) Earthquake Monitoring and Seismic Hazard in Balkan Countries. Springer Publishing, Berlin, 171–187.

Fedorenko, Y.V., Matveeva, T, Beketova, E.B., Husebye, E.S., 2008b. Secondary phase validation - phase classification by polarization. M/s submitted Physics Earth Planetary Interiors.

Goforth, T., Herrin, E., 1981. An automatic seismic signal detection algoritm based on the Welsh Transformer. Bull. *Seismological Society America*, 71, 1351–1360.

Harjes, H.P., Joswig, M., 1985. Signal detection by pattern recognition. In A.U. Kerr (ed.). The VELA Program; A Twenty-Five Year Review of Basic Researc. DARPA, US Government, Washington D.C., USA, 579–584.

Husebye, E. S., Fedorenko, Yu. V., Beketova, E. B., 2002. Enhanced CTBT Monitoring through Modeling, Processing and Extraction of Secondary Phase Information at High Signal Frequencies. 24th Seismic Research Review – Nuclear Explosion Monitoring: Innovation and Integration, September 17–19, Ponte Vedra Beach, FL., 292–301.

Katkalov, Yu., Husebye, E. S., 2008. Cosack Rager field operation – efficient data transfer via mobile phones. Manuscript in preparation.

Kværna, T, Ringdal, F., 1996. Generalized beamforming, phase association and threshold monitoring using a global seismic network. In E.S. Husebye, Dainty, A.M. (eds.), 1996. Monitoring a Comprehensive Test Ban Treaty. Kluwer Academic Publishers, Noordrecht, The Netherlands, 447–446.

Lee, W.H.K., Stewart, S.W., 1981. Principles and Applications of Microearthquakes Networks, Academic Press, Los Angles, CA., 50–60.

Matveeva, T., Fedorenko, Yu. V., Husebye, E. S., 2008. The Karelian Regional Seismic Network in NW Russia. In E. S. Husebye (ed.). Earthquake Monitoring and Seismic Hazard in Balkan Countries. Springer Publishing, Berlin, 163–168.

Mendi, C. D., Husebye, E. S., 1994. Near real time estimation of magnitudes and moments for local seismic events. *Ann. di Geofisica*, 37, 365–382.

Steinert, O., E. S. Husebye, H. Gjoystdal, 1975. Noise Variance Fluctuations and Earthquake Detectability. *J. Geophys*., 41, 289–302.

Accurate Location of Seismic Sources With and Without Travel Time Model

V. Pinsky*

Abstract The problem of accurate seismic event location is a major issue in seismic monitoring. To improve locations much effort has been invested in mapping the 3D seismic velocity structure of the Earth. Likewise, to collect associated ground truth (GT) event information that is event with focal parameter estimates within 1, 5 or 10 km for model validation tests. The accuracy of velocity models currently available are verified for limited areas only, as GT events are too sparse and rare. Obviously, applying an erroneous velocity model would result in a biased event location. However, such errors can be reduced significantly by introducing flexible models containing uncertainty probabilities and this is the problem addressed in this article.

We approach the problem using several methods based on general inverse concepts and robust statistics. Basic observations are relative travel times (RTT), which are tied to bulletin phase pickings at different stations for a given event. The final location solution is the maximum of the location probability density function (PDF) and 90% confidence volume, determined by the grid-based PDF distribution. The PDF location is shown to be a convolution between the a priori PDF of the RTT, and a theoretical PDF, measuring correlation between the model and the observations. The theoretical PDF in turn is represented by M-estimates, providing stability and accuracy of the whole procedure against possible outliers. The approach is illustrated by a pilot study testing a simplified variant of the procedure on a number of GT events contained in the ISC bulletins and compared to the conventional location solutions.

Keywords Epicenter, Ground Truth, relative travel time, outliers, PDF location, M-estimates, robust location, grid-search location

Geophysical Institute of Israel, POB 182, Lod 7100 Israel

* To whom correspondence should be addressed. POB 182, Lod 71100 Israel, vlad@seis.mni.co.il

E.S. Husebye (ed.), *Earthquake Monitoring and Seismic Hazard Mitigation in Balkan Countries.*

1 Introduction

A long standing problem in computational seismology is that of accurately estimating the earthquake or explosion source location in terms of the 4D parameter vector X : latitude, longitude, depth and origin time T_o. A solution to this problem was the least squares approach of Geiger published in 1910. The method is still widely used, although errors of 10–25 km in geographical position are not uncommon and depth estimates are seldom better than 10 km. This is somewhat surprising despite the increased deployment of high quality seismograph stations in recent years. Main factors influencing location accuracies are: (i) network configuration, (ii) Earth heterogeneities, and (iii) phase picking and its proper identification. Note, recently seismologists have taken advantages of new technological developments so local, regional and global data centers collect seismic waveform data in near real time from various kinds of station networks. However, these waveform data are routinely not directly used for event location purposes – but in terms of traditional P – arrival time phase pickings. As mentioned, the data used in this study are extracted from the ISC – bulletins and the reporting stations have an uneven global distribution as shown in Figure 1. Some regions have rather poor station coverage like oceanic ones which may affect epicenter location.

Anyway, with a fixed network configuration there are two alternatives to reduce interference of large scale heterogeneities: (a) construction of explicit 3D Earth velocity models, and (b) building "model independent" location schemes. More recently, new 3D Earth velocity models were constructed based on surface and body waves tomography (Boschi and Dziewonski, 1999; Antolik et al., 2001; Ritzwoller et al., 2003). Together with the Crust Global models (Laske et al., 2002) and databases of collected ground truth events, this has facilitated computation of theoretical and empirical Site-Specific Travel Time Corrections (Firbas, 2000). However, in spite of great efforts invested in introducing 3D travel time tables (Ringdal and Kennett, 2001) large uncertainty still remains for many regions due to uneven sampling, sparse distribution of the GT events as well as uncertainties in a range of acceptable models.

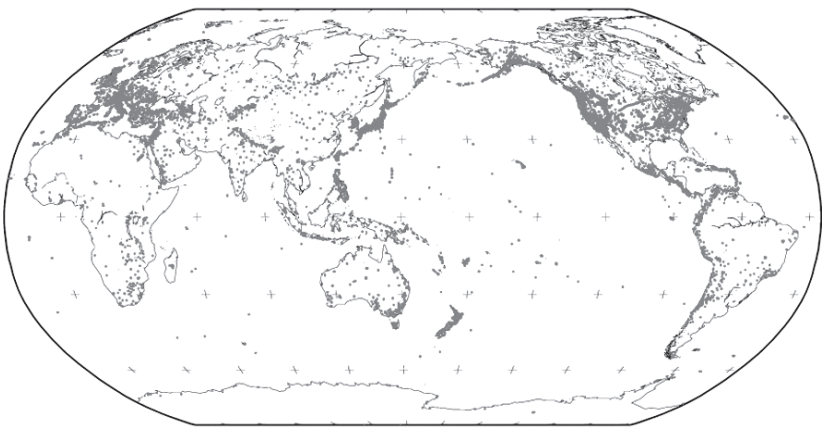

Figure 1 Stations reporting to the ISC

An alternative is "model independent" location schemes usually using a model of relative travel times and assuming homogeneous or simple 1D "velocity" environment for source clusters, as in the double–difference approach of Waldhauser and Ellsworth (2000). A similar "generalized beamforming" approach for automatic event location using a cluster of small arrays have been introduced by Kvaerna and Ringdal (1996). More examples of this and similar approaches tied to using relative arrival times, slowness vector estimates, on P – S derived distance estimate are works of Jih (1999), Pinsky et al. (2006) and Pinsky (2005).

These methods are very attractive because they seemingly minimize velocity uncertainties in the Earth interior. However, such uncertainties will penetrate into velocity models when we increase the size of the array or network apertures needed to provide reliable event location constrains or enlarge event clusters to include, for example, GT events.

A general approach for dealing with different sort of uncertainty using probabilistic formulation of inverse problems is given by Tarantola and Valette (1982) (and upgraded in Tarantola (2005)) which recently has been applied in location procedures by Lomax et al. (2000). The scheme in question allows arbitrary probability distributions for data and parameters, does not require any linear approximation for computation of the target function nor estimation of the confidence area. The latter is straight forward from the posterior PDF grid-based calculation or Monte-Carlo sampling. In turn, a variant of the Non-Gaussian PDF approach of Buland (1986) used for construction of a Least-Squares scheme with variable weights and adjusted through an iterative optimization location routine. This robust algorithm has proved to be more reliable than the standard least squares of Geiger (1910). It serves as a routine location tool for the NEIC (USA) and the ISC (UK) up to now, though the main procedural shortcoming– relatively high probability of convergence to a local minimum – remains.

One of the first probabilistic non-Gaussian non-linear direct grid-search location algorithms was suggested by Sambridge and Kennett (1986). Further development of the probabilistic method is presented in this paper and it is based on the recently developed non-linear grid-search absolute location methods by Pinsky (2000, 2006).

2 Methods for Enhanced Event Location Accuracy

2.1 Deterministic Earth Model and Random Observations

Below we give details on various approaches for enhanced event location performances and also confidence area evaluations. In the next chapter a pilot study applications of these schemes are presented. The unknown 3D parameter vector $\boldsymbol{X}$ of source coordinates Lat, Long, H and origin time T_0 of earthquakes or explosions are given by Least Squares formulation (Geiger, 1910):

$$\{\hat{X},\hat{T}_0\} = \text{argmin}\sum_k \varepsilon_k(X,T_0)^2 \tag{1}$$

where ε_k is the residual term in the k-th travel time equation

$$t_k - \tau(X,Y_k) - T_0 = \varepsilon_k(X,T_0) \tag{2}$$

Equation (2) ties arrival time t_k say of a P-wave to the k-th station with position location vector $\boldsymbol{Y}_k$ with a model travel time function $\tau(\boldsymbol{X},\boldsymbol{Y}_k)$. Normally the travel time is given by a radially symmetric Earth model (time or velocity). These global models are seldom accurate at local and regional distance ranges and this often results in gross hypocenter errors. For achieving better accuracy complicated 3D Earth velocity models are introduced and subsequently validated using relevant GT-event information (Ritzwoller et al., 2003). Occasionally outliers are due to wrong phase pickings and many cause large arrival time errors at local and regional distances.

We shall address this problem by implementing a "robust estimates of location" technique (Andrews et al., 1972; Jeffreys, 1962; Anderson, 1982), the so-called "M-estimates" and the inverse problem theory (Huber, 1981; Tarantola, 2005). The M-estimates techniques allow automatically to delete random outliers and highlight consolidated correct observations by summation of appropriate positive symmetric "bell-shape" functions of residuals Ω:$\{\Omega(x) = \Omega(-x), \text{argmax}(\Omega(x)) = 0\}$, that is:

$$F(X,T_0) = \sum_{\kappa} w_k \Omega(\varepsilon_k(X,T_0)/\sigma_k) \tag{3}$$

where σ_k is a scaling coefficient, w_k is a weighting factor, and solving non-linear equations:

$$\left\{\hat{X},\hat{T}_0\right\} = \underbrace{\arg\max}_{X,T_0} F(X,T_0) \tag{4}$$

Functions

$$\Omega(x) = \exp(-x^2/2) \tag{5}$$

and

$$\Omega(x) = \begin{cases} 1+\cos(x), x\in(-\pi,\pi] \\ 0, x\notin(-\pi,\pi] \end{cases} \tag{6}$$

represent possible sharp-top and obtuse-top patterns of the "bell-shape" function respectively. A location algorithm of the (3), (4) type, described by Anderson (1982) was adapted for an automatic picking-location procedure (Pinsky, 2000) because it effectively suppresses outlier observations which often happen often in case of non-analyst seismogram readings. The form (5) of the M-estimates was used in the EDT version of the robust NonLinLoc location algorithm of Lomax (2005), the form (6) which was qualified by Andrews et al. (1972) and Andrews (1974) as one of the best M-estimates, participate in the Anderson (1982) comparative location study and a "network beamforming" location algorithm of Pinsky (2006).

The sum of the bell-shaped functions being a real positive locally Lebesgue integrable function, can be considered a probability density function (PDF) of the unknown parameters (X, T_0) in terms of Tarantola and Valette (1982). The function $\Omega(x)$ measuring correlation between parameters and the data according to equation (2) is defined as the "theoretical" PDF. To be a real PDF these functions should be

normalised so as to have a unit Lebesgue integral, but on the other hand this is not needed for our purpose.

Let us define the relative travel time (RTT) as $T_{kj} = \tau(X, Y_j) - \tau(X, Y_k)$ - $\tau(\boldsymbol{X},\boldsymbol{Y}_k)$ and a "pseudo-slowness" function β:

$$T_{kj} = T_{kj}\beta\,(X, Y_k, Y_j),\ R_{kj} = R_j - R_k \neq 0 \tag{7}$$

where $R_k = R(X, Y_k)$ is distance along the Earth's great circle (geodetic line) from epicenter $\boldsymbol{X}$ to the station $\boldsymbol{Y}_k$. The "pseudo-slowness" generally depends on the source-station coordinates in the 3D Earth and, for example may be negative, when $R_{k,j}$ is positive and vice versa.

Hence, the equation between observed arrival times t_k and t_j and source coordinates can be written as:

$$t_j - t_k - T_{kj} = t_j - t_k - R_{kj}\beta_{kj} = \varepsilon_{kj} \tag{8}$$

Equation (8) constitutes a "theoretical" stage of knowledge about RTT in terms of Tarantola (2005). Substituting residual ε_{kj} instead of ε_k in (3) we get the PDF of $\boldsymbol{X}$

$$F(X,B) = \sum_{k,j} w_{kj}\Omega[(t_j - t_k - \beta_{kj}R_{kj})/\sigma] \tag{9}$$

which solves the probabilistic inverse problem in a form depending on the vector $\boldsymbol{B}$ of the pseudo-slowness functions $\beta_{kj} = \beta(\boldsymbol{X},\boldsymbol{Y}_k,\boldsymbol{Y}_j)$ and does not depend on origin time T_0.

For the 1D spherical Earth function $\beta_{kj} = \beta(\boldsymbol{X},\boldsymbol{Y}_k,\boldsymbol{Y}_j)$ determined within relatively thin (several degrees thick) concentric rings centred in $\boldsymbol{X}$ will be almost constant. For the 3D Earth we may suppose almost constant β_{kj} within compact sub-networks and across arrays for relatively small segments of the thin concentric rings. When $\boldsymbol{Y}_k,\boldsymbol{Y}_j$ are fixed, β_{kj} is almost constant when the source is contained in a relatively small remote volume. This assumption of partial invariance of β_{kj} is realised in the "Group beamforming" (GB) algorithm.

2.2 Group Beamforming

(GB) is based on splitting a network into M sub-networks W_m, $m = 1, M$. Each W_m is a vector of the corresponding station numbers. Assume that pseudoslowness vector defined above for a pair of stations $\beta_{kj} = \beta_m$, is a constant, when both stations: number k and j belong to the sub-network W_m. In this case we may construct a posterior PDF $F_{GB}\,(X, B)$ in the form of (9) where weights w_{kj}:

$$\{w_{kj} = 1 if\ (k,j) \in W_m, and\ w_{kj} = 0, \text{elsewhere}\}.$$

Joint maximum likelihood estimates of the source coordinates $\boldsymbol{X}$ with the vector of pseudo-slowness values: $B = \{b_1, b_2, \ldots, b_M\}$ are given by maximising the PDF $F_{GB}(\boldsymbol{X},\boldsymbol{B})$:

$$\left\{\hat{X},\hat{B}\right\} = \underbrace{\arg\max}_{X,B} F_{GB}(X,B) \tag{10}$$

Maximum of PDF (9) can be found by any optimisation procedure or by direct grid-search over $\boldsymbol{X}$ and $\boldsymbol{B}$ parameters. Because model parameters $\boldsymbol{B}$ are found jointly with event coordinates $\boldsymbol{X}$, using last event data, the algorithm does not require a priori knowledge of the Earth model. If parameter vector $\boldsymbol{B}$ is considered known a priory exactly from some Earth model or observations it will serve as a parameter in PDF of $\boldsymbol{X}$ described by (9).

2.3 Probabilistic Beamforming

Because the $\boldsymbol{B}$-vector is constant in PDF in (9) and this is equivalent to:

$$F(X,B) = \sum_{k,j} w_{kj} \int \Omega(x-\beta_{kj})'[(t_j - t_k - R_{kj}x)/\Omega]dx \tag{11}$$

where $\delta(x)$ is the Dirac delta-function. In fact, for small arrays the slowness β_{kj} will vary due to local heterogeneities. The distribution of the β_{kj} can be expressed in the form of the PDF f_{kj} (x) of slowness (pseudo-slowness). On the other hand, the PDF $f_{kj}(x)$ can be derived statistically using RTT observations from clustering GT observations. For example, the simple fitting procedure entails calculating the mean and spread of the residual distribution in distance bins at a given confidence interval.

The PDF $f_{kj}(x) = F(x, \beta_{kj}, \upsilon_{kj})$, can be represented, for example by a Gaussian or some other (symmetric) distribution with mean β_{kj}, given by equation (7) and variance υ_{kj}^2 reflecting uncertainty of the RTT model for each pair of stations (k,j) and a grid point in Earth. Anyway, we may substitute the PDF $f_{kj}(x)$ for the delta-function in (11) leading to the PDF

$$F_{PB}(X) = \sum_{k,j=1}^{N} w_{kj} \int f_{kj}(x)'[(t_j - t_k - R_{kj}x)/\Omega]dx \tag{12}$$

From equation (12) we shall derive several cases which are important when actually locating events.

2.4 Important Cases

2.4.1 Range Uncertainty

If, for example, all a priori information we have is that the pseudo-slowness β_{kj} across a network is given an arbitrary value in the interval (b_1, b_2), and other values are impossible, the corresponding PDF of pseudo-slowness will be:

$$f_{kj}(x) = \left\{ \begin{matrix} const, x \in (b_1, b_2] \\ 0, x \notin (b_1, b_2] \end{matrix} \right\}$$

Then the PDF of the source location will be equal to:

$$F(X) = \sum_{k,j} w_{kj} \int_{b_1}^{b_2} \Omega[(t_j - t_k - R_{kj}x)/\sigma]dx \tag{13}$$

For *exponential "theoretical function"* $\Omega(x) = \exp(-x^2/2)$ equation (13) will transform to

$$F(X) = \sum_{k,j} \frac{w_{kj}}{R_{kj}} (F_N[(t_j - t_k - \beta_1 R_{kj})/\sigma] - F_N[(t_j - t_k - \beta_2 R_{kj})/\sigma]) \tag{14}$$

where $F_N(x)$ is a standard normal probability distribution function.

For the cosine *"theoretical" function* $\Omega(x) = \cos(x)$ equation (13) transforms to:

$$F(X) = \sum_{k,j} \frac{w_{kj}}{R_{kj}} (\sin[(t_j - t_k - R_{kj}\beta_1)/\sigma] - \sin[(t_j - t_k - R_{kj}\sigma_2)/\sigma]) \tag{15}$$

and is rewritten as:

$$F(X) = \sum_{k,j} \frac{w_{kj}}{R_{kj}} [\sin(R_{kj}(\beta_2 - \beta_1)/2)\cos(t_j - t_k - R_{kj}(\beta_1 + \beta_2)/2)] \tag{15a}$$

From (16) we can see that the dominant positive impact to the PDF is provided by the station pairs with $R_{kj}(X) \approx 0$ and "correct" average pseudo-slowness. The impact of pairs with different distance to the source is weakened.

2.4.2 Gaussian Uncertainty

Assume the Earth pseudo-slowness model $f_{kj}(x)$ and the theoretical PDF $\Omega(x)$ are normal with averages β_{kj} and $t_j - t_k$ and variances υ_{kj}^2, σ_{kj}^2, respectively. Then from equation (12) we get:

$$F(X) = \sum_{k,j} \frac{1}{\delta_{kj}} \exp[-\frac{1}{2}(t_j - t_k - \beta_{kj}R_{kj})^2/\sigma_{kj}^2] \tag{16}$$

$$\delta_{kj} = (1 + \upsilon_{kj} * R_{kj}/\sigma_{kj})^{0.5} \tag{17}$$

We shall also consider a case when $\Omega(x)$=cos(x) and $f_{kj}(x)$ is normal. This will give:

$$F(X) = \sum_{k,j} \exp[-\frac{1}{4}(\upsilon_{kj}R_{kj}/\sigma_{kj})^2]\cos[(t_j - t_k - \beta_{kj}R_{kj})/\sigma_{kj}] \tag{18}$$

2.5 Confidence Area Evaluation

For evaluation of confidence area $\boldsymbol{A}$ at confidence level α ($\alpha = 0.95$) one has to find a level K of a posterior *normalized* PDF $F(x)$ such that

$$F(x) > K \quad \text{for all} \quad x \in \boldsymbol{A} \quad \text{and} \quad \int_A F(x)dx \geq \alpha \tag{19}$$

Within a grid representation of PDF this integral can be simply approximated by a corresponding integral sum, normalized by the integral sum over the area B, containing the unknown epicenter "for sure".

An alternative approach is a Monte-Carlo simulation, when random values are added to the arrival times (or model travel times) to simulate picking and model errors, and then relocate the event a number of times. The area, limited by the best fitting ellipsoids or lines of the PDF levels, containing $100\alpha\%$ of the locations is a confidence area by definition.

The approximate confidence ellipse has the form:

$$[X - E(X)]^T C^{-1} [X - E(X)] = \chi^2 \tag{20}$$

where X = arg max $F(X)$, χ^2 is a confidence level given by a standard χ^2 distribution and,

$$E(X) = \int XF(X)dX \tag{21}$$

$$\text{and} \quad C = \int XX^T F(X)dX - E(X)E(X)^T \tag{22}$$

can be computed (Tarantola, 1982) via numerical integral approximations.

2.6 Main Variants and Stages of the Location Procedure

The location procedure suggested has in general two-steps. Final location is preceded by initial location due to (1) or (3) using standard travel-time tables. At this stage we get the preliminary source coordinates $\tilde{X}$, travel-time residual *RES*, and empirical PDF of pseudo-slowness (see Sec. 2.4). Then a fine grid (say 1 km step) is established in the area (say 20 × 20 km) around the location $\tilde{X}$, which is subjected to the following grid-search optimisation procedure or variant A or variant B.

Variant A is determined mainly by the "Group Beamforming" above. The network is split into several subsets with presumed constant but unknown (known) slowness (pseudo-slowness β). In this case location is due to equations (9) and (10) and "delivers" source coordinates together with parameter vector $\boldsymbol{B}$.

Variant B The network is taken as a whole (without splitting). Preliminary location result is used to compute slowness (apparent velocity) distribution across the network. Using this information we select the range of pseudo-slowness (β_1, β_2) values and then apply one of the PDF/F/(1×1) formulations in Sec. 2.4 equations (14)–(16) or (peak (peaks) slowness of the distribution (substituted instead of β_{kj}) and utilise one of the formula (17)–(19) with picking RTT scatter σ_{kj}: $\sigma_{kj}^{\ 2} = 2RES^2$, where *RES* is determined above.

2.7 Pilot Study

Variant A case study—location of the calibration 32.5 tons explosion in the Sayarim valley, Israel

A.1. The 32.5 tonnes explosion was recorded and located by the seismic networks of Israel and Jordan, comprising a total of 33 seismic stations (see Figure 2a). Figure 2b depicts the true and computed locations. The currently used location program, based on a local 1D velocity model, gave an epicenter with an error of ~2 km. Applying the Group Beamforming (GB) procedure (Variant A) while sub-dividing the combined seismic network into seven sub-arrays yielded a solution which is within 260 m of the true explosion location.

A.2. We tried to relocate this explosion by using only two sub-arrays (see Figure 2a): one to the north, consisting of four stations and one to the east, consisting of two stations. The GB location result deviates by 0.6 km from the true source position. More GB applications can be found in Pinsky et al. (2006) or in www.free-webs.com/vpinsky.

Variant B case study–comparison of the GT0 Nuclear test locations, using bulletin readings of the first P, Pn, Pg arrivals

In this study the ISC Bulletin data (the EHD catalogue for the first P, Pn, Pg phases arrival times was used to locate a number of nuclear tests with exactly known ignition coordinates (GT0 events is Ground Truth location with zero location error) and thus providing exact location accuracy for each calibration event.

Table 1 shows deviation (in degrees) of the new procedure location estimates from the true locations as compared to the best ISC bulletin locations. Network of stations was considered in Local (0–500 km), Regional (500–3,000 km) and all ranges (0–180). Local and Regional ranges are unavailable for the events N8–N13, as the nearest station in the bulletin starts at the distance range of 2,000 km and larger.

Figures 3–15 demonstrate results of source location for the 13 nuclear tests listed in Table 1. Each figure below comprises the PDF contours (square with circle), PDF maximum (diamond) (the procedure epicentre estimate), the reference epicentre (star) and the ISC location (cross). The outer PDF (equation (20)) contour corresponds to 90% confidence area. The figure captions deliver more details about the events and the location results.

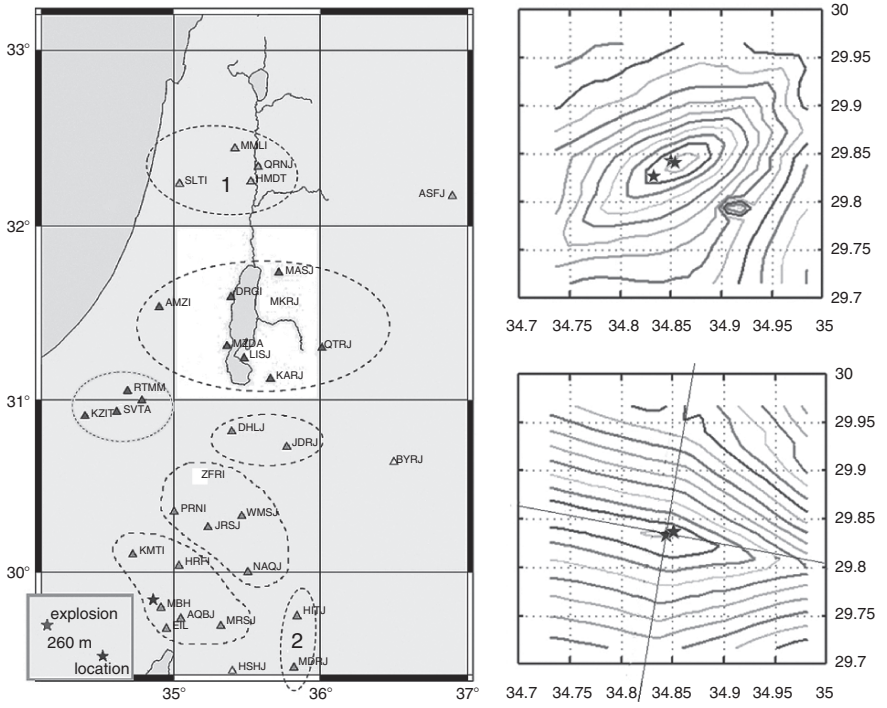

Figure 2 Location of the 32.5 ton calibration explosion is Sayarim valley. (a) The Israeli (ISN) and Jordanian (JSN) seismic station networks are divided into 7 sub-arrays (marked with different colours) yield the GB location marked at the location of the blue star. (b) Contours of the FitFunction of the GB algorithm yielding a location only 260 m from the true location (red star). (c) Two sub-arrays (within elliptic contours in a) provide GB location at the intersection of the respective back azimuths at 600 m away from the true location. The location solution of the standard Geiger method with the 33 ISN and JSN stations is 2 km away from the GT (marked as a green star)

Table 1 Comparison of the Variant B and the ISC locations for the set of 13 NT

				New procedure			
N	Event	Lat	Long	Loc	Reg	ALL	ISC1
1	Bikini1954	11.666	165.387	–	–	0.015	0.1
2	Missisipi1964	31.1420	−89.530	–	0.015	0.02	0.177
3	NewMexico1967	36.678	−107.208	0.025	0.034	0.026	0.034
4	Nevada1968	38.65	−116.200	0.04	0.01	0.015	0.02
5	Colorado1969	39.4058	−107.9081	0.02	0.03	0.03	0.108
6	RatIslands1971	51.472	179.107	0.01	–	0.15	0.128
7	Colorado1973	39.793	−108.367	0.04	0.059	0.02	0.095
8	Sibir1977 N1	69.5367	90.5138	–	–	0.01	0.063
9	Sibir1977 N2	64.1080	99.5580	–	–	0.03	0.033
10	Sibir1978 N3	63.706	125.3209	–	–	0.025	0.083
11	Sibir1978 N4	65.9180	112.5409	–	–	0.04	0.11
12	Sibir1978 N5	66.598	86.2100	–	–	0.02	0.07
13	Ura11978	63.185	63.4320	–	–	0.03	0.08
	Average			–	–	**0.035**	**0.079**

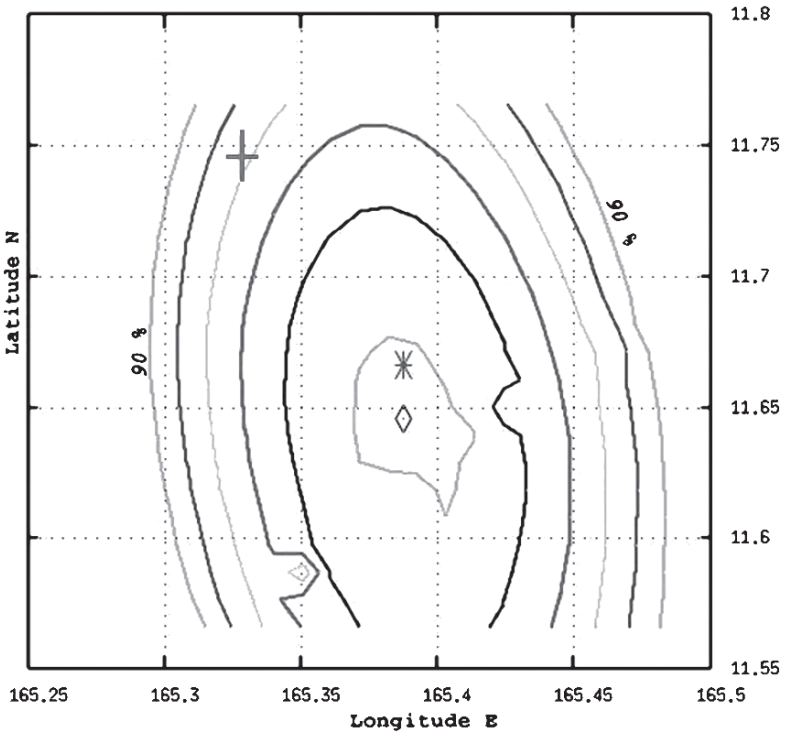

Figure 3 Bikini Atol region Nuclear Test 1954/05/04, 18:10:00, 70 stations, minimum distance $R_{min} = 20.52°$. Location error $\Delta R_{\lozenge} = 0.015°$, $\Delta R^{\dagger} = 0.1°$

3 Discussion and Conclusions

(a) In this pilot study we have tested two robust model free event location algorithms: "Group Beamforming" (GB) and the 4a variant of the "Probabilistic Beamforming" (PB), which exhibited most promising results at different distance ranges, compared to the conventional ISC location procedure.

(b) The demonstrated advantage of these methods relative conventional ones can be partially explained by the less dependency of the new algorithms on model travel times and partially due to inherit filtering of outliers by summation of the bell-shaped Probability Density Functions. On the other hand the shortcomings of the proposed procedures stem from the necessity of tuning the procedure parameters for each given event: for example, select station arrays with "fixed slowness" in the case of the Group Beamforming or select slowness interval $[b_1, b_2]$ and scatter σ in the case of the Probability Beamforming (case 4a). No fixed

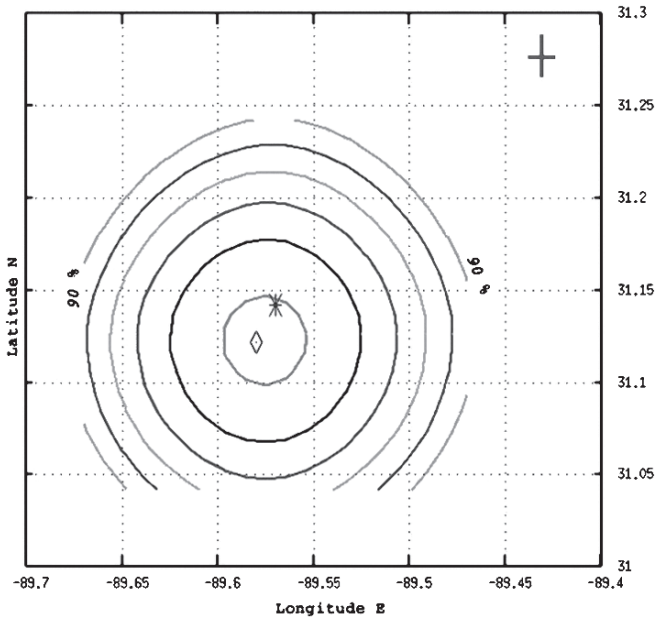

Figure 4 Mississippi 1964/10/22 16:00:00 mb = 4.6, Nuclear test Salmon, 29 stations, gap = 118° minimum distance R_{min} = 5°. Location erorr $\Delta R_{\Diamond} = 0.02°$, $\Delta R_{\dagger} = 0.177°$

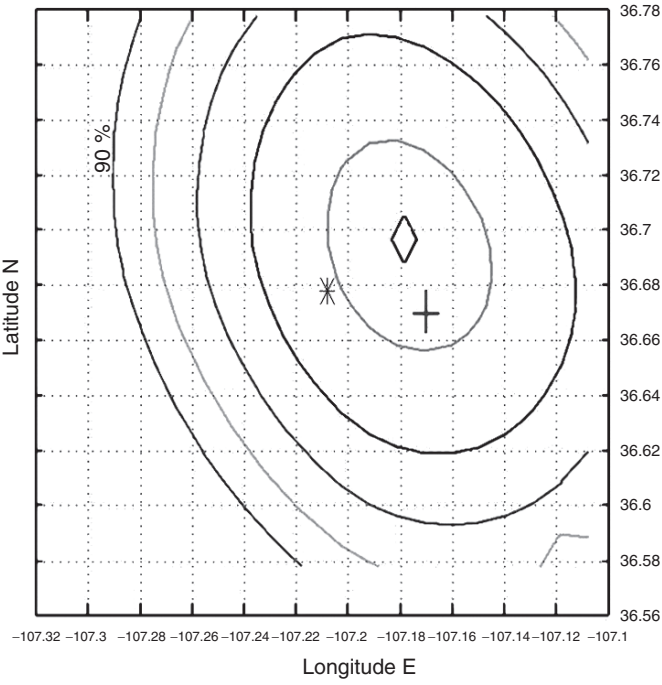

Figure 5 New Mexico 1967/12/10 19:30:00 m_b = 4.8, Nuclear Test, 100 stations, gap = 55°, R_{min} = 1.8°, Location error $\Delta R_{\Diamond} = 0.026°$, $\Delta R_{\dagger} = 0.034°$

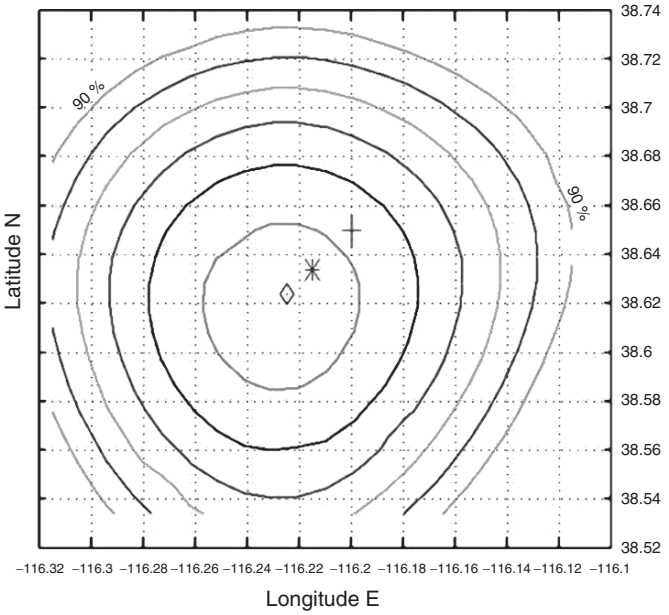

Figure 6 Nevada 1968/01/19 18:15:00 m_b = 6.3, 219 stations, R_{min} = 0.9°, gap = 22°, Location error $\Delta R_{\lozenge}$ = 0.015, $\Delta R_{\dagger}$ = 0.02°

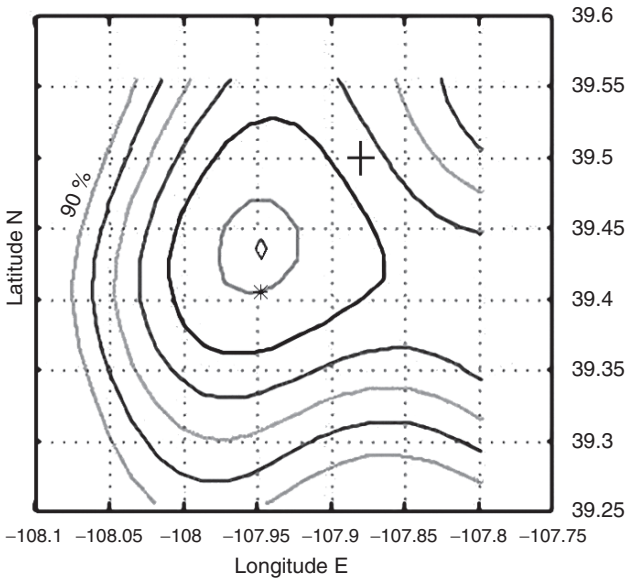

Figure 7 Colorado 1969/09/10 21:00:00 m_b = 5.3, 115 stations, R_{min} = 1.5°, gap = 21°, Location error $\Delta R_{\lozenge}$ = 0.026°, $\Delta R_{\dagger}$ = 0.108°. PDF pattern shows large uncertainty of the epicentre in the South-Eastern direction due to the high regional heterogeneity

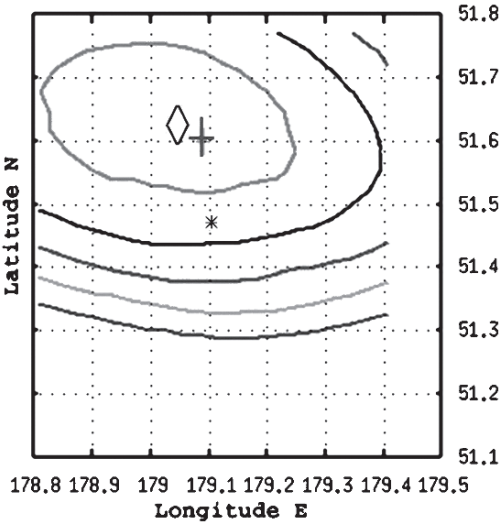

Figure 8 Rat Islands 1971/11/06 21:59:56.00 m_b = 6.5, 372 stations, R_{min} = 0.04°, gap = 28°, Location error $\Delta R_{\Diamond}$ = 0.15°, $\Delta R_{\dagger}$ = 0.128°

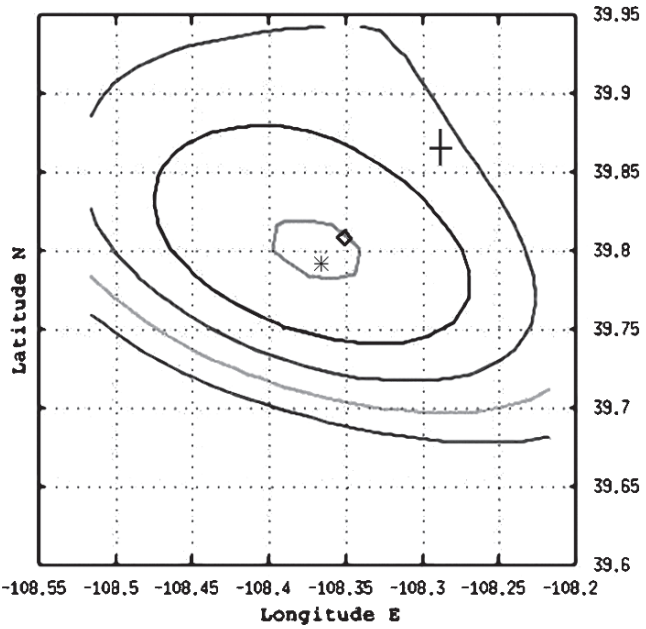

Figure 9 Colorado 1973/05/17 16:00:00.00 m_b = 4.1, 138 stations, R_{min} = 1°, gap = 22°, Location error $\Delta R_{\Diamond}$ = 0.02°, $\Delta R_{\dagger}$ = 0.095°

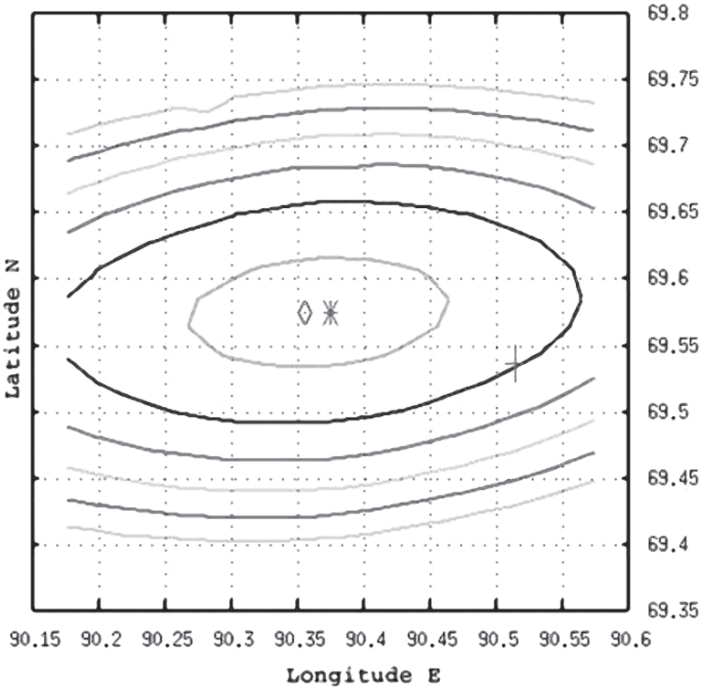

Figure 10 Norhtern Central Sibiria "Sibir N1" 1977/07/26 16:59:57.60 00 m_b = 4.9, 101 stations, R_{min} = 19.7°, gap = 51°, Location error $\Delta R_{\Diamond}$ = 0.01°, $\Delta R_{\dagger}$ = 0.06°

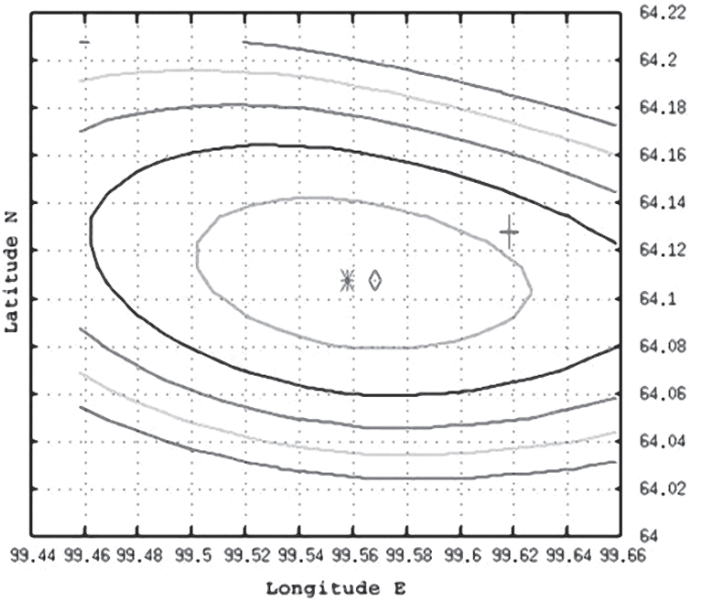

Figure 11 Northern central Sibiria "Sibir N2" 1977/08/20 21:59:58.70 m_b = 5.0, 130 stations, R_{min} = 26°, gap = 85°, Location error $\Delta R_{\Diamond}$= 0.01°, $\Delta R_{\dagger}$ = 0.033°

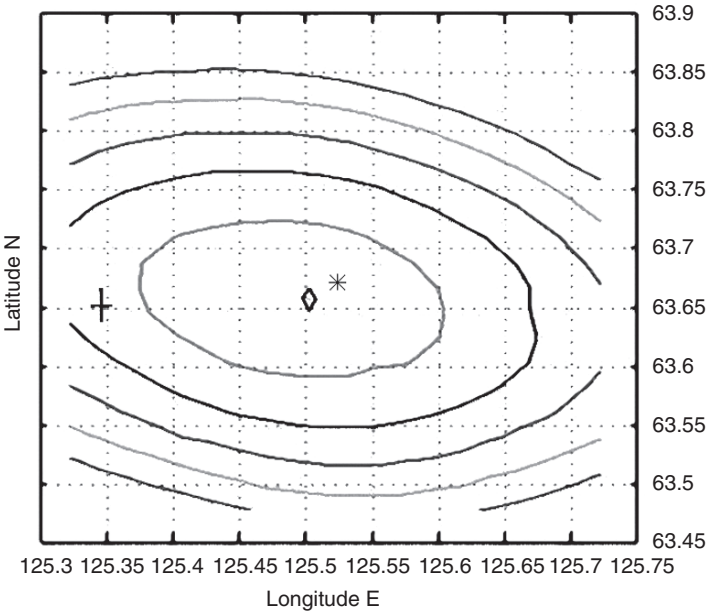

Figure 12 Northern central Sibiria "Sibir N3" 1978/08/09 18:00:00.0 m_b = 5.6, 229 stations, R_{min} = 24.3°, gap = 71°, Location error $\Delta R_{\Diamond}$ = 0.025°, $\Delta R_{\dagger}$ = 0.083°

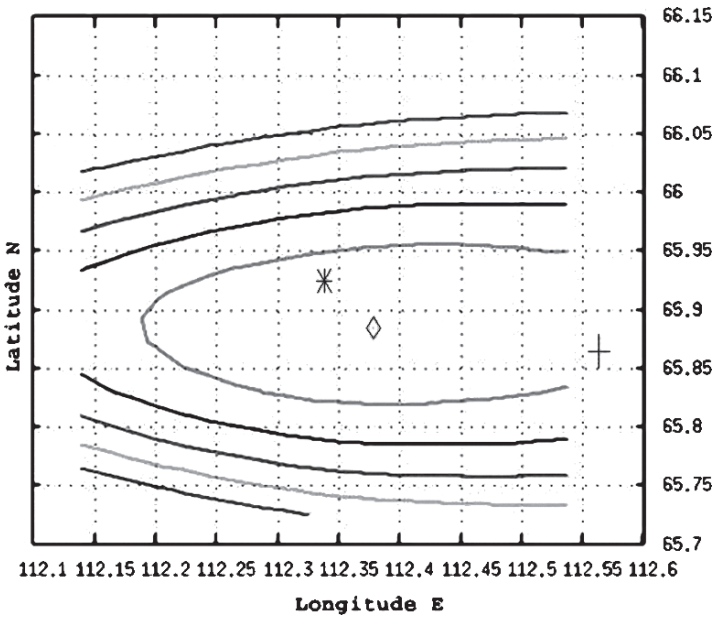

Figure 13 Northern central Sibiria "Sibir N4" 1978/08/24 17:59:57.0 m_b = 5.1, 143 stations, R_{min} = 26°, gap = 96°, Location error $\Delta R_{\Diamond}$ = 0.04°, $\Delta R_{\dagger}$ = 0.11°

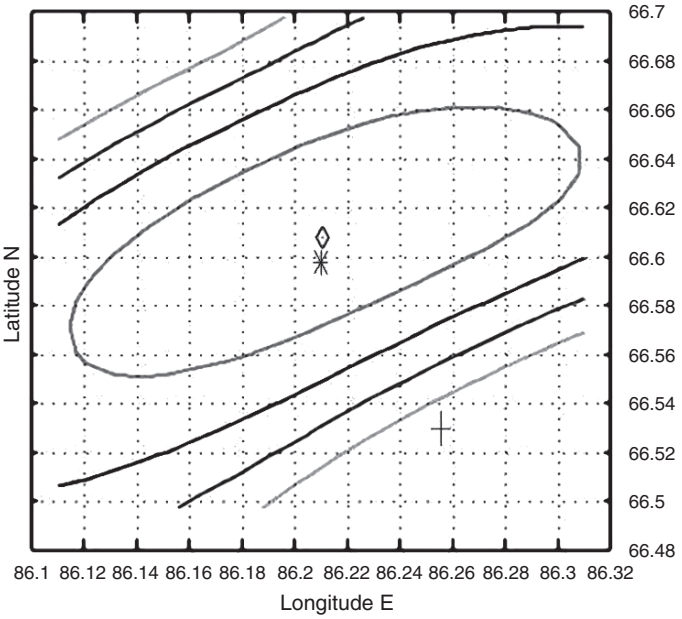

Figure 14 Northern central Sibiria "Sibir N5" 1978/09/21 14:59:57.5 m_b = 5.2, 167 stations, R_{min} = 26°, gap = 49°, Location error $\Delta R_{\lozenge}$ = 0.02°, $\Delta R_{\dagger}$ = 0.07°

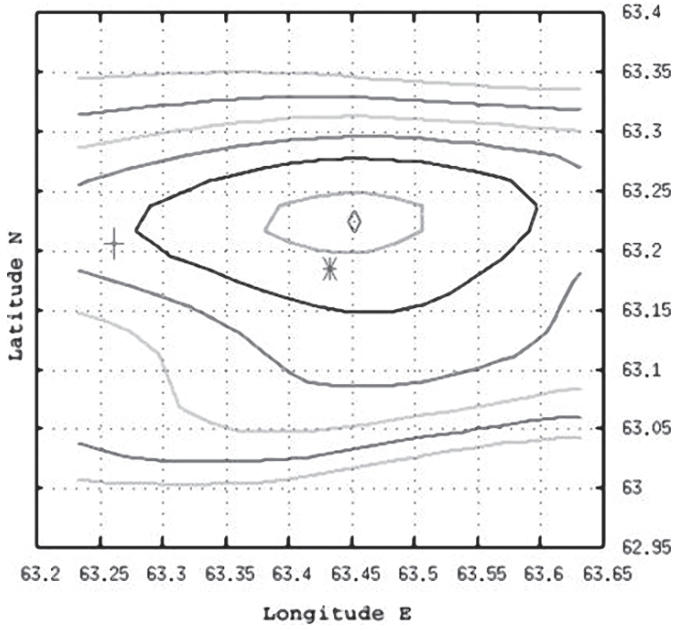

Figure 15 Ural Mountains region 1978/10/17 13:59:57.80 m_b = 5.5, 261 stations, R_{min} = 15.7°, gap = 57°, Location error $\Delta R_{\lozenge}$ = 0.02°, $\Delta R_{\dagger}$ = 0.07°

parameters have been found to be optimum for all cases considered. For example, the b_2 parameter is far more significant than the b_1, when apparent velocities are within the 5–8 km/s – crustal phases interval. Besides, for some values of σ taken from the interval (1–3 s) the location accuracies are in many cases extremely high: within several hundreds of meters, but may degrade for small change of σ. It should be noted that in each case we tried to adjust these parameters to the best sharpness of the PDF form and confidence area size (should be small) and form (circular is preferred). However, reliable and objective truth criteria for the parameter adjustments is still unknown. Presumably, this factor is the reason why confidence area of ±10, ±15 km for most of the cases look so bleak in comparision to the good location results obtained here. In fact, if one refers to the ISC Bulletin, this size of the confidence area statistically corresponds well to the ISC locations on a large sample of the GT0, GT5 events in spite of the small confidence ellipse size reported. The best fixed or case dependant tuning parameter evaluations is seen from massive Monte-Carlo experiments, using hundreds and thousands of the GT5, GT0 events. Such experiments are planned for a future location study.

(c) Further improvements are seen as well in construction of the Earth Uncertainty model in terms of pseudo-slowness PDF or error bars, which will help in better handling of the problem mentioned above. For this purpose the existing GT0 travel time data may be used to compute pseudo-slowness sample distributions using Azimuth-Distance bins. This will make it possible to compute a general form of PDF (12), using tabulated pseudo-slowness distribution parameters.

(d) In addition to using GT0 real data, GT5 (accurate to 5 km) data will essentially broaden the test area. However, the accuracy criterion is not so evident here. To enhance such investigations it is interesting to locate these events using 3D travel time computations, based on existing ray-tracing procedures and simulation of different magnitude scales and arrival patterns by adding of distance-dependent random noise.

(e) Essential shifting of an epicenter may appear as the result of the teleseismic travel time deviations due to the Earth's ellipcity effect, not accounted for here at present. For the travel time ellipcity compensation, the formula of Dziewonski & Gilbert (1976) can be used to calculate phase travel times and distances in a Spherical Earth model. For the distance calculation geodetic latitudes should be transformed to geocentric first, using flattening or eccentric coefficients.

(f) Important question not discussed yet is the event depth determination. All examples above are for nuclear tests, with zero depths. Usually, depth estimations in the international bulletins are not accurate and location by remote network stations only (starting from several degrees to the first station) is often produced with fixed depth. Accurate depth estimations by global network are, therefore, usually due to the depth phases (pP) if present. In the case when local network data are available, local travel time models and Pg, Pn, Sn and Sg readings may produce good depth constrain. The algorithms discussed here are based on the concept of pseudo-slowness of the first P wave arrivals, which is not a depth sensitive parameter for remote stations. Therefore, there is a possibility

of obtaining more accurate epicenter, not influenced by poor depth estimates. On the other hand when close stations are involved, deep and shallow events can possibly be resolved due to the different distance from the source to the station.

(g) The grid-search procedures considered, require initially an epicenter estimate for the grid location. This can be achieved using the arrival order approach (Anderson, 1981) providing the epicentre close to the point of maximum of density intersections of the station pair's bisectors.

Acknowledgements I am thankful to Eystein S. Husebye (BCCS, UoBergen); and Avi Shapira (ISC, UK) for fruitful suggestions during the work on the manuscript.

References

Anderson, K. R., 1981. Epicentral location using arrival time order. *Bull. Seismol. Soc. Am*., 71, 541–546.

Anderson, K. R., 1982. Robust earthquake location using M-estimates. *Physics of the Earth and Plan. Inter*., 30, 119–130.

Andrews D. F., P. J. Bickel, F. R. Hampel, P. J. Huber, W. H. Rogers, J. W. Tukey, 1972. *Robust Estimates of Location*. Princeton University Press, Princeton, NJ, pp 374.

Andrews, D.F., 1974. A robust method for multiple linear regression. *Technometrics*, 16, 523–531.

Antolik, M., Ekstrom, A. M. Dziewonski, 2001. Global event location with full and sparse data sets using three-dimensional model of mantle P-wave velocity. *Pure Appl. Geophys*., 158, 291–317.

Boschi L., A. M. Dziewonski, 1999. High-and-low-resolution images of the Earth's mantle: Implications of different approaches to tomographic modeling. *J. Geoph. Res*., 104, 25, 567–25, 594.

Buland, R., 1986. Uniform reduction error analysis. *Bull. Seismol. Soc. Am*., 76, N1, 217–230.

Dziewonski A. M., Gilbert. F.,1976. The effect of small aspherical perturbations on travel times and re-examination of the corrections for the ellipcity. *J. Geoph. R. Astron. Soc*., 44, 7–17.

Firbas, P., 2000. Location calibration based on 3-D modeling. In Thurber, C.H. and Raninowitz, eds. *Advances in Seismic Event Location,* . Kluwer, 135–162, pp 267.

Geiger, L., 1910. Herdbestimmung bei Erdbeben aus den Ankunftszeiten. Nachrichten von der Königlichen Gesellschaft der Wissenschaften zu Göttingen, Mathematisch-Physikalische Klasse, 331–349. 1912 transliterated in English by F. W. L. Peebles & A. H. Corey: Probability method for the determination of earthquake epicenters from the arrival time only. Bulletin St. Louis University 8, 60–71.

Huber, P. J., 1981. *Robust Statistics*, Wiley, NY, pp 308.

Jeffreys, H.,1962. *The Earth,* Cambridge University Press, Oxford, 4th edn., 93–95.

Jih, R.S., 1999. Epicenter estimation using erroneous crustal model(s) and skew regional networks. *Phys. Earth Planet Inter*., 113, 303–319.

Kvaerna T., F. Ringdal, 1996. Generalized beamforming, phase association and threshold monitoring using a global seismic network. In E. S. Husebye and A. M. Dainty, eds. Monitoring a Comprehensive Test Ban Treaty. NATO ASI Series. Kluwer Academic Press, pp 446–466.

Laske, G., Masters, G., Reif, C., 2002. A New Global Crustal Model at 2×2 Degrees http://mahi.ucsd.edu/Gabi/rem.dir/crust/crust2.html

Lomax, A., 2005. A Reanalysis of the Hypocentral Location and Related Observations for the Great 1906 California Earthquake, *Bull. Seism. Soc. Am*., 91, 861–877.

Lomax, A., Virieux, J., Volant, P., Berge-Thierry, C., 2000. Probabilistic earthquake location in 3D and layered models: Introduction of a Metropolis-Gibbs method and comparison with linear

locations, In Thurber, C.H., and N. Rabinowitz (eds.) *Advances in Seismic Event Location*, Kluwer, Amsterdam, 101–134, pp 267.

Pinsky, V., 2000. Prototype autonomous earthquake locator for regional networks. *Geophys. Res. Lett*., 27, 3549–3552.

Pinsky, V., 2005. Accurate epicenter location with and without travel time model. In Husebye, E. S., Christova, C. (eds). Earthquake Monitoring and Seismic Hazard Mitigation in Balkan Countries. NATO Advanced Research Workshop (ARW); Book of Abstracts, Borovetz, Bulgaria, 11–17 Sep., 2005, 79–83.

Pinsky, V., 2006. Using beamforming for the global network location. *Phys. Earth and Plan. Interiors,* 158, 75–83.

Pinsky, V., Y. Gitterman, A. Hofstetter, A. Shapira, 2006. Robust location of surface explosions by a network of acoustic arrays. *Geoph. Res. Letters,* vol. 33, L02317, doi:10.1029/2005GL024304.

Ringdal, F., B. L. N. Kennett (eds.) 2001. Monitoring the Comprehensive Nuclear Test-Ban Treaty: Special Issue on Source Location, Pageoph, 158, 1–2, Birkhauser, pp 420.

Ritzwoller, M. H., N. M. Shapiro, A. L. Levshin, E. A. Bergman, and E. R. Engdahl, 2003. The ability of a global 3-D model to locate regional events. *J. Geophys. Res*. 108, B7, 2353, ESE 9–1–ESE 9–24.

Sambridge, M. S., Kennett, B. L. N., 1986. A novel method of hypocentre location. *Geophys. J. R. Astron*. Soc. 87, 679–697.

Tarantola, A., Valette, B., 1982. Inverse Problem=Quest for Information. *Journal of Geoph*., 50, 159–170.

Tarantola, A., 2005. Inverse Problems Theory and Methods for Model Parameter Estimation. *SIAM*. pp 342.

Waldhauser, F., Ellsworth, W. L., 2000. A double-difference earthquake location algorithm: Method and application to the northern Hayward fault. *Bull. Seism. Soc. Am*., 90, 1353–1368.

Earthworm Auto-Earthquake Location Performance and Recent Improvements in Seismic Data Acquisition, Processing, Archiving and Dissemination at Kandilli Observatory and Earthquake Research Institute

Childs Dean*, Karabulut Hayrullah[1], Kömeç Ahu[1], and Aktar Mustafa[1,2]

Abstract The Kandilli Observatory Real-Time Automated Seismic Data Processing System (KORTASDPS) has been one of the most important infrastructure developments in the last 5 years at Kandilli Observatory and Earthquake Research Institute (KOERI), Boğaziçi University. KORTASDPS uses the Earthworm (EW) software suite for its real-time processing of seismic data. Primary functions of EW are to serve as real-time data server and auto-detect and locate earthquakes. Performance evaluation of EW was done by comparing its hypocenter catalogs from years 2004 and 2005 with catalogs produced by the National Earthquake Monitoring Center (NEMC) at KOERI which relies on manual detection and location techniques. In general EW performance is highest in northwest Turkey where station density and relative station sensitivity are high. Catalog correlations reveal that this area has an estimated 3.1 low magnitude threshold for a 90% earthquake auto-detection and location reliability. For the rest of the country this low magnitude threshold estimate ranges between 4.4 and 4.6. Three initiatives have been proposed to improve EW auto-detection and location accuracy. These are more accurate timing of emergent phases, use of reliable S phases and an increase in the effective seismic network density with more sensitive and reliable stations. Already expansion and modernization of KOERI's seismic network in 2004 and 2005 have resulted in clear improvements in EW's auto-detection and location performance. A one month pilot analysis was undertaken to understand the nature of the consistent large numbers of EW cataloged seismic events that do not correlate with NEMC. Results show that after careful manual relocation of these events that the majority are not found in either NEMC's preliminary or final catalog and that these events represent almost one third of all events found in the combined EW and NEMC catalogs. Since 2003 the KOERI re-designed digital broadband network has increased from 4 to 33 stations and international shared broadband stations from 2 to 10. The past and planned increases of more sensitive and higher quality seismic stations has and will continue to improve the performance of EW's auto-detection and location

[1] Department of Geophysics, Kandilli Observatory Earthquake Research Institute, Boğaziçi University, Istanbul, Turkey

[2] TUBITAK Marmara Research Center, Earth and Marine Science Institute, Gebze, Turkey

* To whom correspondence should be addresed. E-mail: dean@boun.edu.tr

E.S. Husebye (ed.), *Earthquake Monitoring and Seismic Hazard Mitigation in Balkan Countries.*

reliability and provide a source of information rich data to be used for ongoing and future seismological research activities.

Keywords Earthworm, KOERI, real-time-earthquake-auto-detection, real-time-earthquake-auto-location, Kandilli Observatory

1 Introduction

Since the devastating August 17, 1999, Mw 7.4 Izmit Turkey earthquake it was realized the necessity to modernize the earthquake monitoring and seismic data acquisition infrastructure at Kandilli Observatory and Earthquake Research Institute (KOERI), Boğaziçi University both for monitoring real time seismicity as a public service and to provide a high-quality easy to access digital seismic waveform database for research. To achieve these goals a small group of scientist informally called the "Broadband Group" was formed. This report summarizes the completion and ongoing activities within this group as of December 2005 pertaining to changes in the seismic data acquisition processing and dissemination infrastructure of KOERI. Topics covered are; development, current design, management and performance of the Kandilli Observatory Real-Time Automated Seismic Data Processing System (KORTASDPS) re-design and expansion of the digital broadband seismic station network, and real-time seismic data exchange and archiving.

2 Kandilli Observatory Real-Time Automated Seismic Data Processing System (KORTASDPS)

The development of the KORTASDPS (Childs and Kömeç, 2003) began in early 2001. By November of the same year KORTASDPS was auto-locating its first events whose number has currently reached over 27000. The real-time processing core of KORTASDPS uses the Earthworm (EW) software suite, initially developed by the United States Geological Survey in Menlo Park, California (Johnson et al. 1995). The EW suite is composed of stand alone modules, each module works interactively locally or across a network. The modularity allows seismic network operators to adapt EW to a wide variety of seismic network configurations. Open source code has enabled the expansion and improvement of the EW module suite from contributors worldwide, further increasing its flexibility and robustness.

KORTASDPS was designed to fit the needs of the KOERI real-time earthquake monitoring operations conducted by the National Earthquake Monitoring Center (NEMC) and to feed its seismic data in near real-time to an automated archiving system for post processing. Software from both commercial and freeware sources runs presently on 10 core PCs communicating across a "closed" data network. The primary function of each PC connected to the KORTASDPS closed data network belongs to 1 or 2 of the five operational sub-systems.

1. **Field** PCs are used to configure digital seismic instrumentation and backup data at the station in the event of failed data communication line.
2. **Data Acquisition** PCs interact directly with the seismic stations, record continuous data streams to a hard disk using commercial software, and broadcast the same data stream onto the "closed" data network.
3. ***EW* Real-Time Data Processing** PCs primarily run *EW* modules. They receive the broadcasted data stream from the data acquisition PCs and convert this to *EW* format where it is stored, served by request and re-broadcasted onto the data network. Waveforms from this *EW* formatted data stream are fed to a picker, picks are associated into events, events are located, and finally waveforms are automatically assembled into SAC formatted event files and written to disk. Because these PCs are core to the real-time component of the overall system and because these PCs are relatively difficult to configure on short notice a duplicate or mirror set of computers are run in parallel as a backup.
4. **Data Archiving and Public Distribution** PCs automatically pull SAC format continuous and event based data files from the data processing sub-system and create duplicate copies on their local hard-drives. This continuous SAC data is now open via FTP access to the public. Each month the data is archived to a stable media. Because of its critical importance this sub-system is also mirrored. In addition one PC utilizing the Seiscomp Software Suite is used to distribute seismic data in real-time both nationally and internationally.
5. **The Public Information Access** PC is the KORTASDPS web server. Plans are to make available to the public real-time earthquake location, magnitude and waveform images, produced by the KORTASDPS as well as general information regarding the overall system architecture.

3 Performance of KORTASDPS

3.1 Introduction

The auto-events produced by KORTASDPS EW system can be noise, natural earthquakes, or man made seismic events such as explosions. One of the primary goals of an automated earthquake system is to reduce 'noise events' while simultaneously increasing the detection and accurate location of earthquakes. Unfortunately the suppression of auto-noise-events often leads to the suppression of auto-earthquake-events so an automated system must be optimized or tuned for a given seismic network's particular performance. Nevertheless a well tuned automatic processing system is not by itself sufficient to decrease the false alarm rate while keeping the detection level to a constant. As with all automated systems the quality of input determines the quality of output. Therefore the KORTASDPS system manager must be very familiar with seismic station hardware capabilities, operational status and station site sensitivity in order to understand how to adjust an automated system. Since 2001 the Broadband Group has been managing several key components

of KORTASDPS including the EW system. Direct access to the system has enabled long term rudimentary monitoring of its performance and adjustments to its configuration. This section presents results from the analysis of EW system event auto-locations from years 2004 and 2005.

The earthquake catalog of the NEMC was used to gauge the performance of EW's auto-event locations. As of December 2005 the NEMC continues to manually detect and locate earthquakes throughout Turkey. A seismic analyst is on-site 24 hrs/day 7 days/week. EW is used by the NEMC as a way of coalescing seismic data from the variety of commercial seismic hardware and software into a single seismic data server which is then accessed by the analyst when an earthquake is visually detected on the monitor trace displays. As of December, 2005 there are 42 broadband (3 component), 59 short period analog (single component), and 1 short period digital (3 component) stations flowing into the EW data server in real-time for a total of 102 stations. Analog stations are centrally digitized. Since 2003 the Broadband Group has been monitoring and quantifying KOERI's seismic network performance on a station by station level. Daily State of Health (DSOH) reports are produced for all digital stations and include data recovery percentage, voltages, timing status, and other aspects related to monitoring the health and infrastructure of KORTASDPS. In addition Event State of Health (ESOH) reports are produced when a teleseismic event is large enough to be recorded across the entire network (Childs and Komec, 2003). This allows the determination of a simple dead or alive statistic for all stations especially the analog section of the network which currently comprises 58% of KOERI's network. The freely distributed state of health information is used by decision makers, station maintenance operators, researchers and earthquake monitoring staff. It has been invaluable towards better understanding the quality of input to the EW auto-location system.

3.2 Effective Seismic Network

Because EW's auto-event detection and location performance is intrinsically linked to the state of the seismic network feeding it, an attempt was made to determine the actual "effective seismic network" separately for years 2004 and 2005. In order to be part of the "effective seismic network" a station needed to be installed for a minimum of 8 months of a given year and have had a performance rating of 60% or greater. The latter performance criteria required, for digital stations, a data recovery percentage of 60% or greater for the period in operation and for analog stations a 60% or greater performance based upon ESOH reports. The results of the elimination criteria are below shown in Table 1. The "Effective Seismic Network" criteria for year 2005, though not stringent, eliminated 26% of the then operating stations from the network. This agrees will with ESOH reports which on average show a seismic network functional health of approximately 75%. General observations during relocation of small magnitude events for this study pointed out that some effective network stations consistently recorded readable first arrival phases while other nearby effective network

Table 1 Effective seismic network configurations for years 2004 and 2005

Year	Broadband digital (3 component)	Short period digital (3 component)	Short period analog (1 component)	Total stations "effective network"	Effective network density (km^2/station)
2004	18	1	36	55	14172
2005	30	1	36	67	11634

stations provided consistently no data at all so the rudimentary criteria used in this study as an "effective seismic network" could in the future be updated to take into account a station's sensitivity and signal to noise ratio.

3.3 Correlation Between Auto and Manual Locations

The EW auto-location catalogs for years 2004 and 2005 were correlated with the final 2004 and preliminary 2005 earthquake catalogs produced by the NEMC. The 2005 NEMC preliminary catalog was used for 2005 because a completed "final" catalog was not available during the data processing stage of this analysis. It was necessary to eliminate months April and July of 2004, and February, March and May of 2005 from both catalogs because these sections of the EW catalogs were not available. Correlation of catalogs was completed to the end of November 2005. With exception to some stations to the north and south of the Marmara Sea in northwestern Turkey the NEMC manually locates earthquakes throughout Turkey using essentially the same seismic network configuration as that of EW. Nevertheless some critical location procedures and criteria are different as shown in Table 2. Most notably NEMC has a 5 phase minimum and uses S phases which reduce the minimum number of stations required for a solution to 3. EW has a 4 station minimum and does not use S phases. EW's automatic event detection and location software flowchart and software is shown in Table 3. Each EW software module has its own configuration file which enables the system manager to control its behavior. In this way an EW system can be very specifically tuned to the needs for specific seismic monitoring task.

A catalog correlation criteria of less than 5 s difference in origin time and 50 km in epicentral distance difference was used in the analysis to follow however other more liberal and stringent criteria are shown in Table 4 to give a broader perspective of the results. Table 4 clearly shows that large percentages of earthquakes from both the EW and NEMC catalogs are uncorrelated. For the NEMC the uncorrelated percentages, relative to the total catalog event count, range from 67–74% for both years using the first 2 more stringent correlation criteria shown in Table 4. Comparing the auto-locations with the NEMC final catalog does not necessarily reduce the percentage of uncorrelated NEMC earthquakes as the numbers of both uncorrelated and correlated events can increase however the number of correlated events does increase significantly. Correlation to the end of

Table 2 Event detection and location criteria and procedures used by EW and the NEMC

Ew earthquake auto location criteria	NEMC manual earthquake location preliminary catalog criteria	NEMC manual earthquake location final catalog criteria
Automatic event detection and location (Table 3 for details)	Manual visual event detection by onsite analyst	Same
Only P phases used	P and S phases used	Same
Minimum of 4 stations	No Minimum	Minimum of 3 stations
M_D determined but not used.	M_D determined. M_L for larger magnitudes.	Same + M_B determined
No max azimuthal gap criteria	No max azimuthal gap criteria	Max azimuthal gap criteria of 200 used as a general guideline, exceptions are allowed
No max RMS residual criteria	No max RMS residual criteria	Max RMS residual criteria of 1.0 used as a general guideline, in some cases exceptions are allowed
Single 4 layer Velocity model	Velocity model identical to EW's	Velocity model identical to EW's

Table 3 EW's automatic event detection and location software flowchart

Ew software module name	Functional description
PICK_EW	Continuously time-picks real-time seismic trace data fed from the EW data server
BINDER_EW	Associates picks into events and creates a preliminary location with an event ID. Though not common associated events that have high residuals can be terminated by binder_ew.
EQPROC	Module head which collects information from binder_ew and pick_ew to determine when an event is ready for secondary location processing.
EQBUF	Buffers information received from eqproc
EQCODA	Determines coda length for hypoinverse M_D calculations
EQVERIFY	Tests for noise events and eliminates them.
HYP2000_MGR	Manages EW location data inflow and outflow from hypoinverse (hyp2000). Creates final location. Though not common associated events that have high residuals can be terminated by hyp2000_mgr.

August of a finished not yet distributed section of the NEMC "final" 2005 catalog which became available late in the study revealed that the number of correlated events in the 2.5 s to 25 km and 5 s to 50 km criterion categories increased by 22%. To evaluate the EW auto-location catalogs events produced by seismic network noise must first be removed. Monitoring has shown that the 2004 EW catalog has an average of 65% noise events which if accounted for would give an

Table 4 NEMC and EW event catalog correlation results for years 2004 and 2005

YEAR 2004 (months April and July are not included in the analysis)					
Correlation criteria (origin time and epicentral offset)	Uncorrelated NEMC final catalog with uncorrelated percentages of total catalog		Correlated events	Uncorrelated EW catalog with uncorrelated percentages of total catalog (noise events removed)	
<2.5 s <25 km	2106	71%	844	931	52%
<5 s <50 km	1978	67%	972	804	45%
<10 s <100 km	1873	63%	1077	699	39%
<20 s <200 km	1762	60%	1188	588	33%

YEAR 2005 (months February, March, May and December are not included in the analysis)					
Correlation criteria (origin time and epicentral offset)	Uncorrelated NEMC preliminary catalog with uncorrelated percentages of total catalog		Correlated events	Uncorrelated EW catalog with uncorrelated percentages of total catalog (estimated noise events removed)	
<2.5 s <25 km	2651	74%	914	4114	82% estimate
<5 s <50 km	2461	69%	1101	3927	78% estimate
<10 s <100 km	2277	64%	1285	3743	74% estimate
<20 s <200 km	2090	59%	1472	3556	71% estimate

uncorrelated percentage ranging from 45–52%. For 2005 the noise event monitoring was discontinued Albeit pilot studies for April and June of 2005 have shown that the percentage of auto-noise-events for the EW system has decreased dramatically to less than 30%. This may be due to the addition of 27 digital broadband 3 component and 3 short period analog stations during years 2004 and 2005. This noise-event value can fluctuate monthly on average by approximately 10% as indicated by the 2004 data so a conservative 40% noise-event value estimate was used for year 2005. Based upon the noise estimate uncorrelated earthquakes for EW's 2005 catalog range from 78–82% using NEMC's preliminary catalog and the first 2 more stringent correlation criteria shown in Table 4. For years 2004 and 2005 NEMC uncorrelated percentages of total earthquake catalog remain relatively constant while those of the EW catalog have increased by 58–73%. In addition the percentage of correlated events remains low at 33% and 31% of the total NEMC catalog and 55% and 22% for the EW catalog for years 2004 and 2005 respectively (using <5 s <50 km correlation criteria). Further analysis of EW's uncorrelated seismic events is discussed in section 3.5.

In order to better understand the nature of correlated and uncorrelated NEMC earthquakes, epicenter plots were produced for both 2004 and 2005 grouped into magnitude ranges 2.0–2.9, 3.0–3.9, and 4.0–6.0. Results from 2005 which are nearly identical in character to year 2004 clearly show the effect of network sensitivity as detected by an unbiased observer, the EW auto-locating system.

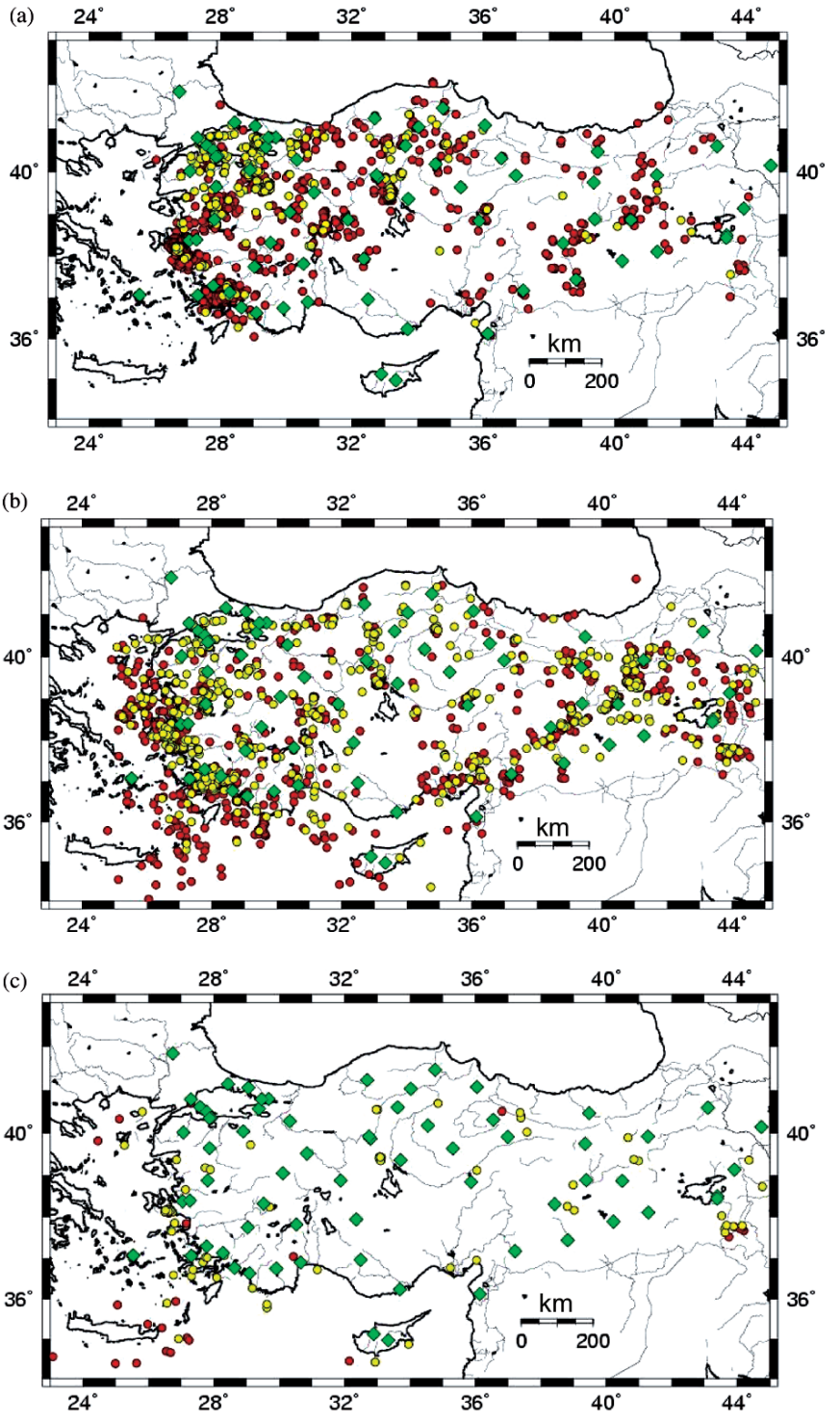
(a)
24°
28°
32°
36°
40°
44°
40°
36°
km
0
200
(b)
(c)

The magnitudes in the range 2.0–2.9 (Figure 1a) shows the best correlation in the northwest and moderately good correlation in north central Turkey. In northwestern Turkey the overall effective network density is higher and a concentration of more sensitive 3 component broadband sensors exists. In north-central Turkey relative effective network density is lower however the predominantly analog seismic stations in this area are consistently healthy. In the west and southwest there is a higher rate of uncorrelated events. This can be explained by the sparse network in areas such as the Izmir region where only 2 to at best 3 stations exists nearby. However in the Bodrum, Gökova Bay region of southwestern Turkey only 9 out of 152 earthquakes located by the NEMC were associated with the EW catalog. The network in this region is composed of a semi-circle arrangement of 4 broadband stations and one short period analog station which half surround the events in question. A look at the ESOH and digital data recovery reports for 2005 shows that broadband station FETY was non-operational for July-October during approximately half of the uncorrelated events in this region and short period station YER was non-operational from March-July during approximately 30% of the uncorrelated events. So the effective network during approximately 80% of the uncorrelated events consisted of 4 stations. This combined with weak arrivals from low magnitude events, noisy station sites (three broadband stations are located at radio tower sites on windy ridges and one broadband is located immediately adjacent to an industrial park) and the non-use of solutions constraining S phases may best explain why the EW system failed to locate events in this area.

In the magnitude range of 3.0–3.9 shown in Figure 1b the ratio of correlated to uncorrelated events has clearly increased relative to Figure 1a. With exception to the Aegean and Mediterranean Sea offshore regions uncorrelated and correlated events are mixed up in the same areas. This reflects that the majority of these events are above the intrinsic minimum magnitude threshold of the network. Figure 2 points out that this intrinsic minimum network detection magnitude threshold is approximately 3 for the manual event location procedure used by the NEMC. For earthquakes located in the offshore regions onshore stations are recording emergent arrivals and the azimuth gap can be very large. Emergent arrivals are often timed late by EW (0.5 to 3 s error) and the lack of S phases in auto-locations of such events can

Figure 1 Correlated EW vs. NEMC catalog events (yellow dots) and uncorrelated NEMC catalog events (red dots) from 2005 less months of February, March and May using a criteria of <5 s in origin time difference and <50 km epicentral difference. Stations belonging to the year 2005 "effective seismic network" are shown as green diamonds. ***(a)*** Magnitude range 2.0–2.9. Note relatively good performance of the EW system in the northwest as demonstrated by a higher density of correlated events. For earthquakes occurring in areas outside of the northwest where network coverage is sparse there are not a sufficient number of good quality station recordings per earthquake for an automatic system to perform well. ***(b)*** Magnitude range 3.0–3.9. Above the effective seismic network's average intrinsic low magnitude threshold of 3.0 there is no clear polarization of correlated and uncorrelated events with exception to offshore regions where azimuthal gaps and epicentral distance to first 3–4 stations are both large considerably hampering accurate auto-locations. In this magnitude range EW's location reliability is clearly improving relative to figure 1a but still remains below 100%. ***(c)*** Magnitude range 4.0–2.9. In this magnitude range EW auto-locations show nearly 100% correlations to the NEMC catalog. As with (a) and (b) uncorrelated events are still found in difficult to locate offshore areas

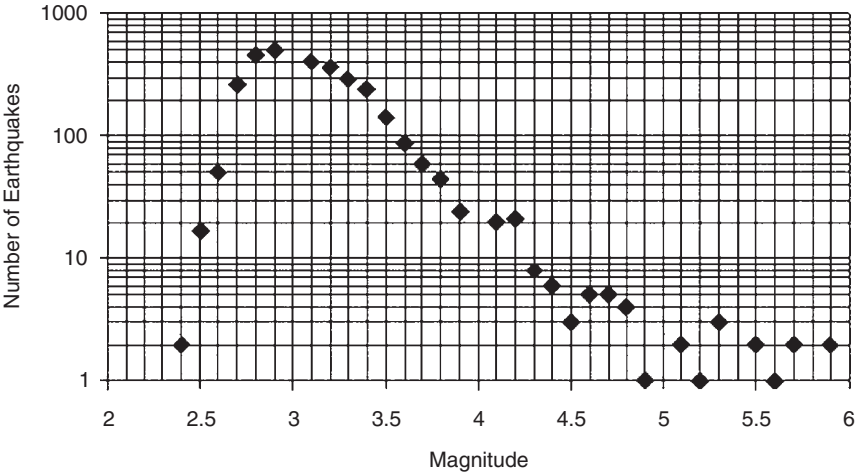

Figure 2 The number of events from NEMC's 2005 earthquake catalog used in this study plotted on a log scale vs. magnitude (90% of which are M_D). Note that the linear trend ends at magnitude 3.0 which represents the average lower magnitude sensitivity for KOERI's seismic network. The NEMC catalog should not be considered complete for events below magnitude 3.0

lead to very unreliable locations. These events may fail at any of 4 levels of the auto-processing. They may; fail to auto-associate, be rejected by the associater after initial association, be rejected by the final hypoinverse location process, or at least have a very large error in origin time and location. KOERI's EW auto-picker configuration has not been tuned. It remains the same as used by the Northern California Seismic Network (NCSN) run by the U.S. Geological Survey in Menlo Park whose seismic station density is more than 10 times greater than that operated by KOERI. Impulsive arrivals for the NCSN are in plentiful supply and the auto-picker is tuned for this. Perhaps the configuration for the EW picker could be better configured or even modified to more accurately time emergent arrivals common with sparse networks without losing the ability to pick impulsive onsets.

In the magnitude range of 4.0–5.5 (Figure 1c) there is nearly a 100% catalog correlation. Only a few events located principally far offshore in the west and southwest remain uncorrelated. Station sensitivity and density are sufficient in this magnitude range for reliable real-time auto-locations.

3.4 Low Magnitude Threshold Estimations for Reliable Earthquake Auto-Detection and Location

Figure 3 shows EW vs. NEMC earthquake correlation percentages relative to total events located by NEMC in 2005 plotted vs. magnitudes. The same < 5 s difference in origin time and < 50 km in epicentral offset criteria is being used here. If we

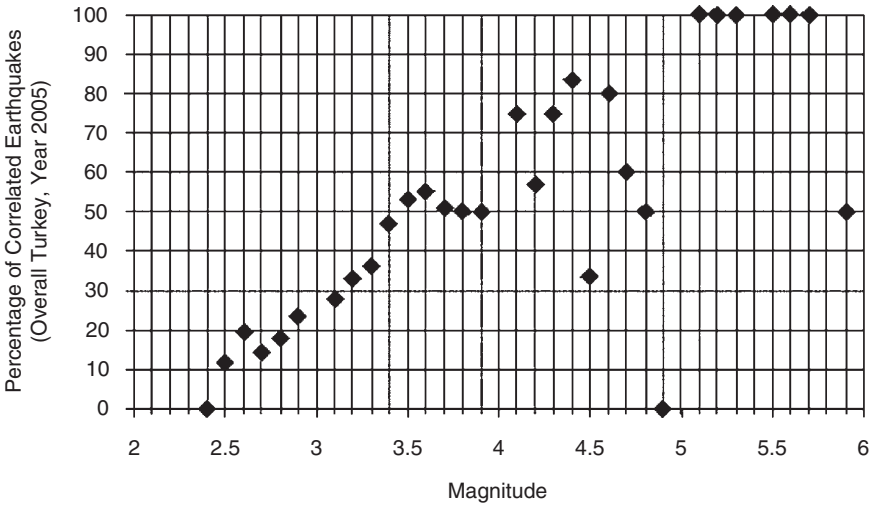

Figure 3 Based upon year 2005 EW and NEMC catalogs this plot shows the percentage of catalog correlated events (with respect to total events located by NEMC). Criteria used in the catalog correlation are <5 s origin time and <50 km epicentral differences. Linear extrapolation of non outlying data points above magnitude 3 give an estimated nationwide EW 90% auto-location reliability threshold of approximately magnitude 4.6. Data from 2004 using the same procedure gives a similar threshold magnitude of 4.4

extrapolate the linear trend of this plot it gives a 4.6 minimum magnitude threshold for 90% reliability of the EW automatic earthquake detection and location for the entire seismic network. A similar 90% reliability plot for the year 2004 (not shown) gives a magnitude threshold of 4.4. These nationwide results are estimates. They can be biased by improper magnitude estimation, incomplete earthquake catalog, limited data above magnitude 4.4 and catalog biasing of the 2.0–4.0 magnitude range from aftershock activity located in areas of sparse network coverage. With exception to magnitude determination all of the biasing effects are known to be present in this plot. For example significant numbers of aftershock earthquakes located by the NEMC from sparse network localities occurred in 2 areas in 2005. These zones being Bala, near Ankara with 291 events and Seferhisar, south of Izmir with 616 events. These 2 zones alone constitute 25% of the 2005 NEMC catalog being used in this study. Anomalous values seen in Figure 3 have epicenters in areas of sparse or no network. For example for magnitudes 3.7 to 3.8, 4.2, 4.5, 4.7 to 5.9 over 85% of these events are located either offshore Turkey to the west and south or in southeastern Turkey near the Iranian border. During the missed magnitude 5.9 event in Seferhisar (Oct. 20, 2140) EW's data server was down with virus problems. Some catalog biasing can be avoided if the EW auto-location threshold reliabilities are evaluated regionally.

It has already been pointed out that seismic network performance is not homogeneous. A closer analysis was made of the Marmara region in northwestern

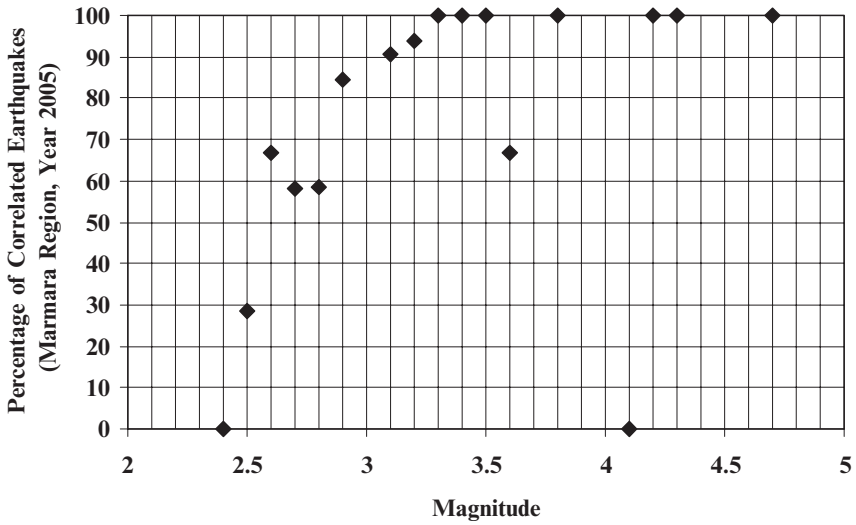

Figure 4 Based upon year 2005 EW and NEMC catalogs this plot shows the percentage of catalog correlated events within the Marmara Region of northwestern Turkey (with respect to total Marmara Region events located by NEMC). This plot shows clearly an estimated Marmara Region EW 90% auto-location reliability threshold of magnitude 3.1. Criteria used in the catalog correlation are <5 s origin time and <50 km epicentral differences. Events considered lie within the latitude range of 39.7 to 41.2 N and longitude range of 26.8 to 30.2 E

Turkey. This area is home to more than 25% of Turkey's population, Turkey's largest city, Istanbul, and a major share of the Turkey's industrial strength. In addition, this area is exposed to considerable threat of a major earthquake which has and likely will be linked to activity associated with the major east-west striking North Anatolian Transform Fault. Figure 4 shows an EW 90% reliable auto-location magnitude threshold of approximately 3.1 for the Marmara Region. During the anomalous magnitude 4.1 event (Nov., 4 2012 UTC) shown in Figure 4 the EW data acquisition and real-time server was not functioning due to a system virus. The uncorrelated magnitude 3.6 event was located by EW's event associater but then killed due to one or more spurious picks.

3.5 A Pilot Study on Uncorrelated Auto-Located Events

As Table 4 shows large numbers of uncorrelated events are found in both the EW and NEMC catalogs. We know that the NEMC uncorrelated events are earthquakes and have already discussed reasons why some of these earthquakes were not detected by the EW system. So what is the nature of the uncorrelated EW events? To find out a detailed look at uncorrelated EW auto-located events from April of 2005 was undertaken. First the April events were viewed and categorized as either

seismic event or noise. The seismic events were then correlated with the NEMC April 2005 catalog. The EW catalog earthquakes that did not correlate with the NEMC April 2005 catalog were then timed and re-located manually and then correlated for a second time with the original NEMC April catalog. The numerical results of this analysis are shown in Table 5 below. Remarkably on the second correlation attempt only 14 or 12% of the total 133 manually re-located EW seismic events correlated with the April 2005 NEMC catalog. To be sure these EW auto-located events were not later discovered in the formation of NEMC's final catalog the same events were correlated with the final April 2005 NEMC catalog giving no difference in the result. Of the 119 uncorrelated EW seismic events 82% locate in northwestern Turkey which includes the seismically active Marmara Region (Lat. range 39.0 – 41.0 N, Long. Range 27.0 – 30.0 E). As shown previously the EW system's detection sensitivity is above average for this area. A summary of the results are shown in the last row of Table 5. For April of 2005 the combining of both automatic and manual earthquake location methods would have increased the number of real-time detected seismic events by nearly 30%.

Table 5 Pilot study for April 2005 data showing results from the re-location of uncorrelated EW auto-located earthquakes

Description	Results
Number of original events from each catalog for April of 2005	EW 388, NEMC 285
Number of seismic and noise events manually found from viewing the EW catalog's associated auto-event files	251 Seismic events, 137 Noise events
Result of 251 EW seismic events cross correlated with NEMC's April catalog with a criteria of <5 s origin time difference and <50 km epicentral offset.	84 Correlated, 167 Uncorrelated
Results of manual locations of 167 uncorrelated EW seismic events.	133 located, 7 teleseisms, 27 not locatable (magnitude too small, not enough stations etc.).
Location details of the 133 manually located EW auto-detected seismic events	Avg. azimuthal gap 208 degrees (58 events <200) Avg. number of picks per event 8.1 Avg. number of stations per event 5.8 Avg. RMS 133 events 0.83
The 133 events manually located EW were again correlated with the Apr 2005 NEMC catalog with a criteria of <5 s origin time difference and <50 km epicentral offset.	14 Correlated, 111 Uncorrelated
Summary of Results There were a combined number of 438 seismic events. Numbers to the right give the percentage in each group.	Only NEMC located 43% Only EW located 27% Jointly located by EW and NEMC 22% Other 8%

4 Re-design and Expansion of KOERI's Digital Broadband Seismic Station Network

4.1 Introduction

Experience in the Broadband Group gained from 3 years of managing, modifying, troubleshooting and monitoring seismic data quality from KORTASDPS prompted a shift in efforts toward modernizing the aging analog seismic station network which feeds KORTASDPS. In March of 2003 a 3 year institute level project was created whose goal was to re-design and expand KOERI's digital broadband seismic network which at that time consisted of four operational stations. Since the initiation of this project the digital broadband seismic network has increased to a total of 33 stations (December, 2005) with an additional 10 international stations arriving in real-time via the Internet (Figure 5). Since 2004 the NEMC has carried on the task of installing and maintaining the most recent broadband stations however a significant number of broadband stations continue to be managed by the Broadband Group.

4.2 General Overview of Re-Designed Broadband Station

All new broadband stations are equipped with a grounding coil and a 220 VAC and phone line voltage surge protection units. Each station has enough backup power to run autonomously for approximately 1 week. Sensor vaults are designed to be thermally

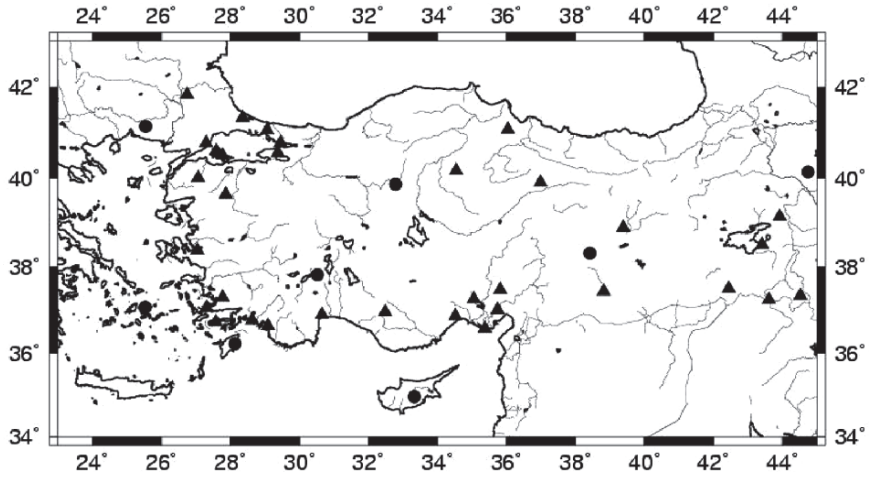

Figure 5 The KOERI real-time broadband station map, December of 2005. Thirty three KOERI operated stations are shown as black triangles and 10 international real-time data exchange stations from FDSN network codes: GE, HL and IU are shown as black circles. Note since March of 2003 there has been greater than a 7 fold increase in permanent KOERI digital broadband stations alone

isolated and an attempt is made to select secure and quiet sites which are also near enough to some form of data communication link. Several data telemetry methods are being used currently. These include: digital lease line, Internet, analog lease line, digital radio, and satellite. The new broadband station design has proven to be inexpensive and robust. Many of the stations installed in 2003 and early 2004 have been in continuous operation since their installation despite the fact that they have not received any maintenance visits. The largest problem to date has centered on the poor service provided by the telecommunications organization.

5 Real-Time Data Exchange and Archiving

5.1 Real-Time Seismic Data Exchange

The rapid increase in high-quality broadband seismic data and improvements in the data collection and processing infrastructure at KOERI has made its position in the international seismic community as a provider of data products much more attractive and attainable. In 2003 the Broadband Group, in cooperation with the ORFEUS Data Center located in the Netherlands, established a first ever real-time sharing of data from KOERI owned broadband stations across the internet using the Seiscomp software suite (Hanka, et. al. 2000). Real-time international seismic data exchange is currently ongoing with the following partners: The National Observatory of Athens (NOA - Athens, Greece), The National Research Centre for Geosciences (GFZ - Potsdam, Germany), The Albuquerque Seismology Laboratory (Albuquerque, USA), The Observatories and Research Facilities for European Seismology (ORFEUS - De Bilt, Netherlands). Such "cross-border" sharing of information is a necessity for most countries interested in earthquakes just outside their borders and helps to create strong international working relationships which are valuable to the scientific community as a whole.

5.2 Seismic Data Archiving

Two separate semi-redundant seismic data archive systems are being operated within KOERI as a crucial component of the KORTASDPS. The primary system run by the NEMC and the secondary or backup system run by the Broadband Group. Comparisons of both systems are summarized below in Table 6.

5.3 Future Developments in Digital Broadband Seismology at KOERI

Kandilli Observatory has a project scheduled to begin in 2006 which will provide for the expansion of the permanent broadband digital network to approximately 55 stations nationwide along with the creation of a 52 broadband instrument pool

Table 6 Comparison of archiving system capabilities for the NEMC and the Broadband Group

Description	NEMC archive	Broadband group archive
Capacity	3 Terabytes	1 Terabyte
Data Format	SAC	SAC
Data Products	Continuous data all stations since Manually extracted event data	Continuous broadband data Manually extracted event data EW auto-event data
Data Accessibility	Public internet access to all waveform data	Data used internally for research. System is a secondary backup to the primary NEMC archive.
Long Term Storage	Data backed up monthly to stable media	Data backed up monthly to stable media

which will be managed by the Geophysics Dept. Also plans exist to increase the number of seismic data and information exchange partners both internationally and nationally thereby stimulating cooperative seismological research and more efficient use of high-quality data gathering resources for all.

6 Conclusions

Since 2000 there have been rapid improvements to the seismic data collecting, processing and archiving infrastructure at the Kandilli Observatory and Earthquake research Institute, Bogaziçi University. The establishment of the complex but robust Kandilli Observatory Real-Time Automated Seismic Data Processing System initiated in 2000–2001 has become the centerpiece of day to day earthquake monitoring operations conducted by the NEMC and has provided easy access to important data products used by the public, decision makers and researchers. Several years of operation and information collection has enabled the quantitative performance evaluation of the earthquake auto-detection and location core of KORTASDPS which uses the EW software suite.

EW's ability to auto-detect and properly locate events is, directly dependent on the earthquakes magnitude, its epicentral distance with respect to the first 4 nearby functioning seismic stations, station azimuthal coverage, and station sensitivity. For magnitudes ranging from 4.0 to 5.5 EW locates nearly 100% of the events with exception to distant events locating offshore to the west and south of Turkey. For magnitudes ranging from 3.0 to 3.9 EW's auto-event location performs moderately well throughout mainland Turkey. Exceptions are the high performance in the northwest Marmara region and the low performance offshore to the west and south. For magnitudes ranging from 2.0 to 2.9 EW performs well in northwestern Turkey where station density and sensitivity are relatively high. The four proposed primary reasons for EW performance deficit are that the EW auto-picks late if at all emergent arrivals, S phases are not used in the location solution, EW is configured to a 4 station minimum as

compared to 3 used by the NEMC and data comes from a low density "effective" seismic network (11634 km^2/station for 2005) composed of a large percentage of low sensitivity stations. Reduction of the hypocenter solution station minimum to 3 will probably cause large increases in spurious locations and noise events. Efforts should therefore be focused on one or more of the 3 remaining problem areas in order to improve EW's auto-detection and location accuracy. Network expansion and upgrade, already underway, has proven effective by increasing the auto-located seismic/noise event ratio thereby lowering the magnitude auto-detection threshold.

Based upon catalog correlation results quantitative analysis of years 2004 and 2005 shows that EW has nationwide a 90% auto-event detection and location reliability lower magnitude threshold with respect to the NEMC catalog between 4.4 – 4.6. Similar analysis for the high seismic risk Marmara Region in northwestern Turkey shows a 90% auto-event detection and location reliability lower magnitude threshold of 3.1. Auto-located earthquake above these magnitudes thresholds could be used as part of a pilot web page based rapid earthquake notification system.

Large percentages of known EW auto-located seismic events remain uncorrelated. The April 2005 pilot study shows that nearly one third of the April of 2005 earthquakes combined from the NEMC and EW catalogs can evade manual detection methods used by the NEMC. The review of auto-locations by NEMC analysts would therefore improve the completeness of real-time earthquake monitoring operations.

Recent expansion and design improvements of KOERI's seismic network including a 7 fold expansion of the digital broadband network in the last 2 years and the planned continued expansion will certainly lower the minimum magnitude threshold for automatic earthquake detection and locations produced by KORTASDP. The now open availability of this new high quality seismic data both in real-time and offline will provide an endless source of fuel for future seismological investigations in Turkey.

Acknowledgements We would like to thank Gonca Örgülü and Doğan Aksari for their work on the KORTASDPS archive sub-system, David Oppenheimer and Lynn Dietz of the United States Geological Survey, Northern California Seismic Network for providing the initial ideas and technical support for the prototype EW system, and the National Earthquake Monitoring Center for providing earthquake catalogs and associated information.

References

Childs, D., Komeç, A., 2003. The Kandilli Observatory Real-Time Automated Seismic Data Processing System, *ORFEUS Newsletter, March, 2003*.
http://www.orfeus-eu.org/newsletter/vol5no1/vol5no1.pdf

Hanka, W., Heinloo, A. and Jäckel, K.-H., Networked Seismographs: GEOFON Real-Time Data Distribution, *ORFEUS Newsletter, December, 2000*.
http://www.orfeus-eu.org/newsletter/vol2no3/vol2no3.pdf

Johnson, C.E., Bittenbinder A., Bogaert B., Dietz L., and Kohler W., 1995. EW: A Flexible Approach to Seismic Network Processing, IRIS Newsletter 14(2), 1–4.

Part V
Seismic Hazard Analysis and Assessment

Data Driven Probabilistic Seismic Hazard Assessment Procedure for Regions with Uncertain Seimogenic Zones

Andrzej Kijko*

Abstract An alternative methodology for probabilistic seismic hazard analysis (PSHA), is described. The approach combines the best features of the "deductive" (Cornell, 1968) and "historical" (Veneziano et al., 1984) procedures. The maximum regional magnitude m_{max} is of paramount importance in this approach and the author present statistical technique that can be used for evaluation of this important parameter. The approach permits the utilization of incomplete and uncertain earthquake catalogues. The technique has been developed specifically for the estimation of seismic hazard at individual sites, without the subjective judgment involved in the definitions of seismic-source zones.

Keywords seismic hazard, m_{max}, incomplete catalogues, no seismic source zones

1 Introduction

Following McGuire (1993), existing procedures of probabilistic seismic hazard analysis (PSHA) fall into two main categories: deductive and historic. The theoretical base for the deductive method was formulated by Cornell (1968). The approach permits the incorporation of geological and geophysical information to supplement the earthquake catalogues. Application of the procedure includes several steps. The initial step requires definition of potential seismic sources, usually associated with geological or tectonic features like faults, and delineation of potentially active regions (zones) over which all available information is averaged. In the next step, seismicity parameters are determined for each seismogenic source zone. Following the most common assumptions made in engineering seismology, viz. that earthquakes are described by a Poisson process and that earthquake magnitudes follow a

Council for Geoscience, Geological Survey of South Africa, Private Bag X112, Pretoria 0001, South Africa

* To whom correspondence should be addressed. email: kijko@geoscience.org.za

E.S. Husebye (ed.), *Earthquake Monitoring and Seismic Hazard Mitigation in Balkan Countries.*

Gutenberg-Richter doubly truncated distribution, the parameters for each seismogenic source zone are: mean seismic activity rate λ (which is the parameter of the Poisson distribution), the level of completeness of the earthquake catalogue m_{min}, the maximum earthquake magnitude m_{max}, and the Gutenberg-Richter parameter b. Assessment of the above parameters requires a seismic event catalogue containing origin times, size of seismic events and spatial locations. Perhaps, then, this allows the calculation of a probability density function (PDF) of distance to the specified site. In the next step a ground-motion relation is selected, giving the cumulative distribution function (CDF) for a required ground motion parameter. The final step requires the integration of individual contributions from each seismogenic zone into a site-specific distribution.

Probably the strongest point of any deductive-type procedure of PSHA is its ability to account for all sorts of deviations from the "standard" model, i.e. it accounts for phenomena such as migration of seismicity, or seismic "gaps". This is possible because the procedure is parametric by nature. Unfortunately, the deductive procedure also has significantly weak points. The major disadvantage stems from the requirement of specifying the seismogenic source zones. Often tectonic provinces or specific active faults have not been identified and mapped and causes of seismicity are not well understood. In addition, the Cornell-based seismic hazard assessment procedure requires, for each zone, a knowledge of the model parameters which cannot be determined reliably for areas that are small or have very incomplete seismic histories.

The second category of PSHA consists of the so-called historic methods (Veneziano et al., 1984), which, in their original form, are non-parametric. These methods require as input data information about past seismicity only, and do not require specification of seismogenic zones. For each historic earthquake, the empirical distribution of the required seismic hazard parameter is estimated by using its value of magnitude, epicentral distance and assumed ground motion attenuation relation. By normalizing this distribution for the duration of the seismic event catalogue, one obtains an annual rate of the exceedance of the required hazard parameter. The major advantage of the method is that a specification of seismogenic source zones is not needed. Furthermore the approach does not require designation of the model. By its nature, the historic method works well in areas of frequent occurrence of strong seismic events, when the record of past seismicity is "reasonably" complete. At the same time, the non-parametric historic approach has significantly weak points. Its primary disadvantage is probably its poor reliability in estimating small probabilities for areas of low seismicity. The procedure is not recommended for an area where the seismic event catalogues are highly incomplete. In addition, in its present form, the procedure is not capable of making use of any additional geophysical or geological information to supplement the pure seismological data. Therefore, a procedure that accepts the varying quality of different parts of the catalogue and does not require specification of seismic source zones would be an ideal tool for analyzing and assessing seismic hazard.

Bearing in mind both the weak and strong points of the above two approaches, the author propose an alternative procedure, which, following the scheme of

McGuire, could be classified as a parametric-historic approach. The new approach combines the best of the deductive and non-parametric historic procedures and, in many cases, is free from the basic disadvantages characteristic of each of the procedures. Since in the proposed approach the maximum regional magnitude m_{max} is of paramount importance, the author present a statistical technique that can be used for evaluation of this important parameter.

2 Estimation of Maximum Regional Magnitude m_{max}

At present there is no generally accepted method for estimating the value of the maximum regional magnitude m_{max}. The methods for evaluating m_{max} fall into two main categories: deterministic and probabilistic.

The deterministic procedure most often applied is based on the empirical relationships between the magnitude and various tectonic and fault parameters. The relationships are variously developed for different seismic areas and different types of faults. In most cases, unfortunately, the value of the parameter m_{max} determined by means of any deterministic procedure is very uncertain. The value of m_{max} can also be estimated purely on the basis of the seismological history of the area, viz. by utilizing seismic event catalogues and appropriate statistical estimation procedures. In this section the author present statistical procedure which can be used for the evaluation of the maximum regional magnitude m_{max}. It is assumed that both the analytical form and the parameters of the distribution functions of earthquake magnitude are known.

Suppose that in the area of concern, within a specified time interval T, there are n main seismic events with magnitudes $M_1, M_2, \ldots, M_n$. Each magnitude $M_i \geq m_{min}$ ($i = 1, \ldots, n$), where m_{min} is a known threshold of completeness (i.e. all events having magnitude greater than or equal to m_{min} are recorded or have been felt in case of macroseismic observations). It is further assumed that the seismic event magnitudes are independent, identically distributed, random values with PDF, $f_M(m|m_{min},m_{max})$ and CDF, $F_M(m|m_{min},m_{max})$ respectively. Parameter m_{max} is the upper limit of the range of magnitudes and thus denotes the unknown maximum regional magnitude which is to be estimated. For the Gutenberg-Richter relation, which is a frequency-magnitude relation, the respective CDF of earthquake magnitudes which are bounded from above by m_{max}, is

$$F_M(m|m_{min},m_{max}) = \begin{cases} 0, & for\ m < m_{min}, \\ \dfrac{1-\exp\left[-\beta\left(m-m_{min}\right)\right]}{1-\exp\left[-\beta\left(m_{max}-m_{min}\right)\right]}, & for\ m_{min} \leq m \leq m_{max} \\ 1, & for\ m > m_{max}. \end{cases} \quad (1)$$

where $\beta = b\ln(10)$, and b is the b-parameter of the Gutenberg-Richter relation.

From the condition that compares the largest observed magnitude m_{max}^{obs} and the maximum expected magnitude during a specified time interval T, after integrating by parts and simple transformations, the maximum regional magnitude m_{max} is (Kijko, 2004)

$$\hat{m}_{\max} = m_{\max}^{obs} + \int_{m_{\min}}^{m_{\max}^{obs}} \left[F_M(m | m_{\min}, m_{\max}^{obs}) \right]^n dm \tag{2}$$

Further modifications of estimator (2) are straightforward. For example, following the assumption that the number of earthquakes occurring in unit time within a specified area obeys the Poisson distribution with parameter λ, after replacing n by λT, estimator (2) becomes

$$\hat{m}_{\max} = m_{\max}^{obs} + \int_{m_{\min}}^{m_{\max}^{obs}} \left[F_M(m | m_{\min}, m_{\max}^{obs}) \right]^{\lambda T} dm \tag{3}$$

It is not difficult to show that for the Gutenberg-Richter-based magnitude CDF (1), the estimator (3) takes the form

$$\hat{m}_{\max} = m_{\max}^{obs} + \frac{E_1(Tz_2) - E_1(Tz_1)}{\beta \exp(-Tz_2)} + m_{\min} \exp(-\lambda T) \tag{4}$$

where $z_1 = -\lambda A_1 / (A_2 - A_1)$, $z_2 = -\lambda A_2 / (A_2 - A_1)$, $A_1 = \exp(-\beta m_{\min})$, $A_2 = \exp(-\beta m_{min}^{obs})$, and $E_1(\cdot)$ denotes an exponential integral function. The above estimator of $m_{\max}$ for the doubly truncated Gutenberg-Richter relation was first obtained by Kijko (1983), who was inspired by discussions with M.A. Sellevoll. Therefore, equation (4) will be denoted as the Kijko-Sellevoll estimator or, in short, K-S. From equations (3) and (4), the approximate variance of the maximum regional magnitude $\hat{m}_{\max}$, estimated according to the K-S procedure, is

$$Var\left(\hat{m}_{\max} \right) = \sigma_M^2 + \left[\frac{E_1(Tz_2) - E_1(Tz_1)}{\beta \exp(-Tz_2)} + m_{\min} \exp(-\lambda T) \right]^2 \tag{5}$$

where σ_M^2 is the variance in the determination of the largest observed magnitude $m_{\max}^{obs}$.

It should be noted that the above approach has several limitations. One of these is the assumption that the β-value in the CDF $F_M(m \mid m_{\min}, m_{\max})$ is known without error. However, β-value uncertainties can be taken into account. Following the assumption that the variation of the β-value in the Gutenberg-Richter-based CDF (1) may be represented by a gamma CDF having parameters p and q, the compound CDF of earthquake magnitudes takes the form (Campbell, 1982)

$$F_M(m | m_{\min} m_{\max}) = \begin{cases} 0 & for\ m < m_{\min}, \\ C_\beta \left\{ 1 - \left[p | \left(p + m - m_{\min} \right) \right]^q \right\}, & for\ m_{\min} \le m \le m_{\max}, \\ 1, & for\ m > m_{\max}. \end{cases} \tag{6}$$

where C_β is a normalizing coefficient. It is not difficult to show that p and q can be expressed through the mean and variance of the β-value, where $p = \bar{\beta}/(\sigma_\beta)^2$ and $q = (\bar{\beta}/\sigma_\beta)^2$. The symbol $\bar{\beta}$ denotes the mean value of the parameter β, σ_β is

the known standard deviation of $\bar{\beta}$ and describes its uncertainty, and C_β is equal to $1/\{1-[p/(p+m_{max}-m_{min})]^q\}$. Equation (6) is known as the Bayesian Exponential-Gamma CDF of earthquake magnitude. Knowledge of equation (6) makes it possible to construct the Bayesian version of the estimator K-S. Thus, following (3) and (5), and through an application of Cramer's approximation, the Bayesian extension of the K-S estimator and its approximate variance becomes

$$\hat{m}_{\max} = m_{\max}^{obs} + \frac{\delta^{1/q}\exp\left[nr^q/\left(1-r^q\right)\right]}{\beta}\left[\Gamma\left(-1/q,\delta r^q\right)-\Gamma\left(-1/q,\delta\right)\right] \tag{7}$$

$$Var\left(\hat{m}_{\max}\right) \cong \sigma_M^2 + \left\{\frac{\delta^{1/q}\exp\left[nr^q/\left(1-r^q\right)\right]}{\beta}\left[\Gamma\left(-1/q,\delta r^q\right)-\Gamma\left(-1/q,\delta\right)\right]\right\}^2 \tag{8}$$

where $\delta = nC_\beta$ and $\Gamma(\cdot,\cdot)$ is the Complementary Incomplete Gamma Function. The Bayesian version of the K-S estimator will be denoted as K-S-B. From the above relations it follows that the assessment of the maximum regional magnitude m_{max} requires knowledge of the area-specific mean seismic activity rate λ and the Gutenberg-Richter parameter b. The maximum likelihood procedure for the assessment of these two parameters is presented in the following sections. Extensive comparisons of performances of K-S and K-S-B estimators are given by (Kijko and Graham, 1998; Kijko, 2004).

3 Assessment of Area-Specific Parameters in Case of Incomplete Data Sets

Since the technique applied for assessment of area-specific seismic hazard parameters is similar to the procedure already described by Kijko and Sellevoll (1992), only the main points of the procedure are presented. Let us assume that in the vicinity of the specified site of the hypothetical engineering structure (HES) (i) the occurrence of the main seismic events in time can be described by a Poissonian process with an area-specific mean activity rate λ, and (ii) earthquake magnitudes are distributed according to the doubly truncated Gutenberg-Richter-based relation (1). Then, the CDF of the largest magnitudes occurring during the time interval t, is (Kijko and Sellevoll, 1992)

$$F_M^{\max}\left(m\middle|m_0,m_{\max},t\right) = \exp\left\{-\lambda_0 t c F_M\left(m\middle|m_0,m_{\max}\right)\right\} \tag{9}$$

where $cF_M(m \mid m_0,m_{max}) = 1-F_M(m \mid m_0,m_{max})$, $\lambda_0 \equiv \lambda(m_0) = \lambda cF_M(m_0 \mid m_{min},m_{max})$ is the mean activity rate of earthquake occurrence within the specified area with magnitude m_0 and above where m_0 is the lower earthquake magnitude in the extreme part of the catalogue, and $m_0 \geq m_{min}$. The parameter $\lambda \equiv \lambda(m_{min})$ is the mean activity rate of

earthquakes with magnitude $m_{\min}$ and above. Magnitude $m_{\min}$ is the minimum threshold magnitude for the entire catalogue (Figure 1).

If the error in the determination of magnitude is assumed to be normally distributed with standard deviation σ_M (Tinti and Mulargia, 1985), the CDF of the apparent magnitude becomes (Gibowicz and Kijko, 1994)

$$F_M\left(m\middle|m_{\min},m_{\max},\sigma_M\right)=F_M\left(m\middle|m_{\min},m_{\max}\right)\cdot D\left(m,\sigma_M\right) \tag{10}$$

where $D(m,\sigma_M) = \{A_1[\mathrm{erf}(y_1) + 1] + A_2[\mathrm{erf}(y_2) - 1] - 2C(m,\sigma_M)A(m)\}/2[A_1 - A(m)]$, $C(m,\sigma_M) = 0.5\exp(\chi^2)[\mathrm{erf}(y_1 + \chi) + \mathrm{erf}((y_2 - \chi)]$, $y_1 = (m-m_{\min})/\sqrt{2}\ \sigma_M$, $y_2 = (m_{\max} - m)/\sqrt{2}\ \sigma_M$, where σ_M denotes the standard error of earthquake magnitude determination, $A(m) = \exp(-\beta m)$, $A_1 = \exp(-\beta m_{\min})$, $A_2 = \exp(-\beta m_{\max})$, and $\mathrm{erf}(\cdot)$ is the error function, $\chi = \beta\sigma_M / \sqrt{2}$, and the magnitude m is unbounded from both ends. Further application of CDF (10) requires additional renormalizations. If m_C is the cut-off value of apparent magnitude, at and above which the earthquakes are complete, then its normalized CDF $\tilde{F}_M(m|m_C, m_{\max}, \sigma_M)$ is zero up to m_C, and is equal to $F_M(m \mid m_{\min},m_{\max},\sigma_M)/[1 - F_M(m_C \mid m_{\min}, m_{\max}, \sigma_M)]$ for $m \geq m_C$. Finally, from the assumed model of apparent magnitude it follows that the "true" mean activity rate $\lambda(m)$ must be replaced by its "apparent" counterpart, $\tilde{\lambda}(m)$ according to the approximate relation $\tilde{\lambda}(m) = \lambda(m)\cdot\exp(\kappa^2)$.

From the definition of PDF and from relations (9) and (10) it follows that the PDF of the strongest earthquake within a period t with apparent magnitude $m \geq m_0$ and standard deviation σ_M, is

$$\begin{aligned} &f_M^{\max}\left(m\middle|m_0,m_{\max},t,\sigma_M\right)\\ &=\tilde{\lambda}_0\tilde{t}f_M\left(m\middle|m_0,m_{\max},t,\sigma_M\right)\cdot\exp\left[-\tilde{\lambda}_0 tc\tilde{F}_M\left(m\middle|m_0,m_{\max},t,\sigma_M\right)\right] \end{aligned} \tag{11}$$

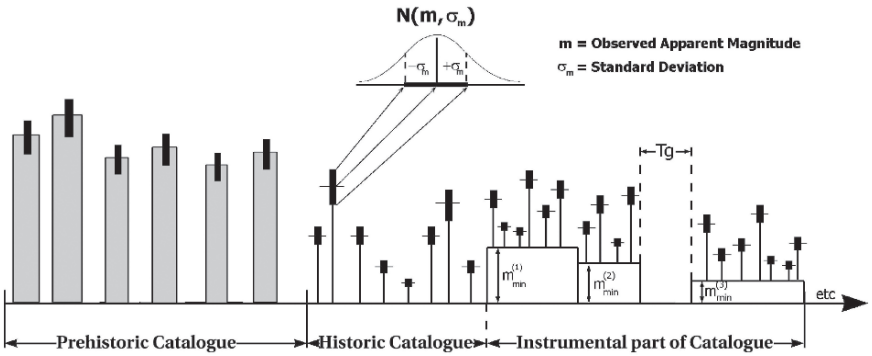

Figure 1 Data which can be used to obtain seismic hazard parameters for the area in the vicinity of the selected site. The approach permits the combination of largest earthquake data and complete data having variable threshold magnitudes

where $c\tilde{F}_M(m|m_0, m_{max}, t, \sigma_M) = 1 - \tilde{F}_M(m|m_0, m_{max}, t, \sigma_M)$. After introducing the PDF (11), one can construct the likelihood function of the strongest earthquake magnitude from the extreme part of the catalogue. Such a function depends on the unknown area-characteristic parameters (λ,β), and becomes

$$L_0(\lambda,\beta) = const \prod_{j=1}^{n_0} f_M^{\max}\left(m_{0j}\middle|m_0, m_{\max}, t_{0j}, \sigma_{M0j}\right) \tag{12}$$

In relation (12), the m_{0j} is the apparent magnitude of the strongest earthquake occurring during the time interval t_j, σ_{M0j} is the value of its standard deviation, $j = 1, \ldots, n_0$, and n_0 is the number of earthquakes in the extreme part of the catalogue.

It is assumed that the second, complete part of the catalogue can be divided into s sub-catalogues (Figure 1). Each of them has a time span T_i and is complete, starting from the known magnitude $m_{min}^{(i)}$. For each sub-catalogue i, m_{ij} is the apparent magnitude, and σ_{Mij} is its standard deviation, $j = 1, \ldots, n_i$, where n_i denotes the number of earthquakes in each complete sub-catalogue and i = 1, …, s. If the size of seismic events is independent of their number, the likelihood function of earthquake magnitudes present in each complete sub-catalogue i, is equal to $L_i(\lambda,\beta) = L_i(\beta)\, L_i(\lambda)$, which is the product of the function of β, $L_i(\beta)$, and the function of λ, $L_i(\lambda)$. Following the definition of the likelihood function of a set of independent observations, the function $L_i(\lambda)$ is given by $const \prod \tilde{f}_M(m_{ij}|m_{min}^{(i)}, m_{max}, \sigma_{Mij})$. The assumption that the number of earthquakes per unit time is a Poisson random variable gives a form of $L_i(\lambda)$ equal to $const\ (\tilde{\lambda}_i t_i)^{n_i}\ ex(-\tilde{\lambda}_i t_i)$, where const is a normalizing factor and $\tilde{\lambda}_1$ is the apparent, mean activity rate for the complete sub-catalogue i. For the ith complete sub-catalogue the true mean activity rate is equal to $\lambda_i \equiv \lambda(m_{min}^{(i)}) = \lambda c F_M(m_{min}^{(i)}|m_{min}, m_{max})$. Functions $L_i(\beta)$ and $L_i(\lambda)$, for $i = 1, \ldots, s$, define the likelihood functions for each complete sub-catalogue. Finally, the joint likelihood function of all data in the catalogue, extreme and complete, is given by:

$$L(\lambda,\beta) = \prod_{i=0}^{n_s} L_i(\lambda,\beta) \tag{13}$$

The maximum likelihood estimates λ and β are the values of $\hat{\lambda}$ and $\hat{\beta}$ that maximize the likelihood function (13). From a formal point of view, the maximum likelihood estimate of m_{max} is simply the largest observed earthquake magnitude m_{min}^{obs}. This follows from the fact that the likelihood function (13) decreases monotonically for $m_{max} \to \infty$. Therefore, by including one of the formulae for m_{max} [the K-S estimator (4) or its Bayesian version (eq. 7)] and by putting $\partial \ln L(\lambda,\beta)/\partial\lambda = 0$ and $\partial \ln L(\lambda,\beta)/\partial\lambda = 0$, we obtain a set of equations determining the maximum likelihood estimate of the area-specific parameters $\hat{\lambda}$, $\hat{\beta}$ and $\hat{m}_{max}$. Such a set of equations is given by Kijko and Sellevoll (1992), and can be solved by an iterative scheme.

4 Assessment of Seismic Hazard for a Given Site

To express seismic hazard in terms of peak ground acceleration (PGA) the aim would be to calculate the conditional probability that a single earthquake of random magnitude M at a random distance R will cause a PGA equal to, or greater than, an acceleration of engineering interest $a_{\min}$. For this purpose the assumption is used that in the range of interest the attenuation curve of the PGA a, has the following form:

$$\ln(a) = c_1 + c_2 \cdot M + \phi(R) + \varepsilon \tag{14}$$

where c_1 and c_2 are empirical constants, M is the earthquake magnitude, and $\phi(R)$ is a function of earthquake distance R. The term ε is the random error which has been observed to have a normal (Gaussian) distribution. Usually $\phi(r)$ is of the form $c_3 \cdot R + c_4 \cdot \ln(R)$, where c_3, and c_4 are empirical constants and $\ln(\cdot)$ denotes the natural logarithm. It can be seen that an application of a straightforward approach, like Cornell's (1968), implies that after γ normalization, the CDF of the logarithm of PGA is:

$$F_X\left(x \middle| x_{\min}, x_{\max}\right) = \frac{\exp\left(-\gamma x_{\min}\right) - \exp\left(-\gamma x\right)}{\exp\left(-\gamma x_{\min}\right) - \exp\left(-\gamma x_{\max}\right)} \tag{15}$$

where $x = \ln(a)$, $\gamma = \beta / c_2$, $x_{\min} = \ln(a_{\min})$, $x_{\max} = \ln(a_{\max})$, and $a_{\max}$ is the maximum possible PGA at the site. From relation (15) it follows that at any given site the logarithm of the PGA is distributed according to the same type of distribution as earthquake magnitude, i.e. negative exponential – the form of the familiar Gutenberg-Richter distribution. The two distributions differ only in the value of their parameters. If the parameter of magnitude distribution is equal to β, the parameter of the distribution of $\ln(PGA)$ is equal to β / c_2.

Equation (15) also implies that the CDF of the logarithm of the largest PGA recorded at the site, within a period of time t, is described by an equation, which is analogous to (9). The CDF of the logarithm of the largest PGA observed at the site is doubly truncated. The first truncation from the bottom, $x_{\min} = \ln(a_{\min})$, represents the chosen threshold of acceleration of engineering interest. The second truncation, $x_{\max} = \ln(a_{\max})$ is an unknown parameter representing the logarithm of the maximum possible PGA at the site. Therefore, for a given $a_{\min}$, the seismic hazard at the site is determined by three parameters: λ, γ and $a_{\max}$.

In order to estimate these parameters, the largest PGAs $a_1, \ldots, a_n$ felt at the site of interest are selected from n consecutive time intervals $t_1, \ldots, t_n$, and the maximum likelihood procedure is used. For a specified $a_{\max}$, the likelihood function of the sample $x_1 = \ln(a_1), \ldots, x_n = \ln(a_n)$ is a function of the unknown parameters λ and γ, and is analogues to (12), the parameter β is replaced by γ, the activity rate for the area, λ, is replaced by the activity rate at the site, λ, and the maximum observed magnitude $m_{\max}^{obs}$ is replaced by the logarithm of the maximum observed PGA, $\ln(a_{\max}^{obs})$.

Similarities between the site-characteristic and area-characteristic distribution functions have further important consequences. From the fact that the CDF of earthquake magnitudes (eq. 1) and the logarithm of PGA recorded at the site (eq. 15) are of the same type, it follows that the value of the maximum possible PGA at the site a_{max} can be estimated according to the same procedure as m_{max}, where in the formulae (1) the respective replacements of parameters are made.

5 Example of Application

5.1 Probabilistic Seismic Hazard Assessment for Specified Site

As an illustration, the procedure as described above was used to estimate the seismic hazard parameters at the site of a hypothetical engineering structure (HES) with latitude $\phi = 33.4$ S and longitude $\lambda = 19.24$ E, located in the territory of South Africa. It is assumed that no information was available which could provide a firm basis for identification and grading of seismic source zones. The procedures were applied to seismic data limited to an arbitrarily chosen distance of 450 km from the site. The compiled catalogue is divided into an incomplete part (historic) and two complete parts (see Figure 1). The first part of the catalogue contains the largest seismic events (with local magnitudes equal to or exceeding $m_0 = 4$) that occurred during the period 1 January 1801–31 December 1970. It was assumed that, for all of these events, the standard deviation in the determination of the magnitudes was 0.4. The second part (from 1 January 1971 to 31 December 1990) includes the complete catalogue of seismic events, from magnitude level $m_{min}^{(1)} = 3.8$ upwards. The uncertainty of magnitude was assumed to be 0.2. The third part (from 1 January 1991 to 31 December 1995) includes the complete data, from magnitude level $m_{min}^{(2)} = 3.5$ upwards. The uncertainty of magnitude was assumed to be 0.1. The strongest known earthquake that occurred within the area was an event of local magnitude $m_L \cong 6.3$ of September 29, 1969. It is assumed that the magnitude of this event was determined with standard error σ_M, equal to 0.25.

Maximization of the likelihood function (13) and application of the K-S estimator for the area surrounding the site of HES gives $\hat{m}_{max} = 6.85 \pm 0.60$, $\hat{\beta} = 2.18 \pm 0.26$, or equivalently $\hat{b} = 0.92 \pm 0.11$, and $\tilde{\lambda}(m_{min} = 2.5) = 9.81 \pm 3.77$. By replacing equation K-S with its Bayesian counterpart, i.e. the K-S-B estimator, the maximization of the likelihood function gives $\hat{m}_{max} = 6.66 \pm 0.44$, $\hat{\beta} = 2.18 \pm 0.26$, or equivalently $\hat{b} = 0.92 + 0.11$, and $\tilde{\tilde{\lambda}}(m_{min} = 2.5) = 9.65 \pm 3.73$. Taking into account that simulation experiments which have shown that the Bayesian estimator K-S-B tends to perform very well (especially in the presence of inevitable deviations from the simple Gutenberg-Richter model), the value $\hat{m}_{max} = 6.66 \pm 0.44$, obtained from applying the K-S-B technique, was used in all further computations.

The horizontal component of the PGA at the site of the HES was calculated using attenuation equation (14) where $c_1 = -3.13$, $c_2 = 0.617$, $c_3 = -0.00675$ and $c_4 = -0.79$ (Ambraseys and Srbulov, 1994). This attenuation equation predicts the mean value of ln(PGA), with a standard deviation $\sigma_{\ln(\mathrm{PGA})}$ equal to 0.62.

Two different approaches to the assessment of maximum PGA at the site, $a_{\max}$, was applied. The first approach is simple and is based on the concept of the "design" earthquake. According to this procedure, $a_{\max}$ is the value of the PGA calculated from ground-motion attenuation formulae by assuming the occurrence of the strongest possible earthquake (e.g. with magnitude $\hat{m}_{\max}$) at a very short distance (say $r_0 = 10$ km). Such a procedure provides the most conservative value of the $a_{\max}$. Unfortunately, there are an overwhelming number of observations world wide that show that the PGA values at short distances from the earthquake hypocentre are extremely scattered. Consequently, in order to apply this simple, deterministic-based procedure, a proper, probabilistic-based analysis of the uncertainty in the estimated PGA has also been incorporated.

The second approach to the assessment of the maximum PGA at the site is purely probabilistic and is based on the fact that the value of maximum possible PGA, $a_{\max}$, at the site of HES can be estimated according to the same equations as the maximum regional magnitude $\mathrm{m}_{\max}$, where in all formulas the parameter β is replaced by $\gamma = \beta/c_2$, the area-specific mean activity rate of seismicity, λ, is replaced by its counterpart, characteristic for the site, and the maximum observed magnitude $\mathrm{m}^{\mathrm{obs}}_{\max}$ is replaced by the logarithm of the maximum observed PGA, $a^{obs}_{\max}$.

To assess the value of $a_{\max}$ according to those two approaches, first a simple model of quantification of potential sources of uncertainty in ground-motion relations will be developed.

Following Tinti and Mulargia (1995), it is assumed that the earthquake magnitude m is determined with an error which is normally distributed and has mean zero and standard deviation σ_{M}. The same assumption is made concerning the error in the determination of earthquake distance r, where the standard deviation of r is denoted as σ_{R}. It can be seen that for an earthquake with an apparent magnitude m, and located at a distance r, the value of ln(PGA) is approximately normally distributed with the mean given by the RHS of equation (14), and the standard deviation given by $\sigma_{\mathrm{TOTAL}} = \sqrt{\sigma^2_{\ln(PGA)} + c_2^2\sigma^2_M + \sigma^2_{\mathrm{R}}(c_3 + c_4/r)^2}$. Therefore, if an earthquake of apparent magnitude m is located at a distance r from the site, the probability that this earthquake will cause a PGA equal to or greater than a is given by

$$\Pr\left[PGA \geq a\right] = 1 - \Phi\left(\frac{\ln(a) - \ln(\bar{a})}{\sigma_{TOTAL}}\right), \tag{16}$$

where $\Phi(\cdot)$ is the normal probability integral, and $\bar{a}$ is the median value of acceleration, with $\bar{a} = a(0.5) = \exp[c_1 + c_2 m + c_3 r + c_4 \ln(r)]$. Equation (16) makes it possible to assess the required value of maximum acceleration at the site together with its uncertainty. Following this approach, the value of $a_{\max}$ is calculated as a median

value of distribution of acceleration (16), calculated at the critical distance r and generated by the largest possible earthquake magnitude m_{max}:

$$\hat{a}_{max} \equiv \hat{a}_{max}(0.5) = \exp[c_1 + c_2 \hat{m}_{max} + c_3 r_0 + c_4 \ln(r_0)] \quad (17)$$

Following relation (16), the upper confidence limit of the $\hat{a}_{max}$, $\hat{a}_{max}$ (0.84) is calculated as a solution of equation (16), where $\Pr[PGA \geq \hat{a}_{max}(0.84)] = 1 - 0.84$, and $\ln(\bar{a}) = \ln(\hat{a}_{max})$. The confidence level 0.84 was chosen by analogy with the normal distribution, for which the upper site confidence limit, with the confidence level 0.84, corresponds to the mean value increased by one standard deviation. For the the selected model of the PGA attenuation, where $\sigma_{\ln(PGA)} = 0.62$, for $\hat{m}_{max} = 6.66$, $\hat{\sigma}_M = 0.44$, $r_0 = 10$ km and $\sigma_R = 5$ km, the resulting median value of maximum PGA $\hat{a}_{max}$, expected at the site of the HES, is equal to 0.40 g, and its 84% upper limit, $\hat{a}_{max}$ (0.84) = 0.82 g. Maximum likelihood solution for the selected site of the HES, for $a_{min} = 0.05$ g, and $\hat{a}_{max} = 0.40$ g, gives $\hat{\lambda} = 0.123 \pm 0.014$ [YEAR^{-1}], and $\hat{\gamma} = 3.49 \pm 0.35$.

The application of K-S and K-S-B procedures gives coincidentally the same value of median acceleration $\hat{a}_{max}$, equal to 0.32 g, while the estimated 84% upper limits $\hat{a}_{max}$ (0.84) are equal to 0.72 and 0.69 g. It is interesting to note that the "design" earthquake approach, which describes the worst scenario and should therefore provide more conservative results, gives $\hat{a}_{max} = 0.40$ g, which is only slightly higher than the $\hat{a}_{max}$ obtained from the application of the K-S and K-S-B procedures. Figure 2 depicts the probabilities that the given value

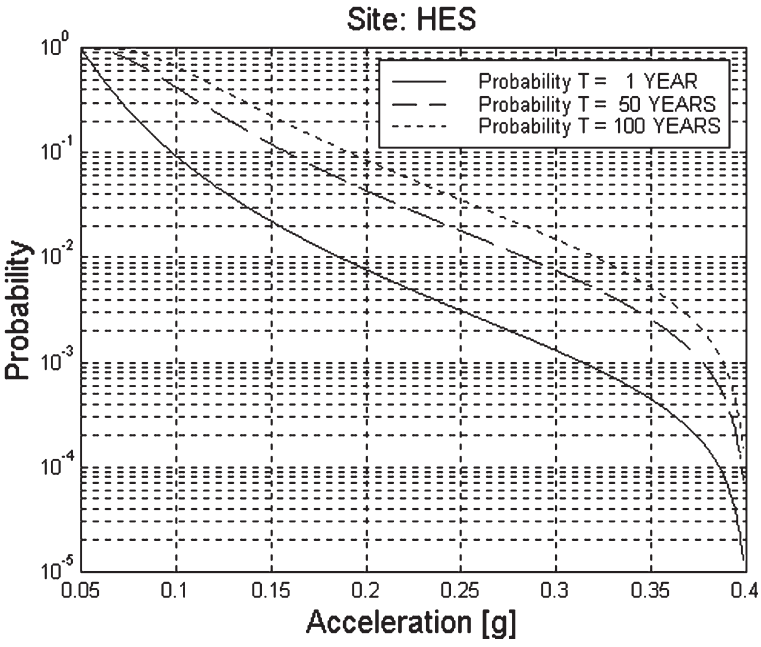

Figure 2 Probabilities that a given PGA will be exceeded in 1, 50 and 100 years for the site of hypothetical engineering structure

of the horizontal component of PGA at the site of the HES will be exceeded in one, 50 and 100 years.

5.2 *Mapping of PSHA for South Africa and Sub-Saharan Africa*

The second example of the application of the technique presented above is the creation of the PGA/ARS hazard maps for South and Sub-Saharan Africa. The maps in figure 3 and 4 show the contoured median values of acceleration (PGA/ARS) with a 10% probability of exceedance in 50 years. The seismic hazard represented here show a 10% in Figures 3 and 4 show a 10% probability of exceeding the calculated PGA and spectral accelerations of 1 Hz respectively, at least once in 50 years. Figure 5 shows similar results for Sub-Saharan Africa.

This methodology has been further extended to include an extensive seismic risk assessment which can project the expected damage and expected monetary losses of a critical structure within an area for a certain period of time.

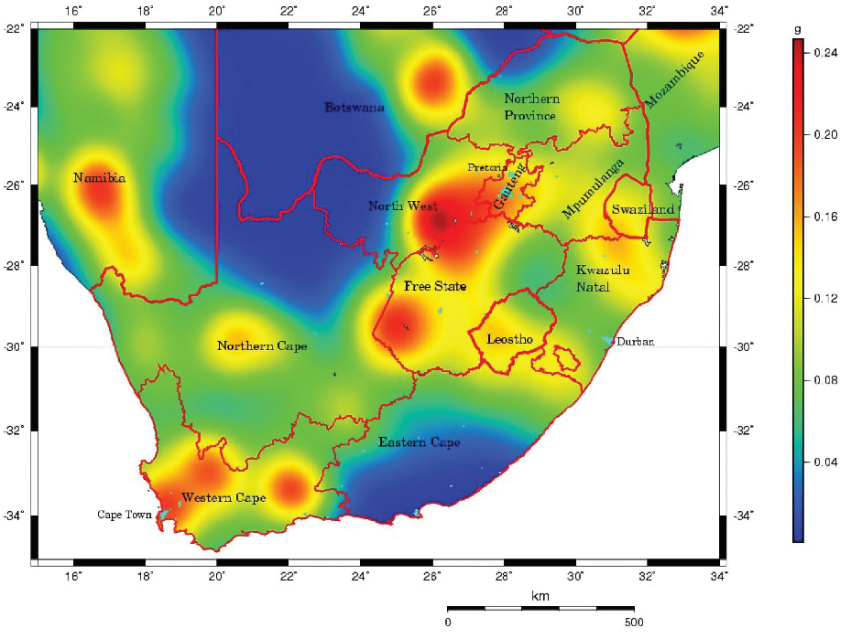

Figure 3 Map of the expected PGA with a 10% probability of being exceeded at least once in a 50-year period for South Africa

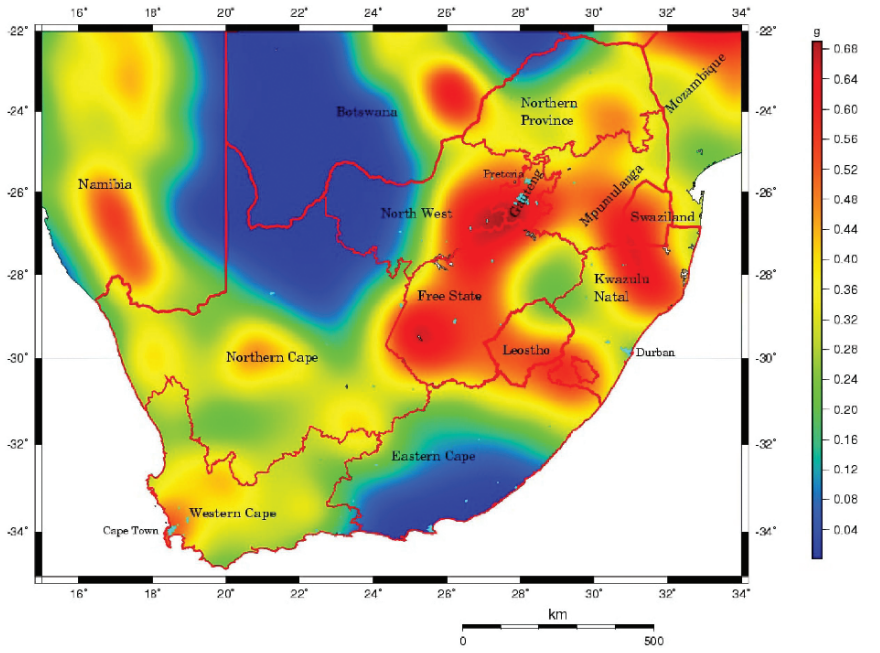

Figure 4 Map of the 1 Hz acceleration response spectra with 10% probability of being exceeded at least once in a 50-year period for South Africa

6 Conclusions

The technique used above for seismic hazard assessment has been developed specifically for the estimation of seismic hazard at individual sites without the subjective judgment involved in the definition of seismic source zones.

This technique combines the best features of the "deductive" (Cornell, 1968) and "historic" (Veneziano et al., 1984) procedures. Since the seismic hazard parameters are estimated by the maximum likelihood procedure, by applying the Bayesian formalism, any additional geological or geophysical information, can be incorporated. The procedure described is consequently capable of giving a realistic assessment of seismic hazard in the areas of both low and high seismicity.

Since the maximum regional magnitude, m_{max}, and the maximum site characteristic PGA, a_{max}, are of cardinal importance in any PSHA, statistical technique which can be used for evaluation of these important parameters is presented.

This approach is particularly useful for the mapping of seismic hazard in areas where both large, historical observations and complete, recent instrumental observations are available. The procedure takes into account incompleteness of the seismic catalogues. The procedure also incorporates uncertainty in earthquake magnitude determination.

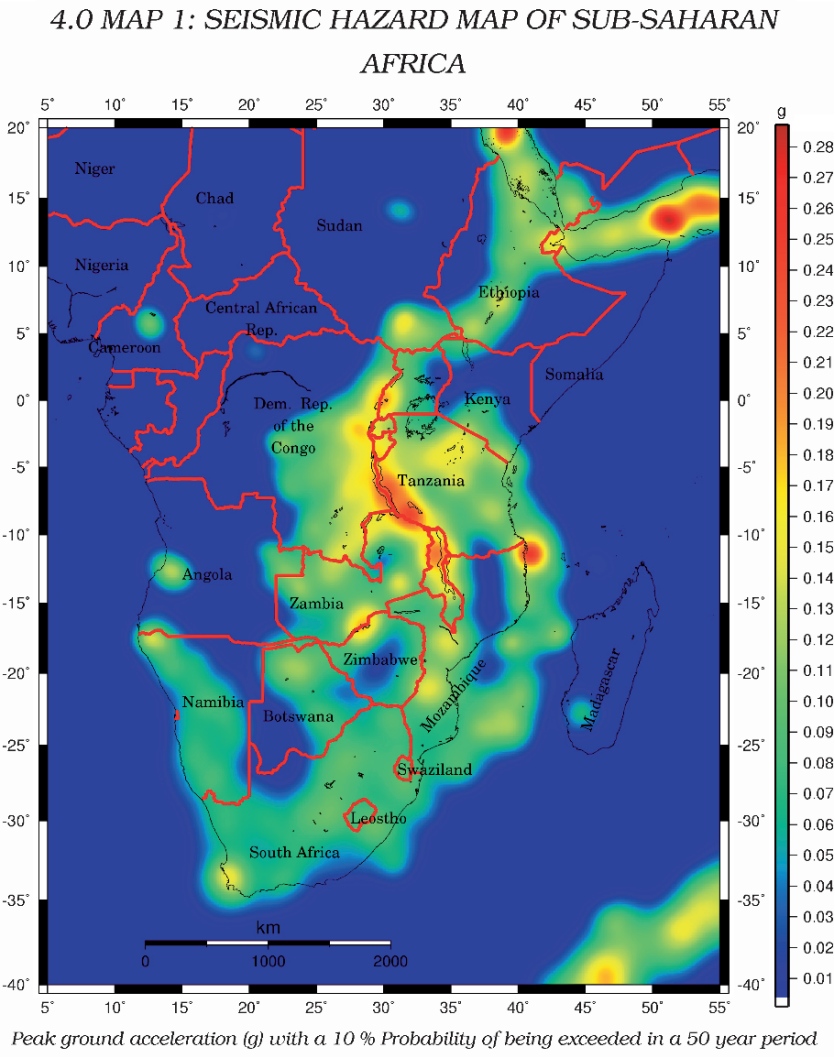

Figure 5 Map of the expected PGA with a 10% probability of being exceeded at least once in a 50-year period for Sub-Saharan Africa

Based on the maximum likelihood principle, a system of equations has been derived for parameters of the models most often used in engineering seismology, viz. a doubly truncated Gutenberg-Richter frequency-magnitude, and a Poisson distribution of earthquake occurrence in time.

The respective computer codes (written in MATLAB and FORTRAN 77 for PC) used for calculation of above examples can be provided free of charge by the author.

References

Ambraseys, N.N., Srbulov, M., 1994. Attenuation of earthquake-induced ground displacements. *Earthquake Eng. Struct. Dyn*. 23, 467–487.

Cornell, C.A., 1968. Engineering seismic risk analysis. *Bull. Seism. Soc. Am*. 58, 1583–1606.

Campbell, K.W., 1982. Bayesian analysis of extreme earthquake occurrences. Part I. Probabilistic hazard model, *Bull. Seism. Soc. Am*., 72, 1689–1705.

Gibowicz, S.J., Kijko, A., 1994. *An Introduction to Mining Seismology*. San Diego, CA: Academic.

Kijko, A., 1983. A modified form of the first Gumbel distribution: model for the occurrence of large earthquakes. Part II: Estimation of parameters. *Acta Geophys. Pol*., 31, 27–39.

Kijko, A., 2004. Estimation of the maximum earthquake magnitude m_{max}. *Pure Appl. Geophys*, 161, 1–27.

Kijko, A., Graham, G., 1998. "Parametric-Historic" procedure for probabilistic seismic hazard analysis. Part I: Assessment of maximum regional magnitude m_{max}. *Pure Appl. Geophys*.

Kijko, A., Sellevoll, M.A., 1992. Estimation of earthquake hazard parameters from incomplete data files, Part II, Incorporation of magnitude heterogeneity. *Bull. Seism. Soc. Am*. 82, 120–134.

McGuire, R.M., 1993. Computation of seismic hazard. *Ann. Di Geofisica*, 36, 181–200.

Tinti, S., Mulargia, F., 1985. Effects of magnitude uncertainties in the Gutenberg-Richter frequency-magnitude law. *Bull. Seism. Soc. Am*. 75, 1681–1697.

Veneziano, D., Cornell, C.A., O'Hara, T., 1984. Historic method for seismic hazard analysis. *Elect. Power Res. Inst*., Report, NP-3438, Palo Alto.

Seismicity and Seismic Hazard Assessment in Greece

Theodoros M. Tsapanos*

Abstract Greece is the most seismically active region in Europe and also rank high (sixth position) on a global scale (Tsapanos and Burton, 1991). Hence reliable seismic hazard assessments are important for sustaining the economical developments of a country like Greece. The objective of such studies and modeling efforts are to obtain long term probabilities of occurrences of seismic events of specified sizes in given time interval.

Primary information for hazard assessments is extensive historical seismicity observations which in case of Greece and adjacent areas dates back to 550 years B.C. Descriptions of the macroseismic effects of several strong earthquakes in this region which occurred between 550 BC – 300 AD have been recovered more recently. As we go back in time the historical records become progressively incomplete and naturally reflects destructive earthquakes in populated areas. Instrumental observations are important in a hazard context both for delineating active faults and also for estimating crustal attenuation properties. Description of the macroseismic effects of several strong earthquakes which occurred in the broad area during the time period 550 BC-300 AD have been found.

In this presentation, I summarize seismic hazard assessment efforts for Greece and give details on shallow and intermediate depths seismicity, maximum observed and expected macroseismic intensities, peak ground accelerations, velocities and displacements. Also strong motions duration are discussed and macroseismic intensity decay with distance for given magnitudes are outlined. The earthquake activity in Greece has an uneven spatial distribution and this is taken into account in the presentations of various hazard measures and their describtions.

Keywords seismicity, seismic hazard, seismic code, Greece

Aristotle University of Thessaloniki, School of Geology, Department of Geophysics, 54124 Thessaloniki, Greece

* To whom correspondence should be addresed. E-mail: tsapanos@geo.auth.gr

E.S. Husebye (ed.), *Earthquake Monitoring and Seismic Hazard Mitigation in Balkan Countries.*

1 Introduction

The seismicity of Greece has been evaluated mainly during the 20th century, though descriptions of the earthquake occurrences have been reported since the middle of 19th century. In Athens the first seismograph (Agamemnone) was installed in 1899 while the first seismometer (Mainka with 2 horizontal components) was installed in Athens in 1911. Later on in 1922 a horizontal seismometer (Wiechert with 2 components) installed, and 6 years later it was supplemented with a vertical seismometer of the same type (Papazachos and Papazachou, 1997).

Presently there are 53 seismological stations equipped with short-period instrumentation in Greece, out of which 36 are in operation under the supervision of the National Observatory of Athens, while 17 belong to the Geophysical Laboratory of the Aristotle University of Thessaloniki. The latter institute operated the first telemetric network in Greece in 1981.

Based on the historical information and instrumental seismicity, the seismic hazard for Greece or parts hereof has been repeatedly assessed since early of 1970-ties. The basic scientific work focus on the geographical distribution of maximum observed intensity (Galanopoulos and Delibasis, 1972), maximum expected macroseismic intensity (Papazachos et al., 1985), peak ground acceleration or velocity (Makropoulos and Burton, 1985) and duration of strong motion (Margaris et al., 1990). Only the major studies are mentioned above.

Detailed knowledge of the attenuation of strong ground motion is very important in seismic hazard studies. The first to study this problem was Makropoulos (1978). Later studies were based on attenuation relations for macroseismic intensities, peak ground accelerations and velocities derived for Greece and the adjacent areas (Papaioannou, 1986; Papoulia and Stavrakakis, 1990, Theodulidis, 1991; Margaris et al., 2002) have made.

Similar studies have been undertaken in other Balkan countries and references is made to the articles of Brlek (2005), Markušić (2005), Rashidov et al., (2005), Solakov et al, (2005), Tóth et al. (2005) and Duni and Kuka (2005). All these references included in the abstract book of NATO ARW which book place in Borovetz, Bulgaria 11–17 Sep. 2005. Full length articles of such studies by Duni and Kuka (pp 55–78), Markusic (pp 79–96), and Tóth et al. (pp 97–110) are included - IBID in this NATO book.

2 Seismicity of Greece

The basic lithospheric process in the Aegean sea is the subduction of the African plate under the Eurasian plate south of Crete forming the Hellenic arc and trench (Papazachos and Comninakis, 1971; Comninakis and Papazachos, 1972; Makris, 1973; Mercier, 1977; McKenzie, 1978; Dewy and Sengor, 1979; Makropoulos and Burton, 1984, Kotzev et al., 2005, 2008).

Chronicles and similar studies of Greek seismicity have been reported since the dawn of Greek civilization dates back to 500 BC . These mainly concerned the

shake-ability and the damages caused in popular areas. Quantitatively type studies have been repeatedly published over the 40 years as the Greece seismograph network became fully operational. In this way quantitative researches that analyzed different parts of Greece, concerning its seismicity based on the horizontal and vertical distribution of seismic energy release, the return periods of earthquakes, and the probability for occurrence of disasterous earthquakes, etc. (Comninakis, 1975, Makropoulos and Burton, 1984; Papazachos, 1990, Tsapanos and Burton, 1991; Hatzidimitriou et al., 1994, Papazachos, 1999; Manakou and Tsapanos, 2000; Tsapanos, 2001, among others).

The networks of Greece Seismological Institutes are continuously recording all the events occurring in Greece and adjacent areas. This adds a new dimension to the relative completeness of the earthquake catalogues for the region for shallow and intermediate depths events as listed in Tables 1 and 2 (Papazachos and Papazachou, 1997).

Obviously, significant improvements in earthquake detectabilities have taken place in this region after the first seismograph installation in 1899. There are two events with magnitudes greater than or equal to 8.0. The first occurred in AD 365 with M=8.3 (SE of Crete island) and the second one occurred in AD 1303 with M=8.0 (in Rhodos island).

In Figures 1 and 2 the seismicity of shallow events and intermediate events, respectively, of Greece is illustrated according to the aforementioned completeness. Notice that no event of focus deeper focus than 180 km ever has been recorded in Greece.

Based on the above completeness of the shallow and the intermediate depth events the quantitative seismicity of Greece can be studied more precisely. Among these investigations is the geographical distribution of the well-known b-value throughout Greece which has been mapped by Papazachos (1999) - See Figure 3.

Table 1 The time periods and the corresponding completeness thresholds of the magnitudes of the six subperiods of the Greek earthquake catalogue for focal depths less than 60 km

1970 – 2000	M = 4.5– 4.9
1950 – 2000	M = 5.0 – 5.1
1911 – 2000	M = 5.2 – 6.4
1845 – 2000	M = 6.5 – 7.2
1500 – 2000	M = 7.3 – 7.8
550 BC-2000	M = 8.0 – 8.3

Table 2 The time periods and the corresponding completeness thresholds of the magnitudes of the four subperiods of the Greek earthquake catalogue (focal depths $61 \leq h \leq 180$ km)

1970 – 2000	M = 5.5 – 5.9
1911 – 2000	M = 6.0 – 6.9
1845 – 2000	M = 7.0 – 7.4
1500 – 2000	M = 7.5 – 8.2

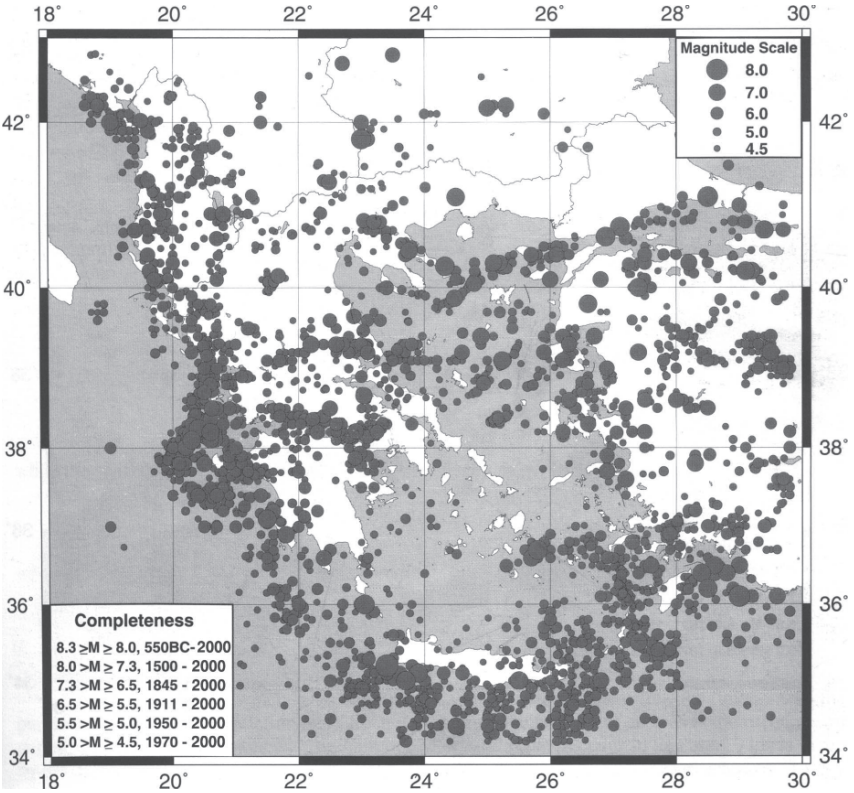

Figure 1 Seismicity of shallow shocks of Greece according to the completeness tabulated in Table 1

The accurate definition of seismic zones or seismogenic areas is important in seismic hazard estimation, which otherwise may cause biased results. Recent studies on seismicity and active tectonics in the Aegean region give new information which is also useful for reliable subdivision of Greece in seismogenic zones (Papaioannou and Papazachos, 2000). We may presume that faults are the seismogenic sources which pose hazards for a number Greece cities, and moreover that major faults are responsible for earthquakes with magnitude $M \geq 6.0$. The lack of knowledge of seismicity parameters for these faults make them unsuitable for this kind of use. However, Papaioannou and Papazachos (1997, 2000) divided Greece in 67 seismogenic sources of shallow shocks and 7 seismogenic sources of intermediate depth earthquakes, based on these new seismological data and moreover on geological, geomorphological and other information, The quantitative seismicity, in terms of the mean return period Tm in the seismogenic sources of shallow events (Figure 4) and the same parameter for the 7 seismogenic sources of intermediate depth earthquakes (Figure 5), was then estimated by these scientists.

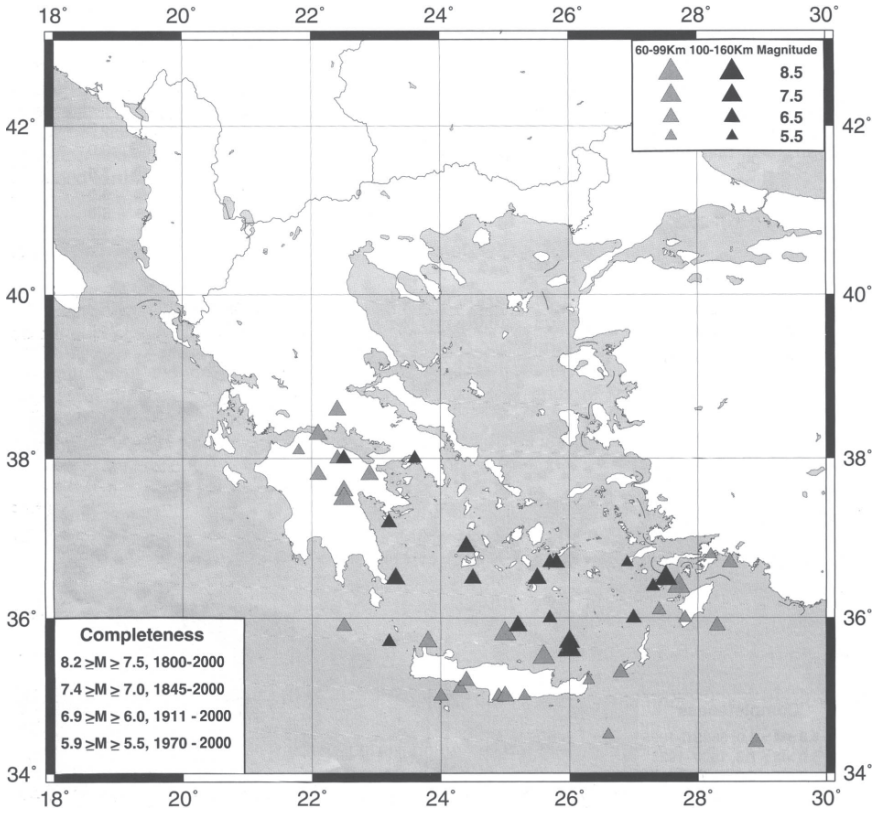

Figure 2 Seismicity of intermediate depth shocks of Greece according to the completeness tabulated in Table 2

3 Seismic Hazard Assessment

Seismic hazard studies in Greece have been published by numerous authors and focus on: (a) the spatial distribution of the maximum observed intensity (Galanopoulos and Delibasis, 1972), (b) the maximum expected macroseismic intensity (Papaioannou, 1984; Papazachos et al., 1985), (c) peak ground accelaration or velocity (Drakopoulos and Makropoulos, 1983; Papaioannou, 1984; Makropoulos and Burton, 1985), and (d) duration of strong ground motion (Margaris et al., 1990; Papazachos et al., 1992). Other related research topics are: (a) simulation of strong ground motions (Stavrakakis, 1985; Stavrakakis et al., 1986; Makropoulos et al., 1990; Margaris, 1994; Theodulidis and Bard, 1995), (b) attenuation of spectral values of strong ground motion (Papazachos et al., 1989; Theodulidis, 1991), (c) site effects (Gazetas et al., 1990; Margaris and Papazachos, 1994; Theodulidis and Tsakalidis, 1994), and (d) response spectra (Theodulidis and Papazachos, 1994).

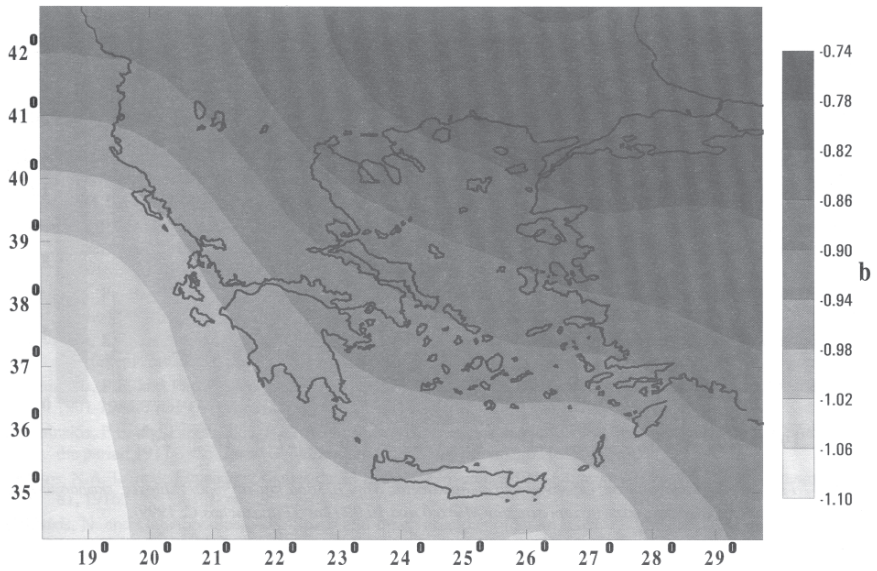

Figure 3 The spatial distribution of the *b*-parameter, of magnitude-frequency relationship, in Greece and the adjacent areas (after Papazachos, 1999)

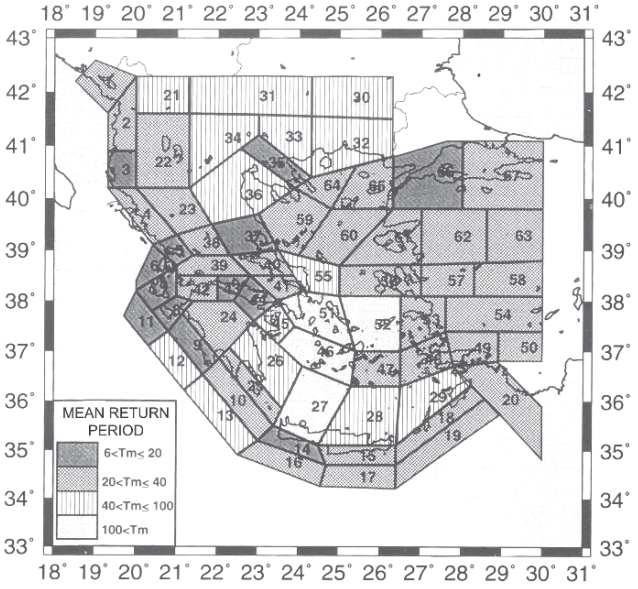

Figure 4 Quantitative expression of Greek seismicity in terms of mean return period, T_m (in years), in the 67 seismogenic sources of shallow seismicity (after Papazachos and Papaioannou, 1997). Based on the mean return period of events with magnitude M=6.3 (the most probable maximum annual magnitude) the whole area are divided in four zones

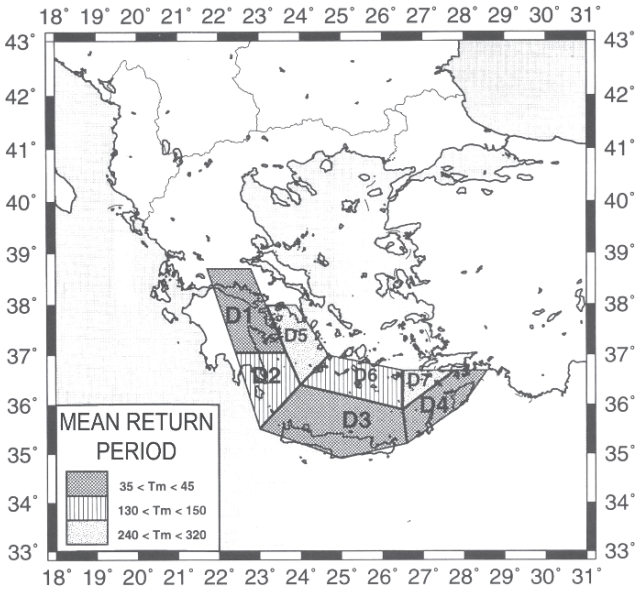

Figure 5 Quantitative expression of Greece seismicity in terms of mean return period, T_m (in years), in the 7 seismogenic sources of intermediate depth seismicity (after Papazachos and Papaioannou, 1997). Based on the mean return period of events with magnitude M=7.0 (most frequently occurring in the Benioff zone of Greece) the whole area divided in three zones

The first to present relations for strong motion attenuation in Greece, after 1970, was Makropoulos (1978). Because of lack of data for Greece he adopted relations derived for other regions and thus obtained, an average attenuation law for PGA in Greece. His equation was of the following type:

$$\log a = \log 2164 + 0.70m \log e - 1.80 \log(r + 20) \quad (1)$$

where α is the acceleration, m is the earthquake magnitude (M_s) and r is the distance (in km)

Papaioannou (1984) derived a relation between the macroseismic intensity *I*, of the shallow shocks of Greece, the distance *Δ* (in Km) and the magnitude *M*:

$$I = 6.59 + 1.18M - 4.5 \log(\Delta + 17) \quad (2)$$

while for the intermediate depth events of the southern Aegean the relation becomes:

$$I = 1.87 + 1.69M - 3.94 \log(D + 30) \quad (3)$$

where M is the earthquake magnitude and D is the distance (in km)

For PGA he proposed the following relation:

$$\log a = \log 5950 + 0.89m \log e - 2.37 \log(r + 23) \quad (4)$$

where m is the earthquake magnitude and r is the distance (in km)

Later Theodulidis (1991) using Greek recordings and defined peak horizontal acceleration γ_m (in cm/sec^2) and for the peak ground velocity υ_m (in cm/sec) respectively, as follow:

$$\log \gamma_m = 1.77 + 0.49M - 1.65 \log(\Delta + 15) \quad (5)$$

$$\log \upsilon_m = 0.39 + 0.61M - 1.62 \log(\Delta + 12) \quad (6)$$

where M is the earthquake magnitude and Δ is the distance (in km)

Recently Margaris et al. (2002) using a comprehensive set of observations obtained the following attenuation relationships for Greece of HPGA γ_m (in cm/sec^2), PGV υ_m (in cm/sec) and PGD d_m (in cm):

$$\log \gamma_m = 4.16 + 0.69M - 1.24 \log(\Delta + 6) + 0.12S \pm 0.70P \quad (7)$$

$$\log \upsilon_m = -1.51 + 1.11M - 1.20 \log(\Delta + 5) + 0.29S \pm 0.80P \quad (8)$$

$$\log d_m = -6.63 + 1.66M - 1.34 \log(\Delta + 5) + 0.50S \pm 1.08P \quad (9)$$

where M is the earthquake magnitude and D is the distance (in km), S is the type of soil: S=*0* is for rock, S=*2* for soft soil and S=*1* for intermediate type of soil. The relationships (7 - 9) represent the attenuation"laws" currently in use in Greece. In Figure (6) we have plotted the attenuation laws (PGA) given by Makropoulos (1978), Papaioannou (184), Theodoulidis (1991), and Margaris et al. (2002) for three different magnitudes

Relations between PGA, PGV and macroseismic intensity in given by Koliopoulos et al. (1998):

$$\log \gamma_m = 0.33I + 0.07 \quad (10)$$

and

$$\log \upsilon_m = 0.33I + 1.10 \quad (11)$$

Based on the above relationships Papazachos and Papazachou (2002) calculated γ_m and υ_m for 5 values of intensity and the results are listed in (Table 3).

An inspection of Table 3 gives that an increase by 1 unit in macroseismic intensity, the values of γ_m and υ_m are almost doubled. Another observation, is that the earthquakes in Greece cause damages, when $I \geq$ VI or PGA exceeds 110 cm/sec^2 ($\approx$0.11g) or PGV exceeds 8 cm/sec (Papazachos and Papazachou, 2002).

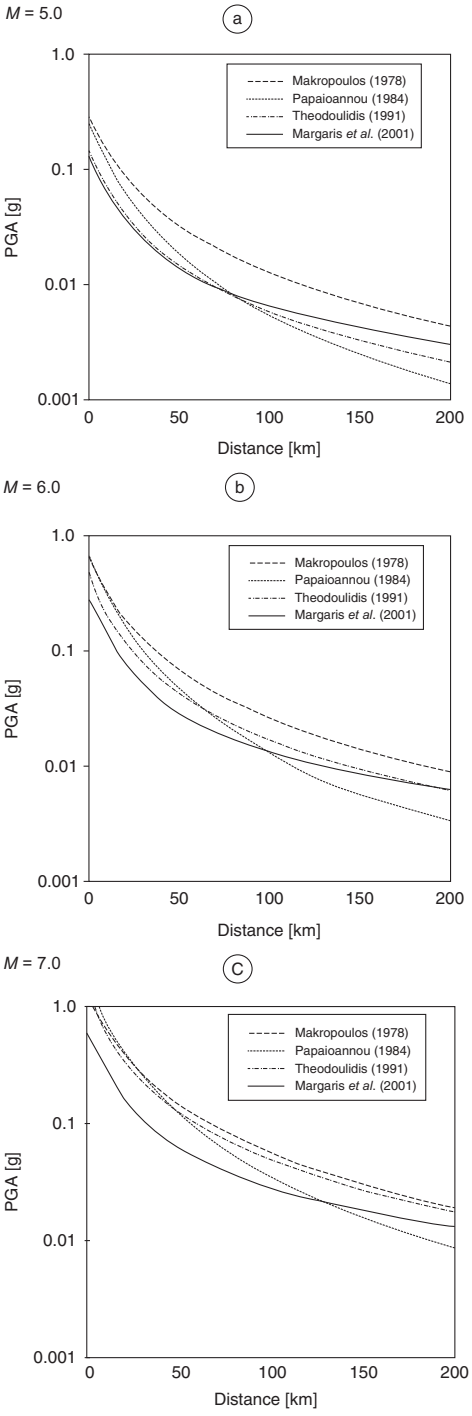

Figure 6 Comparison of the attenuation laws proposed by the four researchers Makropoulos, 1978; Papaioannou, 1984; Theodulidis, 1991 and Magaris et al., 2002.

Table 3 Values for peak ground acceleration and peak ground velocity for 5 values of macroseismic intensity

I	γ_m (in cm/sec^2)	υ_m (in cm/sec)
VI	110	8
VII	240	16
VIII	510	32
IX	1100	75
X	2340	160

Bayesian estimation of seismic hazard for 6 cities of Greece which experienced strong ($M \geq 5.7$) earthquakes during the time period 1986-1996, was studied by Lyubushin et al. (2002). They estimated maximum and quantile values of PGA of the probalistic distribution at selected sites at future time intervals of given lengths. They found that the expected maximum PGA would be more than 2 times greater that the observed PGA at the sites in question.

Koravos et al. (2003) evaluated the maximum earthquake magnitudes in the Aegean area region constrained by tectonic moment release rates. They determined recurrence rates and the maximum earthquake magnitudes for different tectonic zones in the Aegean region (Figure 7) using a combination of instrumental and historical data, plus geodetic observations. On pragmatic grounds they picked maximum magnitudes which are determined either by the seismic or tectonic moment rates release, or the maximum historical magnitude where appropriate. In some areas the seismic moment release rate for a subcatalogue appears to exceed the tectonic moment release rate but no more than a factor of 2 or so, i.e. that is within the errors inherit in seismic moment determinations.

4 Seismic Code in Greece

Studies of the distribution of the strong ground motion throughout Greece have been published by numerous authors, as we mentioned above. A synthetic result of the previous publications is the separation of Greece in four zones, I, II, III and IV (Papazachos et al., 1989) of roughly equal hazard levels proposed by the four seismological research centers of Greece (University of Athens, Aristotle University of Thessaloniki, Geodynamic Institute of the National Observatory of Athens and Institute of Engineering Seismology and Earthquake Engineering-Thessaloniki) and constitutes a part of the Seismic Code of Greece. Each of the above mentioned zones has equal seismic hazard parameters which are expressed in terms of the most probable maximum value of peak ground acceleration PGA as a function of the mean return period T_m, as given below by four equations:

$$\log \gamma_m = 0.266 \log T_m + 1.424 \text{ (zone I)} \tag{12}$$

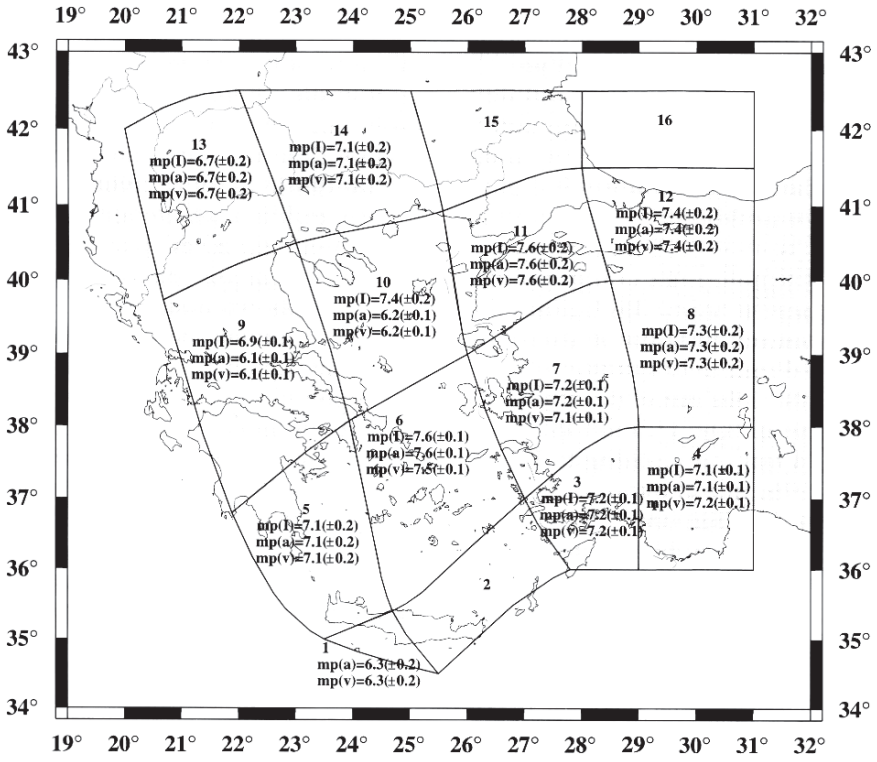

Figure 7 Evaluation of maximum earthquake magnitudes in Aegean area constrained by tectonic moment release. Magnitudes mP(I), mP(a) and mP(v) are derived from Intensity, Acceleration and Velocity, respectively (Koravos et al., 2003)

$$\log \gamma_m = 0.277 \log T_m + 1.579 \text{ (zone II)} \tag{13}$$

$$\log \gamma_m = 0.264 \log T_m + 1.739 \text{ (zone III)} \tag{14}$$

and

$$\log \gamma_m = 0.240 \log T_m + 2.015 \text{ (zone IV)} \tag{15}$$

For return period of $T_m = 475$ years the calculated values of PGA (in g) for the four zones are expressed in the equations 12 - 15: (1) for zone I = 0.12g, (2) for zone II = 0.16g, (3) for zone III = 0.24g and for zone IV = 0.36g. In Figure (8) the division of Greece in four iso-acceleration zones is depicted and moreover this was the official seismic hazard map of Greece until 2003. All of them were included in the former seismic code of Greece, which is written in Greek.

During the period 1986 - 2001 Greece experienced strong and catastrophic earthquakes like the events of Kozani - Grevena (1995, M = 6.6), Aegio (1995,

Figure 8 The former seismic hazard map of Greece which was the official one until 2003. Four zones of 0.12g, 0.16g, 0.24g and 0.36g, are illustrated

M=6.4, Konitsa (1996, M=5.7), Athens (1999, M=5.9), Skyros (2001, M=6.5) and in other places of the country, as well. The data on which the seismic code of Greece were based, had to change as the new knowledge given to Greece seismologists and engineers by this information (earthquakes) must be used. Based on this, a new seismic code of Greece was prepared as a joint work of five seismological research centers of Greece (University of Athens, Aristotle University of Thessaloniki, Geodynamic Institute of the National Observatory of Athens, Institute of Enginnering Seismology and Earthquake Engineering and University of Patra) and become official as of 1/1/2004. Accordingly, the New Seismic Code hasve three (instead of four) zones of seismic hazard (Figure 9), with respective I=0.16g, II=0.24g and zone III=0.36g. We see that the former seismic PGA values of 0.12g (zone I) was incorporated in the new zone I=0.16g. This is the new official seismic hazard map of Greece. All of them were including I in the former seismic code of Greece, which of course is written in Greek.

Figure 9 The new official seismic hazard map of Greece since 1-1-2004. Only three zones of 0.16g, 0.24g and 0.36g are included in the new version

5 Discussion and Conclusions

One approach to analysis of rare, large events is to focus on these events using the statistics of extreme values or Gumbel's (1955) extremes. Gumbel's third asymptotic distribution of extreme values has both a characteristic scale and an estimated maximum event size. Accordingly, Makropoulos (1978) and Makropoulos and Burton (1985) applied this distribution to extreme value data in the area of Greece, and determined the maximum magnitude (ω) for mainland of Greece and determined the maximum magnitude (w or ω) for mainland Greece and some selected cities. The Gumbel's technique have the advantage that it does not require analysis of the whole data set. But as it is suggested by Knopoff and Kagan (1977) Makropoulos and Burton (1985) the error bounds on the maximum magnitude are very large, depending on a combination of the paucity of data and the large extrapolations required. This procedure (Gumbel's method) required fixed time intervals (e.g. 1 year) from which the largest magnitudes are selected.

As it is known the requirement of short time interval is satisfied only for recent instrumentally based catalogues. In order to use historical data sets, the magnitudes must be selected from longer time intervals, and the classical Gumbel's procedure does not provide tools for handling such data sets.

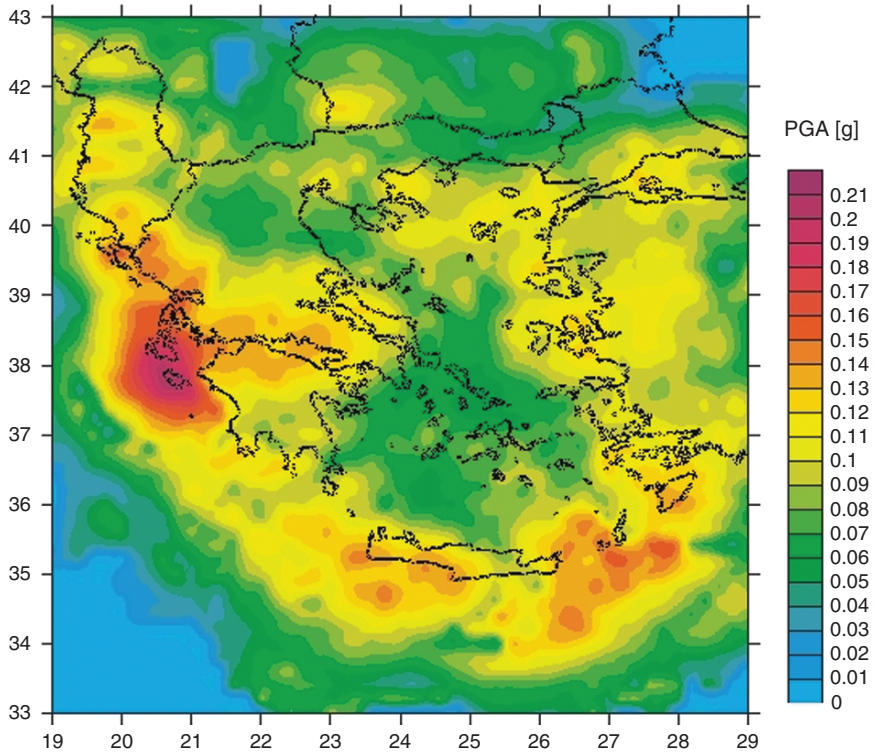

Figure 10 A smoothed probabilistic seismic hazard map of Greece and adjacent areas in terms of PGA values at 10% probability of exceedance at least once in 50 years (after Tsapanos et al., 2004)

In order to overcoming this deficiency Kijko and Sellevoll (1989, 1992) have developed an approach which permits calculation of the maximum likelihood estimates of the parameters of extreme magnitude distributions in the case when the maximum magnitudes are taken from both incomplete (historical) and complete (recorded) earthquake files. Papadopoulos and Kijko (1991) evaluated the maximum regional magnitude m_{max}, assuming a sharp truncation in frequency-magnitude relationship for the seismogenic regions of Greece proposed by Papazachos (1980). Similarly Manakou and Tsapanos (2000) and Tsapanos (2001) estimated m_{max} for Crete and the adjacent area using the maximum likelihood method of Kijko and Sellevoll (1989) by combining both historical and instrumental data on a cellular grid of 0.4° X 0.4° elements.

Very recently Tsapanos et al. (2004) produced a seismic hazard map for Greece. This map was assessed in terms of PGA using the refined approach by (Kijko and Graham, 1998, 1999) and the recent Greek attenuation law derived by Margaris et al. (2002). The procedure has the advantage that does not require any specification of seismic zones.

In this case seismic hazard analysis was performed on the basis of the all seismological observations as well as the instrumental data recorded during the past decades. Only the shallow shocks were taken into account because the attenuation law was derived for shallow earthquakes. A seismic hazard map (Figure 10) was

constructed for the Greek territory. In this map the estimated seismic hazard is specified in terms of the PGA with 10% probability of exceedance in 50 years, corresponding to a return period of 475 years. Note this map is similar to the official seismic hazard map (Figure 9) of Greece. For example Ionian islands show the highest seismic hazard expressed in peak ground acceleration in both maps.

In conclusion we state that a lot of work on seismicity and on seismic hazard evaluation have been done in Greece by: University of Athens, Aristotle University of Thessaloniki, Geodynamic Institute of the National Observatory of Athens (Institute of Geodynamics), Institute of Engineering Seismology and Earthquake Engineering-Thessaloniki and University of Patra. These activities focus on research: (i) time independent seismicity, (ii) time dependent seismicity, (iii) induced seismicity, and (iv) strong ground motions. In the future we foresee that all stations in our country become part of a National Greece Seismological Network for real time earthquake monitoring.

Acknowledgements The author would like to express his sincere thanks to the organizing committee of this workshop and especially the Bulgarian colleagues for their kind hospitality. Also many thanks due to Prof. E. Husebye for constructive criticism of the present work.

References

Brlek, I., (2005). Earthquake activity on the territory of Bosnia and Herzegovina. Abstarcts of NATO ARW "Earthquake monitoring and seismic hazard mitigation in Balkan countries" (edrs. Husebye, E.S. and Christova, C.), Borovetz-Bulgaria 11–17 September 2005, 96–97pp.

Comninakis, P.E. and Papazachos, B.C., (1972). Seismicity of the eastern Mediterranean and some tectonic features of the Mediterranean ridge. Geol. Soc. Am. Bull. 83: 1093–1102.

Comninakis, P.E., (1975). Contribution to the research of seismicity of Greek territory. Ph.D. Thesis, Univ. of Athens, 110pp., (in Greek).

Dewey, J.F. and Sengor, A.M.C., (1979). Aegean and surrounding regions: Complex multiplate and continous tectonics in a convergent zone. Geol. Soc. Am. Bull. 90: 84–92.

Drakopoulos, J. and Makropoulos, K.C., (1983). Seismicity and hazard analysis studies in the area of Greece. Publ. Seism. Lab., Univ. of Athens, 1, 126pp.

Duni, L. and Kuka, N., (2005). Stochastic simulation of ground motions based on data from recent accelerometric records in Albania. Abstarcts of NATO ARW "Earthquake monitoring and seismic hazard mitigation in Balkan countries" (edrs. Husebye, E.S.and Christova, C.), Borovetz-Bulgaria 11–17 September 2005, 108–112 pp.

Galanopoulos, A.G. and Delibasis, K., (1972). Map of maximum observed intensities in Greece (period 1800–1970). Athens.

Gazetas, G., Dakoulas, P. and Papageorgiou. A., (1990). Local soil and source mechanism effect in the 1986 Kalamata (Greece) earthquake. Earthq. Eng. Str. Dyn., 19, 431–456.

Gumbel, L. J.: Statistics of Extemes, Columbia University Press, New York, N.Y., 375 pp. 1955.

Hatzidimitriou, P.M., Karakaisis, G.F., and Papazachos, B.C., (1994). Seismicity of the Aegean sea and surrounding area. Proc. XXIVGen. Ass. Eur. Seism. Comm., Athens 19–24 Sept., 1994, 1, 155–164.

Kijko A., Sellevoll M.A., (1989). Estimation of earthquake hazard parameters from incomplete data files. Part I. Utilization of extreme and complete catalogs with different threshold magnitudes. Bull. Seism. Soc. Am. 79, 645–654.

Kijko A., Sellevoll M.A., (1992). Estimation of earthquake hazard parameters from incomplete data files. Part II. Incorporation of magnitude heterogeneity. Bull. Seism. Soc. Am. 82, 120–134.

Kijko, A and Graham, G., (1998). Parametric-historic procedure for probabilistic seismic hazard analysis. Part I. Estimation of maximum regional magnitude m_{max}. Pageoph, 152, 413–442.

Kijko, A and Graham, G., (1999). Parametric-historic procedure for probabilistic seismic hazard analysis. Part II. Assessment of seismic hazard at specific site. Pageoph, 154, 1–22.

Knopoff, L. and Kagan, Y., (1977). Analysis of the theory of extremes as applied to earthquake problems. J. Geophys. Res., 82, 5647–5657.

Koliopoulos, P.K., Margaris, B.N. and Klimis, N.S., (1998). Duration and energy characteristics of Greek strong motion records. J. Earthq. Eng., 2, 391–417.

Koravos, G.Ch., Main, I.G., Tsapanos, T.M. and Musson, R.M.W. (2003). Maximum earthquake magnitudes in the Aegean area constrained by tectonic moment release rates. Geophys. J. Int., 152, 94–112.

Koravos, G.Ch., Main, I.G., Tsapanos, T.M. and Musson, R.M.W. (2003). Perceptible earthquakes in the broad Aegean area. Tectonophysics, 371, 175–186.

Kotzev, V., King, R.W., Burchfiel, B.C., Todosov, A., Nurce, B., and Nakov, R., (2005). Crustal motion and strain accumulation in south Balkan region inferred from GPS measurements. Abstarcts of NATO ARW "Earthquake monitoring and seismic hazard mitigation in Balkan countries" (edrs. Husebye, E.S. and Christova, C.), Borovetz-Bulgaria 11–17 September 2005, 69–72pp.

Kotzev, V., King, R.W., Burchfiel, B.C., Todosov, A., Nurce, B., Nakov, R., (2008). Crustal Motion and Strain Accumulation in the South Balkan Region Inferred from GPS Measurement. In E.S. Husebye (ed.). Earthquake Monitoring and Seismic Hazard in Balkan Countries. Springer Publishing, Berlin, 19–43.

Lyubushin, A.A., Tsapanos, T.M., Pisarenko, V.F. and Koravos, G.Ch., (2002). Seismic hazard for selected sites in Greece: A Bayesian estimate of seismic peak ground accrleration. Natural Hazards, 25, 83–98.

Makris, J., (1973). Some geophysical aspects of the evolution of the Hellenides. Bull. Geol. Soc. Greece. 10: 206–213.

Makropoulos, K.C., (1978). The statistics of large earthquke magnitude and an evaluation of Greek seismicity. Ph.D. Thesis, Univ. of Edinburgh, 193pp.

Makropoulos, K.C. and Burton, P.W., (1984). Greek tectonics and seismicity. Tectonophysics, 106: 275–304.

Makropoulos, K. C. and Burton, P.W., (1985). Seismic hazard in Greece, II Ground acceleration, Tectonophysics, 117, 259–294.

Makropoulos, K.C., Voulgaris, N. and Likiardopoulos, A., (1990). A multi-methological approach to seismic hazard assessment. A application for Athens (Greece). Proc. Of XXII Gen. Ass. ESC, Barcelona, 585–591.

Manakou, M.V. and Tsapanos, T.M., (2000). Seismicity and seismic hazard parameters evaluation in the island of Crete and surrounding area inferred from mixed data. Tectonophysics, 321, 157–178.

Markušić, S., (2005). Seismicity of Croatia. Abstarcts of NATO ARW "Earthquake monitoring and seismic hazard mitigation in Balkan countries" (edrs. Husebye, E.S. and Christova, C.), Borovetz-Bulgaria 11–17 September 2005, 124–128pp.

Margaris, V.N., Theodulidis, N.P., Papaioannou, Ch.A. and Papazachos, B.C., (1990). Strong motion duration of earthquake in Greece. Proc. XXII Gen. Ass. ESC 2, 865–871.

Margaris, V.N., (1994). Azimuthal dependence of the seismic waves and its influence on the seismic hazard assessment in the area of Greece. Ph.D. Thesis, Univ. of Thessaloniki, 324pp.

Margaris, V.N. and Papazachos, B.C., (1994). Implications of the azimuthal variations of seismic intensities in seismic hazard assessment. ESC XXIV, Gen. Ass., Athens, 3, 1718–1728.

Margaris, V.N., Papazachos, C.B., Papaioannou, Ch.A. Theodulidis, N., Kalogeras, I. and Skarlatoudis, A., (2002). Empirical attenuation relations for the strong ground motion parameters of shallow earthquakes in Greece. Proc. 2nd Congress of Engin. Seismology and Earthquake Engineering 28–30 November 2001, Thessaloniki.

McKenzie, D., (1978). Active tectonics of the Alpine-Himalayan belt: the Aegean sea and the surrounding regions. Geophys. J. R. astr. Soc. 55: 217–254.

Mercier, J., (1977). Principal results of a neotectonic study of the Aegean arc and its location within the eastern Mediterranean. In: Proc. VI Coll. Geol. Aegean Region, Athens, 1977, I. G.M.R., Athens, Greece. III: 1281–1291

Papadopoulos, G.A. and Kijko, A., (1991). Maximum likelihood estimation of earthquake hazard parameters in the Aegean arc from mixed data. Tectonophysics, 185, 277–294.

Papaioannou, Ch.A., (1984). Attenuation of seismic intensities and seismic hazard in the area of Greece. Ph.D. Thesis, Aristotle Univ. of Thessaloniki, 200pp.

Papaioannou, Ch.A., (1986). Seismic hazard assessment and long term earthquake prediction in southern Balkan region. Proc. 2nd Int. Reg. Sem. on Earthq. Prognostics (edit. A. Vogel and K. Brandes), Berlin 223–241.

Papaioannou, Ch.A. and Papazachos, B.C., (1997). Seismic hazard in Greece based on new seismotectonic data. In: Abstr. IASPEI 29th Gen. Assembly, Thessaloniki, 18–28 August 1997, p. 294.

Papaioannou, Ch.A. and Papazachos, B.C., (2000). Time-independent and time-dependent seismic hazard in Greece based on seismogenic sources, Bull. Seismol. Soc. Am., 90, 22–33.

Papazachos, B.C., (1980). Seismicity rates and long term earthquake prediction in the Agean area. Quaterniones Geodaesiae. 3, 171–190.

Papazachos, B.C., (1990). Seismicity of the Aegean and the surrounding area. Tectonophysics, 178, 287–308

Papazachos, B.C. and Comninakis, P.E., (1971). Geophysical and tectonic features of the Aegean arc. J. Geophys. Res., 76: 8517–8533.

Papazachos, B.C., Kiratzi, A.A., Hatzidimitriou, P.M. and Theodulidis, N.P., (1985). Regionalization of seismic hazard in Greece. Proc. 12th Reg. Sem. on Earthq. Eng. EAEE_ EPPO, Halkidiki, Greece, 12pp.

Papazachos, B.V., Makropoulos, K., Latousakis, J. and Theodulidis, N., (1989). Elaboration of a map of seismic hazard in Greece. 2nd rep. For the program of OASP, 24pp. (in Greek).

Papazachos, B. C., Margaris, V.N., Theodoulidis, N.P. and Papaioannou, Ch. A., (1992). Seismic hazard assessment in Greece based on strong motion duration. Proc. 10th W.C.E.E., 1, 425–430.

Papazachos, B.C. and Papazachou, C.B., (1997). The earthquakes of Greece. Ziti Publications, Thessaloniki, 304pp.

Papazachos, B.C. and Papazachou, C.B., (2002). The earthquakes of Greece. Ziti Publications, 2nd Edition, Thessaloniki, 317pp.

Papazachos, C.B., (1999). An alternative method for a reliable estimation of seismicity with an application in Greece and surrounding area, Bull. Seismol. Soc. Am., 89, 111–119.

Papoulia, J.E. and Stavrakakis, G.N., (1990). Attenuation laws and seismic hazard assessment. Natural Hazards, 3, 49–58.

Rashidov, T., Erdick, M., Safac, E., Turdukulov, A. and Ashrabov, A., (2005). Seismic risk assessment and mitigation in Tashkent (Uzbekistan) and Bishkek (Kyrgystan). Abstarcts of NATO ARW "Earthquake monitoring and seismic hazard mitigation in Balkan countries" (edrs. Husebye, E.S.and Christova, C.), Borovetz-Bulgaria 11–17 September 2005, 153–157pp.

Stavrakakis, G.N., (1985). A contribution of the Bayes statistics for seismic hazard assessment and simulation of the expected strong ground motion. Ph.D. Thesis, Univ. of Athens, 294pp.

Stavrakakis, G.N., Drakopoulos, J. and Makropoulos, K.A., (1986). A model for the seismic hazard assessment in southwestern Peloponnesus and synthesized ground motion for the city of Kalamata. Ann. Geol. Pays Hell. 233–249.

Solakov, D., Simeonova, S. and Christoskov, L., (2005). Seismicity and seismic hazard modelling in Bulgaria. Abstarcts of NATO ARW "Earthquake monitoring and seismic hazard mitigation in Balkan countries" (edrs. Husebye, E.S.and Christova, C.), Borovetz-Bulgaria 11–17 September 2005, 162–165pp.

Theodulidis, N.P., (1991). Contribution to the study of strong motion in Greece. Ph.D. Thesis, Univ. of Thessaloniki, 500pp.

Theodulidis, N.P. and Papazachos, B.C., (1994). Seismic hazard in Greece in terms of spectral values. 7th Congr. Geolog. Soc. Of Greece, Thessaloniki, May 25–27.

Theodulidis, N.P. and Tsakalidis, K., (1994). Site effects on strong motion recorded over simple geology structure. The case of Lefkas and Argostoli (Ionian islands,Greece). ESC XXIV, Gen. Ass., Athens, 3, 1640–1659.

Theoduludis, N.P. and Bard, P-Y., (1995). Strong ground motion simulation of large earthquakes. Proc. 10th Eur. Conf. Eartq. Eng., 1, 269–274.

Tóth, L., Gyöiri, E., Mónus, P. and Zsiros, T., (2005). Seismicity and seismic hazard in and around Hungary. Abstarcts of NATO ARW "Earthquake monitoring and seismic hazard mitigation in Balkan countries" (edrs. Husebye, E.S. and Christova, C.), Borovetz-Bulgaria 11–17 September 2005, 169–172pp.

Tsapanos, T.M. and Burton, P.W., (1991). Seismic hazard evaluation for specific seismic regions of the world. Tectonophysics, 194, 153–169.

Tsapanos, T.M., (2001). Earthquake hazard parameters estimated in Crete island and the adjacent area. Pageoph, 158, 1691–1718.

Tsapanos, T.M., Mantyniemi, P. and Kijko, A., (2004). A probabilistic seismic hazard assessment in Greece and the surrounding region including site-specific considerations. Annals of Geophysics, 47 (6), 1675–1688.

Are Rock Avalanches and Landslides Due to Large Earthquakes or Local Topographic Effects? A Case Study of the Lurøy Earthquake of August 31, 1819, A 3D Finite Difference Approach

T.R.M. Kebeasy,[1] E.S. Husebye[2]*, and S. Hestholm[3]

Abstract The Lurøy earthquake of August 31, 1819, with MS ~ 5.8 is, by many colleagues, rated as the largest in NW Europe in historical times (pre-1900) and even up to present. Local shaking manifestations were most spectacular with rock, stone and mud avalanches, mast-high waves in nearby Rana fjord and even liquefaction was reported. Most surprisingly, at epicentral distances exceeding 100 km except for Stockholm 800 km away, very few macroseismic observations are available. Another peculiarity was the lack of any significant housing damage even in the Lurøy parish itself. In a recent paper, we postulated that the earthquake was of moderate size, reestimated at MS ~ 5.1, but of shallow depth between 5 and 10 km causing the intense local shaking. In this article, we add a new dimension to the many Lurøy earthquake studies namely simulating the seismic wavefield response of Lurøy itself and adjacent areas characterized by steep topographic reliefs. We use a 3D finite difference scheme and compute ground motion in the 2–8 Hz band for a shear wave source with a focal depth of 5 km. Water covered areas are replaced by crystalline crust due to the sparsity of dense bathymetric data.

Main results are that the topography of the Lurøy, close to the mountain peak at 685 m, causes wavefield amplification by a factor of 20 and even stronger. Further away in the Rana fjord and surrounding areas, we also got strong amplification in particular where the relief is sharpest thus explaining triggering of avalanches in a quantitative manner. In other words, macroseismic observations would be biased upward due to the topographic focusing effects and unless properly corrected for may increase the final earthquake magnitude estimate. We take these results to strongly support our claim that the historic Lurøy earthquake was of moderate size of MS ~ 5.1 and not at MS ~ 6.0 class as claimed by many colleagues. The largest magnitude estimates stem from including outlier observations in Kola and Stockholm. Finally, downscaling of maximum earthquake magnitude would also lower the seismic risk levels significantly.

[1] Schlumberger Cambridge Research, High Cross, Madingley Road, Cambridge, CB3 OEL, United Kingdom

[2] Bergen Center for Computational Science, UNIFOB/UoBergen, Bergen, Norway

[3] Shell International Exploration and Production, Inc., Houston, TX, USA

* To whom correspondence should be addressed. E-mail: esh@bccs.uib.no

E.S. Husebye (ed.), *Earthquake Monitoring and Seismic Hazard Mitigation in Balkan Countries.*

Keywords 3D synthetic seismogram, topography amplification, rock avalanches, mast high waves, magnitude bias, lurøy EQ

1 Introduction

Historical earthquake observations are essential for mapping the seismicity for a given region over a reasonable time span like 500 years. These data in turn are extensively used for probabilistic seismic hazard analysis (PSHA) for nuclear power plants, huge industrial installations and for metropolitan cites in earthquake prone areas. In this context, the largest occurring earthquakes contribute the most to the risk level estimate where the ground motion is represented with a relatively simple parameter such as peak ground acceleration (PGA) for a given time interval and area (e.g., see Kijko, 2008, ibid).

Working with historical earthquake data for NW Europe (Mantyniemi et al., 2004) the impression is that in the past large earthquakes occurred relatively more frequently. In addition, most intriguingly, historical events are far too often the largest in many regions of the world. Questions remain as to whether there is any scientific proxy for such a claim or just subjective feelings on our side? A common explanation is that, for intraplate earthquakes, the recurrence time is much longer so we simply have not yet experienced stronger events. However, since magnitude estimates of historical events are tied to macroseismic observations (felt/observed by human beings), an explanation perhaps lies in the handling of the macroseismic data at hand. For example, Kjellen (1910) located the Lurøy earthquake in north Sweden albeit he had access to detailed Norwegian descriptions of this event like that of Keilhau (1836). Likewise, Grunthal and Wahlstrøm (2003) reports several gross errors including fake events in catalogues from central, northern and northwestern Europe. Initially, the magnitude estimate relied upon an assumed correlation between maximum epicentral intensity and magnitude. This was later replaced by the correlation of magnitude to the size of the often elliptically/circularly shaped felt area of intensity III and IV. A potential flaw here is that intensity observations are subjective in nature and rarely corrected for local site condition. In Fennoscandia the claim by many fellow scientists is that just after the melting about 10,000 years ago of the large glacier covering the region, part of the energy release was in the form of large magnitude earthquakes (Olesen et al., 1999; Wu et al., 1999; Hicks et al., 2000; Stewart et al., 2000). The recently discovered neotectonic faults mostly in northern Fennoscandia are taken in support of such statements. The most prominent of which is the Pårve fault being 150 km long with fault scarp of 10–15 m Hence, large earthquake could occur in this region (glacial rebound driven) and in support of this claim the Lurøy earthquake of August 31, 1819 with MS ~ 5.8–6.2 (Muir Wood, 1989) is taken as a manifestation.

Muir Wood (1989) stated that the Lurøy earthquake of August 31, 1819 is one of the largest known pre-1900 Fennoscandinavian earthquakes. His magnitude assessment was based upon the large areal extent of: (i) the intensity III macroseismic observations including one from Stockholm 800 km away, and (ii) rock avalanche and landslides in the vicinity of the epicentre. In a recent paper about this earth-

quake, Husebye and Kebeasy (2004) presented a re-assessment of the macroseismic observations that lead to a significant reduction of the felt area and therefore 'lowered' the Lurøy earthquake magnitude to MS ~ 5.1. This result is not entirely popular among many colleagues primarily because: (i) observation of rock avalanches and mast-high waves in the vicinity of the epicentre are not easily reconciled with a MS ~ 5 earthquake, and eventually (ii) the downscaling of the magnitude significantly lowers the seismic risk levels not only for Lurøy but also the adjacent offshore areas. Recently, the Husebye and Kebeasy (2004) paper has come under severe attacks from colleagues; Wahlstrøm (2004) and Bungum and Olesen (2005) both claiming that the magnitude downgrading of the Lurøy 1819 and the Kattegat 1759 earthquakes were wrong and due to faulty data analysis. In replies to these accusations Husebye and Kebeasy (2005) and Husebye (2005) maintained that their analyses were correct and saw no compelling reason to upgrade their magnitude estimates for these two earthquakes. Husebye draw attention to the recent Kaliningrad earthquake of 21 September 2004, and ML magnitude 5.0 which was felt over larger areas than those in Kattegat and Lurøy but the latter are given magnitudes at c.5.8–6.0 as mentioned above (Husebye and Mantyniemi, 2005). Why this heated discussion of event magnitudes of some large historical earthquakes? The reason appears foremost to be that lower magnitudes imply lower hazard levels and hence less need for excessive earthquake risk research ventures. In case of the Husebye (2005) paper even the journal editor took part; he removed critical comments on the Bungum and Olesen paper in the Husebye (2005) (author not notified) and ensured that a severe blunder in Bungum and Olesen were corrected prior to publication initially claimed to be carefully screened.

A new approach to settle ongoing debates on the size of historical earthquakes and likely future damage potential is the introduction of wavefield synthetics for corroborating past earthquake damage and corresponding macroseismic observations. An adequate example here, Kebeasy and Husebye (2003b) demonstrated that the once presumed largest earthquake in Scandia (S. Sweden & Denmark), the Kattegat earthquake of December 22, 1759, was over-sized as the macroseismic observations extending far south into N. Germany were not corrected for wavefield amplification nor focus effects in the Danish and N. German sedimentary basins. Unless accurately accounting for such effects the corresponding magnitude estimates would be upward biased.

This article is intended to demonstrate whether these reported rock avalanches and landslides in the vicinity of Lurøy earthquake epicentre were triggered because of an exceptionally large earthquake or alternatively strong wavefield amplification due to local surface topography. The technique used is 3D finite difference (FD) wavefield modelling based on the formulation of Hestholm and Ruud (1998, 2002) and Hestholm et al. (2006). However, due to the heavy computations involved in 3D modelling, we are unable to capture the whole area within one model volume so it was subdivided into 2 smaller ones. The first comprises the Lurøy islands and the second Hemnes and Utskarpen in the Rana fjord (Figure 1). Also, we consider this article as a sequel to that of Husebye and Kebeasy (2004) and Husebye (2005) in support of their claim to downscale the Lurøy earthquake magnitude to a more realistic estimate.

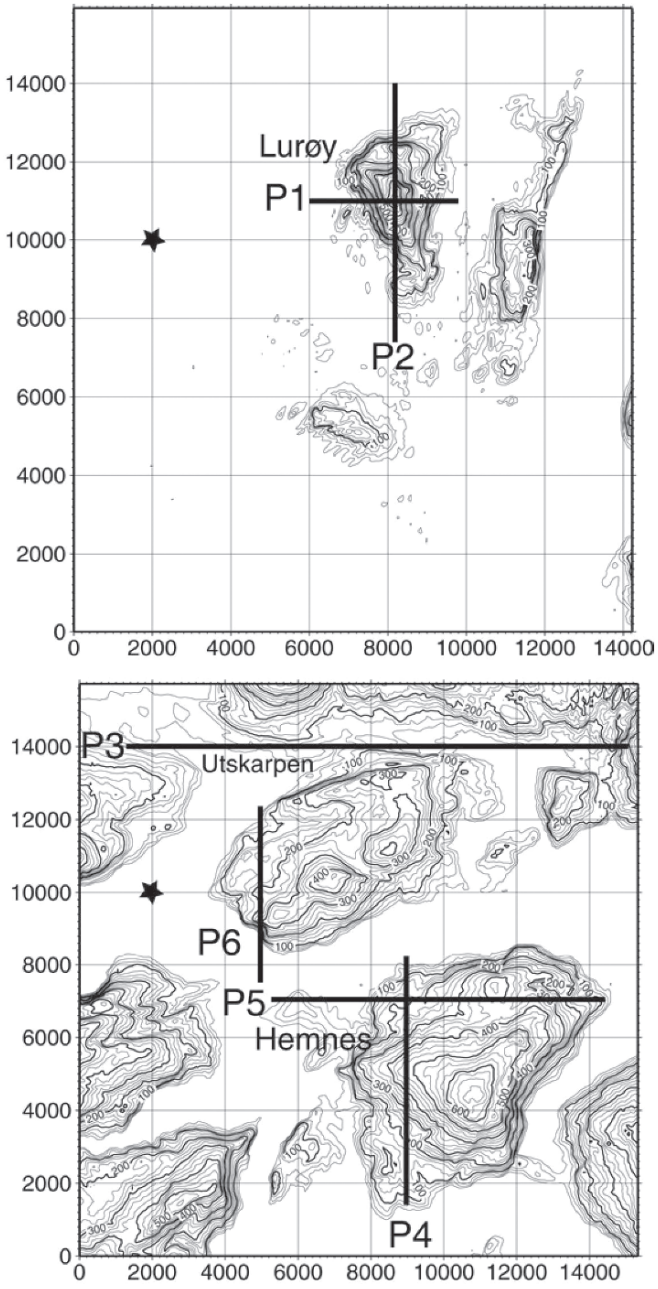

Figure 1 Topographic maps of (top) the Lurøy island ($14.2 \times 16\,km^2$) and (bottom) Hemnes and Utskarpen in the Rana fjord ($15.4 \times 18.2\,km^2$). The latter is about 50 km east of Lurøy. Y- and X-axes coincide with North and East respectively. Results are displayed at intervals of 200 m along the respective profiles. The star indicates the source location. The source depth for both models is set to 5 km

2 The 3D FD Modelling Approach and Model Construction

The importance of topography on the seismic wavefield was demonstrated by Bannister et al. (1990) identifying P-to-Rg converted in the teleseismic P-wave coda. They used NORESS array records to pinpoint nearby hills where the phase conversions took place irrespective of azimuth of the incoming P-waves. At that time synthetic modelling of P-waves, P-to-S-conversions, scattering and topography reflections were out of question due to excessive computational requirements and moreover finite difference solutions of the elastic wave equation were at a preliminary stage. An early significant contribution was that of Hestholm et al. (1994) who calculated 2D synthetics for a $80 \times 500\,km^2$ model over a time span of 60 s. Further refinements from other scientists (e.g. Moczo et al., 1995, 1999: Pitarka, 1999; Olsen et al., 2000) combined with continuous development of faster computers resulted in 3D FD-solutions for the viscoelastic wave equation, even for models with free surface topography (see Hestholm and Ruud, 1998, 2002). In the present study, we used the latter approach. The 3D viscoelastic finite-difference code with free surface topography boundary conditions implemented (Hestholm and Ruud, 2002; Hestholm et al., 2006), is parallelized using Message Passing Interface (MPI) to run by domain decomposition parallellization on several computer nodes to accommodate for large areas and/or higher frequencies in seismic wavefield modelling. The code applied in the present work was refined and Matlab wrappers were added for user-friendliness.

Seismic surveys (Kinck et al., 1993) imply that the crustal thickness in and around the Lurøy area is about 30 km and reasonably homogeneous with a gradual P-velocity increases from 6.1 km/s at the surface down to 7.1 km/s above Moho. Elevations are moderate with mountain peaks in the 600–800 m range compared with 1,200–1,400 m on the mainland. Depths of nearby fjords seldom exceed 250 m There is insufficient data on the subsoil coverage in this area to constrain a detailed 3D model. On the other hand, we have obtained digital topographic data with spatial sampling of 25 m from Statens Kartverk (the national mapping agency of Norway). Water covered areas are represented as crystalline crust as bottom topography data is lacking. Besides, we did not have the software tools for producing models with 3D boundary layers. The question in this context is whether this model simplification would severely decline the quality of the wavefield synthetics? The answer is ‘no’ since on land, subsurface topographic features do not produce severely distorted wavefields but mostly small amplitude coda waves.

A spatially pure shear source with a temporal Ricker profile (derivative of a Gaussian) of central frequency of 2.5 Hz was used to simulate earthquakes in the experiments. It may be argued that this model represents an oversimplification for the problem at hand, and in particular that a line source is more appropriate for events with magnitudes above 5. Nor is any magnitude scaling attempted, say for M5 synthetics versus M6 ones. The Hestholm et al.(2006) work implies that the mentioned simplification is not quite critical inasmuch as both true focal location and event magnitude are unknown. The same apply to the loading

needed for triggering the reported avalanches and land slide in Utskarpen. In the latter case rainy weather for weeks appears to be a requisite at least for land slides and hence such phenomena preferably take place in spring (snow melting) and the rainy October and November. The Lurøy earthquake occurred on 31 August 1819, which was the first sunny day after 3 weeks of continuous rainy weather.

Absorbing boundary conditions were incorporated in the form of 1 km thick damping layers along the sidewalls and bottom of the model using Cerjan et al. (1985) exponential damping method. Although reflecting boundaries is generally a problem that tends to persist in seismic modeling, for our Lurøy synthetics we found that such reflections were minimal. This is due to our extensive empirical experience with adjusting the absorption coefficient as a function of thickness of absorbing strips, given various categories of models. Visually the artificial wall reflections were very small and hence did not distort the wavefield in any significant manner. A time step of 3 ms was used in the computations of the synthetic wave field. The three particle velocity components of the synthetic wave field are computed at all grid points of the free surface. The data is extracted along the profiles shown in Figure 1. To demonstrate the amplification, we use a 5% damped response spectrum (Kebeasy and Husebye, 2003a). In this analysis, the spectral amplitudes of the filtered traces were normalized to the corresponding traces of a plane model of crystalline rock at the same distance range.

3 Lurøy Islands Model and Hemnes and Utskarpen in the Rana Fjord Models

The surface area of the model is $14.2 \times 16\,km^2$ (Figure 1) with a depth of 7.5 km and uniform 0.05 km spatial sampling. The source was located to the west of Lurøy Island and at a depth of 5 km underneath the island. However, the latter results will not be shown, but referred to in the results section. The synthetic seismograms are calculated along two profiles; SN and WE on Lurøy Island (Figure 1). The P-velocity is uniformly set to 6.1 km/s and a Poisson ratio value of 0.25 is used for P-to-S-velocity conversion. For details on the physical model set-up we refer to Table 1.

In this case, the model is $15.4 \times 18.2 \times 8\,km^3$ with the same spatial sampling (Figure 1) as for the Lurøy model. The source was located to the west of the model at a depth of 5 km. However, source location is not based on seismotectonic considerations. We are limited by the model dimensions, and the source location has to be within the model block. The synthetic seismograms are calculated along four profiles (Figure 1) coinciding where the rock avalanches and landslides that were reported. Again, model details are in Table 1.

Table 1 Physical model parameters for both Lurøy Island and Hemnes and Utskarpen in the Rana fjord area.

Model parameters	Lurøy model	Hemnes and Utskarpen model
Vp	6,100 m/s	6,100 m/s
Vs	3,526 m/s	3,526 m/s
P	2.75 g/cm^3	2.75 g/cm^3
Qp	350	350
Qs	155	155
dx = dy = dz	50 m	50 m
Dt	0.003 s	0.003 s

4 Seismological and Geological Mapping of the Rana Fjord Country

In contrast to the physical parameters given in Table 1, information bearing on the seismological and geological frameworks for the Lurøy earthquake is generally lacking. Lurøy and adjacent Rana fjord area are part of the Nordland county (between 65.0° and 68.5° North), has a relatively high seismic activity but mostly in terms of small magnitude (ML < 3.0) events (Bungum et al., 1979). The only known exception is the Bodø earthquake of 15 Dec. 1962, and ML ~ 4.8. The Lurøy event took place at c.2.30 pm and many farmers were out in the field since the sky was clear after more than 3 weeks of persistent raining. The strongest shaking was reported from Lurøy (an island) but also in the Rana fjord proper.

The most striking observational features features were rock avalanches in Lurøy and Hemnesberget while at Utskarpen also a landslide was reported. In the Rana fjord itself mast high waves were observed and by us taken to reflect excitations caused by stone avalanches falling into the sea. The probable earthquake triggering of the mentioned avalanches are very exceptional but on the other hand such phenomenon are not unusual in certain areas of Norway where soil is dominated by clay sediments. The common denominator here is very wet weather like the 'rainy' October and November months and during snow melting in spring time. The strongest shaking was reported from the Lurøy area so we, like Muir Wood (1989), put the epicenter close to this island while Ambressey's (1985) used a location 100 km further east. Kjellen (1910) for some unexplainable reason located the Lurøy earthquake further east on the coast of the Bothnian Bay in Sweden. A peculiarity of the Lurøy earthquake is intense shaking in the Rana fjord area but no housing damages reported. Furthermore, a few observations from areas 700–1200 km away exist, but as mentioned some of these are considered to be outliers from places like Stockholm, NW Finland and Kola. If the latter are taken to be representative measures of felt area radii and hence of the extent of the felt area per se and then used for calculating the macroseismic MS magnitude of 5.8–6.2 by Muir Wood (1989) and Ambresseys (1985). Since details on epicenter location for this earthquake are lacking we cannot forward a specific faulting mechanism for this

event – elsewhere in Norway we find both normal and strike slip source mechanisms (Hicks, 1996; Hicks et al. 2000).

As mention, no detailed bathymetry maps exist for the Rana fjord area so the ocean parts of the models used, are replaced by upper crustal material. Likewise, sediment coverage on land is not known and hence replaced by upper crustal material. Some colleagues may consider that the lack of seismological and geological information in our synthetic modeling effort would limit the usefulness of our wavefield simulation efforts to which we disagree. For example, 2-D synthetics produced an amplitude amplification pattern reminiscent of housing damage pattern of a recent Egyptian earthquake for the city of Cairo (Kebeasy and Husebye, 2003a).

To summarize, the Lurøy earthquake took place almost two centuries ago and its epicenter or its focal depth are not well constrained. The most striking macroseismic observations originated from the Lurøy Island and its neighboring places hence we locate the epicenter there. Regarding focal depth, most small earthquakes in this area have shallow foci so our standard depth is 5 km. Also, for computational reasons we are forced to use a shallow source to keep the source inside our model, and to some extent also artificial reflections from the model boundaries may distort results if the source is far away. However, we are essentially testing whether local topography amplifies the destructive shear waves by say an order of magnitude. We also test whether more moderate sized earthquakes suffice for explaining macroseismic features usually attributed to magnitude 6 and larger earthquakes.

5 Results

The amount of observational data at hand is impressive as each grid point is represented by a 3-component seismograms with duration of 6 s and 11 s for the Lurøy Island and Hemnes and Utskarpen respectively and at a sampling rate of 0.015 s. Also note that the 3-component is oriented in the familiar North/South and East/West directions but the vertical component is perpendicular to the slope of the free surface with embedded topography. For signal power estimation the 'varying' site record orientation is of no consequences while polarization would be somewhat affected but being of little practical importance. The synthetic seismograms are obtained along six profiles covering the areas where rock, stone avalanches and landslides were reported (Figure 1). Two perpendicular profiles (P1 and P2) oriented west-east and south–north intersecting on the highest peak of Lurøy Island. The first source is located to the west of Lurøy Island and a second source underneath the island. Four profiles (P3–P6) traverse Hemnes and Utskarpen in the Rana fjord. Since model sizes are restricted by computer constraints, we have located the source focus about 50 km eastwards for simulating shakings in Hemnes and Utskarpen in the Rana fjord. Furthermore, we exclusively use the horizontal components to investigate amplification, since the vertical component exhibits weaker amplification and most of the damage reported is tied to shear waves. Note, all the synthetic seismograms shown here have the same amplitude scale.

Initially, we investigate influence of the source location to Lurøy Island on the synthetic wavefield. Amplification for the western source is 20% less than that of the

source underneath the island. However, the amplification pattern is similar across the island. This is to be expected since we are dealing with wave interferences, which has a more dominant effect than a particular source location. Another characteristic feature is that record duration is short with the S-pulse within 2 s of the P-pulse. In fact, these seismograms have similar appearances to those stemming from underground nuclear explosions with main P-duration of just a few seconds. This implies that the shallow focal depths and the confined volume of the Lurøy Island cause interferences to take place within a few seconds so there is no 'room' for generating S-wave coda as most of the signal energy rapidly leaks away from the island.

To illustrate the simulated shaking of Lurøy Island caused by the strong, local earthquakes on August 31, 1819, we display the two horizontal synthetic components along the two profiles (P1 and P2) across the island with their spectral amplification (Figures 2 and 3). A common feature here is that the N–S component shows higher

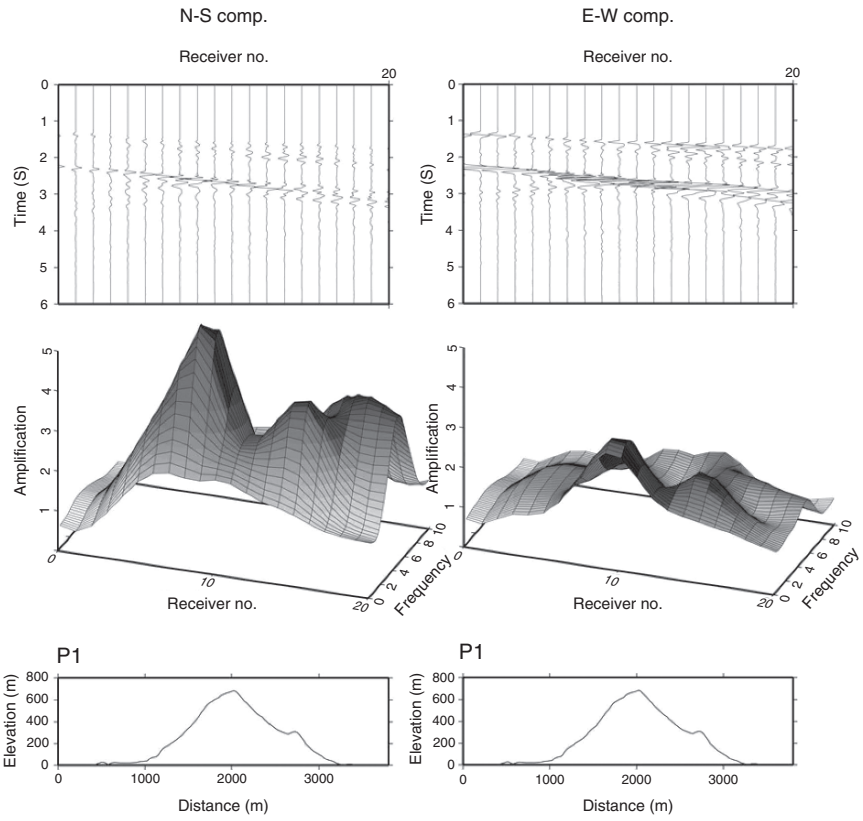

Figure 2 Synthetic seismograms for Lurøy model along the P1-profile for transverse (SH-waves; N–S) and radial (SV-waves; E–W) components respectively and the receiver spacing is 200 m. In the middle, ground motion amplification is displayed as a function of frequency and distance along the profile and the bottom is the topography relief along the profile. Amplification is strongest in the N–S component and coincides with a relative steep slope near the mountain peak

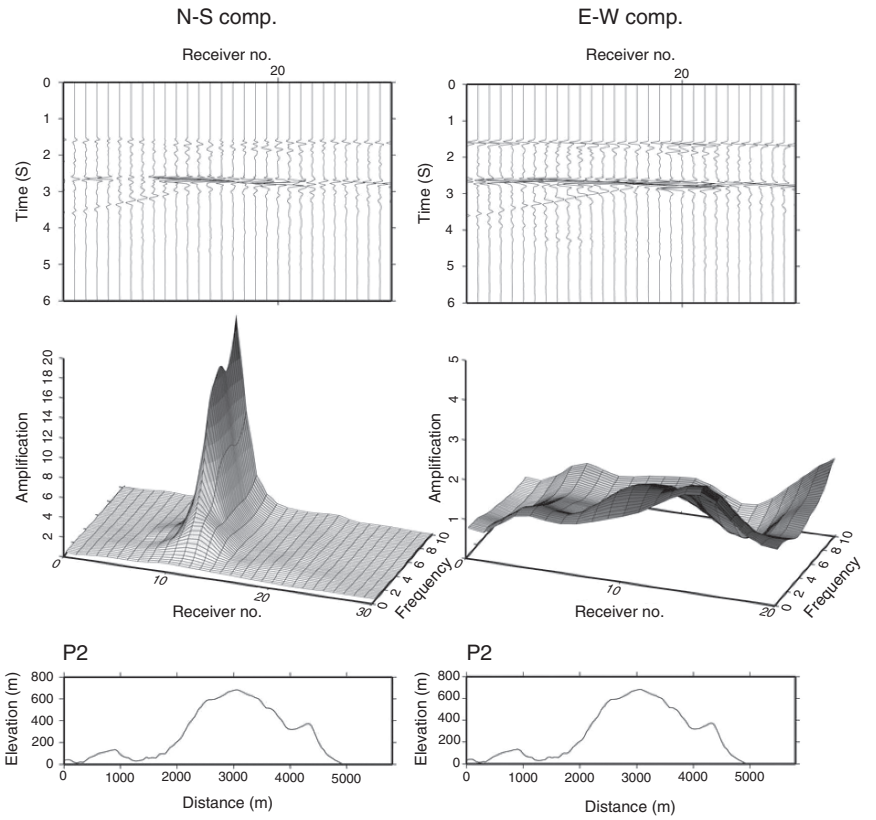

Figure 3 Synthetic seismograms of the two horizontal component of P2 with their spectral amplification and the topography elevation along the profile. The receiver spacing is 200 m. Amplification is a factor of 10 on the N–S component and closely coincides with where the rock avalanche was observed on Lurøy. Note that most of the amplification is focused on the southern part of P2 from the peak

amplification on the slopes than that of the E–W component. The explanation is that the E–W component roughly coincides with the radial (P–SV) component for this specific source – island configuration and the N–S component coincides with the (SH) transverse component. Inspecting the N–S components of P1 and P2 show that the amplification increases along the mountain slope and reaches its maximum just before the peak of the island. However, the N–S component along P2 shows much higher amplification (a factor of 20) than that of P1 (a factor of 5). Geli et al. (1988) pointed out the importance of the shape ratio (the mountain height (h) relative to its half width (l)) on the amplification. Furthermore, the amplification ratio between crest/base increases with increasing

shape ratio (h/l < 0.7). This explains the high amplification along P2 where h/l is 0.35, whereas the h/l for P1 is 0.7. Noteworthy, the maximum amplification along P2 coincides closely with where the rock avalanche on Lurøy Island took place. In addition, the amplification shows frequency dependency among the different profiles.

As mentioned, we cannot make the model excessively large so in order to simulate the wavefield in the Rana fjord area, we literally moved the source eastwards (Figure 1). Figures 4–7 exhibit amplification along the profiles (P3–P6), traversing Hemnes and Utskarpen. Similar to P1 and P2, the N–S component shows higher amplification than that of the E–W component for P3

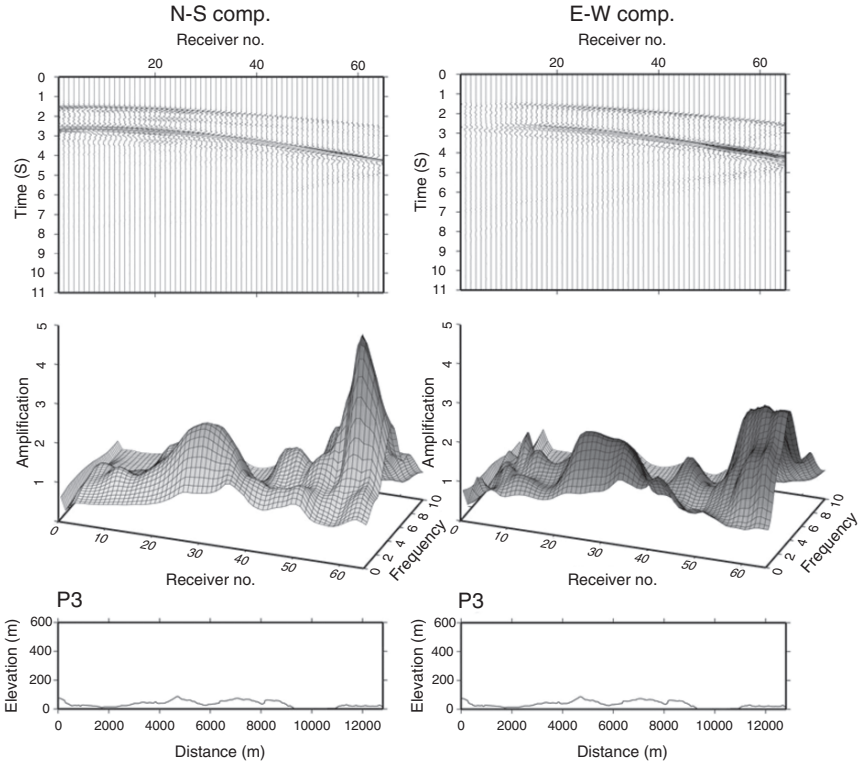

Figure 4 Synthetic seismograms for Hemnes and Utskarpen model of the two horizontal component of P3 with their spectral amplification and the topography elevation along the profile. Also, the amplification is most noticeable on the N–S component, as the case for Lurøy. Amplification along P3 is modest at a factor of about 3, including the low relief around Utskarpen area (Figure 1). However, at the end of the profile, the amplification increases to a factor of 5, coincident with the increasing slope towards inland mountain. Captions Otherwise as in Figure 3

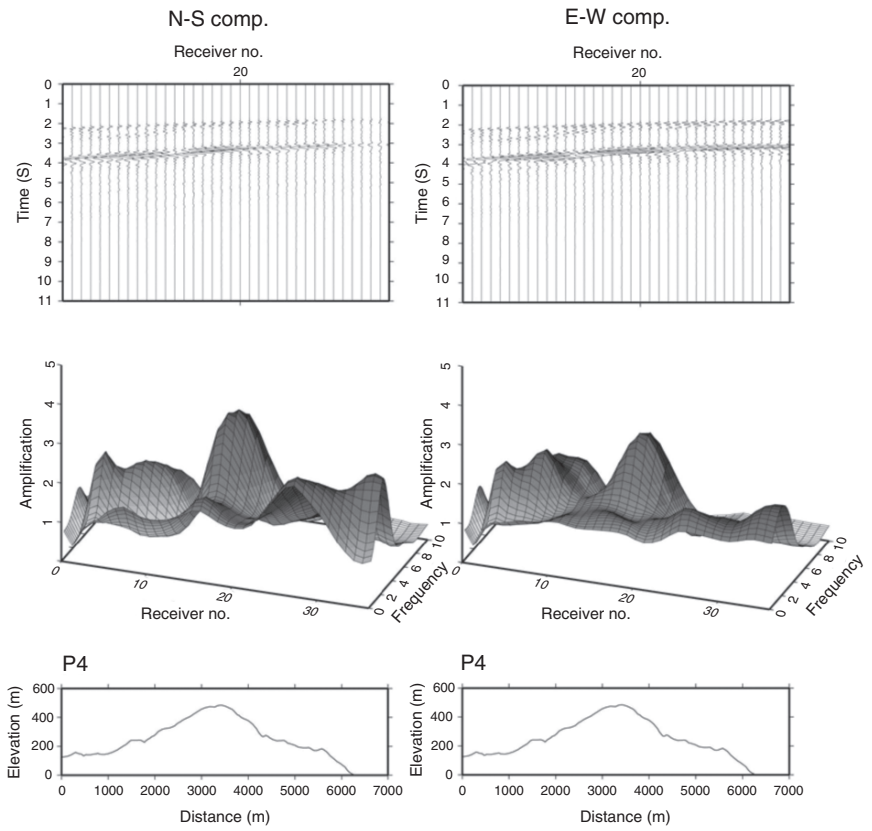

Figure 5 Amplification along P4 increases with the slope and attains its maximum near the highest part of Hemnes Mountain. However, the amplification varies rapidly along P4. Captions otherwise as in Figure 4

to P6. Amplification along P3 is modest at a factor of about 3, including the low relief around Utskarpen area (Figure 1). However, at the end of the profile, the amplification increases to a factor of 5 (Figure 4), coincident with the increasing slope towards inland mountains. Amplification along P4 increases with the slope and attains its maximum near the highest part of Hemnes Mountain. Nevertheless, the amplification varies rapidly along P4 and may reflect the 3D nature of the topography. This is clearly observed along P5 traversing the same mountain. Again, the highest amplification along P4 (a factor of 5) and P5 (a factor of 7) coincides with the reported rock avalanche near Hemnes (Figures 5 and 6). Similarly to P4 and P5, P6 exhibits the highest wavefield amplification by a factor of 10 (Figure 7) and again where the rock avalanche was reported.

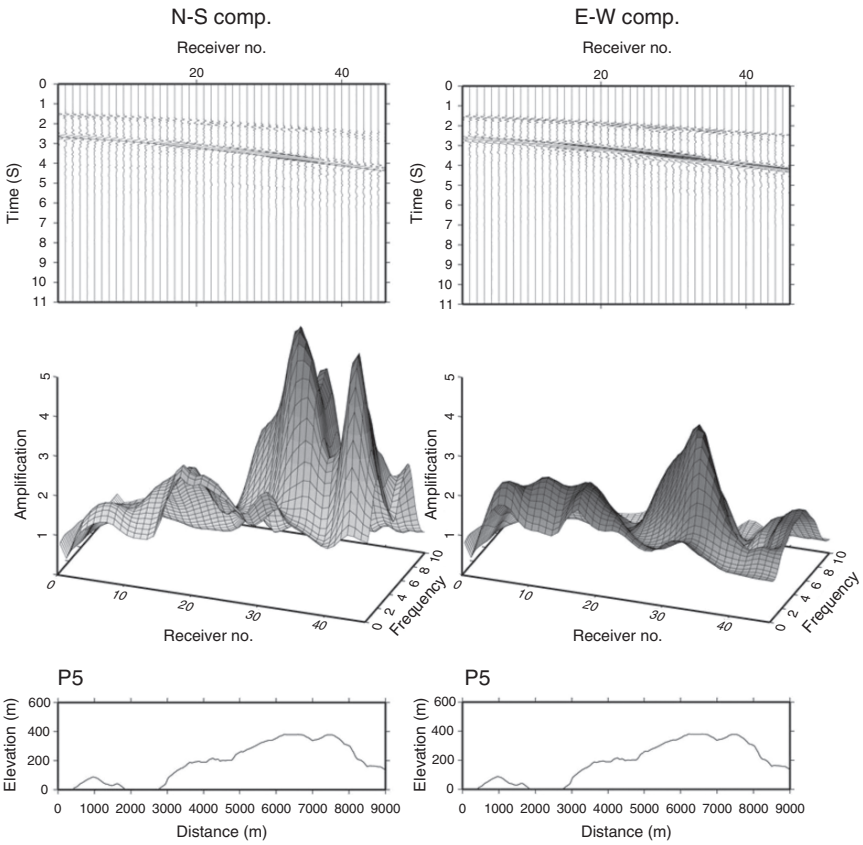

Figure 6 Amplification increases along the slope of Hemnes Mountain. Note a relatively small trough near the peak of the mountain towards the end of the profile, results on a second peak amplification, easily seen on the N–S component. Captions otherwise as in Figure 4

6 Discussion

The influence of topographic features on seismic ground motion has been reported repeatedly over time and far more frequent after the San Fernando earthquake in 1971. Geli et al. (1988) summarized the available studies and noted that amplification associated with topography is frequency dependent. Moreover, the amplification is larger for horizontal than vertical motion as demonstrated here.

The principal aim of our endeavour is to demonstrate that topography cannot be ignored in most seismic hazard studies, as is presently the case. The empirical site response estimates based upon spectral ratios of ambient noise records or from S-wave coda are not adequate substitutes in this sense as (i) noise is mainly Rayleigh waves, and (ii) focusing effects mainly stem from wavefield interferences. Hence, in

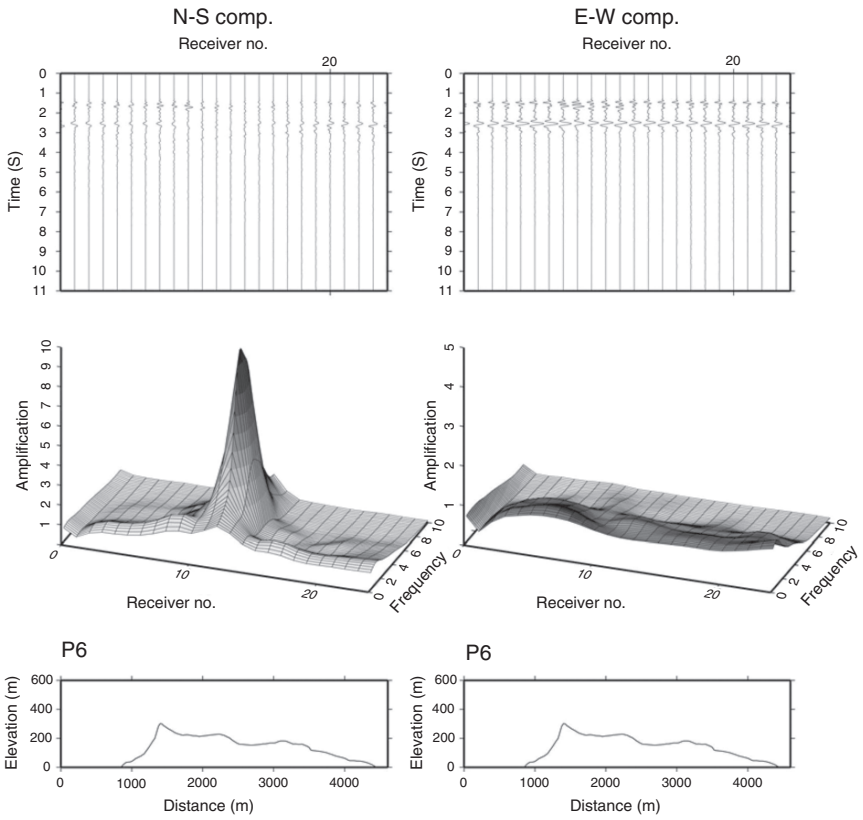

Figure 7 Synthetic seismograms of the two horizontal component of P6 with their spectral amplification and the topography elevation along the profile. The receivers spacing is 200 m. The amplification shows as one strong peak near the peak of the profile and comprises most of frequency band. Captions otherwise as in Figure 3

our 3D simulations of the Lurøy earthquake of 1819 we are foremost interested in the shaking of the Lurøy Island itself as the most vivid macroseismic reports stem from this island as well as some other place such as Hemnes and Utskarpen (in the Rana fjord), Træna and Tonnes. For wavefield synthetics to be meaningful we have to extract wave parameters, which can be related to the reported shaking and damage that mimic the macroseismic observations at hand (Table 2). For low-story housing most of the potential damage is in the range of 3–10 Hz whereas for triggering avalanches low-frequency waves of long time duration are most effective. However, explosion-type sources of short duration are used for triggering snow avalanches and occasionally removing hanging cliffs in a controlled manner (Mokrov et al., 2000). From the above results, we have demonstrated that even short duration pulses acting in an environment of rugged topography can produce sufficient amplification of the ambient wavefield to trigger rock avalanches.

Table 2 Tabulations of macroseismic information bearing on the Lurøy earthquake 31. Other locations have been added (in particular the Nordland counties, north to Henningsvær and south to Brønnøysund) where this earthquake should have been felt but there were no reports of it. Also, information that seems unreliable is included. The locations are grouped in terms of direction and epidistance relative to the Lurøy earthquake location given at the top of the table. Material and reportings used, are taken from the works of Heltzen (1834), Keilhau (1836) and Kolderup (1913) – intensity values from Husebye and Kebeasy (2004)

Place	Latitude (° N)	Longitude. (° E)	Distance (km)	Azimuth (degree)	Comments
Lurøy	66.41	12.91			Avalanche (VIII)
Near Field					
Nesna	66.20	13.02	24	168	Felt (VI)
Dønnes	66.20	12.58	28	212	Felt (VI)
Utskarpen	66.28	13.56	32	114	Landslide (VI)
Træna	66.50	12.10	37	286	Avalanche (VI)
Hemnesberget	66.22	13.62	37	124	Avalanche (VI)
Sadnessjøen	66.02	12.62	46	197	
Mjølan	66.33	14.13	55	98	
North (N)					
Bodø	67.25	14.25	110	32	Felt (III)
Røst	67.52	12.10	128	344	
Saltdal	67.10	15.40	133	54	Felt (V)
Sørland	67.67	12.68	140	356	
Svolvær	68.23	14.55	214	18	
Selsøya	68.32	15.27	234	24	Felt (III)
Stokmarkness	68.55	14.90	252	19	
Henningsvær	68.15	8.18	280	316	
Senja	69.00	16.80	335	28	Felt? (III)
Tranøy	69.13	17.43	357	30	Felt? (III)
South (S)					
Brønnøysund	65.47	12.22	109	197	
Vega	65.50	11.90	110	204	
Leka	65.08	11.70	157	201	
Rørvik	64.85	11.23	189	205	
Overhalla	64.47	11.92	221	192	Felt (III)
Namsos	64.47	11.50	225	197	Felt (?)
Steinkjer	64.02	11.47	274	195	Felt (?)
Levanger	63.73	11.30	306	195	Felt (?)
Stadsbygda	63.50	10.10	343	203	Felt (III)
Trondheim	63.40	10.40	352	200	Felt (?)
Far South (FS)					
Brekken	62.63	11.87	422	187	Felt (III)
Rørøs	62.57	11.38	433	190	
Lillehammer	61.10	10.45	602	192	
Oslo	59.90	10.73	731	190	
Bergen	60.38	5.32	767	213	
Stockholm	59.35	18.00	824	160	Felt (II)
East (E)					
Åsele	64.18	17.32	321	138	Felt (III)

(continued)

Table 2 (continued)

Place	Latitude (° N)	Longitude. (° E)	Distance (km)	Azimuth (degree)	Comments
Lycksele	64.57	18.45	327	126	Felt (III)
Umeå	63.84	20.10	440	127	Felt (II)
Arpela	66.00	24.00	499	90	Felt (II?)
Haparanda	65.78	24.00	503	92	Felt (II?)
Tornea	66.00	25.00	543	89	Felt (II?)
Uleaborg	65.10	25.46	589	98	Felt (II?)

Naturally, we cannot be very specific about the rock avalanches associated with the Lurøy earthquake in 1819 except that it is unique in the annals of earthquake occurrence in Norway. On the other hand, rock falls and avalanches are not quite uncommon and besides are most frequent in wet environments like spring thaw in April and heavy raining in the autumn months October and November (Ambraseys, 1985). A notable aspect of rock falls is their occasional generating of tidal waves in the fjord of W. Norway if the released masses are large enough. Villages in Loen and Tafjord were destroyed and many people perished when hit by such tidal waves in 1905 and 1936 respectively (Husebye and Kebeasy, 2004). Moreover, clay and mud slides are quite common in certain parts of Norway, around the Oslo fjord, Namdalen and also in the Rana fjord (Utskarpen) and as for rock avalanches mostly in a wet environment. These phenomena to be triggered by earthquakes are often hinted but with the Lurøy Island exception, evidence in support of such hypothesis is generally lacking.

Works on rock stability (e.g., Selby, 1980; Kramer. 1996; Kliche, 1999) do not provide any clear explanation for the 1819 rock avalanches since it is a complex subject depending on slope angle, lengths and widths of joints etc. Field geologists measure these parameters prior to issuing statements on rock stabilities say of road escarpments. Likewise, for clay mud flows reflecting that the original clay become almost fluid when water saturated and then may slide even for tiny slope angles of a few degrees typically of Utskarpen. Snow avalanche modeling implies that seismic load of relatively long duration that is SH-coda waves is efficient in their triggering. Practical experiments with dynamite and mortar grenades may also trigger snow avalanches and this kind of source with high intensity and short duration must have triggered the reported Lurøy earthquake avalanches. The avalanche in Lurøy itself did not fall directly into the sea so the ‘mast-high waves’ reports were confined to the Rana fjord. In other words, the waves in the sea are secondary earthquake effects. Similarly, reported ‘milky and muddy rivers’ are attributed to the relative strong shakings in the mountainous parts of the region as implied by our wavefield synthetics.

High intensities normally lead to high magnitude estimation for historical earthquakes, since we are lacking instrumental records for objective size studies. Here we have demonstrated that the high intensities reported at Lurøy Island, Hemnes and Utskarpen during the 1819 Lurøy earthquake probably were the consequence of local topography and not necessarily a large magnitude event. This corroborates

our earlier conclusion (Husebye and Kebeasy, 2004) in which we demonstrated that the magnitude of Lurøy earthquake was overestimated based on misinterpretation of the felt areal extent of intensity III. Foremost, we have demonstrated that extensive uses of 3D synthetic wavefield analysis add a new dimension to interpretations of the many partly vivid historical earthquake descriptions.

7 Conclusion

We have reinvestigated the spectacular Lurøy earthquake of August 31, 1819 which is generally classed as the largest in NW Europe in historical times (Muir Wood, 1989). In contrast to such studies, our focus is on a physical understanding of the macroseismic information at hand and not on re-examination of old annals and newspaper clippings in libraries. Despite handicapped by limitations in model sizes and number of runs to be made for the computer intensive 3D wavefield synthetics we conclude:

- Rugged topography will produce strong ground motion amplification.
- Both for Lurøy itself and Hemnes in Rana fjord the reported rock avalanche areas coincide closely with the calculated high amplification areas. The Utskarpen landslide area also has relatively high amplification but less than the mountainous areas.
- Reported 'mast high waves' are probably related to rock avalanches falling into the Rana fjord – not so at Lurøy and hence no 'mast high' waves three.
- Reported 'milky and muddy' rivers originating in the mountains are also related to strong ground shaking.
- No housing damages except for a few chimneys falling down; as expected with a moderate size Lurøy earthquake and most wavefield amplification is in the uninhabited mountain areas.
- Effects of topography cannot be ignored in seismic hazard assessment or in analysis of historic macroseismic observations.
- The magnitude of the 1819 Lurøy earthquake is considered overestimated and should be lowered to a more realistic estimate as calculated in Husebye and Kebeasy, 2004.

Acknowledgements The authors sincerely thank the Research Council of Norway (Programme for Supercomputing) through a grant of computing time. The particular code version applied in this work was refined through a collaborative project between The University of Texas at Dallas, TX, and the Cold Regions Research and Engineering Lab, US Army, NH, during 2001–2002.

References

Ambraseys, N. N., 1985. The seismicity of Western Scandinavia. *Earthq. Eng. Struct. Dyn*. 13, 361–399.

Bannister, S. C., Husebye, E. S., Ruud, B. O., 1990. Teleseismic P-coda analyzed by three component and array technique – deterministic location of topographic P-to-Rg scattering near the NORESS array. *Bull. Seism. Soc. Am*. 80, 1969–1986.

Bungum, H, Hokland, B. K., Husebye, E. S. Ringdal, F., 1979. An exceptional intraplate earthquake sequence in Meløy, Northern Norway. *Nature,* 280, 5717, 32–35.

Bungum, H., Olesen O., 2005. The 31st of August 1819 Lurøy Earthquake revisited. *Norwegian J. Geology*, 85, 245–252.

Cerjan, C., Kosloff, D., Kosloff, R. and Reshef, M., 1985. Short note on a non-reflecting boundary condition for discrete acoustic-wave and elastic-wave equations. *Geophysics*, 50, 705–708.

Geli, L., Bard, P. Y., Jullien, B., 1988. The effect of topography on earthquake ground motion: a review and new results. *Bull. Seism. Soc. Am*. 78, 42–63.

Grunthal, G., Wahlstrøm, R., 2003. A Mw based earthquake catalogue for central, northern and northwestern Europe using a hierarchy of magnitude conversions. *J. of Seismology,* 7, 507–531.

Heltzen, I. A., 1834. *Ranens beskrivelse*. Rana Museum og Historielag. *Mo i Rana*, 290 .

Hestholm, S. O., Husebye, E. S., Ruud, B. O., 1994. Seismic wave propagation in complex crust – upper mantle media using 2D finite difference synthetics. *Geophys. J. Int*. 118, 643–670.

Hestholm, S. O., Ruud, B. O., 1998. 3-D finite difference elastic wave modeling including surface topography. *Geophysics*, 63, 613–622.

Hestholm, S., Moran, M., Ketcham, S., Anderson, T., Dillen, M., McMechan, G., 2006. Effects of free-surface topography on moving-seismic-source modeling. *Geophysics*, 71, T159–T166.

Hestholm, S. O., Ruud, B. O., 2002. 3D free-boundary conditions for coodinate-transform finite-difference seismic modeling. *Geophys. Prosp*. 50, 463–474.

Hicks, E.C., 1996. Crustal stresses in Norway and surrounding areas as derived from earthquake focal mechanism solutions and in-situ stress measurements. M.Sc. Thesis, Dept. of Geology, UoOslo, Oslo, Norway, 164 pp.

Hicks, E. C., Bungum, Lindholm, C. D., 2000. Seismic activity, inferred crustal stresses and seismotectonics in the Rana region, northern Norway. *Quaternary Science Reviews*, 19, 1423–1436.

Husebye, E. S., 2005. Comments on the Lurøy earthquake controversy. *Norwegian J. Geology* 85, 253–256.

Husebye, E. S., Kebeasy, T. R. M., 2004. A re-assessment of the 31st of August 1819 Lurøy earthquake – Not the largest in NW Europe. *Norwegian J. Geol*. 84, 57–66.

Husebye, E. S., Kebeasy, T. R. M., 2005. Historical earthquakes in Fennoscandia – how large?. *Physics Earth Planetary Interior* 149, 355–359.

Husebye, E. S., Mäntyniemi, P., 2005. The Kaliningrad, West Russia earthquake on the 21st of September – surprise events In a very low-seismicity area. *Physics Earth Planetary Interiors*, 153, 227–236.

Kebeasy, T. R. M., Husebye, E. S., 2003a. A finite-difference approach for simulating ground responses in sedimentary basins: qualitative modeling of the Nile Valley, Egypt. *Geophy. J. Int*. 154, 913–924.

Kebeasy, T. R. M., Husebye, E. S., 2003b. Revising the 1759 Kattegat earthquake questionnaires using synthetic wave field analysis. *Physics of Earth & Planetary Interiors*, 139, 269–284.

Keilhau, B. M., 1836. Efterretninger om jordkjælv i Norge. *Magasin for Naturvidenskaperne*, 12, 83–165.

Kijko, A., 2008. Data driven probabilistic seismic hazard assement procedure for regions with uncertain seismogenic zones. In E.S. Husebye (ed.) Earthquake Monitoring and Seismic Hazard in Balkan Countries. Springer Publishing, Berlin, 237–251. ibid.

Kjellen, R., 1910. Sveriges jordskalf. Forsøk til en svensk landsgeografi. *Gøteborgs Høgskolas Årsskrift,* 15, 1–211.

Kinck, J. J., Husebye, E. S., Larsson, F. R., 1993. The moho depth distribution in Fennoscandia and the regional tectonic evolution from Archean to Permian times. *Precambrian Res*. 64, 23–51.

Kliche, C. A., 1999. Rock slope stability. Socity for Mining, Metallurgy, and Exploration (SME), *Inc., Littleton*, CO.

Kolderup, C. F., 1913. Norges jordskjΦlv med sΦrlig hensyn til deres utbredelse i rum og tid. *Bergen Museum Aarbok,* 8, 152.

Kramer, S. L., 1996. *Geotechnical earthquake engineering* Prentice-Hall, New York 653 pp.

Mäntyniemi, P., Husebye, E. S, Kebeasy, T. R. M., Nikonov, A. A., Nikulin, V., Pacesa, A., 2004. State-of-the-art of historical earthquake research in Fennoscandia and the Baltic Republics. *Annali Di Geofisica*, 47, 611–619.

Moczo, P., Rovelli, A., Labak, P., Malagnini, L., 1995. Seismic response of the geological structure underlying Roman Colosseum. *Annali di Geofisica* 38, 939–956.

Moczo, P., Lucka, M., Kristek, J., Kristekova, M., 1999. 3D displacement dinite differences and a combined memory optimization. *Bull. Seismol. Soc. Am*. 89, 69–79.

Mokrov, E., Chernouss, P., Fedorenko, Yu. V., Husebye, E. S., 2000. The influence of seismic effects on avalanche release. In Proceed. Int. Snow Sci. Workshop ISSW-2000, Big Sky, MT, 338–341.

Muir Wood, R., 1989. The Scandinavian earthquakes of 22 December 1759 and 31 August 1819, Disasters, 12, 223–236.

Olesen. O., Dehls, J., Olsen, L., Blikra, L. H., Rise, L., Bungum, H., Lindholm, C. D., Hicks, E., Riis, F., Bockmann, L., 1999. *Mor Norge rører på seg,* GEO 2, 12–17.

Olsen, K. B., Nigbor, R., Konno, T., 2000. 3D viscoelastic wave propagation in the upper Borrego Valley, California, constrained by Borehole and surface data. *Bull. Seis. Soc. Am*. 90, 134–150.

Pitarka, A., 1999. 3D elastic finite difference modeling of seismic wave propagation using staggered-grid non-uniform spacing. *Bull. Seism. Soc. Am*. 89, 54–68.

Selby, M. J., 1980. A rock mass strength classification for geomorphic purposes: with tests from Antarctica and New Zealand. *Zeitschrift fur Geomorphologie*, 24, 31–51.

Stewart, I. S., Sauber, J., Rose, J., 2000. Glacio-seismotectonics: ice sheets, crustal deformation and seismicity. *Quarterly Sci. Rev*. 19, 1367–1389.

Wahlstrøm, R., 2004. Two large historical earthquakes in Fennoscandia still large. *Phys. Earth Planet. Inter*. 145, 253–258.

Wu, P., Johnston, P., Lambeck, K., 1999. Postglacial rebound and fault instability in Fennoscandia. *Geophys. J. Int*. 139, 657–670.